

**NASA CONTRACTOR
REPORT**

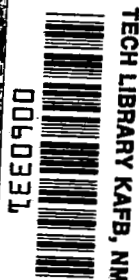


NASA CR 1219 v.5 c.1

LOAN COPY

KIRTLAND AFB, N. M.

NASA
CR
1219
v.5
c.1



**EXPERIMENTAL INVESTIGATION
IN AN ANNULAR CASCADE SECTOR OF
HIGHLY LOADED TURBINE STATOR BLADING**

V - Performance of Two Tangential Jet Blades

by James L. Bettner

Prepared by
GENERAL MOTORS
Indianapolis, Ind.
for Lewis Research Center



0060331

1. Report No. NASA CR-1675	2. Government Accession No.	3. Recipient's Catalog No.	
4. Title and Subtitle EXPERIMENTAL INVESTIGATION IN AN ANNULAR CASCADE SECTOR OF HIGHLY LOADED TURBINE STATOR BLADING V - PERFORMANCE OF TWO TANGENTIAL JET BLADES		5. Report Date November 1970	
		6. Performing Organization Code	
7. Author(s) James L. Bettner		8. Performing Organization Report No. EDR 5315	
9. Performing Organization Name and Address General Motors Indianapolis, Indiana		10. Work Unit No.	
		11. Contract or Grant No. NAS 3-9404	
12. Sponsoring Agency Name and Address National Aeronautics and Space Administration Washington, D.C. 20546		13. Type of Report and Period Covered Contractor Report	
		14. Sponsoring Agency Code	
15. Supplementary Notes			
16. Abstract <p>Two low reaction tangential jet turbine stator blade configurations were tested in a six-blade annular cascade. A plain blade, designed to the same aerodynamic requirements, was tested for performance comparison. The two tangential jet configurations differed by and were identified by the axial position of the jet slot. The slot was located at approximately 38 percent of the axial chord for the number 1 blade and at about 57 percent for the number 2 blade. The tangential jet blade surface contours were identical to the plain blade, except in the aft suction surface region which was modified to accommodate the jet slots. Three jet slot sizes of 0.020, 0.030, and 0.040 inch with three secondary flow rates for each slot were investigated for both number 1 and 2 blades. Secondary flow rates of up to nearly 7.5 percent of the primary flow were investigated. All configurations were tested at the design values of inlet gas angle and Mach number.</p>			
17. Key Words (Suggested by Author(s)) Turbines Cascade sectors Turbine blades Highly loaded blades		18. Distribution Statement Unclassified - unlimited	
19. Security Classif. (of this report) Unclassified	20. Security Classif. (of this page) Unclassified	21. No. of Pages 164	22. Price * \$3.00

FOREWORD

The research described herein, which was conducted by the Allison Division of General Motors, was performed under NASA contract NAS 3-9404. The work was done under the technical management of Mr. Edward L. Warren and Mr. Stanley M. Nosek, Airbreathing Engines Division and Fluid System Components Division, respectively, NASA Lewis Research Center. The report was originally issued as Allison EDR 5315, Volume V, March 1970.

TABLE OF CONTENTS

	<u>Page</u>
Summary and Conclusions	1
Introduction	3
Symbols	4
Tangential Jet Blade Performance	7
Velocity and Pressure Distributions	9
Surface Velocity Distribution	9
Surface Pressure Distribution	10
Tangential Lift Coefficient	11
Flow Visualization Results.	12
Suction Surface Separated Flow Patterns.	12
Pressure Gradient and Secondary Flow Requirements	13
Downstream Gas Angle and Tangential Velocity.	14
Average Downstream Gas Angles.	14
Change in Tangential Velocity and Reaction Across Blade Row.	14
Contour Plots.	15
Results at the Blade Trailing Edge (Station 3)	15
Results Downstream of the Blade Trailing Edge (Station 4)	16
Kinetic Energy Loss Coefficient	16
Downstream Gas Angle.	17
Mass Averaged Loss and Boundary Layer Parameters	17
Results at the Blade Trailing Edge (Station 3)	17
Aerodynamic Loss Data	17
Boundary Layer Parameters	19
Results Downstream of the Blade Trailing Edge (Station 4)	20
Aerodynamic Loss Data	20
Boundary Layer Parameters	20
Summary of Tangential Jet Blade Performance	21
References	24
Tables	25
Figures	31

LIST OF TABLES

<u>Table</u>	<u>Title</u>	<u>Page</u>
I	Design data for the plain and tangential jet blades	25
II	Experimental results for tangential jet No. 1 blade and plain blade	26
III	Experimental results for tangential jet No. 2 blade and plain blade	27
IV	Tangential jet and plain blade tangential force results . . .	28
V	Tangential jet and plain blade tangential lift coefficient results	29
VI	Tangential jet blade and plain blade measured and design change in tangential velocity across blade row	30

LIST OF ILLUSTRATIONS

<u>Figure</u>	<u>Title</u>	<u>Page</u>
1	Tangential jet blade No. 1 assembly.	31
2	Tangential jet blade No. 2 assembly.	32
3	Tangential jet blowing blade profiles and passages	33
4	Sketch of baffle installation details	34
5	Bench test slot-to-downstream suction surface flow pattern.	35
6	Annular cascade test rig.	36
7	Measured and predicted surface critical velocity ratio distribution for tangential jet blade No. 1	37
8	Measured and predicted surface critical velocity ratio distribution for tangential jet blade No. 2	38
9	Measured and predicted surface critical velocity ratio distribution for plain blade hub section.	39
10	Measured and predicted surface critical velocity ratio distribution for plain blade mean section.	40
11	Measured and predicted surface critical velocity ratio distribution for plain blade tip section	41
12	Mean section suction surface diffusion developed by various tangential jet configurations	42
13	Measured mean section surface static pressure distribution for all tangential jet configurations	43
14	Variation of corrected tangential force with secondary flow for the plain and tangential jet blades	44
15	Variation of corrected tangential force with jet momentum coefficient for plain and tangential jet blades	45
16	Variation of the jet contribution to the total mean section lift with percentage of secondary flow rate for all tangential jet configurations.	46
17	Effect of secondary flow rate on tangential lift coefficient for various blade configurations	47
18	Variation of tangential lift coefficient with jet momentum coefficient.	48
19	Flow visualization results for the tangential jet No. 1 blade with 0.020-in. jet slot and 1.00% secondary flow ($C_{jm} = 0.0045$)	49
20	Flow visualization results for the tangential jet No. 1 blade with 0.20-in. jet slot and 2.60% secondary flow ($C_{jm} = 0.0244$)	50
21	Flow visualization results for the tangential jet No. 1 blade with 0.020-in. jet slot and 4.00% secondary flow ($C_{jm} = 0.0456$)	51

<u>Figure</u>	<u>Title</u>	<u>Page</u>
22	Flow visualization results for the tangential jet No. 1 blade with 0.030-in. jet slot and 2.50% secondary flow ($C_{jm} = 0.0052$)	52
23	Flow visualization results for the tangential jet No. 1 blade with 0.030-in. jet slot and 4.10% secondary flow ($C_{jm} = 0.036$)	53
24	Flow visualization results for the tangential jet No. 1 blade with 0.030-in. jet slot and 6.30% secondary flow ($C_{jm} = 0.0752$)	54
25	Flow visualization results for the tangential jet No. 1 blade with 0.040-in. jet slot and 3.20% secondary flow	55
26	Flow visualization results for the tangential jet No. 1 blade with 0.040-in. jet slot and 3.98% secondary flow ($C_{jm} = 0.0407$)	56
27	Flow visualization results for the tangential jet No. 1 blade with 0.040-in. jet slot and 5.62% secondary flow ($C_{jm} = 0.0582$)	57
28	Flow visualization results for the tangential jet No. 1 blade with 0.040-in. jet slot and 7.44% secondary flow ($C_{jm} = 0.0854$)	58
29	Flow visualization results for the tangential jet No. 2 blade with 0.020-in. jet slot and 1.96% secondary flow ($C_{jm} = 0.0164$)	59
30	Flow visualization results for the tangential jet No. 2 blade with 0.020-in. jet slot and 3.02% secondary flow ($C_{jm} = 0.0339$)	60
31	Flow visualization results for the tangential jet No. 2 blade with 0.020-in. jet slot and 3.54% secondary flow ($C_{jm} = 0.0424$)	61
32	Flow visualization results for the tangential jet No. 2 blade with 0.030-in. jet slot and 2.01% secondary flow ($C_{jm} = 0.0177$)	62
33	Flow visualization results for the tangential jet No. 2 blade with 0.030-in. jet slot and 2.99% secondary flow ($C_{jm} = 0.0344$)	63
34	Flow visualization results for the tangential jet No. 2 blade with 0.030-in. jet slot and 4.02% secondary flow ($C_{jm} = 0.0487$)	64
35	Flow visualization results for the tangential jet No. 2 blade with 0.040-in. jet slot and 2.00% secondary flow ($C_{jm} = 0.0161$)	65

<u>Figure</u>	<u>Title</u>	<u>Page</u>
36	Flow visualization results for the tangential jet No. 2 blade with 0.040-in. jet slot and 3.00% secondary flow ($C_{j_m} = 0.0315$)	66
37	Flow visualization results for the tangential jet No. 2 blade with 0.040-in. jet slot and 4.00% secondary flow ($C_{j_m} = 0.0483$)	67
38	Plain blade flow visualization results for inlet hub static-to-total pressure ratio of 0.74 (design value) .	68
39	Tangential jet flow as a function of cavity-to-inlet total pressure ratio	69
40	Tangential jet flow requirements to prevent flow separation	70
41	Circumferential variation of tangential jet No. 1 downstream gas angle with secondary flow rate at 13.04-in. radial position and 0.040-in. slot size	71
42	Comparison of measured and predicted radial distribution of downstream gas with secondary flow rate for all tangential jet configurations.	72
43	Measured and predicted radial variation of the plain blade average downstream gas angle	73
44	Variation of mean section average gas angle at Station 4 with secondary flow for each blade configuration.	74
45	Effect of blade configuration and secondary flow rate or blade row mean section reaction.	75
46	Variation of position and shape of tangential jet No. 1 trailing edge wake with increase in the amount of secondary flow.	76
47	Plain blade exit wake survey total pressure distribution for radial position $R = 12.97$ in.	77
48	Contours of kinetic energy loss coefficient across one tangential jet No. 1 blade passage at Station 3 (0.020-in. slot, $\dot{m}_j/\dot{m}_p = 1.00\%$)	78
49	Contours of kinetic energy loss coefficient across one tangential jet No. 1 blade passage at Station 3 (0.020-in. slot, $\dot{m}_j/\dot{m}_p = 2.60\%$)	79
50	Contours of kinetic energy loss coefficient across one tangential jet No. 1 blade passage at Station 3 (0.02-in. slot, $\dot{m}_j/\dot{m}_p = 4.00\%$).	80
51	Contours of kinetic energy loss coefficient across one tangential jet No. 1 blade passage at Station 3 (0.030-in. slot, $\dot{m}_j/\dot{m}_p = 2.50\%$)	81

<u>Figure</u>	<u>Title</u>	<u>Page</u>
52	Contours of kinetic energy loss coefficient across one tangential jet No. 1 blade passage at Station 3 (0.030-in. slot, $\dot{m}_j/\dot{m}_p = 4.10\%$)	82
53	Contours of kinetic energy loss coefficient across one tangential jet No. 1 blade passage at Station 3 (0.030-in. slot, $\dot{m}_j/\dot{m}_p = 6.30\%$)	83
54	Contours of kinetic energy loss coefficient across one tangential jet No. 1 blade passage at Station 3 (0.040-in. slot, $\dot{m}_j/\dot{m}_p = 3.98\%$)	84
55	Contours of kinetic energy loss coefficient across one tangential jet No. 1 blade passage at Station 3 (0.040-in. slot, $\dot{m}_j/\dot{m}_p = 5.62\%$)	85
56	Contours of kinetic energy loss coefficient across one tangential jet No. 1 blade passage at Station 3 (0.040-in. slot, $\dot{m}_j/\dot{m}_p = 7.44\%$)	86
57	Contours of kinetic energy loss coefficient across one tangential jet No. 2 blade passage at Station 3 (0.020-in. slot and $\dot{m}_j/\dot{m}_p = 1.96\%$)	87
58	Contours of kinetic energy loss coefficient across one tangential jet No. 2 blade passage at Station 3 (0.020-in. slot and $\dot{m}_j/\dot{m}_p = 3.02\%$)	88
59	Contours of kinetic energy loss coefficient across one tangential jet No. 2 blade passage at Station 3 (0.020-in. slot and $\dot{m}_j/\dot{m}_p = 3.54\%$)	89
60	Contours of kinetic energy loss coefficient across one tangential jet No. 2 blade passage at Station 3 (0.030-in. slot and $\dot{m}_j/\dot{m}_p = 2.0\%$)	90
61	Contours of kinetic energy loss coefficient across one tangential jet No. 2 blade passage at Station 3 (0.030-in. slot and $\dot{m}_j/\dot{m}_p = 2.99\%$)	91
62	Contours of kinetic energy loss coefficient across one tangential jet No. 2 blade passage at Station 3 (0.030-in. slot and $\dot{m}_j/\dot{m}_p = 4.02\%$)	92
63	Contours of kinetic energy loss coefficient across one tangential jet No. 2 blade passage at Station 3 (0.040-in. slot and $\dot{m}_j/\dot{m}_p = 2.0\%$)	93
64	Contours of kinetic energy loss coefficient across one tangential jet No. 2 blade passage at Station 3 (0.040-in. slot and $\dot{m}_j/\dot{m}_p = 3.00\%$)	94
65	Contours of kinetic energy loss coefficient across one tangential jet No. 2 blade passage at Station 3 (0.040-in. slot and $\dot{m}_j/\dot{m}_p = 4.00\%$)	95
66	Contours of kinetic energy loss coefficient across one blade passage—plain blade exit wake survey.	96

<u>Figure</u>	<u>Title</u>	<u>Page</u>
67	Circumferential variation of trailing edge midspan region wake \bar{e} distributions for the 0.040-in. slot No. 1 and No. 2 jet blades	97
68	Contours of kinetic energy loss coefficient at Station 4 for tangential jet blade No. 1 (0.020-in. slot, $\dot{m}_j/\dot{m}_p = 1.0\%$).	98
69	Contours of kinetic energy loss coefficient at Station 4 for tangential jet blade No. 1 (0.020-in. slot, $\dot{m}_j/\dot{m}_p = 2.6\%$).	99
70	Contours of kinetic energy loss coefficient at Station 4 tangential jet blade No. 1 (0.020-in. slot, $\dot{m}_j/\dot{m}_p = 4\%$).	100
71	Contours of kinetic energy loss coefficient at Station 4 for tangential jet blade No. 1 (0.030-in. slot, $\dot{m}_j/\dot{m}_p = 2.5\%$).	101
72	Contours of kinetic energy loss coefficient at Station 4 for tangential jet blade No. 1 (0.030-in. slot, $\dot{m}_j/\dot{m}_p = 4.2\%$).	102
73	Contours of kinetic energy loss coefficient at Station 4 for tangential jet blade No. 1 (0.030-in. slot, $\dot{m}_j/\dot{m}_p = 6.4\%$).	103
74	Contours of kinetic energy loss coefficient at Station 4 for tangential jet blade No. 1 (0.040-in. slot, $\dot{m}_j/\dot{m}_p = 3.94\%$)	104
75	Contours of kinetic energy loss coefficient at Station 4 for tangential jet blade No. 1 (0.040-in. slot, $\dot{m}_j/\dot{m}_p = 5.64\%$)	105
76	Contours of kinetic energy loss coefficient at Station 4 for tangential jet blade No. 1 (0.040-in. slot, $\dot{m}_j/\dot{m}_p = 7.48\%$)	106
77	Contours of kinetic energy loss coefficient at Station 4 for tangential jet blade No. 2 (0.020-in. slot, $\dot{m}_j/\dot{m}_p = 1.97\%$)	107
78	Contours of kinetic energy loss coefficient at Station 4 for tangential jet blade No. 2 (0.020-in. slot, $\dot{m}_j/\dot{m}_p = 3.00\%$)	108
79	Contours of kinetic energy loss coefficient at Station 4 for tangential jet blade No. 2 (0.020-in. slot, $\dot{m}_j/\dot{m}_p = 3.50\%$)	109
80	Contours of kinetic energy loss coefficients at Station 4 for tangential jet blade No. 2 (0.030-in. slot, $\dot{m}_j/\dot{m}_p = 2.01\%$)	110
81	Contours of kinetic energy loss coefficient at Station 4 for tangential jet blade No. 2 (0.030-in. slot, $\dot{m}_j/\dot{m}_p = 3.08\%$)	111

<u>Figure</u>	<u>Title</u>	<u>Page</u>
82	Contours of kinetic energy loss coefficient at Station 4 for tangential jet blade No. 2 (0.030-in. slot, $\dot{m}_j/\dot{m}_p = 4.04\%$)	112
83	Contours of kinetic energy loss coefficient at Station 4 for tangential jet blade No. 2 (0.040-in. slot, $\dot{m}_j/\dot{m}_p = 2.03\%$)	113
84	Contours of kinetic energy loss coefficient at Station 4 for tangential jet blade No. 2 (0.040-in. slot, $\dot{m}_j/\dot{m}_p = 3.00\%$)	114
85	Contours of kinetic energy loss coefficient at Station 4 for tangential jet blade No. 2 (0.040-in. slot, $\dot{m}_j/\dot{m}_p = 3.85\%$)	115
86	Contours of kinetic energy loss coefficient—plain blade downstream wake survey	116
87	Contours of downstream gas angle measured from axial for the tangential jet blade No. 1 (0.020-in. slot, $\dot{m}_j/\dot{m}_p = 1.0\%$)	117
88	Contours of downstream gas angle measured from axial for the tangential jet blade No. 1 (0.020-in. slot, $\dot{m}_j/\dot{m}_p = 2.67\%$)	118
89	Contours of downstream gas angle measured from axial for the tangential jet blade No. 1 (0.020-in. slot, $\dot{m}_j/\dot{m}_p = 4.0\%$)	119
90	Contours of downstream gas angle measured from axial for the tangential jet blade No. 1 (0.030-in. slot, $\dot{m}_j/\dot{m}_p = 2.5\%$)	120
91	Contours of downstream gas angle measured from axial for the tangential jet blade No. 1 (0.030-in. slot, $\dot{m}_j/\dot{m}_p = 4.2\%$)	121
92	Contours of downstream gas angle measured from axial for the tangential jet blade No. 1 (0.030-in. slot, $\dot{m}_j/\dot{m}_p = 6.4\%$)	122
93	Contours of downstream gas angle measured from axial for the tangential jet blade No. 1 (0.040-in. slot, $\dot{m}_j/\dot{m}_p = 3.94\%$)	123
94	Contours of downstream gas angle measured from axial for the tangential jet blade No. 1 (0.040-in. slot, $\dot{m}_j/\dot{m}_p = 5.64\%$)	124
95	Contours of downstream gas angle measured from axial for the tangential jet blade No. 1 (0.040-in. slot, $\dot{m}_j/\dot{m}_p = 7.48\%$)	125
96	Contours of downstream gas angle measured from axial for the tangential jet blade No. 2 (0.020-in. slot, $\dot{m}_j/\dot{m}_p = 1.97\%$)	126

<u>Figure</u>	<u>Title</u>	<u>Page</u>
97	Contours of downstream gas angle measured from axial for the tangential jet blade No. 2 (0.020-in. slot, $\dot{m}_j/\dot{m}_p = 3.00\%$)	127
98	Contours of downstream gas angle measured from axial for the tangential jet blade No. 2 (0.020-in. slot, $\dot{m}_j/\dot{m}_p = 3.50\%$)	128
99	Contours of downstream gas angle measured from axial for the tangential jet blade No. 2 (0.030-in. slot, $\dot{m}_j/\dot{m}_p = 2.0\%$)	129
100	Contours of downstream gas angle measured from axial for the tangential jet blade No. 2 (0.030-in. slot, $\dot{m}_j/\dot{m}_p = 3.08\%$)	130
101	Contours of downstream gas angle measured from axial for the tangential jet blade No. 2 (0.030-in. slot, $\dot{m}_j/\dot{m}_p = 4.04\%$)	131
102	Contours of downstream gas angle measured from axial for the tangential jet blade No. 2 (0.040-in. slot, $\dot{m}_j/\dot{m}_p = 2.03\%$)	132
103	Contours of downstream gas angle measured from axial for the tangential jet blade No. 2 (0.040-in. slot, $\dot{m}_j/\dot{m}_p = 3.00\%$)	133
104	Contours of downstream gas angle measured from axial for the tangential jet blade No. 2 (0.040-in. slot, $\dot{m}_j/\dot{m}_p = 3.85\%$)	134
105	Contours of downstream gas angle—measured from axial—plain blade downstream wake survey	135
106	Radial variation of circumferentially mass-averaged kinetic energy loss coefficient at trailing edge (Station 3) for all tangential jet configurations	136
107	Plain blade exit wake survey—kinetic energy loss coefficient at Station 3.	137
108	Circumferential variation of mass flow rate per unit depth near the cascade center passage mean section for two tangential jet blade configurations	138
109	Variation of overall mass-averaged kinetic energy loss coefficient with percent of secondary flow at tangential jet blade No. 1 trailing edge	139
110	Variation of overall mass-averaged kinetic energy loss coefficient with percent secondary flow at tangential jet blade No. 2 trailing edge	140
111	Radial variation of boundary layer displacement thickness at trailing edge (Station 3) for all tangential jet configurations.	141
112	Plain blade exit wake survey—displacement thickness distribution at Station 3	142

<u>Figure</u>	<u>Title</u>	<u>Page</u>
113	Radial variation of boundary layer shape factor of trailing edge (Station 3) for tangential jet configurations	143
114	Plain blade exit wake survey—shape factor distribution at Station 3.	144
115	Effect of secondary flow on trailing edge mean section δ^* and H for tangential blades 1 and 2	145
116	Radial variation of circumferentially mass-averaged kinetic energy loss coefficient at Station 4 for all tangential jet configurations.	146
117	Plain blade downstream wake survey—kinetic energy loss coefficient distribution at Station 4	147
118	Variation of overall mass-averaged kinetic energy loss coefficient with percent secondary flow at tangential jet blade No. 1, Station 4	148
119	Variation of overall mass-averaged kinetic energy loss coefficient with percent secondary flow at tangential jet blade No. 2, Station 4	149
120	Radial variation of boundary layer displacement thickness at Station 4 for all tangential jet configurations	150
121	Radial variation of boundary layer shape factor at Station 4 for tangential jet configurations.	151
122	Plain blade downstream wake survey-shape factor distribution at Station 4	152

EXPERIMENTAL INVESTIGATION IN AN ANNULAR CASCADE SECTOR OF HIGHLY LOADED TURBINE STATOR BLADING

BY J. L. Bettner
Allison Division of General Motors

SUMMARY AND CONCLUSIONS

Two tangential jet blade configurations have been tested in a six-blade annular cascade. A plain blade, designed to the same aerodynamic requirements, was tested for comparison. The two tangential jet configurations differed by and were identified by the axial position of the jet slot. The slot was located at approximately 38% of the axial chord for the No. 1 blade and at about 57% for the No. 2 blade. The tangential jet blade surface contours were identical to the plain blade, except in the aft suction surface region which was modified to accommodate the jet slots. Three jet slot sizes of 0.020, 0.030, and 0.040 in. with three secondary flow rates for each slot were investigated for both No. 1 and 2 blades. All configurations were tested at the design values of inlet gas angle and Mach number. The combinations of jet slot height and secondary flow rates produced a range of mean section jet momentum coefficient, C_{jm} , values of up to 0.085. The momentum coefficient is the ratio of jet-to-total-stream momentum that exists at the blade trailing edge and is defined as

$$C_{jm} = \frac{\dot{m}_j U_j}{(\dot{m}_p + \dot{m}_j) W_{m_3}}$$

Neither of the two tangential jet blades achieved all of design point aerodynamic conditions, although the effectiveness in increasing suction surface diffusion and preventing flow separation was demonstrated. That the design conditions were not satisfied points out that (1) the incorporation of tangential jets in turbomachine blade rows is a difficult and subtle design problem and (2) insufficient design information currently exists. The contribution of the present investigation lies in the fact that it provides:

- Some insight as to where to locate tangential jet slots for maximum effectiveness
- Information as to how much secondary flow momentum must be supplied for the mainstream flow to be able to negotiate a given adverse pressure gradient

The tangential jet blades were designed such that the No. 1 and No. 2 slots would be located upstream and downstream, respectively, of the plain

blade separation point. However, the experimental location of the plain blade suction surface flow separation point occurred downstream of its predicted location. Because of this, both No. 1 and 2 tangential jet slots were actually positioned upstream of the plain blade flow separation point.

The No. 1 blade required from 4 to 5% secondary flow to prevent suction surface flow separation while the No. 2 blade needed only about 3%. This was a result of the more severe adverse pressure gradient which existed downstream of the No. 1 slot. However, the blade cavity pressure ratio required to supply the necessary secondary flow was less for the No. 1 blade than for the No. 2 blade. This was primarily caused by the differences in static pressure that existed at the slot exit for the two jet configurations.

The aerodynamic performance of the No. 1 blade was superior to that of the No. 2 blade in that it more closely approached the coincident satisfaction of gas angle, lift, lift coefficient, and loss levels. The trailing edge loss levels were over 50% greater for the No. 2 blade than they were for the No. 1 blade.

Even though the capability in preventing flow separation was demonstrated, incorporation of the tangential jet on the suction surface did not produce a blade which had improved performance over the plain blade. Secondary flows of 4% and greater were required to produce tangential lift coefficient values, gas turning, and suction surface diffusion value levels that were equivalent to the plain blade. The tangential jet blades, as designed herein, have the inherent deficiency of promoting flow separation at the slot lip. The losses associated with this separation must first be overcome with substantial amounts of secondary flow before the prime function of reenergizing the conventional boundary layer can be accomplished.

INTRODUCTION

Increasing interest in developing lightweight, highly loaded gas turbine engines confronts the designer with the problem of maintaining a high level of engine performance. One cause of performance loss in present engines is the condition of the gas flow separating from the blading surfaces. When flow separation is experienced in a blade passage, there is a loss in available kinetic energy, mixing losses are increased, and the desired change in tangential momentum of the gas is not attained. The use of boundary layer control devices offers a possible means of preventing flow separation in maintaining performance in turbomachinery. The NASA-Lewis Research Laboratory contracted Allison Division of General Motors to conduct an experimental research program to evaluate the aerodynamic performance of highly loaded turbine stator blades incorporating several kinds of boundary layer control devices. The following four concepts are being investigated:

- Vortex generators
- Tandem airfoils
- Jet-flapped blowing
- Tangential jet blowing

This report covers the performance evaluation of the tangential jet concept of boundary layer control. Two axial locations of the jet slot—approximately at 38 and 57% of the axial chord—were investigated. For each slot axial location three jet heights, with three secondary flow rates for each jet height, were investigated. All configurations were tested at the design values of inlet gas angle and Mach number. Blade surface static pressure and velocity distributions along with flow visualization results, aerodynamic loss, and boundary layer data are presented.

The analysis and design of all the blade configurations are presented in Volume I. The program base-line level of aerodynamic performance generated by a plain blade and the subsequent evaluation of a corotating vane and a triangular plow-type vortex generator with respect to plain blade performance are established in Volume II. Volume III presents the aerodynamic evaluation of the tandem blade. The aerodynamic performance of the jet flap configuration is presented in Volume IV.

SYMBOLS

A	area, in. ²
C _j	jet momentum coefficient
C _x	blade axial chord, in.
D _s	suction surface diffusion factor, $1 - \frac{(W/W_{cr})_2}{(W/W_{cr})_{max}}$
\bar{e}	kinetic energy loss coefficient
F	force, lb _f
g	acceleration of gravity, $\frac{lb_m}{lb_f} \frac{ft}{sec^2}$
H	boundary layer shape factor
\bar{hb}	jet-flap slot size, in.
ℓ	blade length, in.
M	Mach number
\dot{m}	mass flow rate, lb _m /sec
O	throat dimension, in.
P	pressure, psia
R	radial position, in.; Reaction, $R_m = 1 - \frac{(W/W_{cr})_o^2}{(W/W_{cr})_4^2} \Big]_m$
s	blade spacing, in.
T	temperature, °R
te	blade trailing edge radius, in.
tl	blade leading edge radius, in.
U _j	jet velocity, ft/sec

W	mainstream flow velocity, ft/sec
X	axial coordinate
α	tangential jet slot angle measured from axial, degrees
β	gas angle measured from tangential, degrees
Δ	change in variable
δ_i	ratio of blade cavity air total pressure to standard sea level conditions
δ_o	ratio of inlet air total pressure to standard sea level conditions
δ^*	dimensionless boundary layer displacement thickness
θ_{cr}	squared ratio of critical velocity at blade row inlet to critical velocity at standard sea level temperature
θ^*	dimensionless boundary layer momentum thickness
θ	circumferential position, degrees
ρ	density, lb _m /ft ³
σ_x	axial chord solidity, C_x/s
ψ	gas angle measured from axial, degrees
ψ_t	tangential lift coefficient
$\bar{\omega}$	total pressure loss coefficient

Subscripts

0	station at stator inlet
1	station at blade throat
2	station immediately upstream of trailing edge inside blade passage
3	station immediately downstream of blade trailing edge
4	station two inches (measured from the axial direction) downstream of the blade trailing edge

Baro barometric conditions

cr conditions at Mach number of unity

h hub

i blade interior

j jet

ℓ local, lower limit of integration

m mean

ma mass averaged

oa overall

p primary

ps pressure surface

ss suction surface

st static

T total

TJ1 tangential jet No. 1

TJ2 tangential jet No. 2

t tip

u tangential velocity, upper limit of integration

x axial component

y tangential direction

TANGENTIAL JET BLADE PERFORMANCE

The concept of boundary layer control with a tangential jet is to energize the boundary layer region with a high energy tangentially blown jet. Energy addition into this region should allow the boundary layer fluid to proceed further into an adverse pressure gradient before experiencing flow separation than an unblown or conventional boundary layer flow.

The six-blade annular cascade assemblies of tangential jet No. 1 and 2 configurations are shown in Figures 1 and 2, respectively. Design and performance results of the program base-line plain blade are presented in References 1 and 2. The tangential jet blades were designed to have surface contours identical to the plain blade except in the aft suction surface region which was modified to accommodate the tangential jet slot step. The only difference between the two jet configurations was the axial location of the jet slot. The location of the jet slots, as the function of percent axial chord, is as follows:

	<u>Tangential jet slot position (% C_x)</u>		
	<u>Hub</u>	<u>Mean</u>	<u>Tip</u>
Tangential jet No. 1	39.56	38.30	37.91
Tangential jet No. 2	58.24	56.51	55.49

These blades were designed so that the No. 1 jet configuration was located slightly upstream of the predicted plain blade point of flow separation. The No. 2 jet configuration was designed to be blowing into a separated flow region. Blade section profiles and relative position with adjacent airfoils for both jet configurations are shown in Figure 3.

The cavity inside the blades was fed through the hub section from a plenum chamber located below the blade base. Bench tests on individual tangential jet blades demonstrated that the secondary jet flow had a large positive radial component. The blades were designed on the premise that when a particle of jet fluid left the jet slot at a particular radial location, it remained at the radial location and moved only in the axial-tangential plane. The internal geometry of the airfoils had to be modified to minimize this radial component to produce a more satisfactory distribution of jet velocity. This change was accomplished by blanking off the portion of the available flow area in the region of the jet slot at the hub section which forced the flow to "bleed" through a porous metal baffle that was positioned along the blade length. The baffle is shown installed in the blade in Figure 4. Because the blade was capped at the tip section, the secondary flow tended to stagnate on the upstream side of the baffle, pass through the holes in the

baffle in a nearly circumferential direction, and then flow out through the jet slot. A 0.030-in. dia hole was drilled in the hub section blank material to keep from starving the hub cavity region of secondary flow. A line of lampblack-mineral oil fluid was placed immediately downstream of the slot on a jet No. 1 configuration which was bench tested in still air surroundings. The resulting suction surface flow pattern (Figure 5) indicated that a satisfactory radial distribution of jet velocity existed at the jet slot.

Blade No. 3 was instrumented with static pressure taps primarily on the hub, mean, and tip sections of its suction surface, while blade No. 4 was similarly instrumented on its pressure surface. This arrangement of static pressure taps permitted definition of the blade surface static pressure distribution through the center passage of the cascade. Design data for the tangential jet blades and the plain blade are given in Table I. Experimental data for all of the tangential jet configurations and the plain blade are presented in Tables II and III. The leading edges of blades No. 1 and 6 were matched to a set of inlet guide walls, contoured to generate a free vortex flow immediately upstream of the blade row. The plain blade was tested both with and without contoured exit guide walls. No exit guide walls were used on the tangential jet blade tests. Details of the guide walls and the test rig are given in Reference 1. The aft end of the test rig with a plain blade mounted in position is shown in Figure 6.

As listed in Tables VII and IX of Reference 1, the design values of secondary flow for each jet slot were to be:

Jet slot size (in.)	Design jet flow \dot{m}_j/\dot{m}_p (%)	
	Tangential jet No. 1	Tangential jet No. 2
0.020	2.59	3.05
0.030	4.17	4.62
0.040	5.72	6.20

Experimental results for three secondary flow rates for each slot size were obtained. The design values of the secondary flow were achieved for the No. 1 configuration. However, attainment of the limiting cavity total pressure at relatively small values of secondary flow restricted the secondary flow rates to only about 4% of the primary flow for the tangential jet No. 2 blade. The values of secondary flow obtained experimentally were:

Experimental jet flow \dot{m}_j/\dot{m}_p (%)

<u>Jet slot size (in.)</u>	<u>Tangential jet No. 1</u>	<u>Tangential jet No. 2</u>
0.020	1.00	1.96
	2.60	3.02
	4.00	3.54
0.030	2.50	2.00
	4.10	2.99
	6.30	4.02
0.040	3.98	2.00
	5.62	3.00
	7.44	4.00

Information concerning the kind of instrumentation and associated accuracy is presented in Reference 1. Actual conduct of the test and data reduction procedure is delineated in Reference 2.

VELOCITY AND PRESSURE DISTRIBUTIONS

Surface Velocity Distribution

The hub, mean, and tip section surface velocity distributions for the tangential jet No. 1 configurations are shown in Figure 7. Similarly, Figure 8 shows the surface velocity results for the No. 2 configuration. The plain blade velocity distributions are shown on Figures 9, 10, and 11.

As shown in Figure 12 for the mean section, the diffusion capability increased with secondary flow rate. Approximately 7% secondary flow was required to develop the same diffusion as did the plain blade. However, the design mean section value of 0.4 was not attained. The details as to how the diffusion was increased are examined by considering, for example, the velocity distributions for the 0.020-in. slot configuration of Figure 7. As the secondary flow was increased, an increase in suction surface velocity immediately upstream of the slot was observed while the flow decelerated in the trailing edge region. With only 1% secondary flow, the mainstream flow separated from the step on the surface at the slot lip, diffused slightly into the increased flow area downstream of the slot, and remained in a strongly separated state to the blade trailing edge. This condition is characterized by the constant value of 0.90 for the velocity ratio downstream of the slot to the trailing edge. Separation of the flow from the suction surface resulted in a reduction of effective flow area which produced the

larger-than-design velocity ratios at the blade trailing edge. As the secondary flow was increased, the boundary layer was progressively energized to the point where the flow reattached itself to the suction surface immediately downstream of the slot and remained attached to the trailing edge region. The resulting velocity distributions can be seen in Figure 7 to be approaching the theoretical (unseparated flow) velocity distribution as the secondary flow is increased from 1 to 2.6% and, finally, to 4% of the primary flow rate.

Because all blade configurations were tested at the same inlet Mach number, the reattaching of the flow to the suction surface resulted in an increase in flow area with subsequent decrease in free stream velocity, blade row reaction, and expansion ratio.

The No. 1 blade mean section velocity distributions of Figure 7 show that between 4 and 5% secondary flow was required to attain (at least on the aft 50% of the blade chord) the theoretical surface velocity distribution. The No. 2 blade mean section results of Figure 8 show that only about 3 to 4% secondary flow was required to produce the design suction surface velocity distribution in the aft region of the blade. However, the No. 2 blade pressure surface results have larger values and do not agree as well with the theoretical predictions as those for the No. 1 blade. As will be demonstrated in the following discussion, less lift was, therefore, generated by the No. 2 blade.

Surface Pressure Distribution

The surface static pressure distributions that correspond to the mean section velocity distributions are shown in Figure 13. The tangential force resulting from the static pressure differential per unit blade length was computed by passing a smooth curve through the static pressure data points and by graphically determining the area between the P_{st} versus C_x curves. The total lift on the airfoil mean sections was considered to be the sum of the lift as a result of the static pressure differential and the change in tangential component of jet momentum. These blade forces are tabulated in Table IV.

Mean section unit corrected force per pound of corrected primary flow results are presented as a function of secondary flow rate in Figure 14. Also, a jet momentum coefficient was defined as

$$C_{jm} = \frac{\dot{m}_j U_j}{(\dot{m}_p + \dot{m}_j) W_{m_3}}$$

where W_{m_3} refers to the mainstream velocity that existed at the trailing edge location; the subscript m denotes that calculations were performed only at the mean section. Bench tests showed that a 17.5 in. Hg pressure drop existed across the internal baffle when the blade cavity pressure was maximum at 60 in. Hg abs. The jet velocity was computed by assuming that the jet expanded from the total pressure just upstream of the slot (but downstream of the internal baffle) to the static pressure at the slot exit (shown in Figure 13 for each configuration). These jet momentum coefficient data are also shown in Table V. The mean section corrected force data are plotted against jet momentum coefficient in Figure 15. These results show that with increasing secondary flow the lift generated on the airfoil per pound of primary flow progressively decreases with the No. 1 configuration. They also show that for the No. 2 jet configuration the corrected lift was at least constant and perhaps even increased slightly with secondary flow. This was primarily a result of the orientation of the No. 2 jet on the suction surface (Figure 3). The No. 2 jet was able to efflux jet flow more in the tangential direction and thus, for the same secondary flow rate, contribute more to the total lift on the airfoil than was the No. 1 jet configuration. This observation is confirmed by Figure 16. Over the range of secondary flows investigated, the No. 2 jet contributed to the total lift on the airfoil at a rate of approximately three times that of the No. 1 configuration. This resulted in the slope of the corrected total force-secondary flow curves being less negative for the No. 2 blade.

The results of Figures 14 and 15 show that the No. 2 jet configuration was less effective in achieving the design lift than was the No. 1 jet blade. The loading was less on the No. 2 blade because, as is shown in Figure 45, the No. 2 blade reaction was less. The reduced reaction may have been caused by the throat areas which were larger than required.

Tangential Lift Coefficient

The expansion ratio across the cascade had to be varied to maintain the correct inlet Mach number for each tangential jet blade test; it was desirable, therefore, to present the performance results in terms of a parameter that would reflect the effects of a variable expansion ratio. Such a parameter is the mean section tangential lift coefficient, ψ_{t_m} , presented in Figure 17 and listed in Table V.

ψ_{tm} is essentially the ratio of the lift generated by an airfoil to the total-to-static pressure drop across the airfoil and is defined as

$$\psi_{tm} = \frac{s}{C_x} \left[\frac{\rho_{st4} W_{x4} \Delta W_{u_{O-4}}}{(P_{T_O} - P_{st4}) g} \right]_m = \left[\frac{F_{yT}/\ell}{C_x(P_{T_O} - P_{st4})} \right]_m$$

The design value of ψ_{tm} was 1.09 for the plain blade. The effect of increasing secondary flow was to cause a very slightly increasing design value of ψ_{tm} for the tangential jet blades.

The results of Figure 17 were obtained by dividing the corrected tangential force on the airfoil by essentially the required corrected expansion ratio across the cascade. Both the lift and expansion ratio decreased with increased secondary flow but the expansion ratio fell at a faster rate, the net result being an increase in ψ_{tm} with increasing secondary flow. The

design value was satisfied by the No. 1 blade with approximately 6% secondary flow ($C_{jm} \approx 0.07$). Again, it can be seen in Figure 17 that the tan-

gential jet No. 2 configuration was considerably less effective in achieving the design value than was the tangential jet No. 1 blade.

The plain blade passed slightly less than design flow at less than design expansion ratio. It also generated less than design lift as shown by Figures 14 and 15. As far as the lift coefficient is concerned, however, the design value was satisfied. ψ_{tm} is also presented as a function of jet

momentum coefficient in Figure 18.

FLOW VISUALIZATION RESULTS

Suction Surface Separated Flow Patterns

Application of the lampblack-mineral oil flow visualization technique demonstrated that the tangential jet concept can prevent flow separation from occurring on blading suction surfaces. Results for each of the No. 1 jet blade configurations tested are presented in Figures 19 through 28 and results for the No. 2 blade are shown in Figures 29 through 37. Flow visualization results for the plain blade are shown in Figure 38. It can be seen from Figure 38 that flow separation occurred on the plain blade suction surface. However, the actual location of the separated region was far enough downstream of the predicted location that both tangential jet slots were upstream of the separation point. The separated flow regions that

were eliminated by the tangential jets were those created by the jet slot step. These results show that between 4 and 5% secondary flow ($C_{j_m} \approx 0.04$

to 0.05) was required for the No. 1 jet blade to prevent flow separation, while only about 3% secondary flow ($C_{j_m} \approx 0.035$) was required for the No.

2 blade. This is the direct result of having a less severe adverse pressure gradient on the suction surface from the slot to the trailing edge on the No. 2 jet blade than the No. 1 jet blade. Since blade No. 2 had the less severe adverse pressure gradient to negotiate, it could prevent flow separation from occurring with a lesser amount of secondary flow than blade No. 1 required.

The cavity total pressures required to produce the secondary flow rates are illustrated in Figure 39. The No. 2 jet configuration cavity pressure ratio-secondary flow rate characteristic was far less sensitive to slot size than was the No. 1 jet configuration. Also, the cavity pressure ratio required to supply the necessary secondary flow was less for the No. 1 blade than for the No. 2 blade. This was primarily caused by the higher static pressure that existed at the No. 2 slot exit.

Pressure Gradient and Secondary Flow Requirements

Figure 40 presents the adverse pressure gradient developed on the suction surface from the jet locations to the trailing edge of the various jet blade configurations. These pressure gradient data were obtained from Figure 13 and are presented as a function of jet momentum coefficient. Based on the surface velocity distribution plots of Figures 7 and 8 and the flow visualization photographs (Figures 19 through 37), regions of C_{j_m} re-

quired to prevent flow separation from the suction surface are noted on Figure 40. For instance, with the No. 1 jet configuration, a corrected adverse pressure gradient of 2.0 was developed on the suction surface and negotiated (no separation with $C_{j_m} \approx 0.042$ ($\dot{m}_j/\dot{m}_p \approx 4\%$). Whereas, on the No. 2 blade a $\Delta P_{stj-3}/\delta_0 \Delta X_{ssj-3}$ of approximately 1.7 was generated between the slot location and the trailing edge and required C_{j_m} of about 0.034 ($\dot{m}_j/\dot{m}_p \approx 3\%$).

These data provide the designer with some insight as to what to expect in secondary flow requirements to negotiate a given adverse pressure gradient when the tangential jet is located upstream of the predicted point of flow separation.

DOWNSTREAM GAS ANGLE AND TANGENTIAL VELOCITY

Average Downstream Gas Angles

A radial-circumferential survey of total temperature, total pressure, and gas angle was performed in a plane located 2 in. downstream of the blade trailing edge. A typical circumferential variation of gas angle with increasing secondary flow rate at a fixed radial position is presented in Figure 41. In general, the gas angle (measured from axial) tends to increase with increasing secondary flow. It may also be observed that when viewed aft-looking-forward the circumferential position of the blade wakes moves slightly in the counterclockwise direction as the secondary flow rate is increased.

Gas angle data such as that shown in Figure 41 were averaged over each circumferential sweep to obtain only the radial variation of gas angle as a function of slot size and secondary flow rate combinations. These data are presented in Figures 42 and 43 for the two tangential jet and the plain blades. Included in these figures is the theoretical distribution of downstream gas angle for the respective secondary flow rates. These data show that, in general, increased gas turning was accomplished by increasing the secondary flow rates. This is further demonstrated in Figure 44 where the angles at the mean section are plotted as a function of secondary flow. These data show that turning is increased with secondary flow and the design value is achieved with between 4 and 5% secondary flow. The reason is not clear why the tangential jet No. 2, 0.020-in. slot angle data does not correlate with secondary flow rate as well as the other jet blade configurations.

Change in Tangential Velocity and Reaction Across Blade Row

The tangential jet and plain blades were designed to accomplish the same change in tangential velocity across the blade row. Based on design inlet gas angles, inlet and exit critical velocity ratios, including loss and downstream gas angle measurements, the experimental change in tangential velocity was computed and is compared with the plain blade and design values in Table VI. Positive and negative deviation in Table VI represent, respectively, greater than and less than design values of ΔW_u across the blade row. Table VI illustrates that, in general:

- No. 1 blade effected a larger change in tangential velocity across the blade row than did the No. 2 blade
- Correlation of ΔW_u was similar to that of the corrected lift (Figure 14) with secondary flow for both the No. 1 and 2 jet configurations (That is, the change in tangential velocity across the blade row decreased for the No. 1 blade, but was nearly constant for the No. 2 blade as the secondary flow was increased.)

Nearly all of the tangential jet configurations were deficient in satisfying the design, ΔW_u . The configurations that most nearly satisfied the design values were the small, secondary flows through the No. 1 blade 0.020-in. slot. Figure 14 shows that these configurations also most nearly satisfied the design corrected force values. However, Figure 44 showed that, in general, the greatest discrepancy between measured and design gas angle occurred at the low values of secondary flow. Thus, it may be concluded from the blade lift and ΔW_u calculations and the gas angle measurements that neither the tangential jet No. 1 or No. 2 blades satisfied all of the design point conditions.

The design values of secondary flow for the No. 1 jet blade were:

\overline{hb} (in.)	\dot{m}_j / \dot{m}_p (%)
0.020	2.59
0.030	4.17
0.040	5.72

Further, the design value of reaction across the blade row was 22.35% at the mean section. Figure 45 presents the experimental values of blade row reaction as a function of percent secondary flow and shows that, in general, less than design values were obtained. It can be observed, however, that the design value was obtained with the 0.020-in. slot TJ1 configuration with its design secondary flow of 2.6%. However, it has been previously noted that flow separation at the slot lip with the resulting large blockage occurred in the mainstream passage for this configuration slot size-secondary flow rate combination. Therefore, it may be concluded that since less than design reaction was obtained, once flow separation was prevented by the addition of secondary flow, the resulting throat passage areas were larger than required to achieve the design velocity diagrams. The throat area for the No. 2 jet configuration also appears to have been too large as its blade row reaction was even less than the No. 1 blade.

CONTOUR PLOTS

Results at the Blade Trailing Edge (Station 3)

Total pressure radial-circumferential surveys were performed immediately behind the blade trailing edge for the purpose of determining the Station 3 loss and boundary layer characteristics for each blade configuration.

A typical total pressure trace result for the No. 1 tangential jet 0.040-in. slot blade with four values of secondary flow at a radial location of 12.97 in. is shown in Figure 46. Similar data for the plain blade are shown in Figure 47.

Progressive increase in the amount of secondary flow appeared to shrink the wake in both the circumferential and axial directions. When viewed aft-looking-forward, the circumferential movement of the wake was in the counterclockwise direction. There was no evidence of total pressure excess in wakes of any of the tangential jet blade configurations. Apparently, sufficient mixing of the jet and freestream had taken place by the time the flow reached the trailing edge that only conventional type wakes of Figure 46 were measurable.

Data of the type shown in Figure 46 were assembled in the form of contour plots of kinetic energy loss coefficient and are presented in Figures 48 through 56 for the No. 1 blade configuration and Figures 57 through 65 for the No. 2 blade. Similar plain blade \bar{e} data are shown in Figure 66. All of these results show for a given slot size for both the No. 1 and 2 blades that the circumferential extent of the high loss wake region was reduced as the secondary flow was increased. It can be observed that the hub regions for the No. 1 and 2 blades are quite different. A fairly large region of moderately large loss existed in the hub region for the No. 1 blade, whereas this was a very low loss region for the No. 2 blade. It may also be observed from Figures 54 and 65 for similar conditions of secondary flow and jet slot size for the No. 1 and 2 blades that the No. 2 blade appeared to have a slightly lower overall loss level than did the No. 1 blade. This condition is more clearly shown in Figure 67 where the \bar{e} circumferential distributions in the neighborhood of the trailing edge mean section are presented for the 0.040-in. jet slot and approximately 4% secondary flow for the No. 1 and 2 blades. The peak loss level for the No. 1 blade was more than 0.95 but only about 0.80 for the No. 2 blade.

Results Downstream of the Blade Trailing Edge (Station 4)

Kinetic Energy Loss Coefficient

Contour plots of kinetic energy loss coefficient were also assembled from the total pressure surveys performed in a plane 2 in. (measured axially) downstream of the blade trailing edges. These results are shown in Figures 68 through 76 for the No. 1 blade and Figures 77 through 85 for the No. 2 blade. Plain blade results are included in Figure 86. There is nothing substantially different between these No. 1 and 2 jet blade loss contour plots. Under similar circumstances of secondary flow and slot size the No. 1 and 2 blades exhibited about the same wake shape and loss level. They generally show that for a fixed slot size the regions of larger loss were decreased by increased secondary flow. They also show a larger loss region very near the hub section, but this has been attributed to the flow separating from the rig hub wall casing at Station 4.

Downstream Gas Angle

Contour plots of the gas angle, measured from the axial direction 2 in. downstream of the trailing edge, are shown in Figures 87 through 104 for all of the tangential jet blade configurations. Figure 105 illustrates the plain blade gas angle contour plot. The theoretical radial distribution of the gas angle, based on a 4% loss in total pressure across the cascade and including the effects of mass addition, is shown as the right-hand ordinate of Figures 87 through 104. These plots show how overturning of the gas from the axial direction in the hub region was experienced by all of the tangential jet configurations. They also show that for a fixed slot size, increasing the secondary flow resulted in an increase in turning toward the tangential direction. As has been mentioned earlier, this increase in turning toward the tangential direction with increased secondary flow is the result of the flow reattaching itself to the suction surface downstream of the slot. The only region in which the plain blade experienced design or overdesign turning was near the hub section.

MASS AVERAGED LOSS AND BOUNDARY LAYER PARAMETERS

Results at the Blade Trailing Edge (Station 3)

Aerodynamic Loss Data

Circumferentially mass averaged values of \bar{e} at each radial depth were computed by Equation (6) of Reference 2 and are shown for both tangential jet and plain blades in Figures 106 and 107, respectively. The numerical integrations were performed in the circumferential direction encompassing the points of minimum total pressure in the wakes of blades No. 3 and 4.

For a given slot size, the \bar{e} results show that, in general, for the range of secondary flow rates investigated, increasing the amount of secondary flow decreased the circumferentially mass averaged loss level. These results substantiate the trends shown in the tangential jet loss contour plots because the hub section was a region of high loss for the No. 1 blade but it was a region of very low loss for the No. 2 blade. The reason for this is not clear. The loss data of Figure 107 show that the plain blade had regions of large loss in the midspan and tip regions. The plain blade hub section loss, however, was quite small. These results also agree with the trends described by the plain blade loss contour plot of Figure 66.

There is, however, an apparent contradiction between these mass averaged loss data and local kinetic energy loss distributions presented earlier in Figure 67 for the No. 1 and 2 blades with 0.040-in. jet slots and 4% secondary flow. In Figure 67 it was shown that on an area-averaged

basis the loss for the No. 1 blade was greater than it was for the No. 2 blade. However, if the 0.040-in. slot, 4% secondary flow TJ1 and TJ2 loss levels of Figure 106 are compared, it is seen that on a mass averaged basis the reverse trend is indicated; (i.e., the loss for blade No. 2 is larger than for blade No. 1). This circumstance is primarily attributed to mass averaging of the losses using the distribution of mass in the wakes of these two blade configurations. The distribution of mass flow rate per unit depth in the midspan region for these two configurations is shown in Figure 108. The static pressure at the radial positions in question was assumed constant in the circumferential direction and used with the plenum total temperature and surveyed total pressure to compute the circumferential distribution of mass flow per unit depth shown in Figure 108. The circumferentially mass averaged loss results were computed by an expression of the form

$$\bar{\epsilon} = \frac{\int_{\theta_l}^{\theta_u} \bar{\epsilon}_l \rho_{st} W r d\theta}{\int_{\theta_l}^{\theta_u} \rho_{st} W r d\theta}$$

The numerator represents the summation of the product of the local loss coefficient times the local element of mass flow per unit depth. The denominator represents the mass flow per unit depth. Since the denominator of the expression had nearly the same value for both the tangential jet No. 1 and No. 2 blades, the answer as to why the No. 2 blade had the largest mass averaged loss level must lie in the numerator of the expression. In order for the integral of the local loss times mass flow to be largest for the No. 2 blade, it must have more mass in its wake since the No. 2 local loss was less than for the No. 1 blade. This can be seen to be the case in Figure 108. The freestream level of mass flow per unit depth was less for the No. 2 blade, but in the wake region the No. 2 blade had the larger amount of mass flow.

An overall flow passage mass averaged value of kinetic energy loss coefficient was computed at the trailing edges (Station 3) of the No. 1 and 2 blades and is illustrated as a function of the amount of secondary flow in Figures 109 and 110, respectively. A fair amount of scatter did exist in these computed $\bar{\epsilon}_{Oa_{ma}}$ results and a curve was passed through the points to indicate general trends. Examination of Figures 109 and 110 shows that the loss level for both No. 1 and 2 blades decreased with increasing secondary flow. Over the relatively small range of secondary flows tested with

the No. 2 blade, the loss level was substantially higher than it was for the No. 1 blade. Figure 109 shows from the general trend curve that a No. 1 blade trailing edge loss level equivalent to that of the plain blade was attained with about 4.0% secondary flow. This corresponds to a jet momentum coefficient of about 0.04. A further increase in the amount of secondary flow produced a loss level that was less than that for the plain blade.

Boundary Layer Parameters

Radial variation of the displacement thickness and the boundary layer shape factor are shown in Figure 111 for the various tangential jet blade configurations. Similar plain blade data are shown in Figure 112. In general, the momentum thickness was nearly independent of the effects of varying jet slot size and amount of secondary flow rate. This was not the case for the displacement thickness which was quite sensitive to the variations of jet slot size and amounts of secondary flow. It can be noted that for a given slot size across nearly the entire radial span of the blade that the displacement thickness shrank or thinned out rather markedly as the secondary flow was increased. As the jet progressively prevented flow separation from the suction surface and shrank the size of the blade wake, the size of the displacement thickness (which reflects a blockage of the flow path area) was likewise reduced in size.

The boundary layer shape factor ($H = \delta^* / \theta^*$) results of Figure 113 show the effects of the tangential jet configurations simultaneously on δ^* and θ^* . It can be seen that δ^* has the controlling influence on H since θ^* was nearly unaffected by jet slot size and flow rate combinations. These results clearly show how the shape factor, H , is progressively reduced as flow separation is inhibited by increasing secondary flow. The plain blade H data of Figure 114 show that when gross separation is experienced on the suction surface—as it was on the plain blade—a rather erratic radial variation in H values resulted. This is seen to also be the case particularly with the No. 1 jet blade and was only overcome by relatively large amounts of secondary flow (4.0% for the 0.020-in. slot and over 5% for the larger slot sizes). This was not so much the case for the No. 2 jet blade as its suction surface adverse pressure gradient downstream of the slot was less severe than that for the No. 1 blade. Flow separation was prevented with a resulting reasonably smooth radial variation of H with about 3% secondary flow ($C_{j_m} \approx 0.035$).

The effect of secondary flow on the boundary layer parameters of the No. 1 and 2 jet blades is further demonstrated by presenting only the mean section δ_m^* and H_m as a function of \dot{m}_j / \dot{m}_p in Figure 115. They show that both δ_m^* and H_m are consistently smaller for the No. 2 blade. Further, δ_m^* and H_m decrease in magnitude to their unseparated values at a faster rate with increasing secondary flow than they do for the No. 1 blade.

Results Downstream of the Blade Trailing Edge (Station 4)

Aerodynamic Loss Data

Circumferentially mass averaged kinetic energy loss coefficients were computed at each of the 10 surveyed radial positions for each tangential jet configuration and are shown in Figure 116. Similar plain blade results are included as Figure 117 for comparison purposes. These tangential jet data show that, for a given slot size, the losses decreased slightly with increased secondary flow. Also, the tangential jet No. 2 blade loss appeared, to a small extent, to be larger than the No. 1 blade. The losses both No. 1 and 2 blades were large near the hub section, but this is attributed to the flow separating off the rig hub casing wall at this axial station.

Even though the performance evaluation is somewhat clouded by having the flow separate from the hub casing wall, overall mass averaged kinetic energy loss coefficients were computed for the two tangential jet blades and are illustrated in Figures 118 and 119. The most interesting observation concerning these loss data is that $\bar{e}_{oa_{ma}}$ is a fairly strong function of slot

size for the No. 1 blade but not for the No. 2 blade. This observation holds whether the $\bar{e}_{oa_{ma}}$ is correlated with \dot{m}_j/\dot{m}_p as in Figure 118 or with C_{jm} .

The reason why the loss is a function of the slot size for one configuration but not the other is not clear. The mass averaged loss results of Figure 119 show that at least at small secondary flow rates the loss for the No. 2 blade is larger than that for the No. 1 blade.

Boundary Layer Parameters

Boundary layer displacement thicknesses were computed at Station 4 for the various tangential jet configurations and are presented in Figure 120. At this axial station the effects of slot size and secondary flow combinations are slight on both the displacement and momentum thickness. They are slightly stronger on the displacement thickness.

At this axial location all of the tangential jet configurations have about the same size of displacement thickness which decreases very slightly with increased secondary flow.

The radial variation of boundary layer shape factor, $H = \delta^*/\theta^*$, is shown in Figure 121 for the various tangential jet blade configurations and in Figure 122 for the plain blade. H was reasonably uniform over the entire blade span and decreased from about 1.5 to 1.3 for the No. 1 blade and from 1.3 to 1.1 for the No. 2 blade as the amount of secondary flow was increased.

SUMMARY OF TANGENTIAL JET BLADE PERFORMANCE

Two tangential jet blade configurations have been tested in a six-blade annular cascade. A plain blade, designed to the same aerodynamic requirements, was tested for comparison. The two tangential jet configurations differed by and were identified by the axial position of the jet slot. The slot was located at approximately 38% of the axial chord for the No. 1 blade and at about 57% for the No. 2 blade. The tangential jet blade surface contours were identical to the plain blade, except in the aft suction surface region which was modified to accommodate the jet slots. Three jet slot sizes of 0.020, 0.030, and 0.040 in. with three secondary flow rates for each slot were investigated for both No. 1 and No. 2 blades. The combinations of jet slot height and secondary flow rates produced a range of mean section jet momentum coefficient, C_{jm} , values of up to 0.085. The momentum coefficient is the ratio of jet-to-total stream momentum that exists at the blade trailing edge and is defined as

$$C_{jm} = \frac{\dot{m}_j U_j}{(\dot{m}_p + \dot{m}_j) W_{m_3}}$$

Neither of the two tangential jet blades designed and tested herein achieved all of the design point aerodynamic conditions, although the effectiveness of the tangential jet concept in preventing flow separation was demonstrated. The fact that the design conditions were not satisfied points up the following two problems.

- Incorporation of tangential jets in turbomachine blade rows is a difficult and subtle design problem.
- Insufficient design information currently exists.

The contribution of the present investigation lies in the fact that it provides some insight as to where to locate tangential jet slots for maximum effectiveness and supplies information as to how much secondary flow momentum is required through a given tangential jet slot size for the mainstream flow to be able to negotiate a given adverse pressure gradient.

The following is a list of the outstanding observed design and performance characteristics of the subject tangential jet blades.

1. The tangential jet blades were designed such that the No. 1 and 2 slots would be located upstream and downstream, respectively, of the plain separation point. However, the experimental location of the plain blade suction surface flow separation point occurred downstream of its predicted location. Because of this, both No. 1 and No. 2 tangential jet slots were actually positioned upstream of the plain blade flow separation point.

2. The No. 1 blade required from 4 to 5% secondary flow to prevent suction surface flow separation while the No. 2 blade needed only about 3%. This was caused by the more severe adverse pressure gradient which existed downstream of the No. 1 slot. However, the blade cavity pressure ratio required to supply the necessary secondary flow was less for the No. 1 blade than for the No. 2 blade. This was primarily a result of the differences in static pressure that existed at the slot exit for the two jet configurations.
3. The blade row expansion ratio and reaction decreased with increased secondary flow for both tangential jet configurations. The corrected lift decreased for the No. 1 blade but remained essentially constant with secondary flow for the No. 2 blade. This was attributed to the orientation of the jet on the suction surface which allowed the No. 2 jet thrust to be a larger percentage of the total lift on the airfoil than the No. 1 jet thrust.
4. Neither No. 1 nor 2 tangential jet blade satisfied the design corrected lift although the design tangential lift coefficient was satisfied by the No. 1 blade with about 6% ($C_{jm} \approx 0.07$) secondary flow.
5. For a given tangential jet geometry of slot size and axial location, an increase in secondary flow increased the blade row suction surface diffusion.
6. For both tangential jet configurations, an increase in jet flow generally resulted in an increase in gas turning.
7. Up to nearly 7.5% secondary flow was available to the No. 1 jet blade, whereas because of attainment of the limiting cavity pressure this was restricted to 4.0% for the No. 2 blade.
8. The aerodynamic performance of the No. 1 blade was superior to that of the No. 2 blade in that it more closely approached the coincident satisfaction of gas angle, lift, lift coefficient, and loss levels. The loss at the trailing edge of the No. 1 jet configuration was very near the plain blade loss level. These loss levels were over 50% greater for the No. 2 blade than they were for the No. 1 blade.

In conclusion, even though the capability in preventing flow separation was demonstrated, incorporation of the tangential jet on the suction surface did not produce a blade which had improved performance over the plain blade. Secondary flows of 4% and greater were required to produce tangential lift coefficient values, gas turning, and suction surface diffusion

value levels that were equivalent to the plain blade. The tangential jet blades, as designed herein, have the inherent deficiency of promoting flow separation at the slot lip. The losses associated with this separation must first be overcome with substantial amounts of secondary flow before the prime function of reenergizing the conventional boundary layer can be accomplished.

REFERENCES

1. Bettner, J. L. "Experimental Investigation in an Annular Cascade Sector of Highly Loaded Turbine Stator Blading." NASA CR-1219, Analyses and Design, Vol I. July 1968.
2. Bettner, J. L. "Experimental Investigation in an Annular Cascade Sector of Highly Loaded Turbine Stator Blading." NASA CR-1323, Performance of Plain Blade and Effect of Vortex Generators, Vol II. October 1968.

Table I.

Design data for the plain and tangential jet blades.

	Hub	Mean	Tip
C_x , in.	1.365	1.5925	1.820
s , in.	1.01267	1.22967	1.44678
σ_x	1.348	1.293	1.258
$X_j)_{TJ1}$, in.	0.540	0.610	0.690
$X_j)_{TJ1}$, % C_x	39.56	38.30	37.91
$X_j)_{TJ2}$, in.	0.795	0.900	1.010
$X_j)_{TJ2}$, % C_x	58.24	56.51	55.49
t_l , in.	0.0546	0.0637	0.0728
t_e , in.	0.0175	0.0175	0.0175
β_o , degrees	36.08	41.66	46.37
ψ_1 , degrees	47.85	43.02	38.73
$W/W_{cr})_o$	0.703	0.623	0.572
$W_{ss}/W_{cr})_{max}$	1.350	1.189	1.082
$W/W_{cr})_4$	0.799	0.707	0.647

Table II.

Experimental results for tangential jet No. 1 blade and plain blade.

		Tangential jet No. 1 blade									
Jet slot size, in.		0.020			0.030			0.040			Plain blade
Secondary flow rate, %		1.00	2.60	4.00	2.50	4.10	6.30	3.98	5.62	7.44	
Actual primary flow rate, lb _m /sec		1.480	1.480	1.400	1.350	1.260	1.260	1.380	1.280	1.290	
Equivalent primary flow rate, lb _m /sec		1.054	1.086	1.085	1.045	1.023	1.045	1.059	1.021	1.031	0.996
Plenum total pressure, in. Hg abs		49.400	42.028	39.728	40.168	38.268	37.301	39.937	38.421	38.321	37.481
Barometric pressure, in. Hg abs		29.200	29.288	29.228	29.368	29.368	29.301	29.487	29.421	29.421	29.306
P _{T_O} /P _{st_{4h}}		1.507	1.465	1.400	1.394	1.333	1.313	1.383	1.333	1.330	1.288
P _{T_O} /P _{Baro}		1.486	1.435	1.359	1.368	1.303	1.273	1.354	1.306	1.303	1.279
Plenum total temperature, °R		554	551	550	560	560	555	545	544	544	525
θ _{cr}		1.068	1.062	1.060	1.079	1.079	0.069	1.050	1.048	1.048	1.012
δ _O		1.450	1.405	1.328	1.342	1.279	1.247	1.335	1.284	1.281	1.253
Actual secondary flow rate, lb _m /sec		0.0148	0.0385	0.0560	0.0337	0.0516	0.0794	0.0549	0.0719	0.0959	---
Blade cavity total pressure, in. Hg abs		27.950	44.430	55.930	30.520	35.220	47.600	38.820	37.720	48.620	---
Blade cavity total temperature, °R		554	544	543	560	554	551	535	538	538	---
P _{T_i} /P _{T_O}		0.6440	1.0571	1.4078	0.7598	0.9203	1.2761	0.9720	0.9817	1.2687	---
Inlet critical velocity ratio	Hub	0.695	0.707	0.701	0.707	0.705	0.707	0.695	0.696	0.704	0.703
	Mean	0.650	0.663	0.656	0.641	0.640	0.643	0.645	0.626	0.636	0.633
	Tip	0.602	0.616	0.609	0.569	0.571	0.574	0.558	0.552	0.561	0.559

Table III.

Experimental results for tangential jet No. 2 blade and plain blade.

		Tangential jet No. 2 blade									
Jet slot size, in.		0.020			0.030			0.040			Plain blade
Secondary flow rate, %		1.96	3.02	3.54	2.01	2.99	4.02	2.00	3.00	4.00	
Actual primary flow rate, lb _m /sec		1.430	1.390	1.410	1.370	1.340	1.340	1.400	1.370	1.350	
Equivalent primary flow rate, lb _m /sec		1.081	1.081	1.104	1.029	1.029	1.030	1.059	1.058	1.063	0.996
Plenum total pressure, in. Hg abs		40.150	39.350	39.160	39.943	38.820	38.487	39.660	38.630	37.880	37.481
Barometric pressure, in. Hg abs		29.646	29.646	29.615	29.543	29.320	29.387	29.264	28.933	28.977	29.306
P _{T_O} /P _{st_{4h}}		1.380	1.355	1.354	1.380	1.359	1.351	1.386	1.368	1.341	1.288
P _{T_O} /P _{Baro}		1.354	1.327	1.322	1.352	1.324	1.310	1.355	1.335	1.307	1.279
Plenum total temperature, °R		534	543	545	522	515	507	522	516	516	525
θ _{cr}		1.029	1.046	1.050	1.006	0.992	0.977	1.006	0.994	0.994	1.012
δ _O		1.342	1.315	1.309	1.335	1.297	1.286	1.325	1.291	1.266	1.253
Actual secondary flow rate, lb _m /sec		0.028	0.042	0.050	0.028	0.040	0.054	0.028	0.041	0.054	---
Blade cavity total pressure, in. Hg abs		37.65	50.05	58.82	36.943	47.120	58.537	36.560	45.83	51.080	---
Blade cavity total temperature, °R		530	536	537	514	514	503	524	515	507	---
P _{T_I} /P _{T_O}		0.9377	1.2719	1.5020	0.9248	1.2138	1.5209	0.9218	1.1863	1.5068	---
Inlet critical velocity ratio	Hub	0.707	0.700	0.706	0.700	0.700	0.703	0.703	0.705	0.701	0.703
	Mean	0.639	0.634	0.638	0.640	0.644	0.647	0.633	0.635	0.631	0.633
	Tip	0.566	0.563	0.566	0.575	0.584	0.588	0.558	0.559	0.556	0.559

Table IV.

Tangential jet and plain blade tangential force results.

	Slot size (in.)	% \dot{m}_j / \dot{m}_p	C_{jm_3}	F_{yT_m} / ℓ	$\sqrt{\theta_{cr}}$	\dot{m}_p	$\frac{F_{yT_m} / \ell}{\dot{m}_p \sqrt{\theta_{cr}}}$
Tangential jet No. 1 blade	0.020	1.00	0.0045	9.985	1.033	1.480	6.531
		2.60	0.0244	9.598	1.030	1.480	6.296
		4.00	0.0456	8.586	1.029	1.400	5.960
	0.030	2.50	0.0052	8.154	1.039	1.350	5.813
		4.10	0.0368	7.446	1.039	1.260	5.688
		6.30	0.0752	7.050	1.034	1.260	5.411
	0.040	3.98	0.0407	8.282	1.025	1.380	5.855
		5.62	0.0582	7.812	1.024	1.280	5.960
		7.44	0.0854	7.790	1.024	1.290	5.897
Tangential jet No. 2 blade	0.020	1.96	0.0164	6.893	1.014	1.430	4.754
		3.02	0.0339	6.756	1.023	1.390	4.751
		3.54	0.0424	6.853	1.025	1.410	4.742
	0.030	2.01	0.0177	6.912	1.003	1.370	5.030
		2.99	0.0344	6.759	0.996	1.340	5.064
		4.02	0.0487	6.772	0.988	1.340	5.115
	0.040	2.00	0.0161	6.740	1.003	1.400	4.800
		3.00	0.0315	6.635	0.997	1.370	4.858
		4.00	0.0483	6.510	0.997	1.350	4.837
Plain blade				6.980	1.006	1.240	5.600
Design value				7.040	1.000	1.050	6.705

Table V.

Tangential jet and plain blade tangential lift coefficient results.

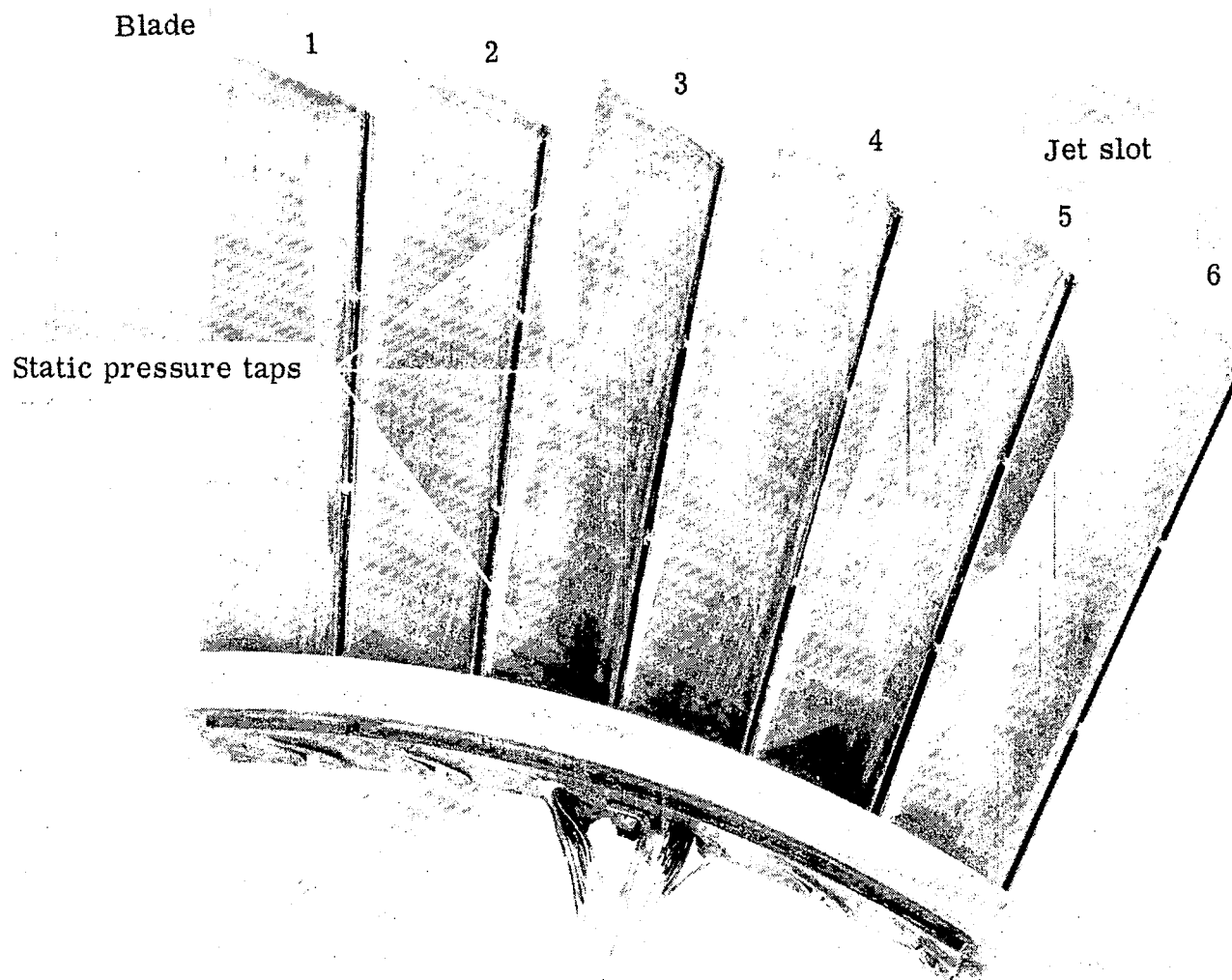
	Slot size (in.)	% \dot{m}_j/\dot{m}_p	$C_{j_{m_3}}$	$\frac{F_{yT_m}}{\delta_o \ell}$	$\frac{P_{st_{4m}}}{\delta_o}$	$\psi_{t_m} = \frac{F_{yT_m}/\delta_o \ell}{C_x(P_{T_o} - P_{st_4})/\delta_o}$
Tangential jet No. 1	0.020	1.00	0.0045	6.886	10.107	0.942
		2.60	0.0244	6.831	10.372	0.992
		4.00	0.0456	6.465	10.830	1.050
	0.030	2.50	0.0052	6.076	10.855	0.993
		4.10	0.0368	5.822	11.326	1.085
		6.30	0.0752	5.653	11.485	1.106
	0.040	3.98	0.0407	6.204	10.942	1.037
		5.62	0.0582	6.084	11.311	1.128
		7.44	0.0854	6.081	11.340	1.138
Tangential jet No. 2	0.020	1.96	0.0164	5.137	10.970	0.866
		3.02	0.0339	5.137	11.165	0.913
		3.54	0.0424	5.236	11.189	0.937
	0.030	2.01	0.0177	5.177	10.980	0.875
		2.99	0.0344	5.211	11.147	0.922
		4.02	0.0487	5.266	11.202	0.946
	0.040	2.00	0.0161	5.087	10.927	0.848
		3.00	0.0315	5.140	11.064	0.889
		4.00	0.0483	5.142	11.267	0.942
Plain blade				5.570	11.580	1.122
Design value				7.040	10.397	1.090

Table VI.

Tangential jet blade and plain blade measured and design change in tangential velocity across blade row.

Tangential jet No. 1 blade												
		0.020-in. jet slot			0.030-in. jet slot			0.040-in. jet slot			Plain blade	Design value
	\dot{m}_j/\dot{m}_p (%)	1.00	2.60	4.00	2.50	4.10	6.30	3.98	5.62	7.44		
Hub	W_u (% deviation)	1224.47 -1.88	1230.53 -1.39	1130.03 -9.44	1277.50 +2.37	1222.76 -2.01	1070.71 -14.19	1138.04 -8.80	1115.33 -10.62	1114.36 -10.70	1136.01 -8.96	1247.87
Mean	W_u (% deviation)	1079.73 +5.07	1065.31 +3.66	1013.03 -1.42	1010.10 -1.71	984.45 -4.20	986.72 -3.98	1030.15 +0.24	994.31 -3.24	1027.53 -0.01	940.59 -8.47	1027.65
Tip	W_u (% deviation)	939.66 +7.55	919.45 +5.24	859.74 -1.60	870.30 -0.30	835.23 -4.40	813.22 -6.92	859.93 -1.62	828.96 -5.12	836.78 -4.20	776.91 -11.08	873.71

Tangential jet No. 2 blade												
		0.020-in. jet slot			0.030-in. jet slot			0.040-in. jet slot			Plain blade	Design value
	\dot{m}_j/\dot{m}_p (%)	1.96	3.02	3.54	2.01	2.99	4.02	2.00	3.00	4.00		
Hub	W_u (% deviation)	1278.74 +2.47	1249.93 +0.16	1267.98 +1.61	1281.21 +2.67	1266.89 +1.52	1267.82 +1.59	1242.77 -0.41	1283.45 +2.85	1252.55 +0.38	1136.01 -8.96	1247.87
Mean	W_u (% deviation)	996.94 -2.99	991.96 -3.47	1004.79 -2.22	959.49 -6.63	953.35 -7.23	981.99 -4.44	966.47 -5.95	963.87 -6.21	952.35 -7.33	940.59 -8.47	1027.65
Tip	W_u (% deviation)	848.41 -2.89	835.17 -4.41	841.75 -3.66	822.37 -5.88	820.29 -6.11	819.10 -6.25	806.05 -7.70	803.56 -8.03	790.66 -9.51	776.91 -11.08	873.71



5315V-151

Figure 1. Tangential jet blade No. 1 assembly.

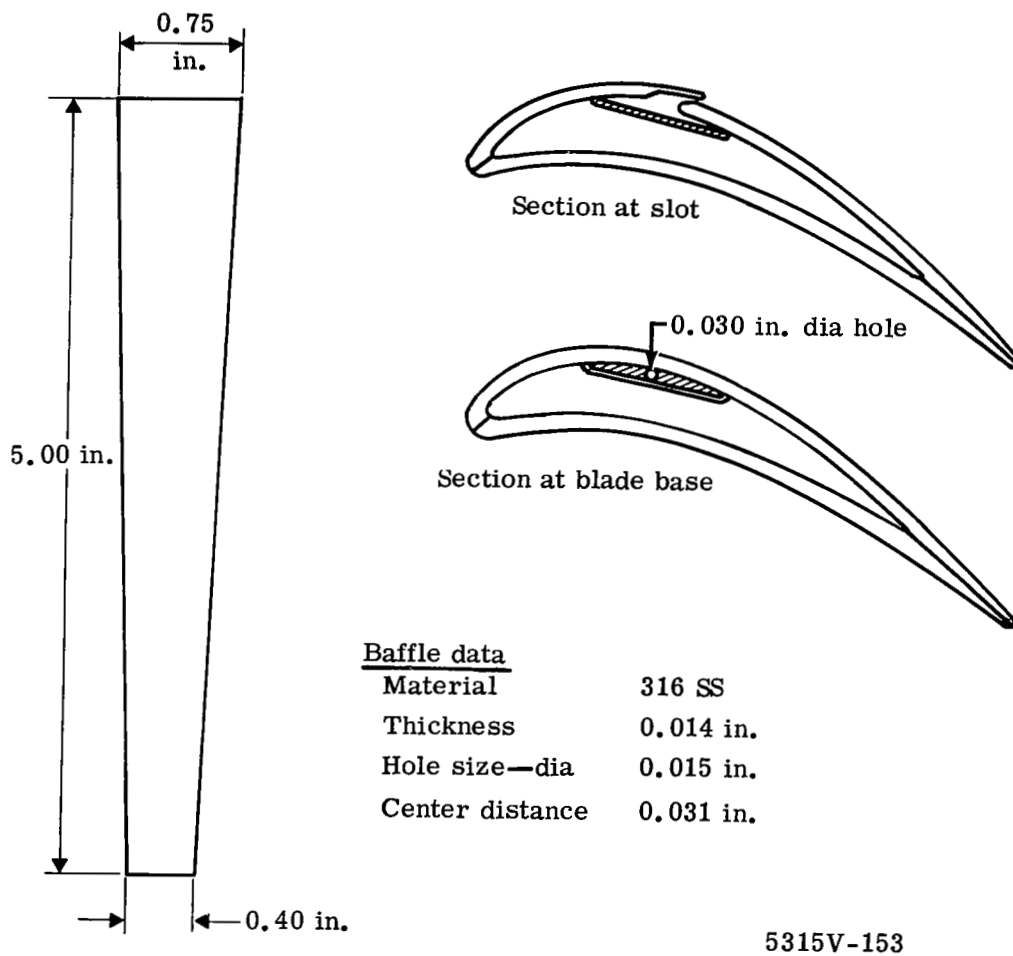


Figure 4. Sketch of baffle installation details.

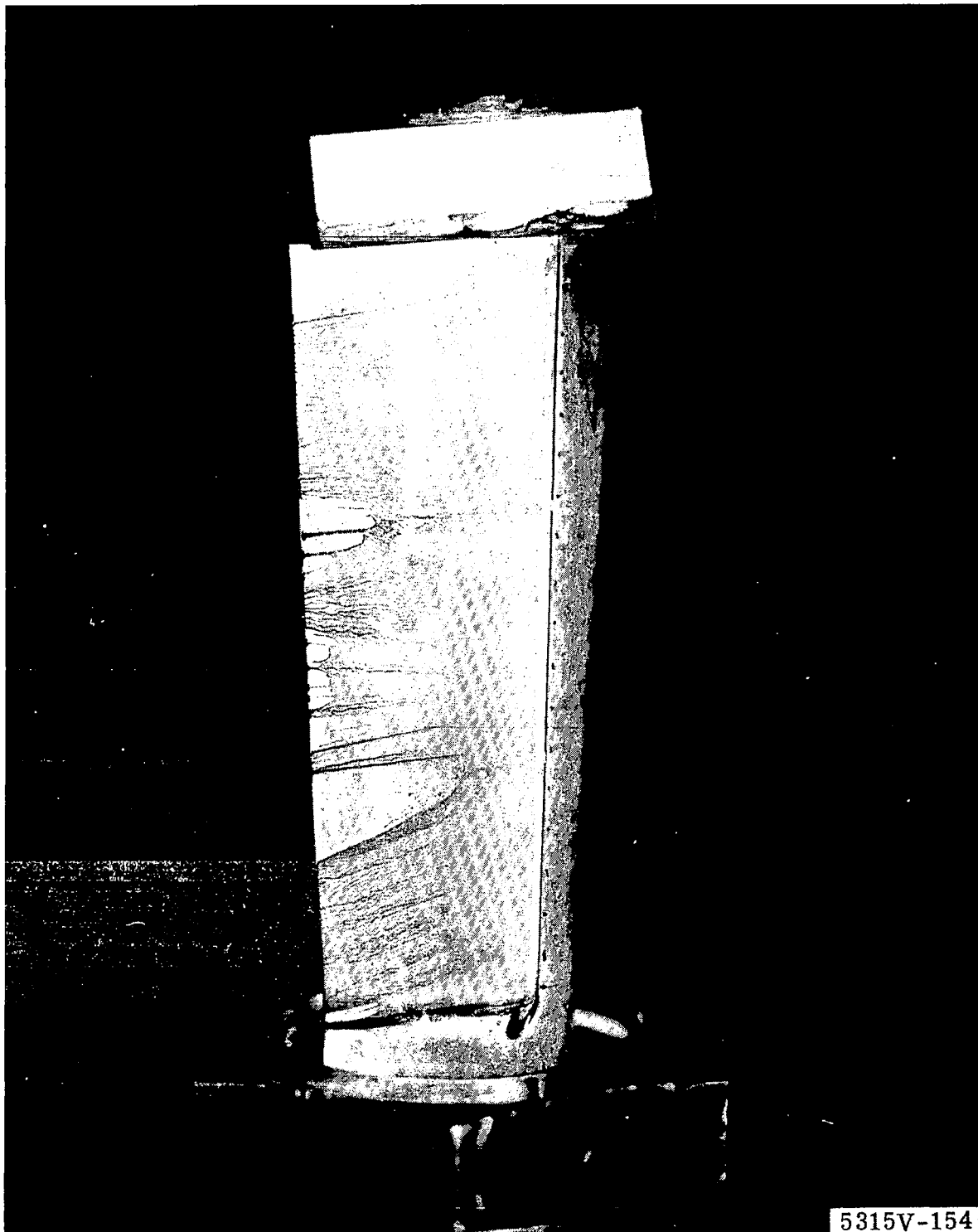


Figure 5. Bench test slot-to-downstream suction surface flow pattern.

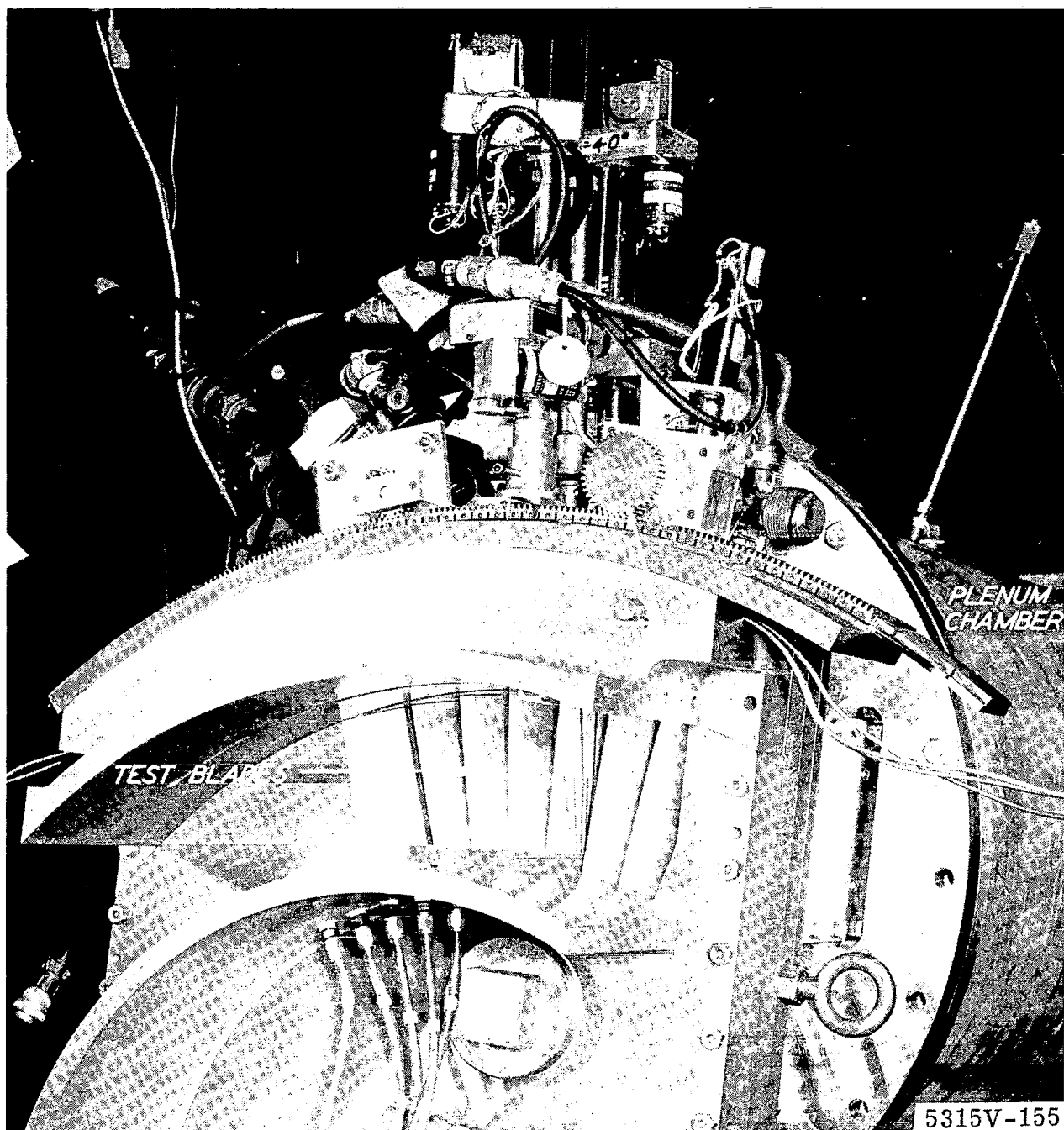


Figure 6. Annular cascade test rig.

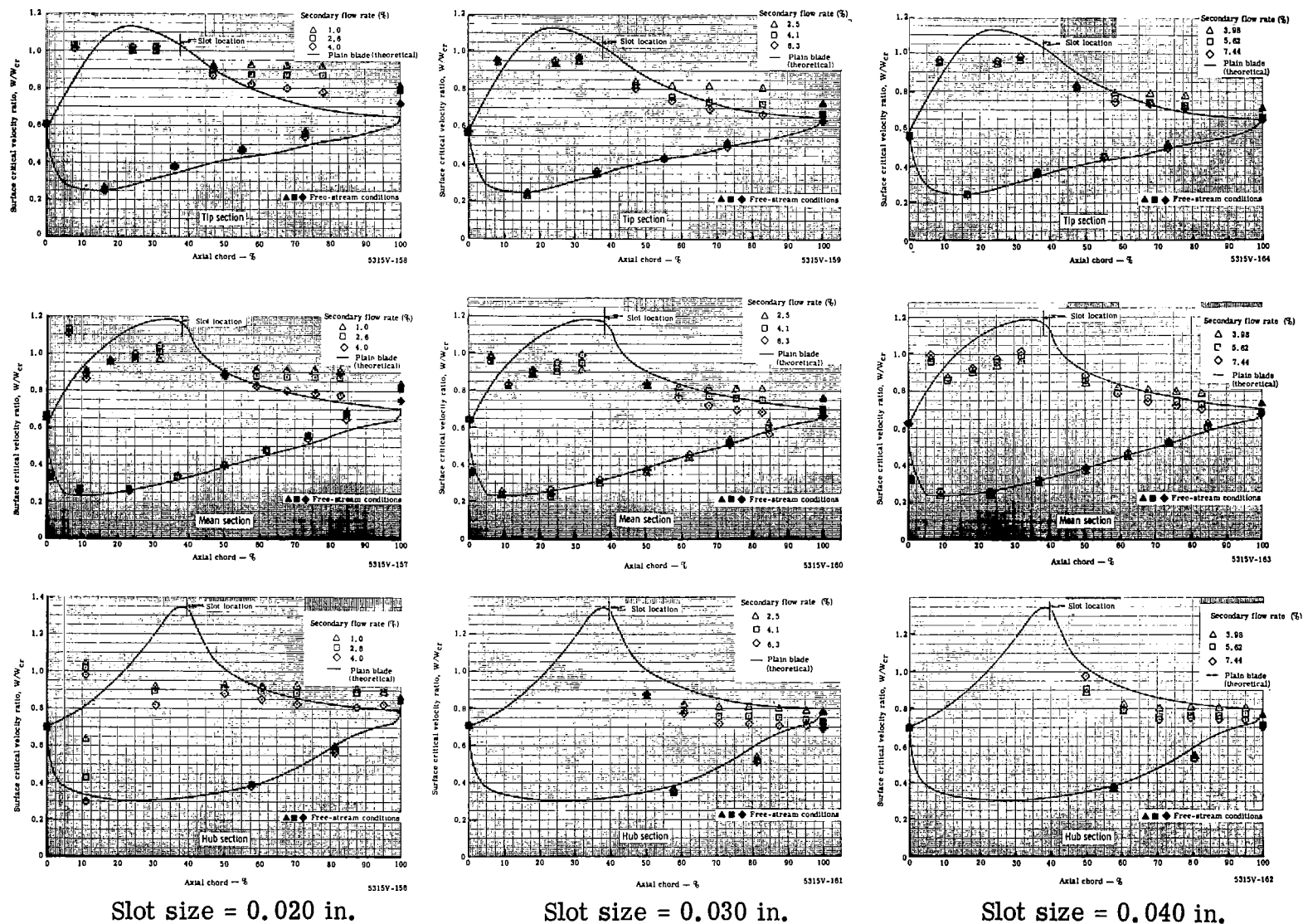
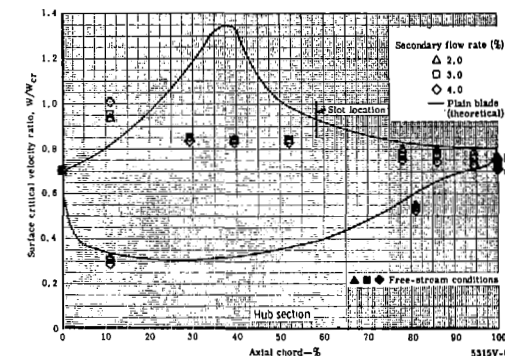
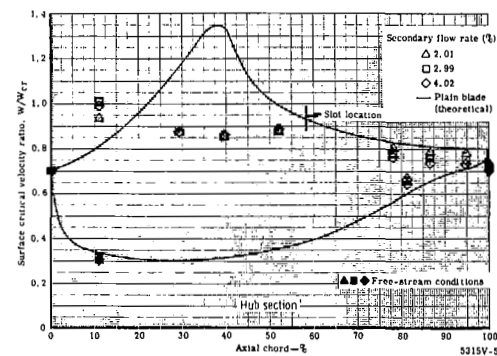
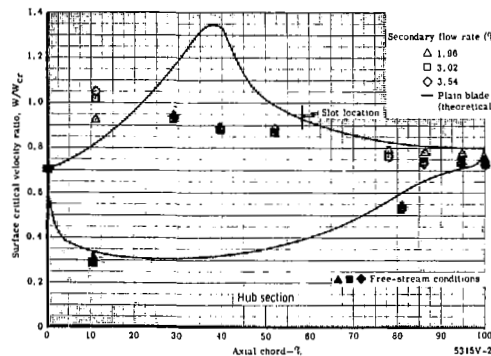
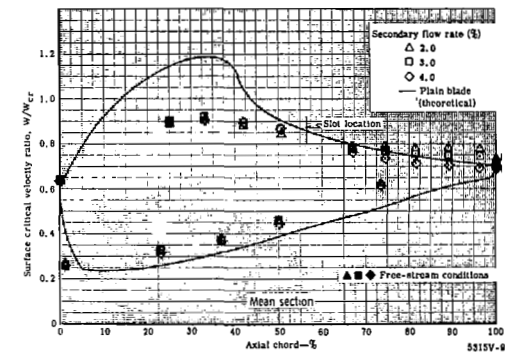
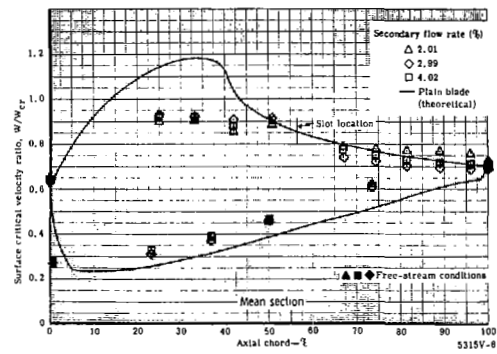
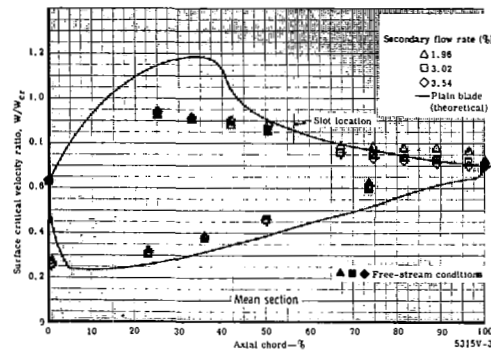
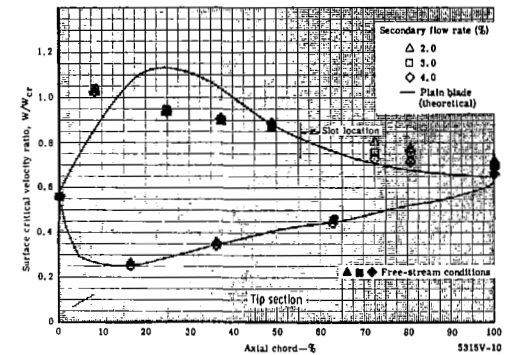
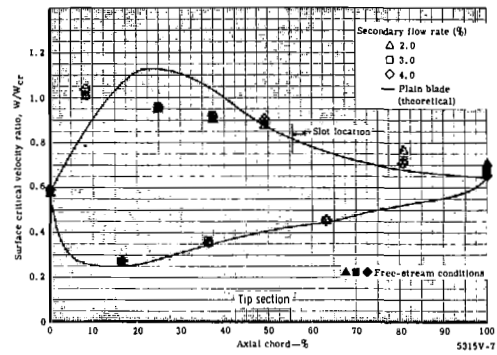
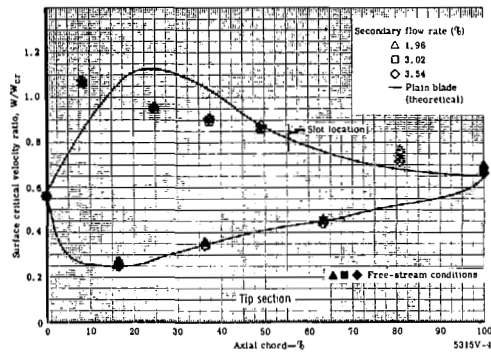


Figure 7. Measured and predicted surface critical velocity ratio distribution for tangential jet blade No. 1.



Slot size = 0.020 in.

Slot size = 0.030

Slot size = 0.040 in.

Figure 8. Measured and predicted surface critical velocity ratio distribution for tangential jet blade No. 2.

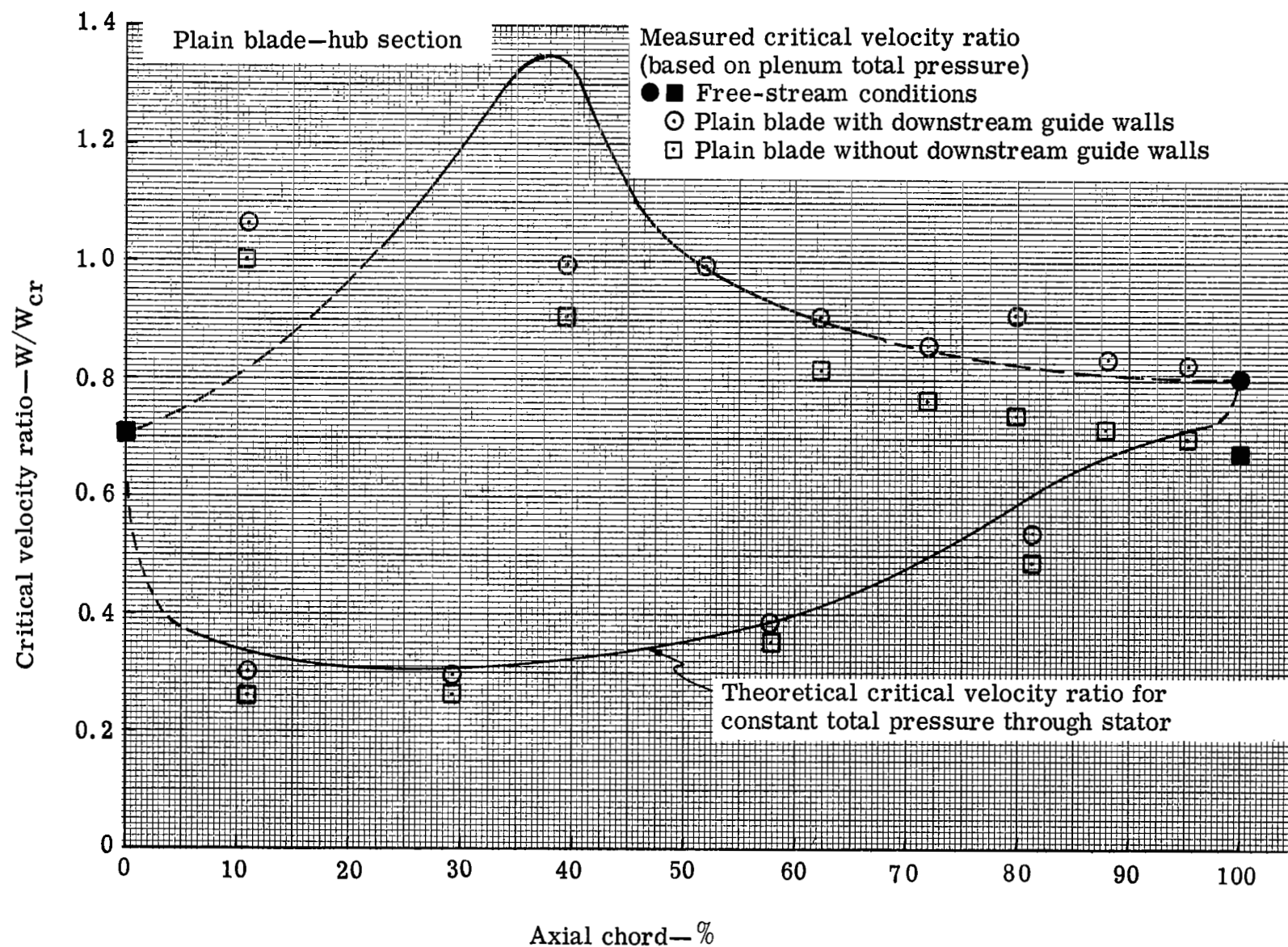
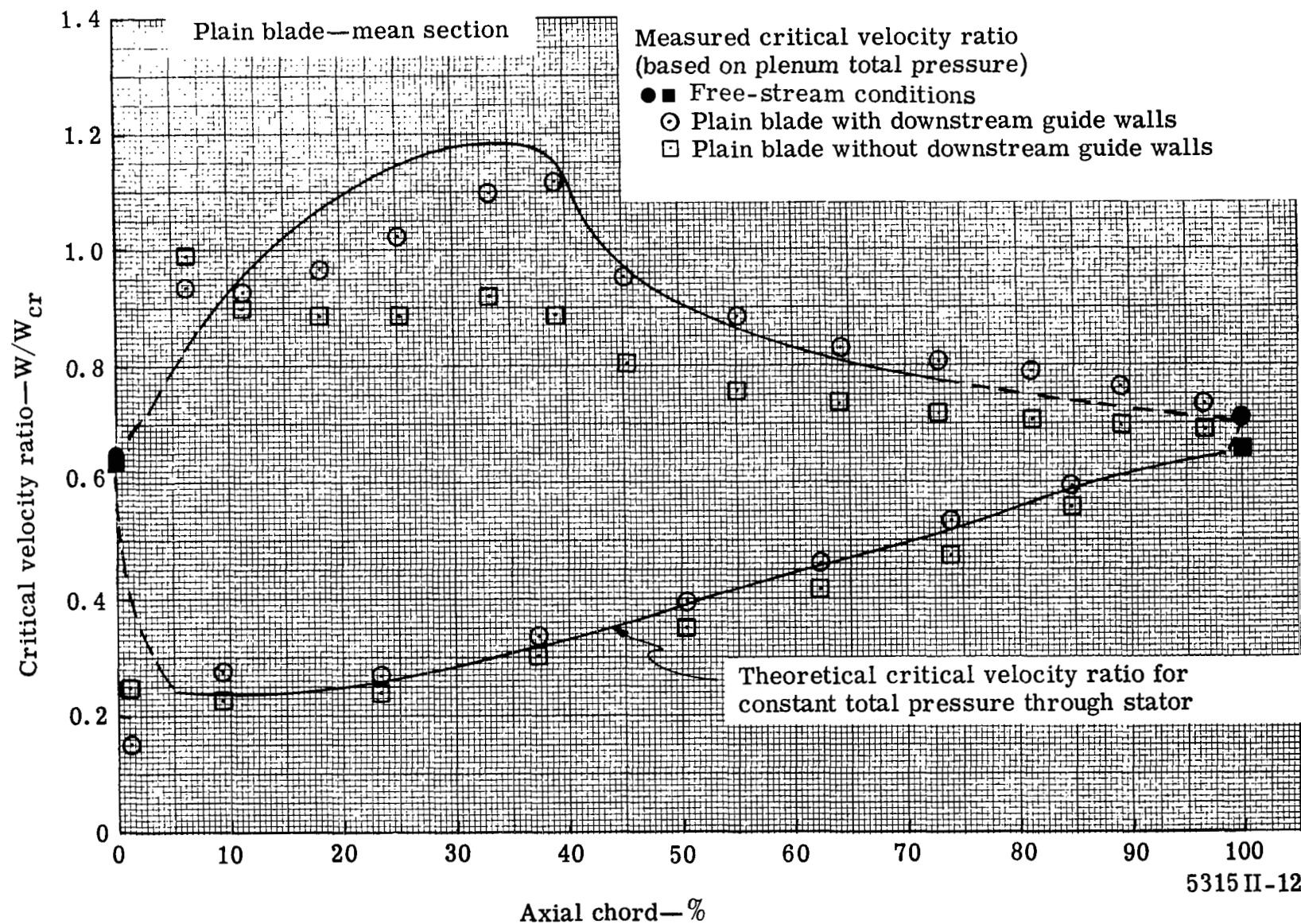


Figure 9. Measured and predicted surface critical velocity ratio distribution for plain blade hub section.



5315 II-12

Figure 10. Measured and predicted surface critical velocity ratio distribution for plain blade mean section.

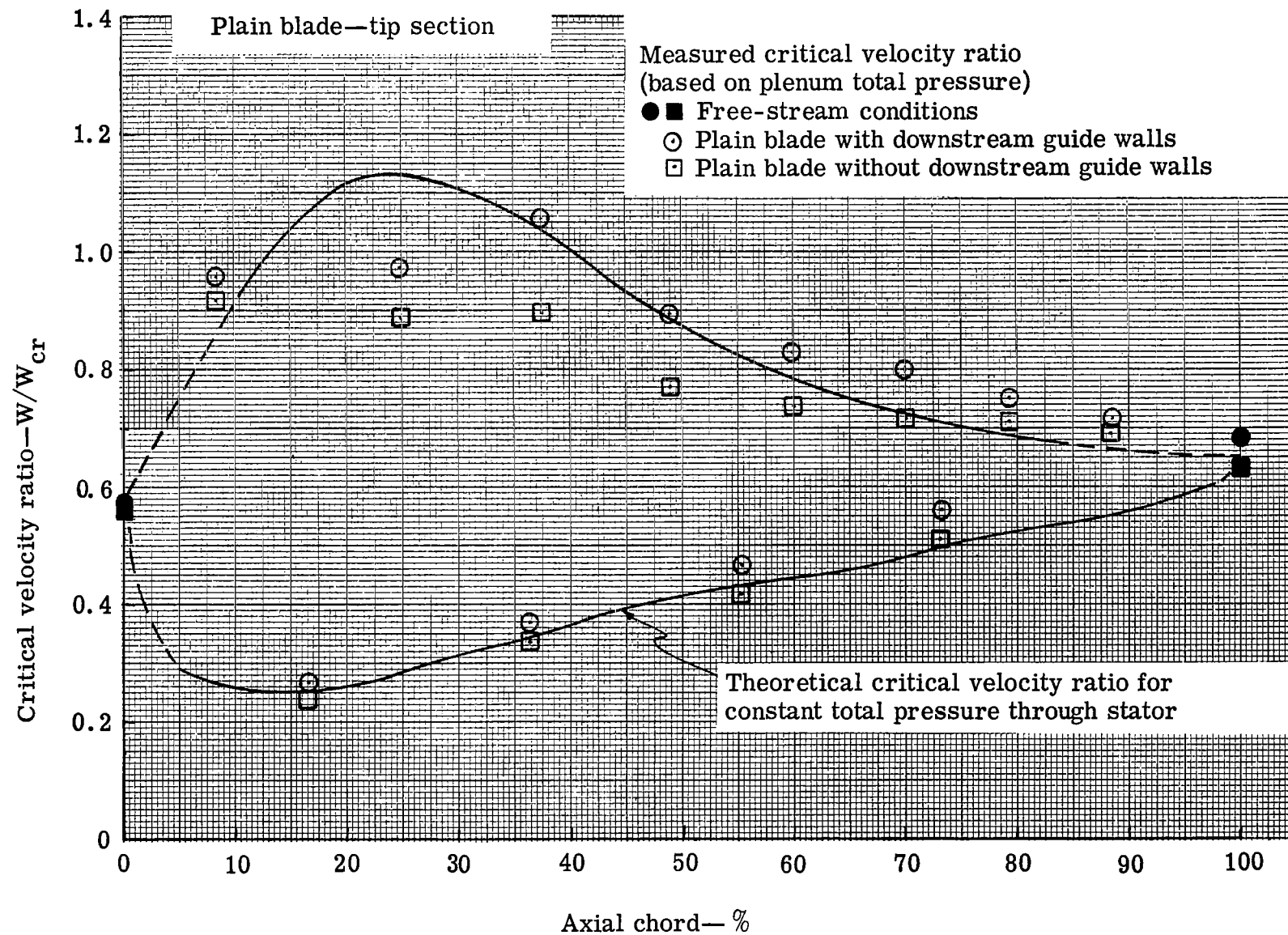


Figure 11. Measured and predicted surface critical velocity ratio distribution for plain blade tip section.

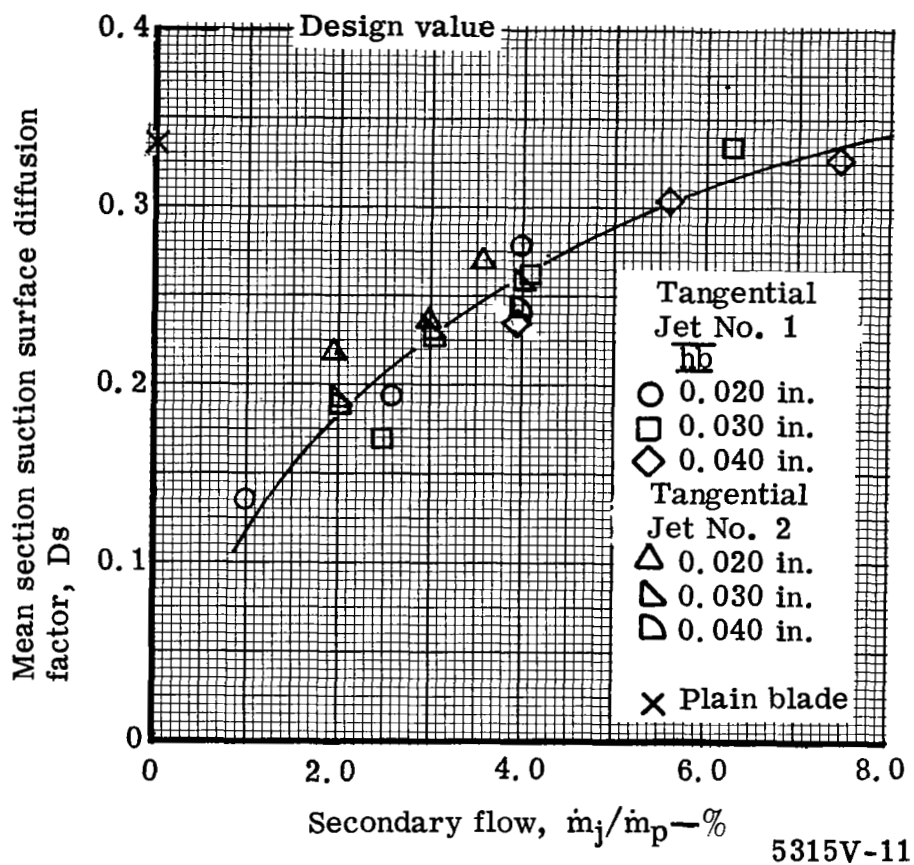
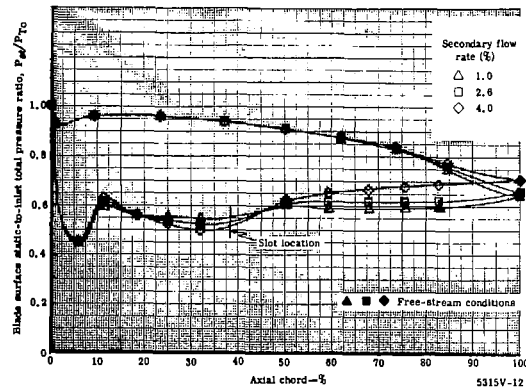
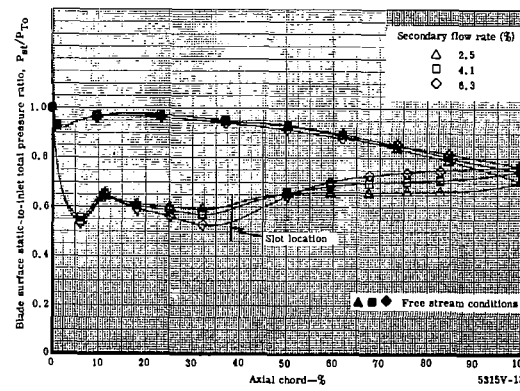


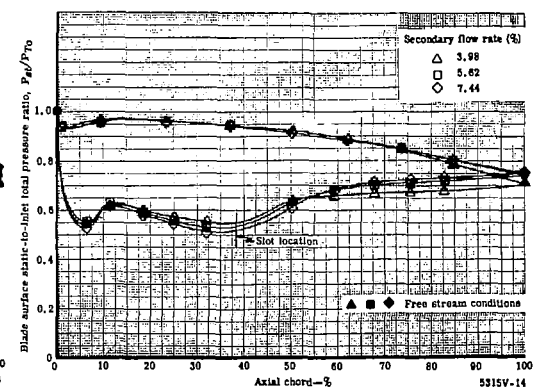
Figure 12. Mean section suction surface diffusion developed by various tangential jet configuration.



Slot size = 0.020 in.

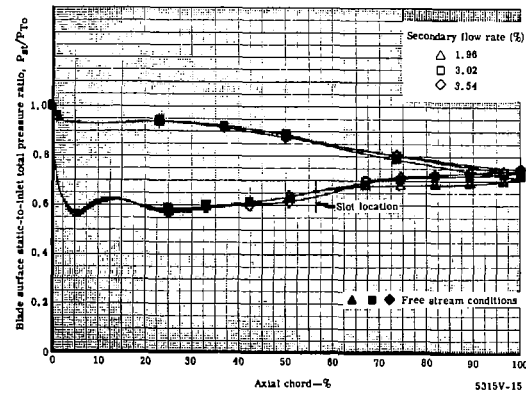


Slot size = 0.030 in.

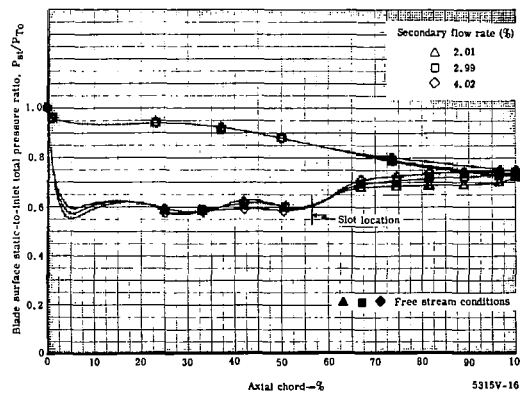


Slot size = 0.040 in.

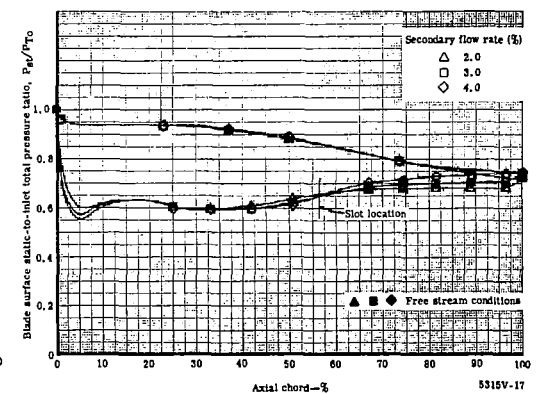
Tangential jet blade No. 1



Slot size = 0.020 in.



Slot size = 0.030 in.

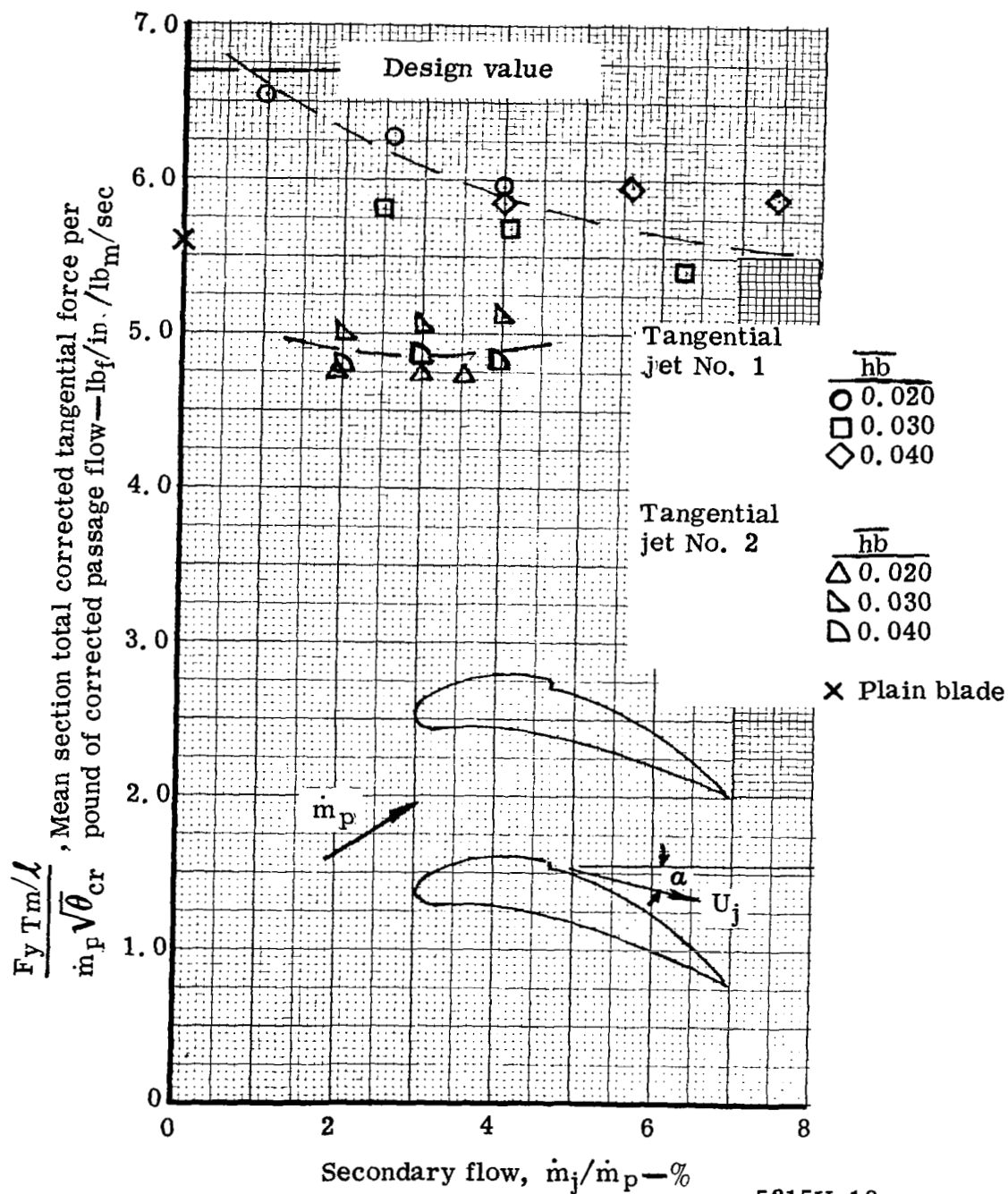


Slot size = 0.040 in.

Tangential jet blade No. 2

Figure 13. Measured mean section surface static pressure distribution for all tangential jet configurations.

$$\frac{F_y T_m / \ell}{\dot{m}_p \sqrt{\theta}} = \frac{\dot{m}_j U_j \sin \alpha}{\ell} \int_0^{C_x} (P_{st_{ps}} - P_{st_{ss}}) dx$$

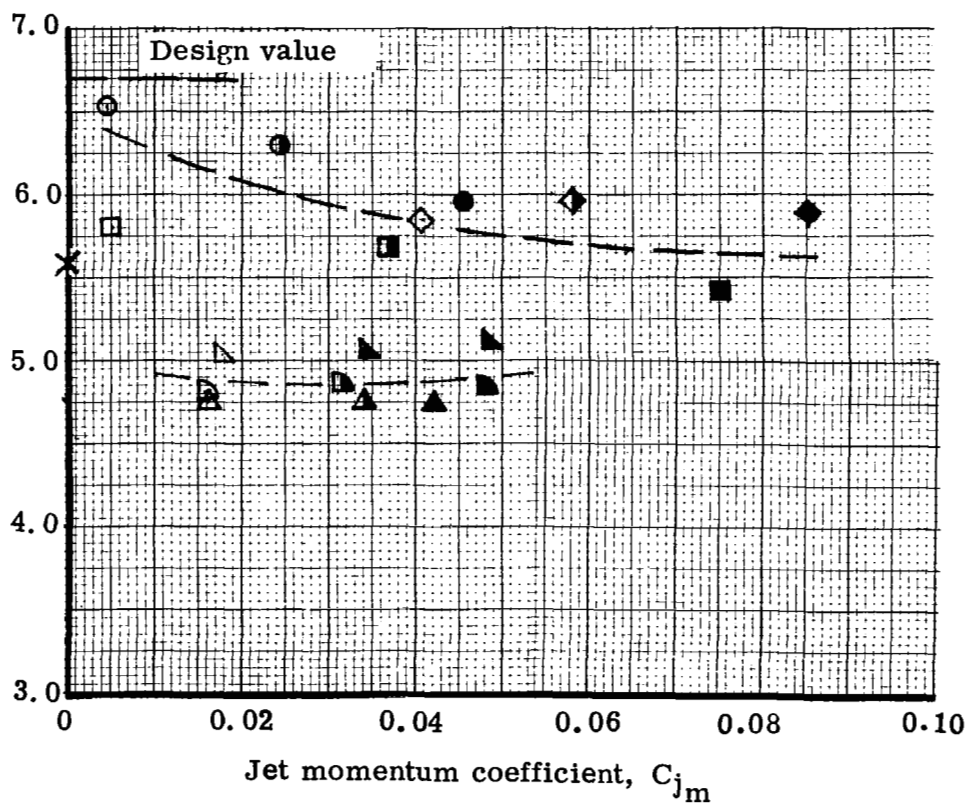


5315V-18

Figure 14. Variation of corrected tangential force with secondary flow for the plain and tangential jet blades.

$\frac{F_y T_m / L}{\dot{m}_p \sqrt{\theta_{cr}}}$, Mean section total corrected tangential force per pound of corrected passage

flow—lb_f/in. /lb_m/sec



5315V-19

Figure 15. Variation of corrected tangential force with jet momentum coefficient for plain and tangential jet blades.

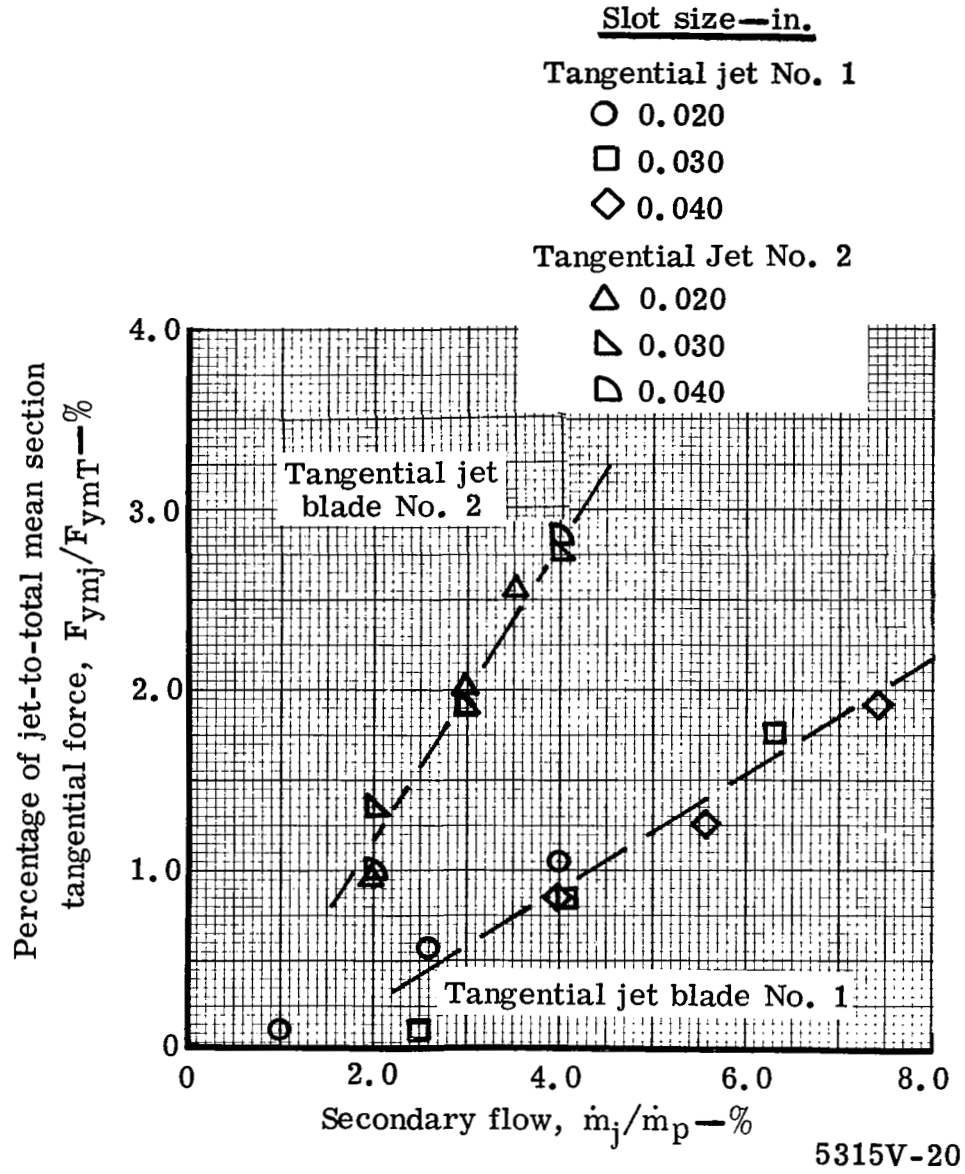


Figure 16. Variation of the jet contribution to the total mean section lift with percentage of secondary flow rate for all tangential jet configurations.

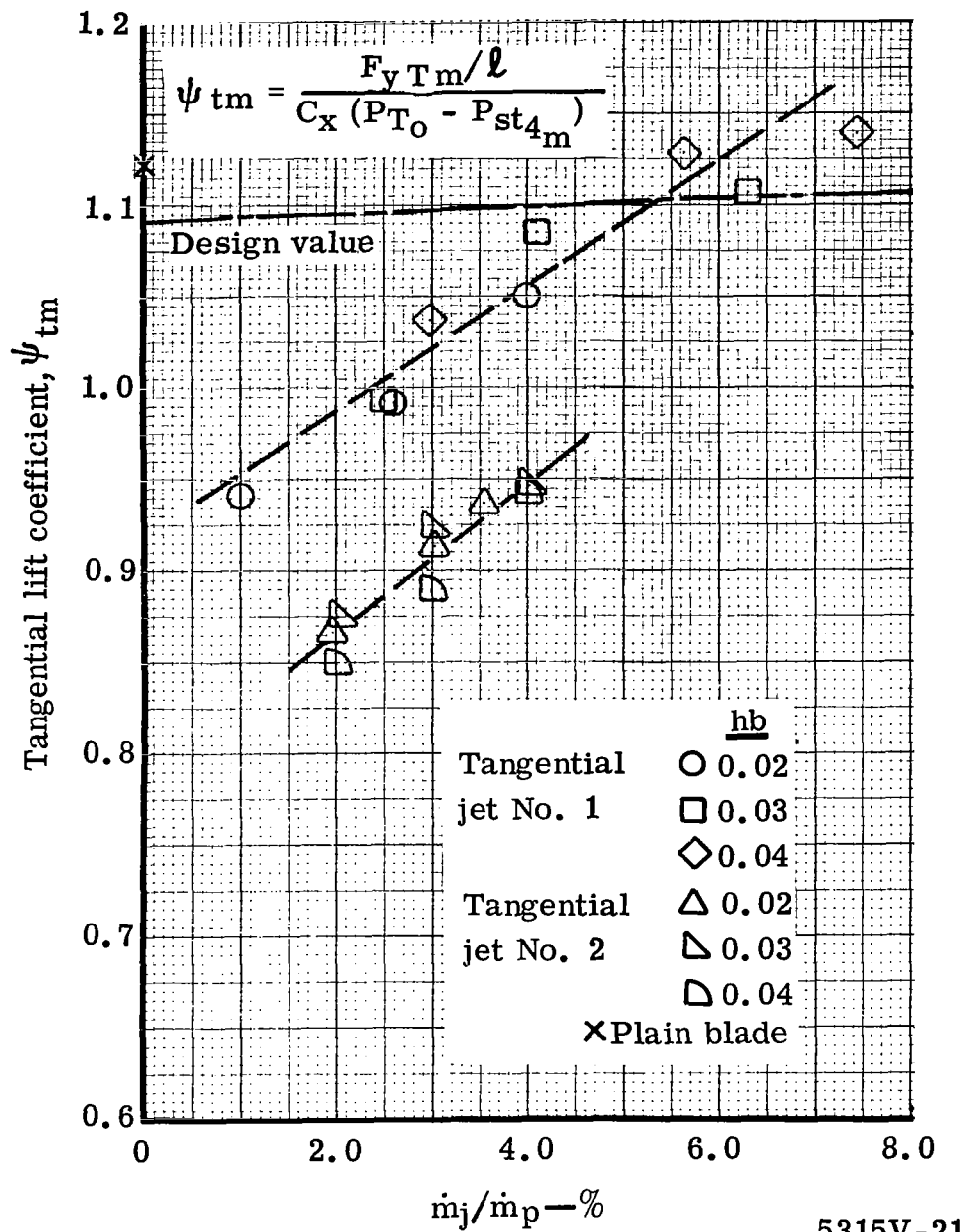


Figure 17. Effect of secondary flow rate on tangential lift coefficient for various blade configurations.

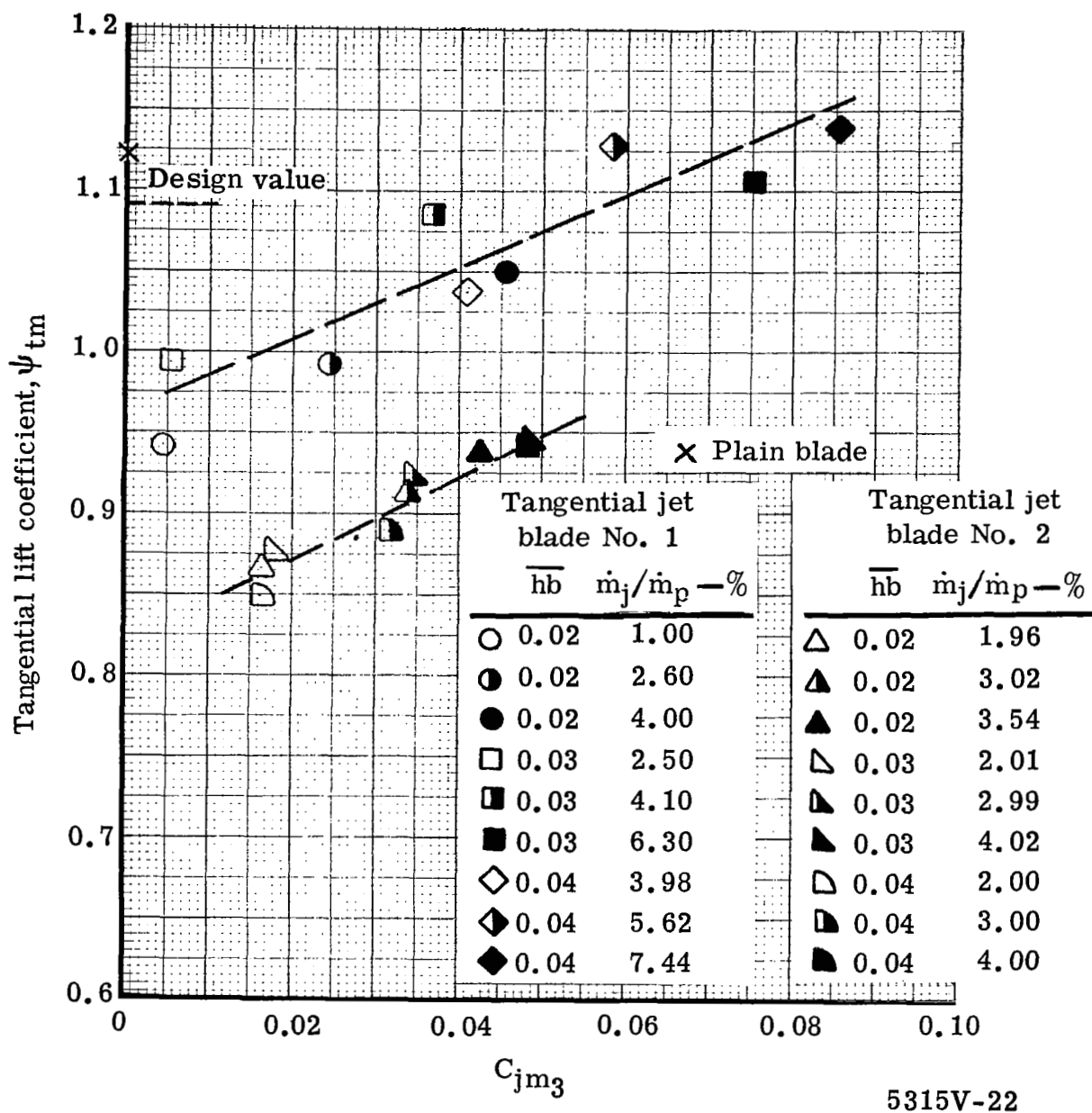


Figure 18. Variation of tangential lift coefficient with jet momentum coefficient.



Vane No. 2



Vane No. 3



Vane No. 4

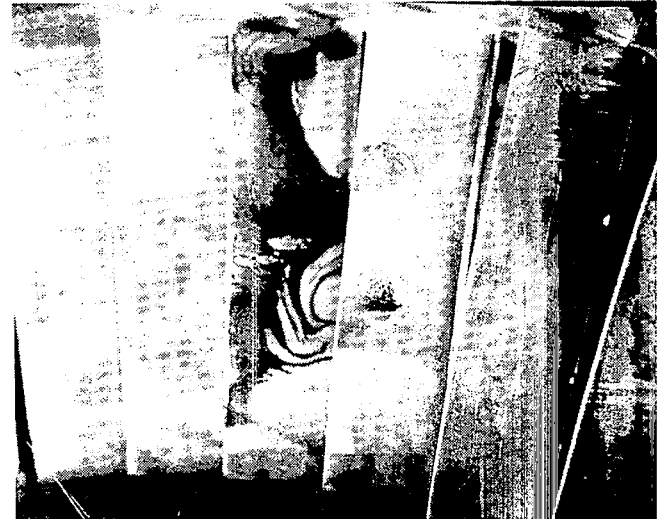


Vane No. 5

Figure 19. Flow visualization results for the tangential jet No. 1 blade with 0.020-in. jet slot and 1.00% secondary flow ($C_{jm} = 0.0045$).



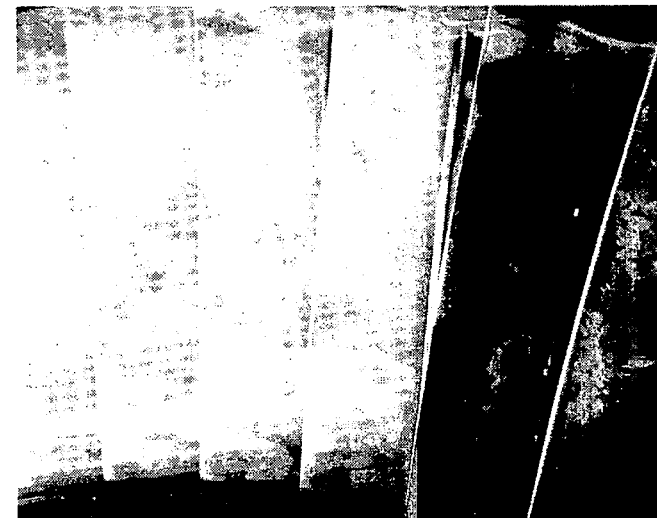
Vane No. 2



Vane No. 3

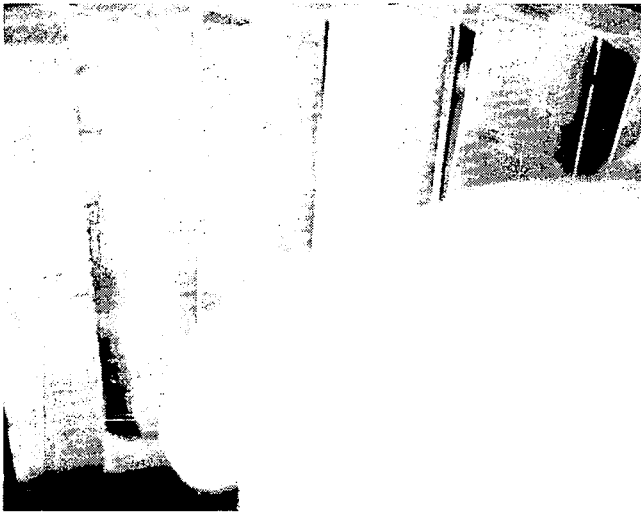


Vane No. 4



Vane No. 5

Figure 20. Flow visualization results for the tangential jet No. 1 blade with 0.020-in. jet slot and 2.60% secondary flow ($C_{jm} = 0.0244$).



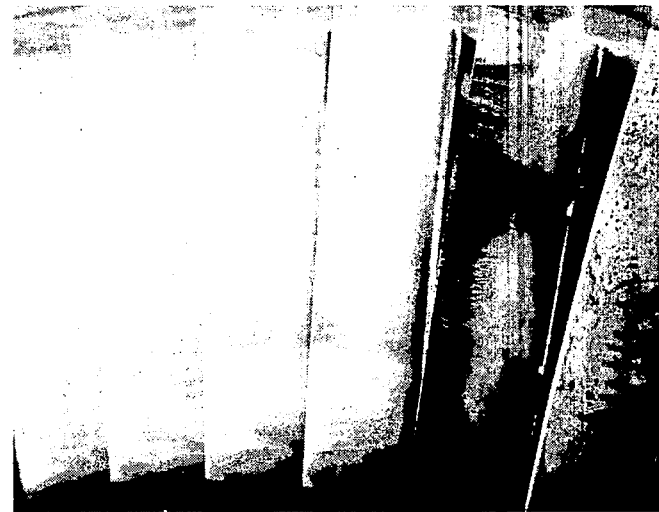
Vane No. 2



Vane No. 3

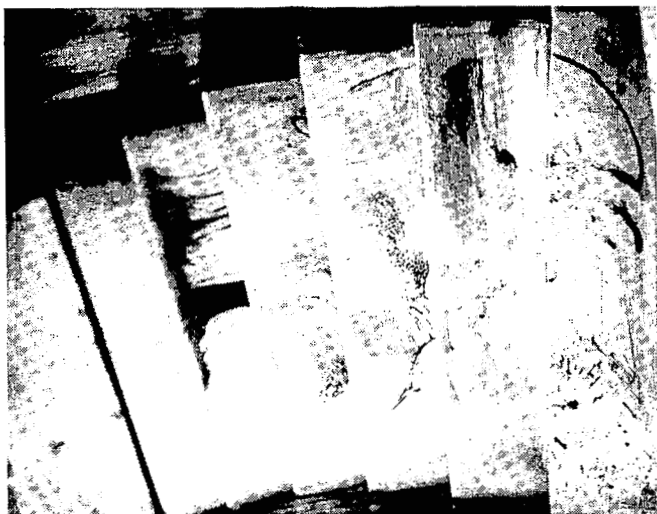


Vane No. 4

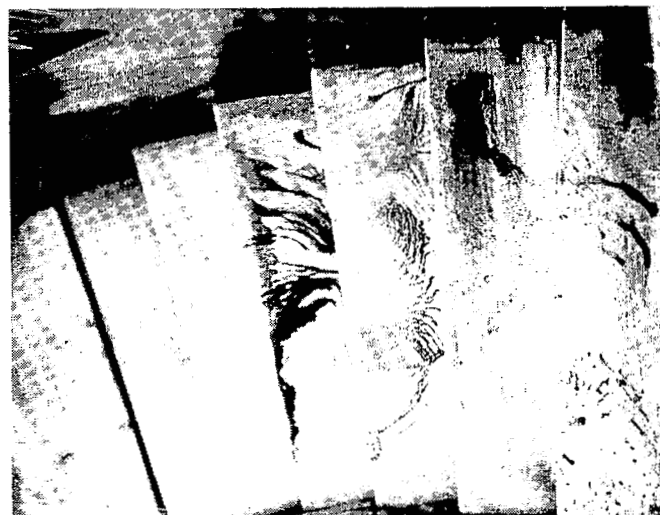


Vane No. 5

Figure 21. Flow visualization results for the tangential jet No. 1 blade with 0.020-in. jet slot and 4.00% secondary flow ($C_{jm} = 0.0456$).



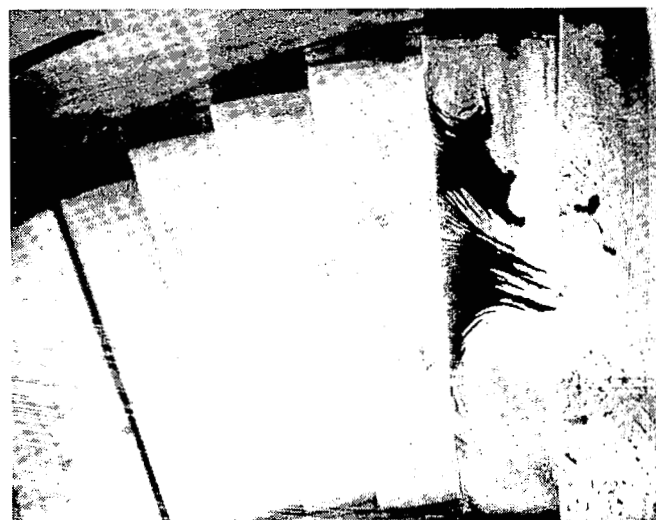
Vane No. 2



Vane No. 3



Vane No. 4



Vane No. 5

Figure 22. Flow visualization results for the tangential jet No. 1 blade with 0.030-in. jet slot and 2.50% secondary flow ($C_{j_m} = 0.0052$).



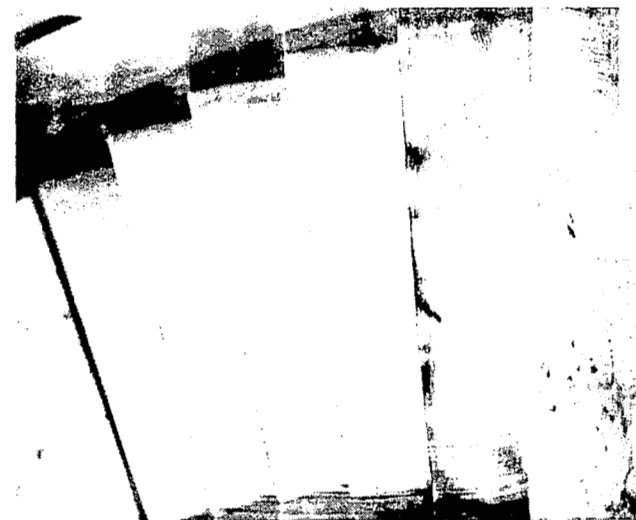
Vane No. 2



Vane No. 3

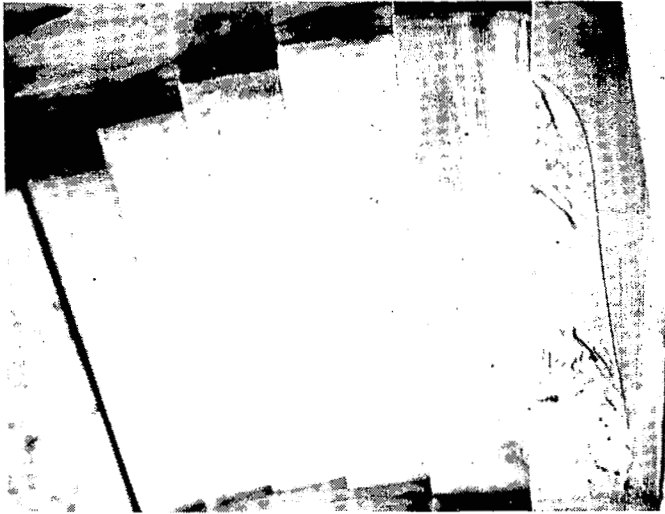


Vane No. 4

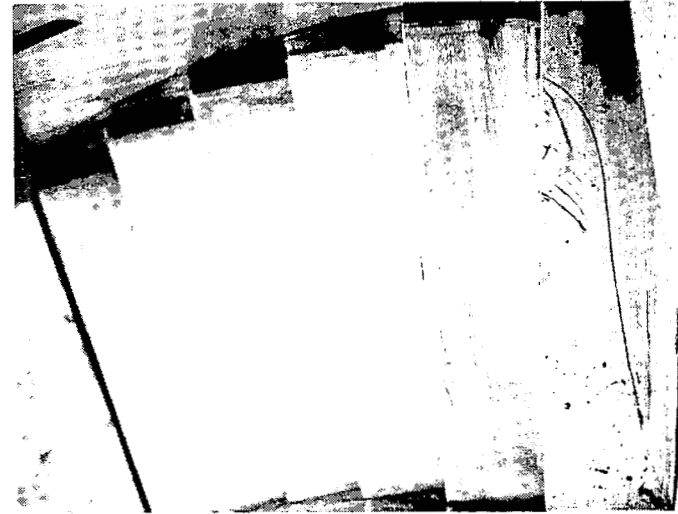


Vane No. 5

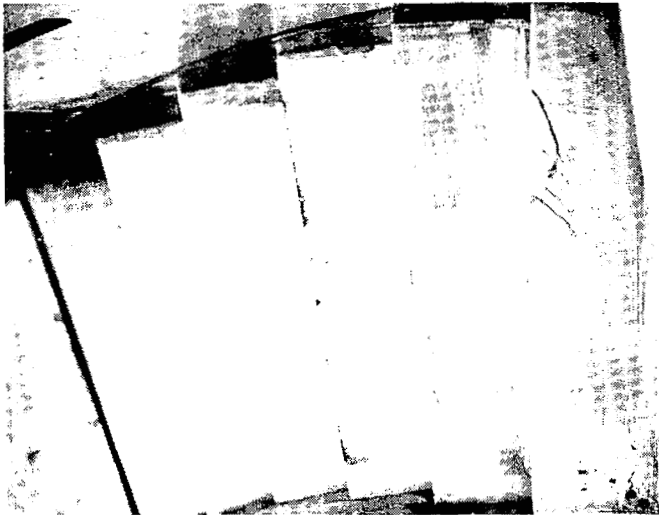
Figure 23. Flow visualization results for the tangential jet No. 1 blade with 0.030-in. jet slot and 4.10% secondary flow ($C_{jm} = 0.036$).



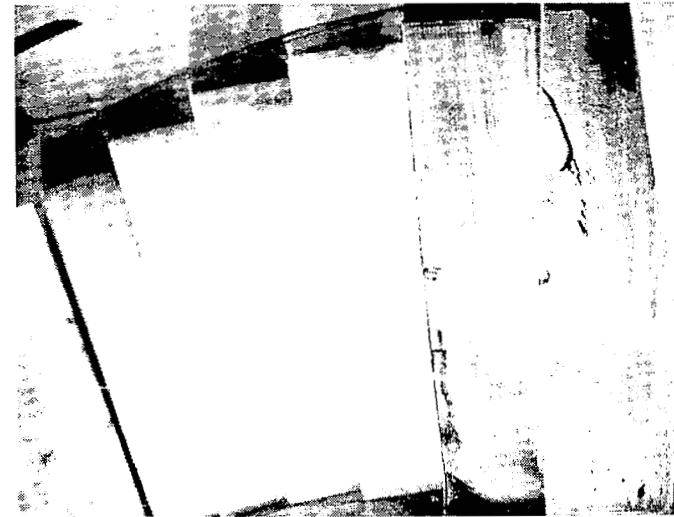
Vane No. 2



Vane No. 3

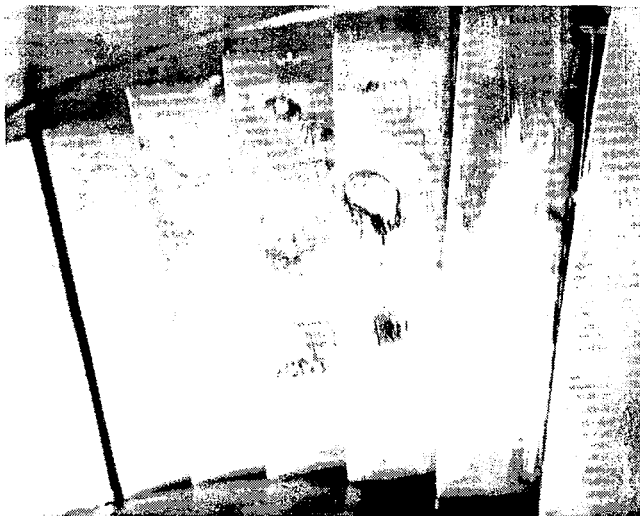


Vane No. 4



Vane No. 5

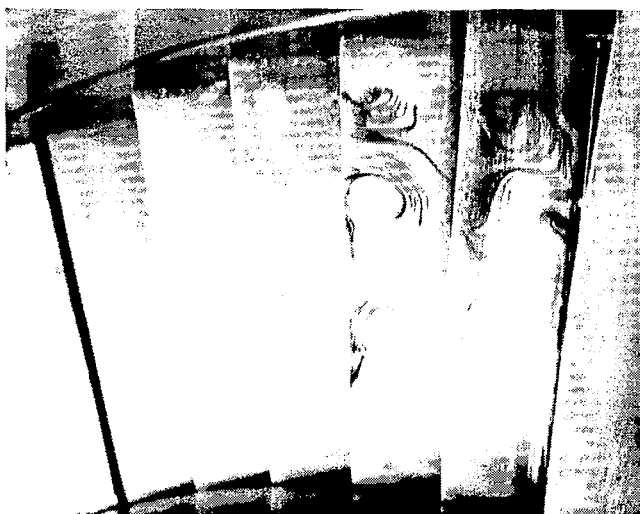
Figure 24. Flow visualization results for the tangential jet No. 1 blade with 0.030-in. jet slot and 6.30% secondary flow ($C_{jm} = 0.0752$).



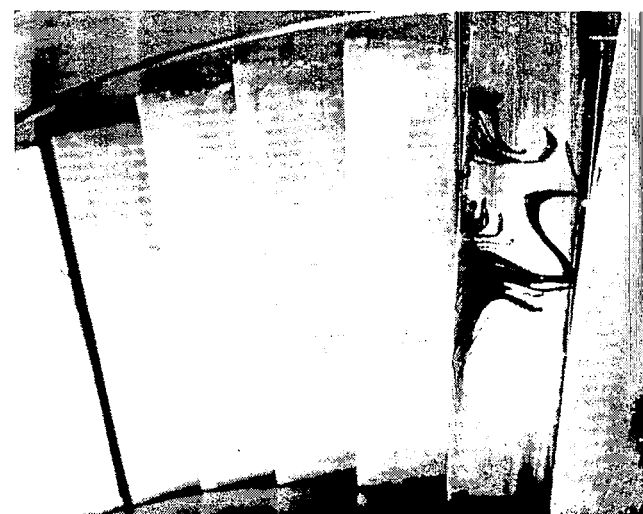
Vane No. 2



Vane No. 3

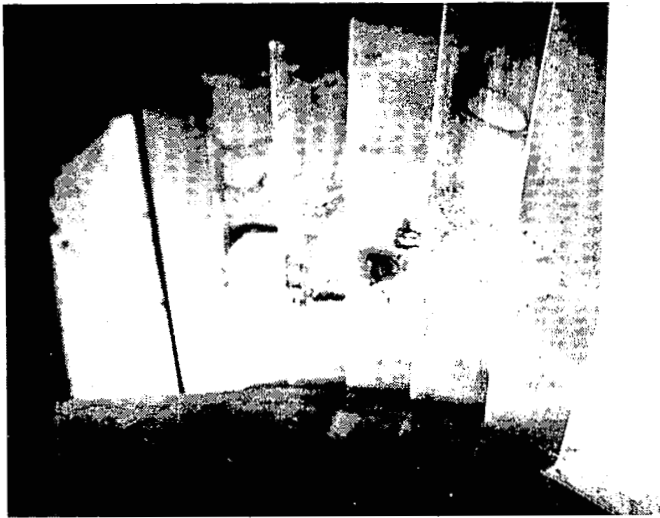


Vane No. 4



Vane No. 5

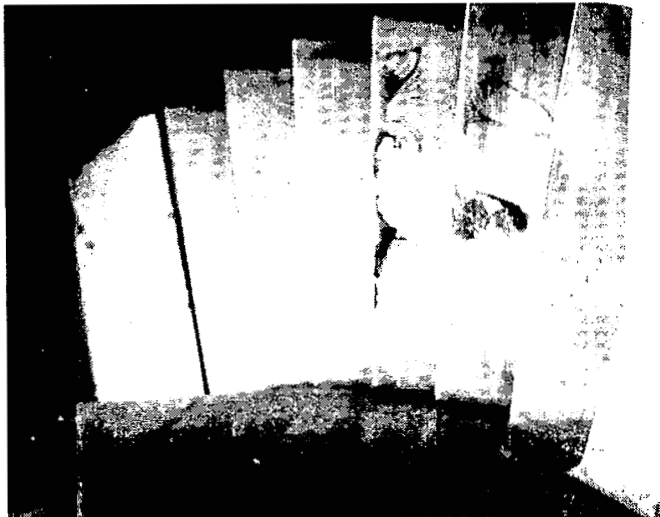
Figure 25. Flow visualization results for the tangential jet No. 1 blade with 0.040-in. jet slot and 3.20% secondary flow.



Vane No. 2



Vane No. 3

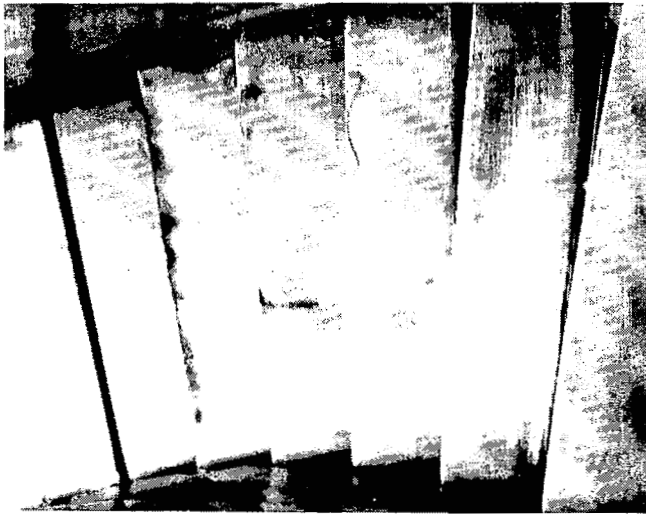


Vane No. 4

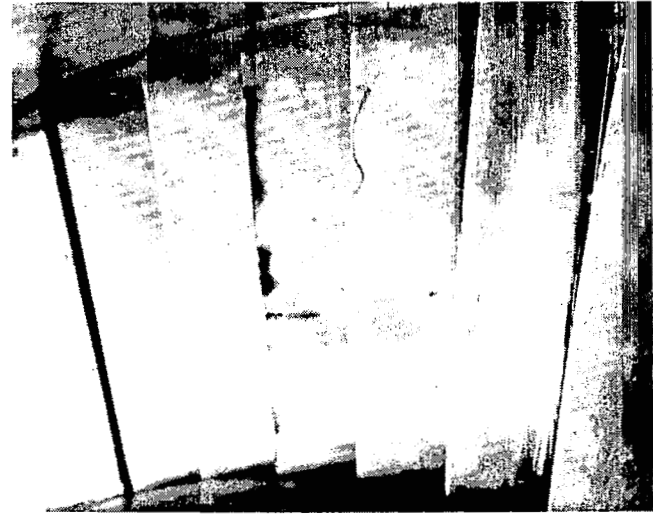


Vane No. 5

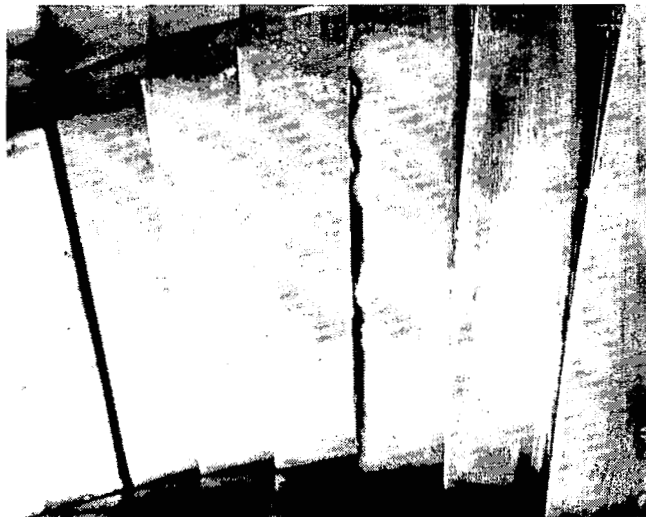
Figure 26. Flow visualization results for the tangential jet No. 1 blade with 0.040-in. jet slot and 3.98% secondary flow ($C_{jm} = 0.0407$).



Vane No. 2



Vane No. 3

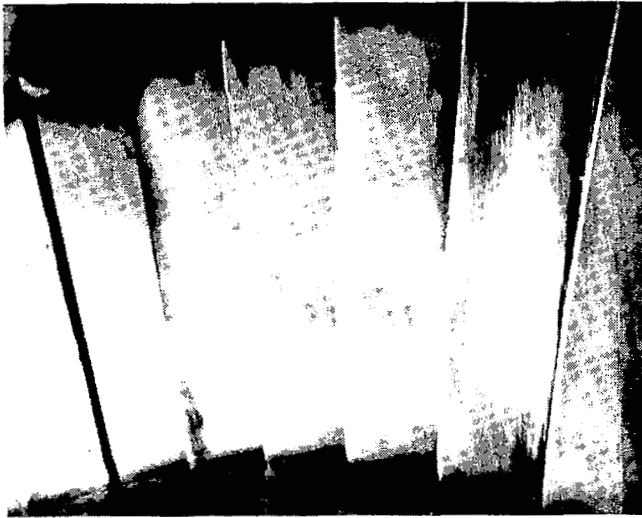


Vane No. 4



Vane No. 5

Figure 27. Flow visualization results for the tangential jet No. 1 blade with 0.040-in. jet slot and 5.62% secondary flow ($C_{jm} = 0.0582$).



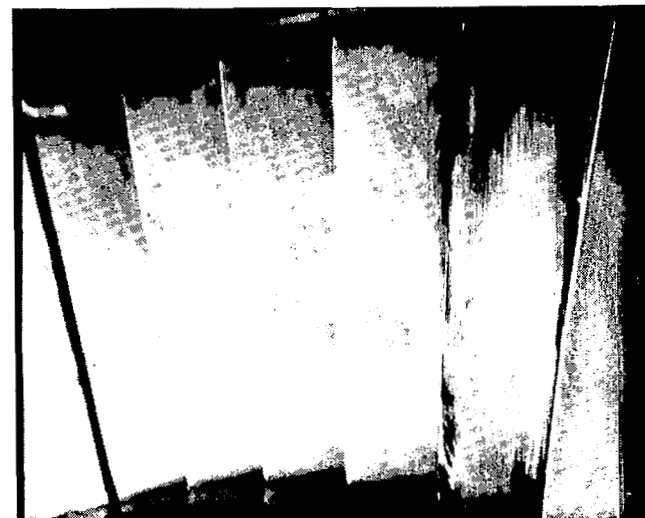
Vane No. 2



Vane No. 3



Vane No. 4



Vane No. 5

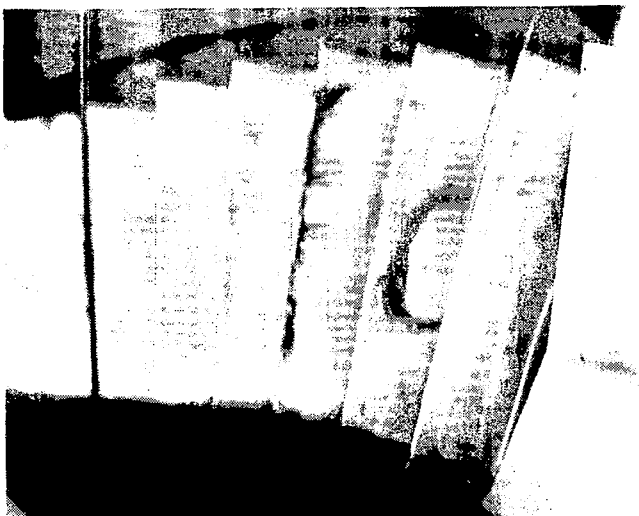
Figure 28. Flow visualization results for the tangential jet No. 1 blade with 0.040-in. jet slot and 7.44% secondary flow ($C_{jm} = 0.0854$).



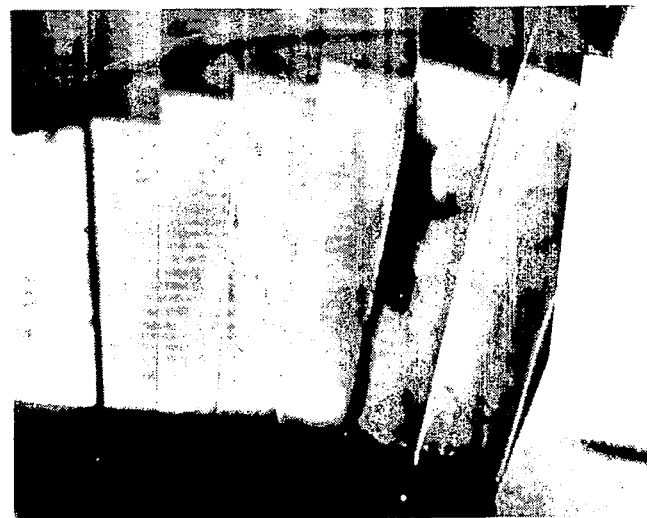
Vane No. 2



Vane No. 3



Vane No. 4

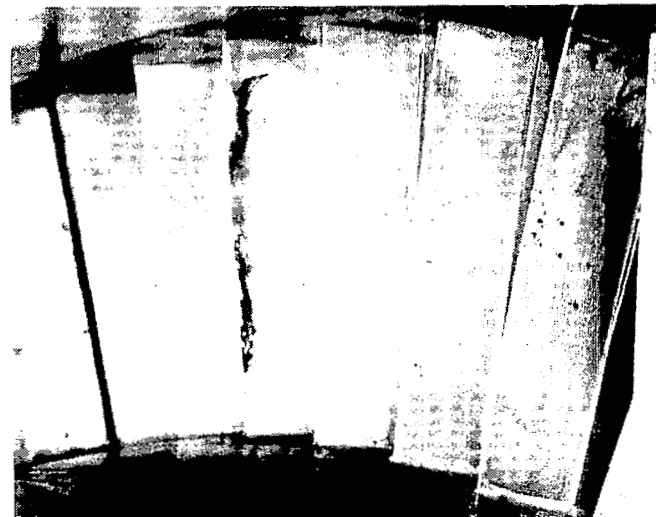


Vane No. 5

Figure 29. Flow visualization results for the tangential jet No. 2 blade with 0.020-in. jet slot and 1.96% secondary flow ($C_{j_m} = 0.0164$).



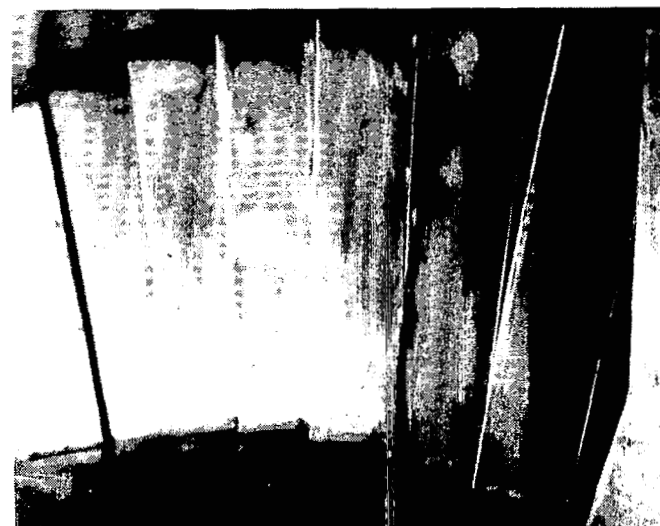
Vane No. 2



Vane No. 3

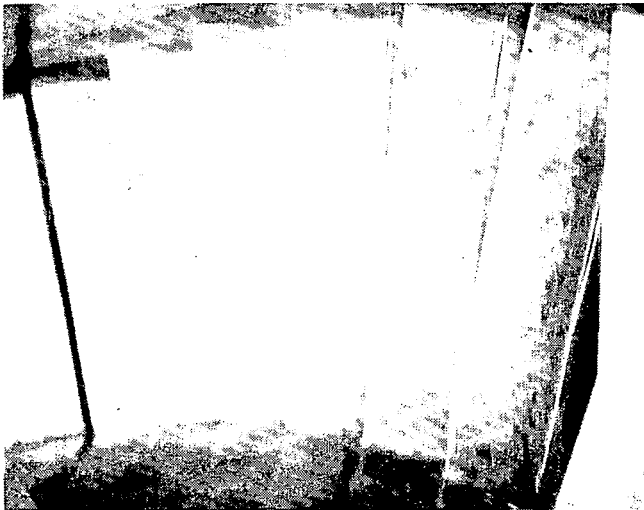


Vane No. 4



Vane No. 5

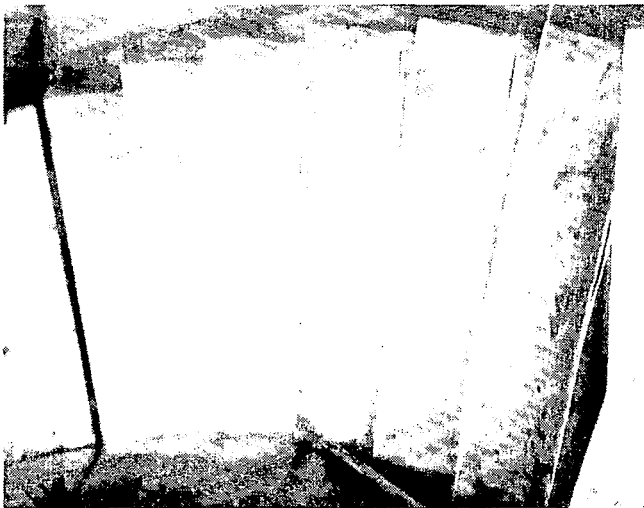
Figure 30. Flow visualization results for the tangential jet No. 2 blade with 0.020-in. jet slot and 3.02% secondary flow ($C_{jm} = 0.0339$),



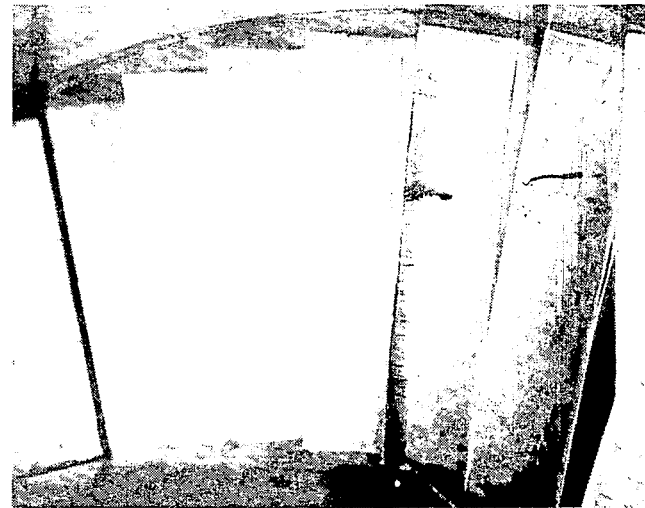
Vane No. 2



Vane No. 3



Vane No. 4



Vane No. 5

Figure 31. Flow visualization results for the tangential jet No. 2 blade with 0.020-in. jet slot and 3.54% secondary flow ($C_{j_m} = 0.0424$).



Vane No. 2



Vane No. 3



Vane No. 4



Vane No. 5

Figure 32. Flow visualization results for the tangential jet No. 2 blade with 0.030-in. jet slot and 2.01% secondary flow ($C_{jm} = 0.0177$).



Vane No. 2



Vane No. 3

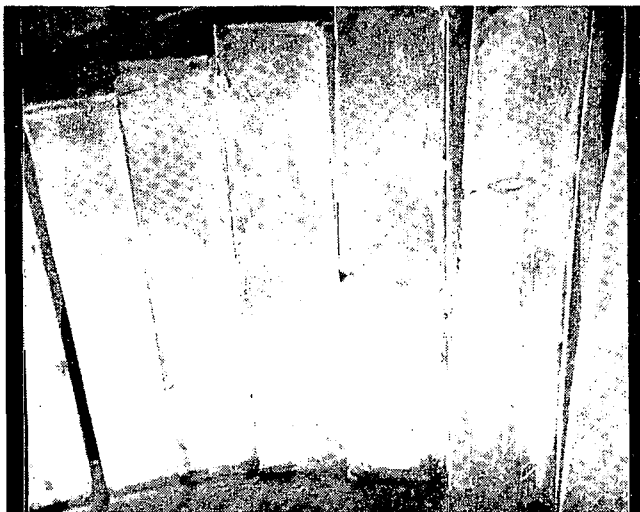


Vane No. 4

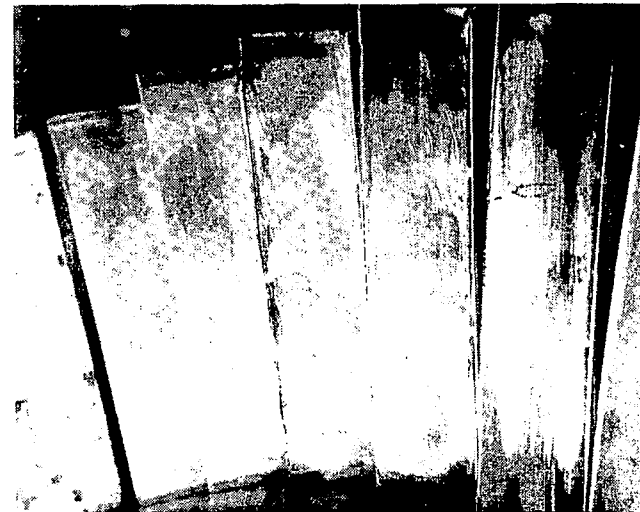


Vane No. 5

Figure 33. Flow visualization results for the tangential jet No. 2 blade with 0.030-in. jet slot and 2.99% secondary flow ($C_{j_m} = 0.0344$).



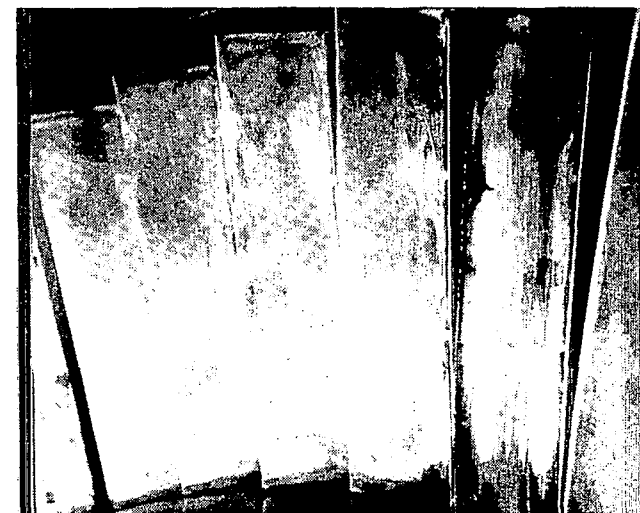
Vane No. 2



Vane No. 3

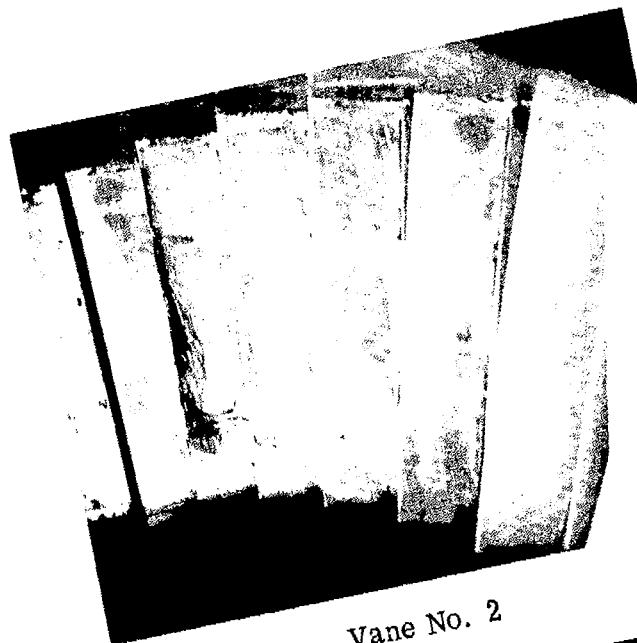


Vane No. 4

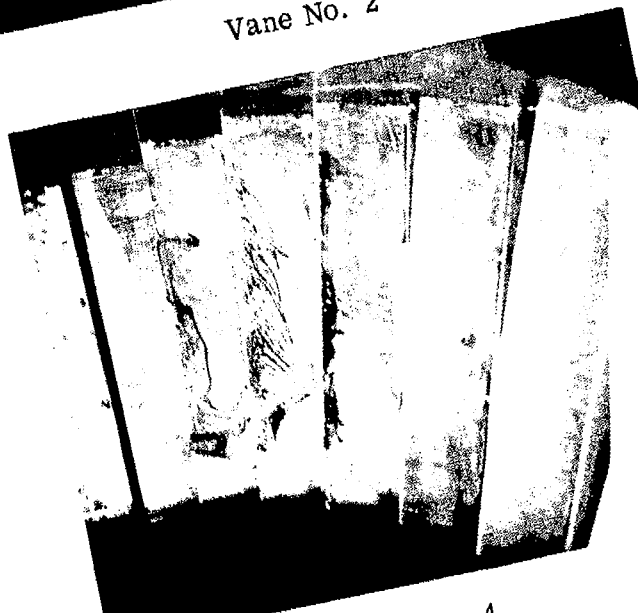


Vane No. 5

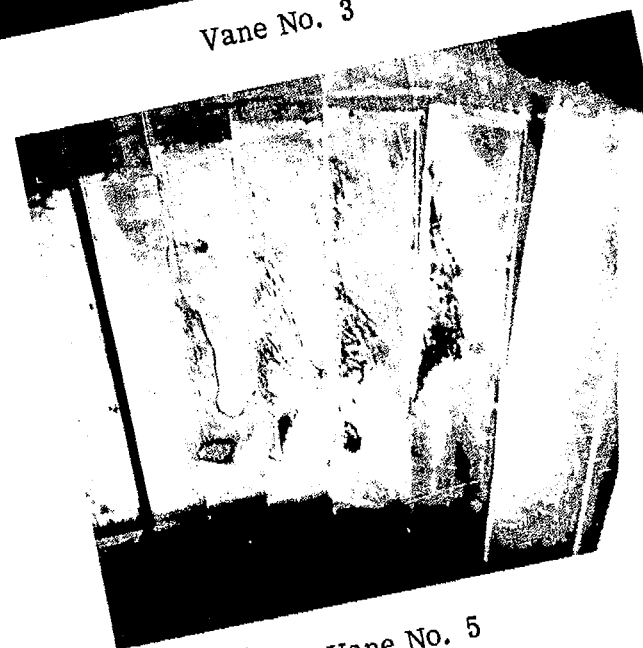
Figure 34. Flow visualization results for the tangential jet No. 2 blade with 0.030-in. jet slot and 4.02% secondary flow ($C_{jm} = 0.0487$).



Vane No. 2

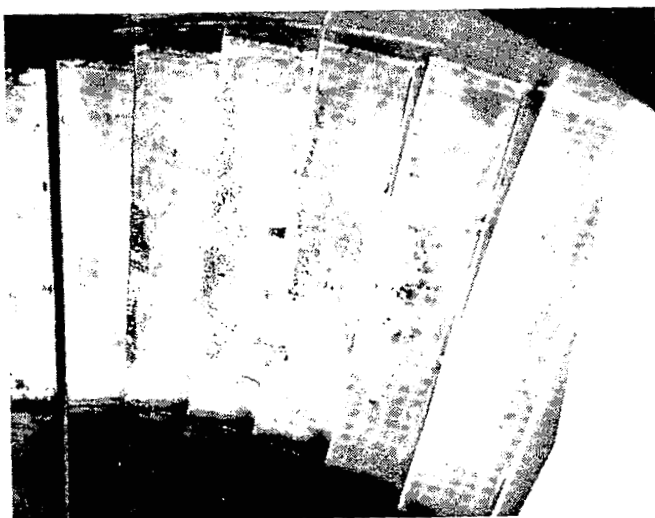


Vane No. 3

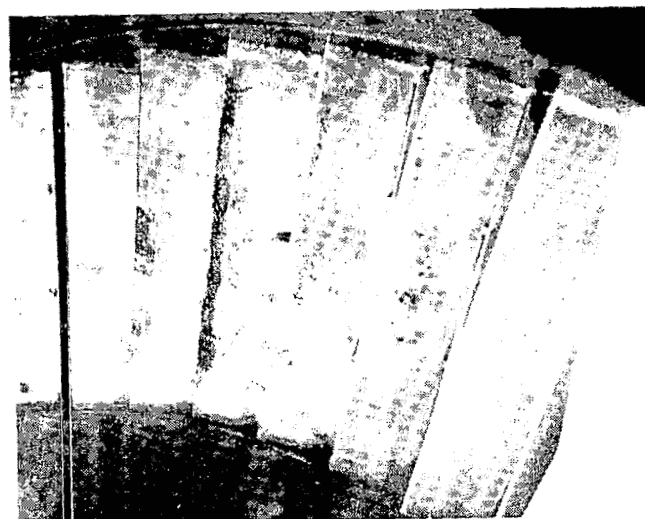


Vane No. 5

the tangential jet No. 2 blade with 0.040-in. jet
- 0.0161).



Vane No. 2



Vane No. 3



Vane No. 4



Vane No. 5

Figure 36. Flow visualization results for the tangential jet No. 2 blade with 0.040-in. jet slot and 3.00% secondary flow ($C_{j_m} = 0.0315$).



Vane No. 2



Vane No. 3



Vane No. 4

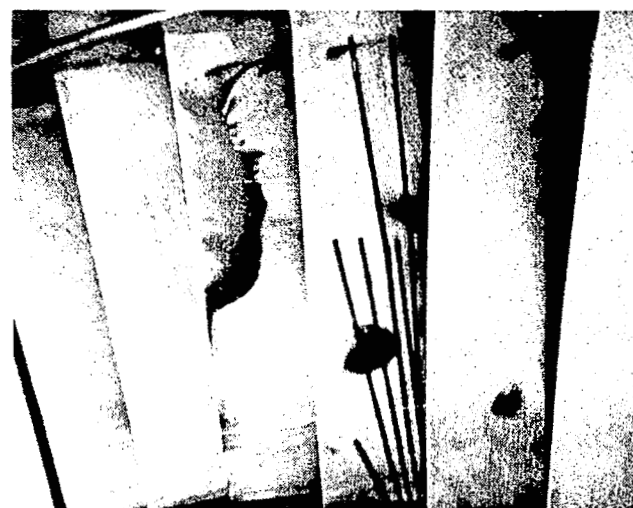


Vane No. 5

Figure 37. Flow visualization results for the tangential jet No. 2 blade with 0.040-in. jet slot and 4.00% secondary flow ($C_{jm} = 0.0483$).



Vane No. 2



Vane No. 3



Vane No. 4



Vane No. 5

Figure 38. Plain blade flow visualization results for inlet hub static-to-total pressure ratio of 0.74 (design value).

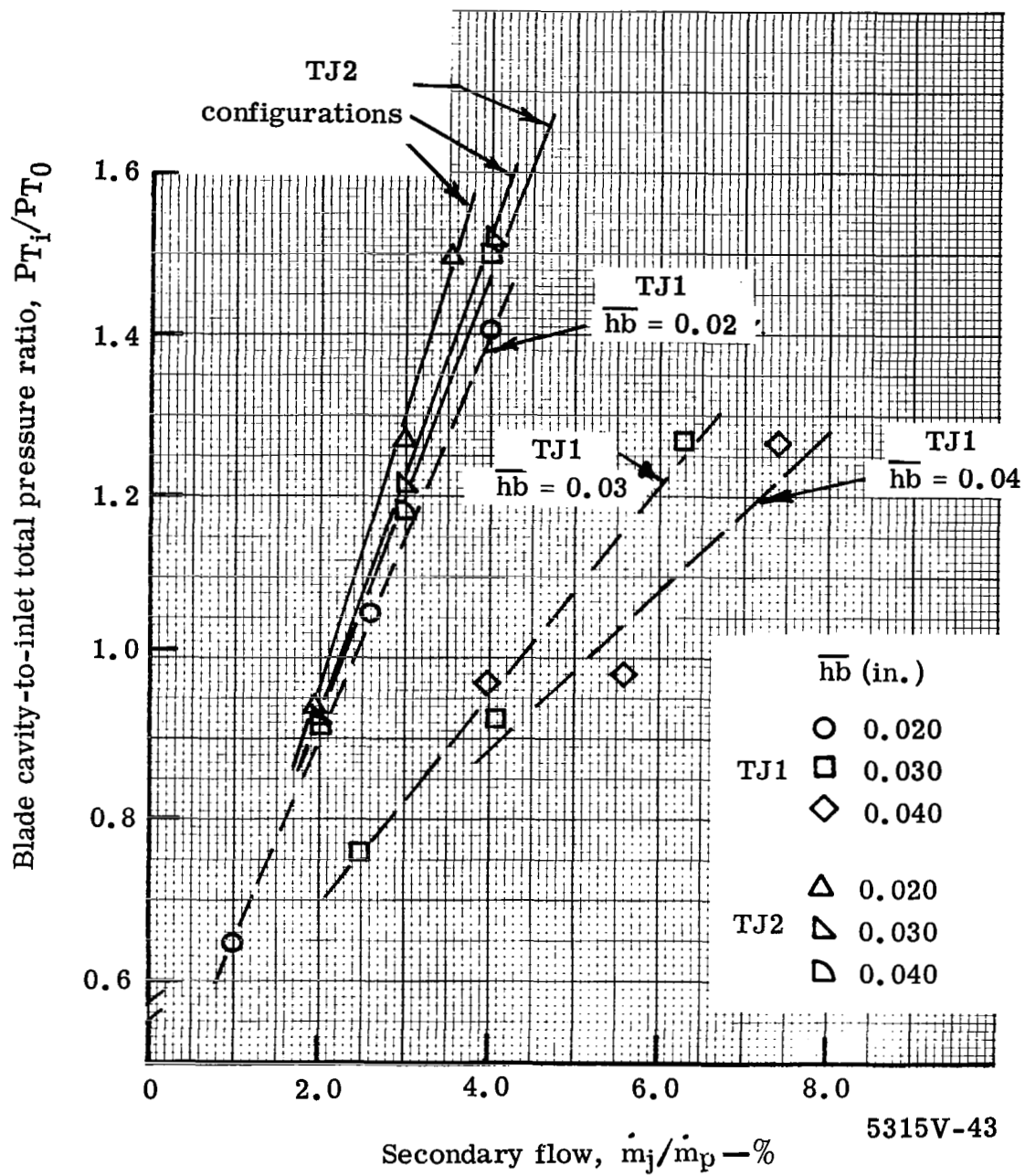


Figure 39. Tangential jet flow as a function of cavity-to-inlet total pressure ratio.

Tangential jet blade No. 1

Tangential jet blade No. 2

	$\bar{h}b$	m_j/m_p
○	0.02	1.00
◐	0.02	2.60
●	0.02	4.00
◻	0.03	2.50
◼	0.03	4.10
■	0.03	6.30
◊	0.04	3.98
◈	0.04	5.62
●	0.04	7.44

	$\bar{h}b$	m_j/m_p
△	0.02	1.96
▲	0.02	3.02
▲	0.02	3.54
◁	0.03	2.01
◁	0.03	2.99
◁	0.03	4.02
◁	0.04	2.00
◁	0.04	3.00
◁	0.04	4.00

TJ1

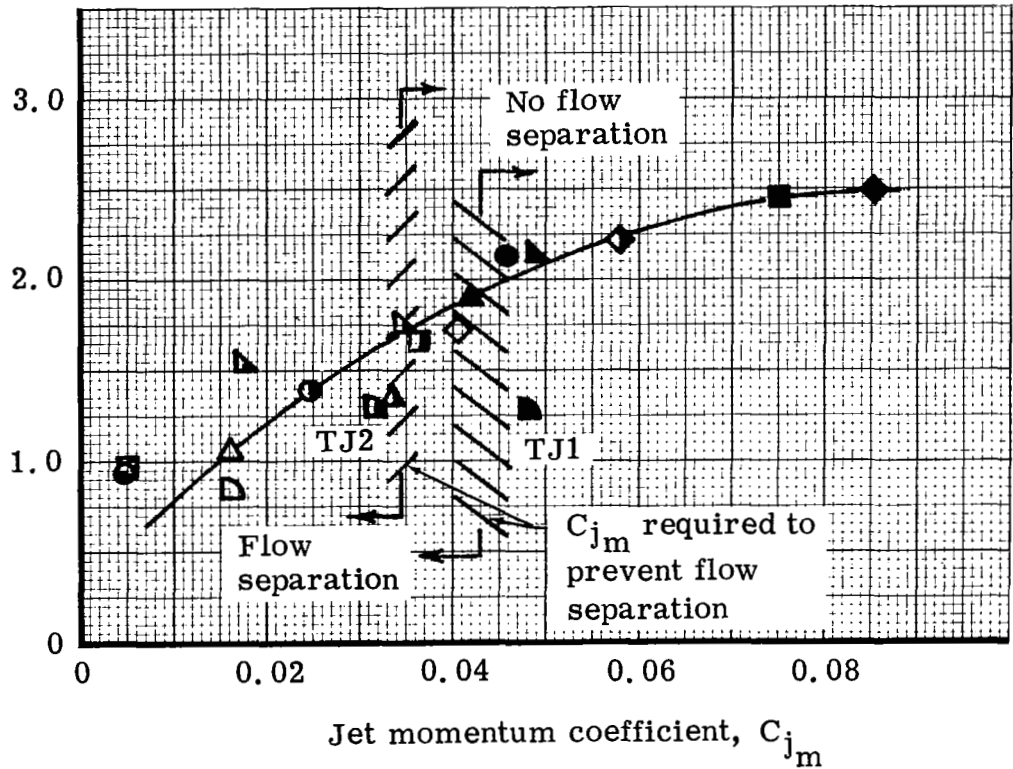
TJ2

ΔX_{ssj-3}

1.345 in.

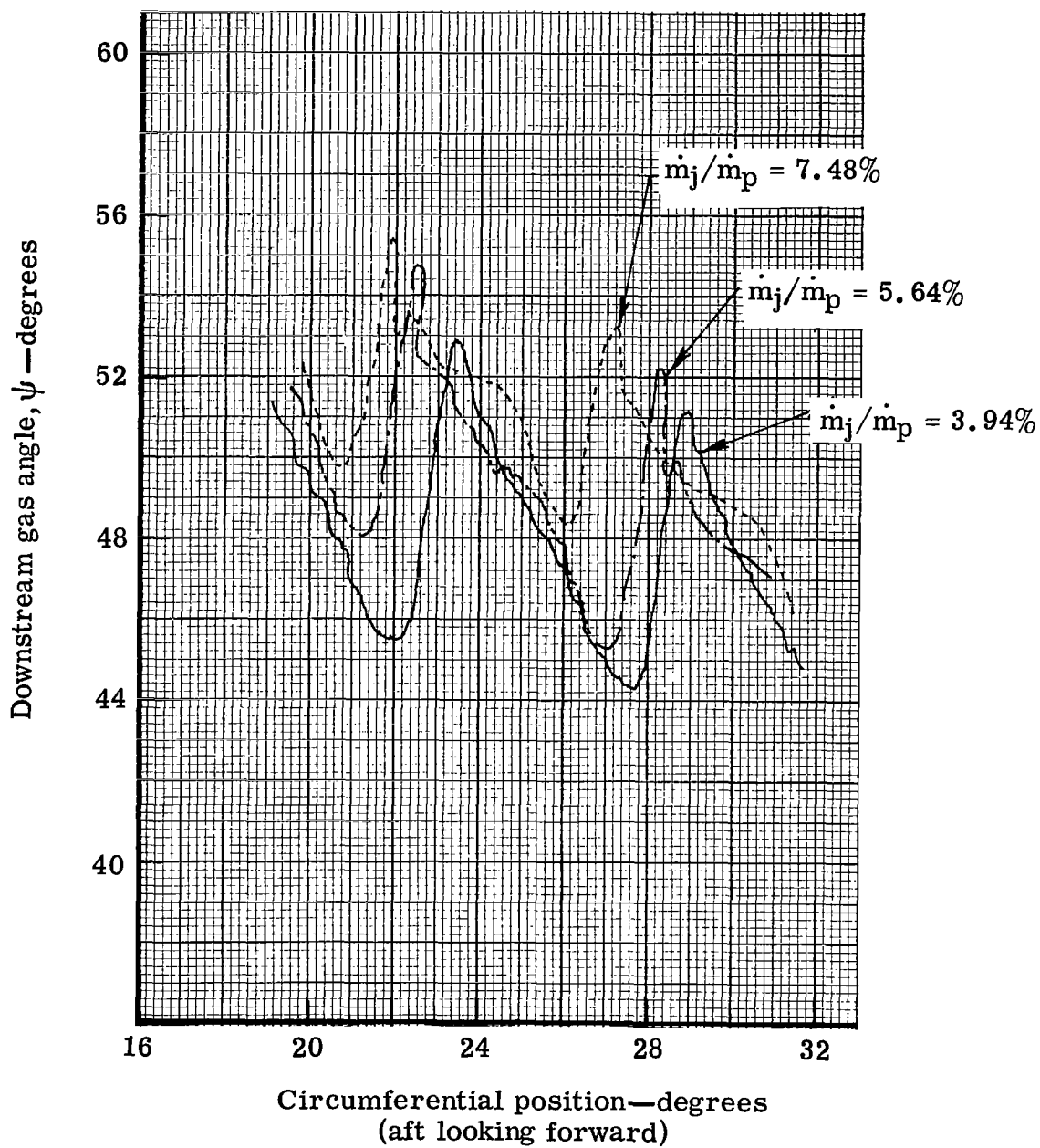
1.027 in.

Jet slot location to trailing edge
developed adverse pressure gradient,
 $P_{stj-3}/\delta_0 \Delta X_{ssj-3} - \text{psia/in.}$



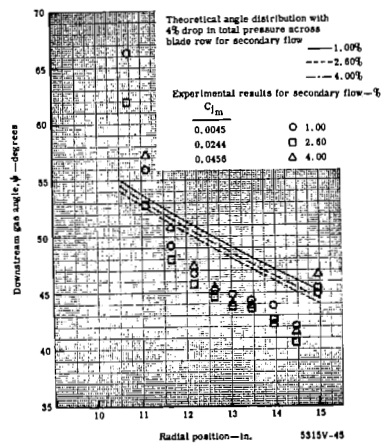
5315V-44

Figure 40. Tangential jet flow requirements to prevent flow separation.

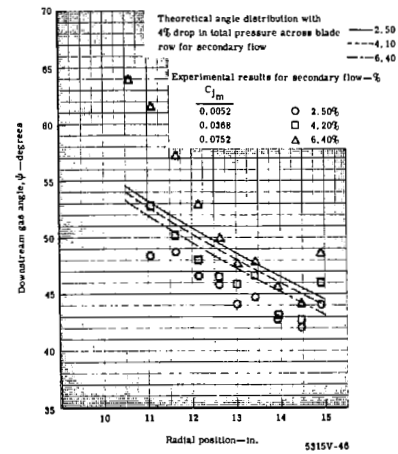


5315V-42

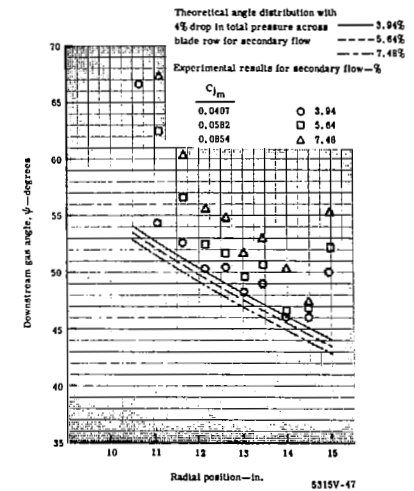
Figure 41. Circumferential variation of tangential jet No. 1 downstream gas angle with secondary flow rate at 13.04-in. radial position and 0.040-in. slot size.



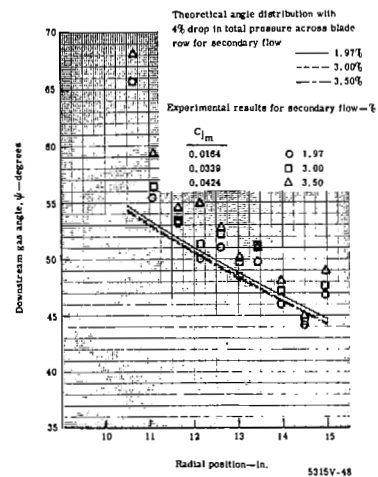
Slot size = 0.020 in.



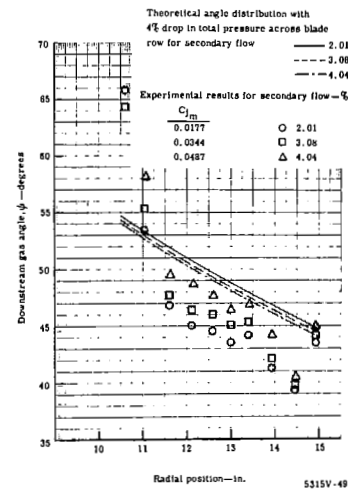
Slot size = 0.030 in.
Tangential jet blade No. 1



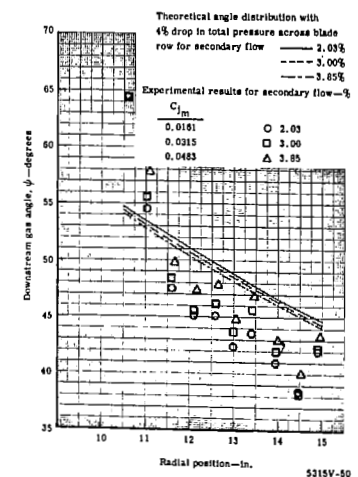
Slot size = 0.040 in.



Slot size = 0.020

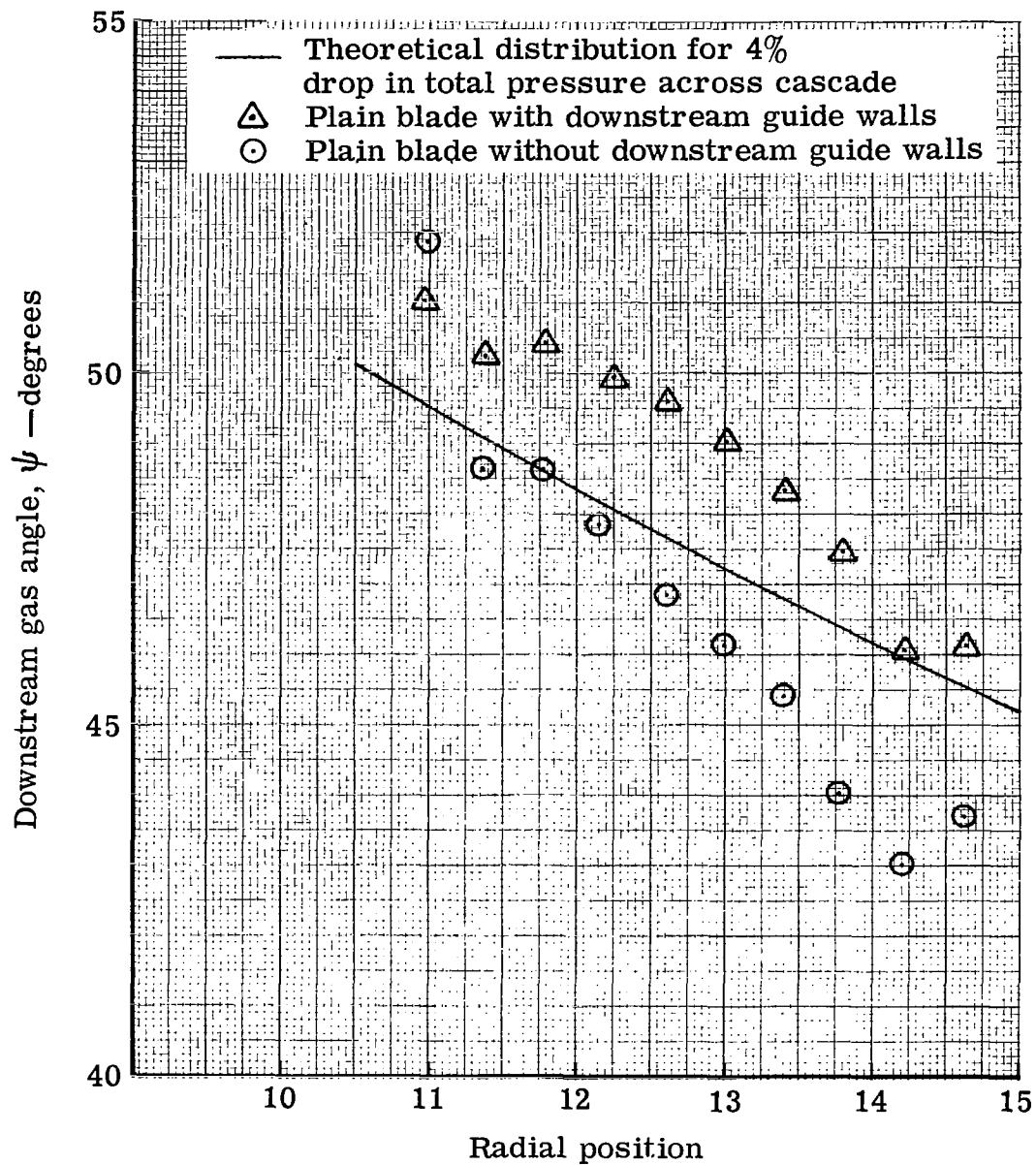


Slot size = 0.030 in.
Tangential jet blade No. 2



Slot size = 0.040 in.

Figure 42. Comparison of measured and predicted radial distribution of downstream gas with secondary flow rate for all tangential jet configurations.



5315-20

Figure 43. Measured and predicted radial variation of the plain blade average downstream gas angle.

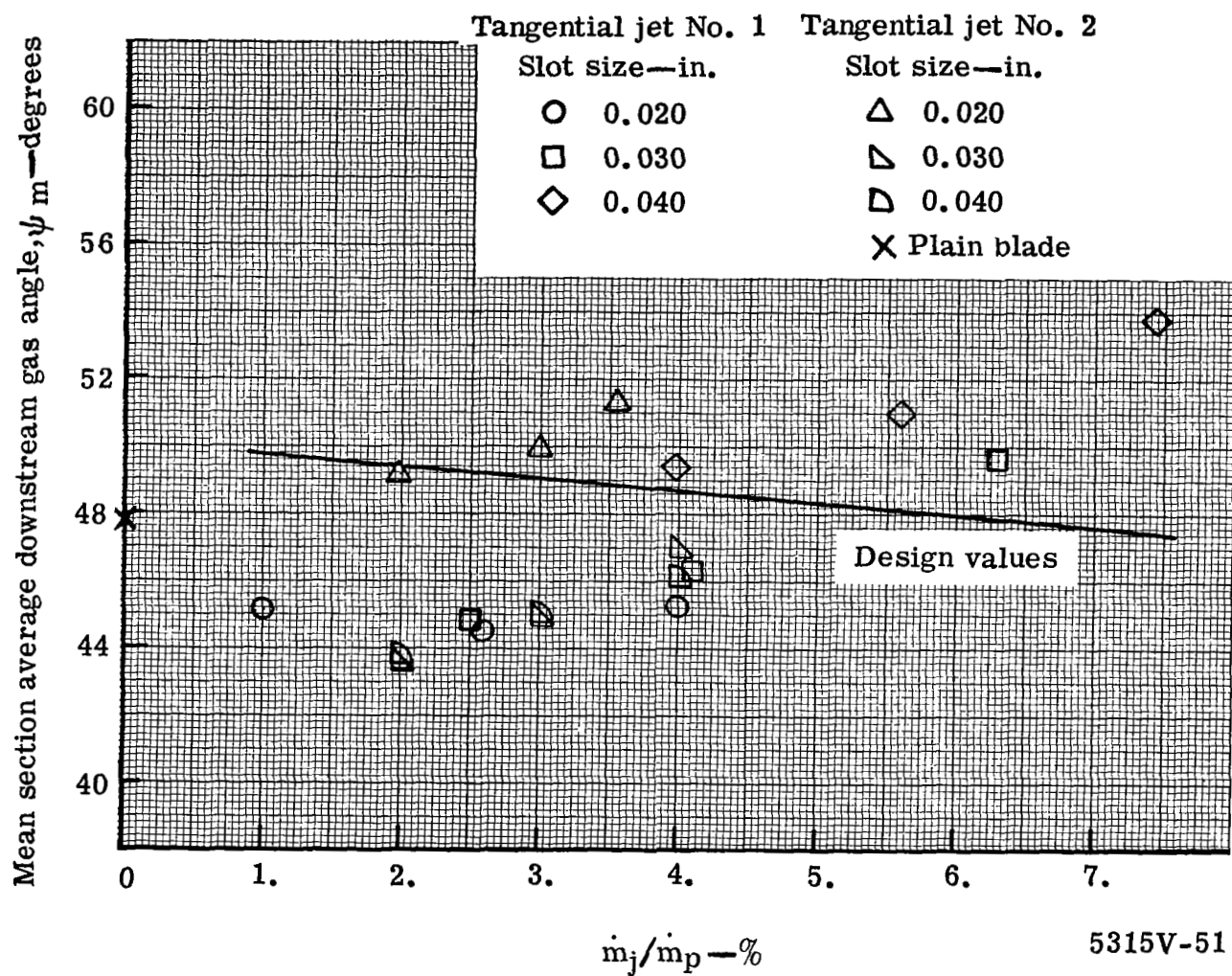


Figure 44. Variation of mean section average gas angle at Station 4 with secondary flow for each blade configuration.

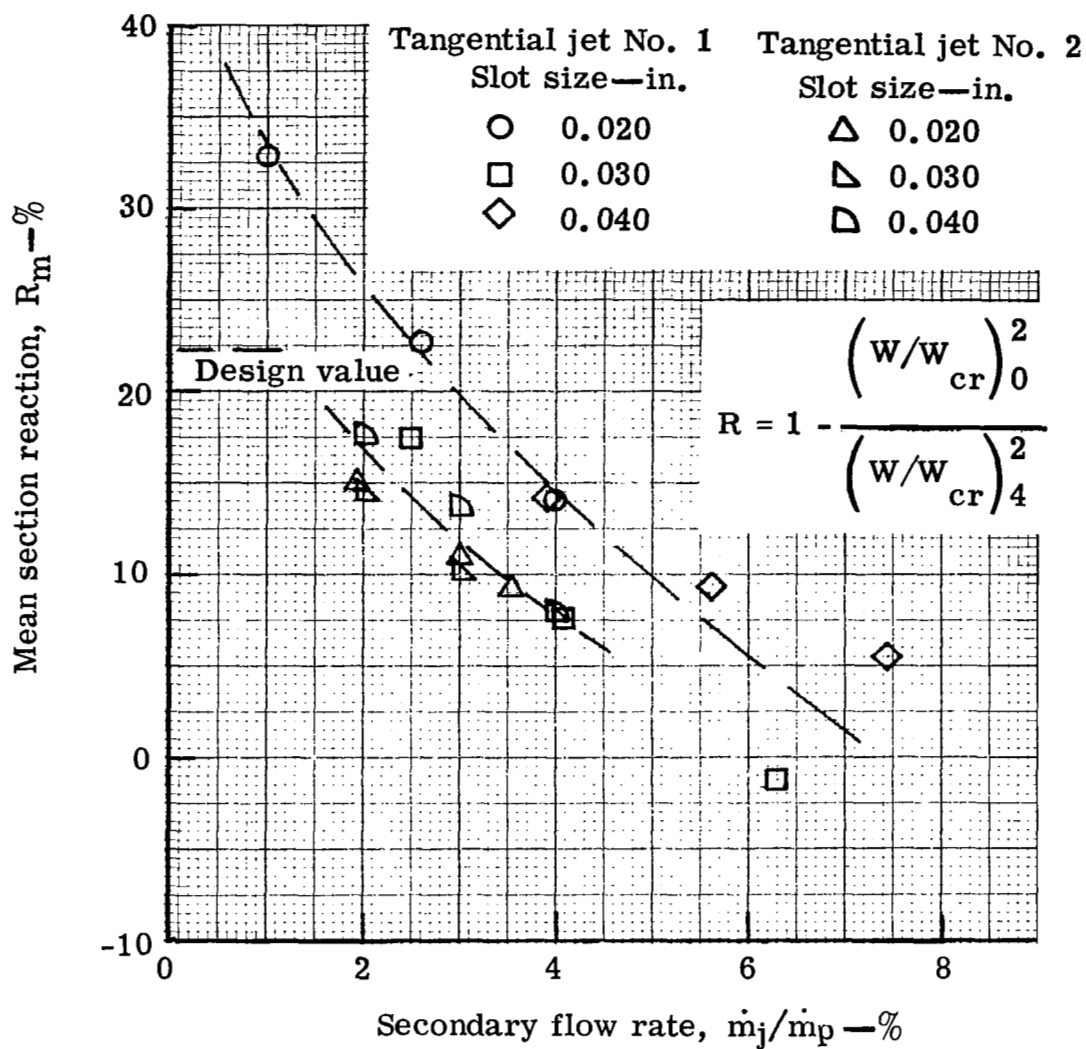
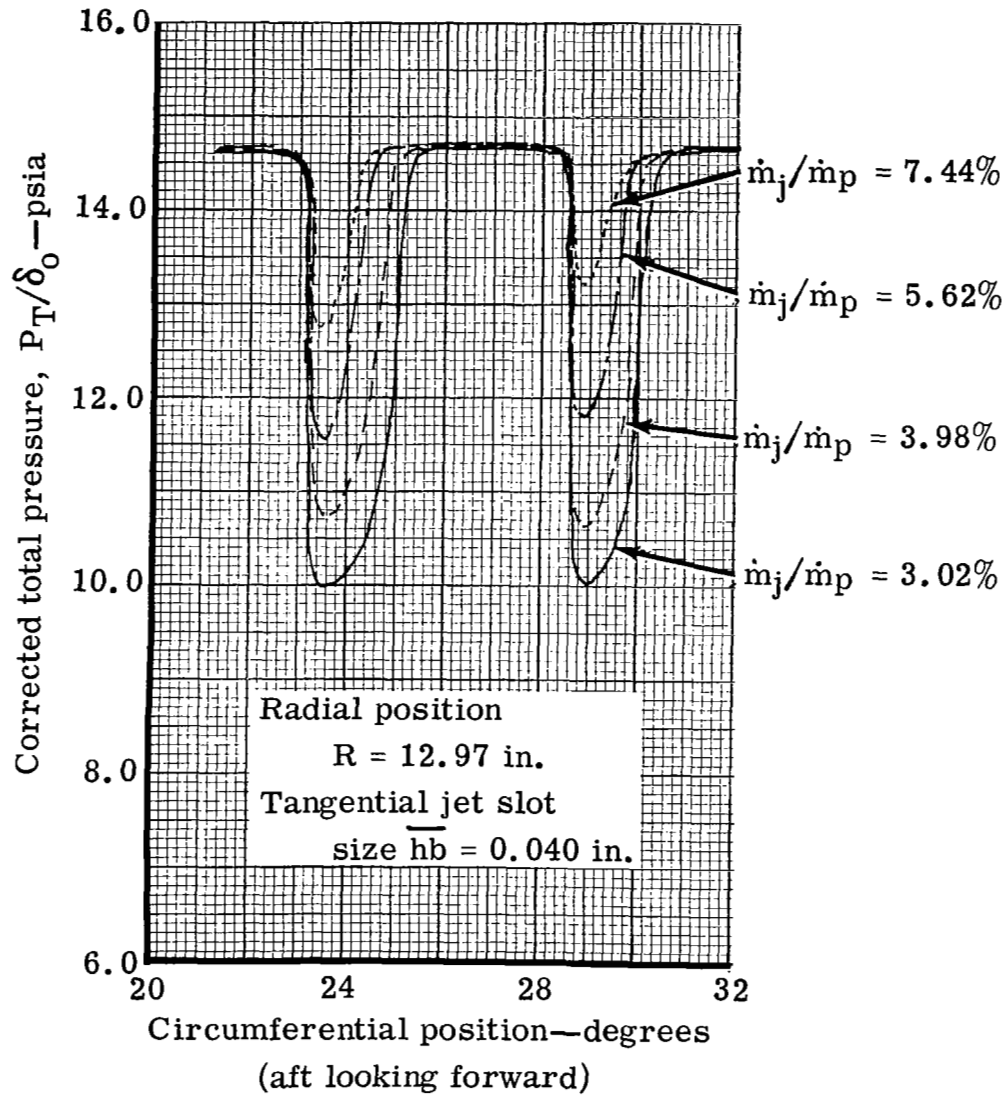


Figure 45. Effect of blade configuration and secondary flow rate or blade row mean section reaction.



5315V-53

Figure 46. Variation of position and shape of tangential jet No. 1 trailing edge wake with increase in the amount of secondary flow.

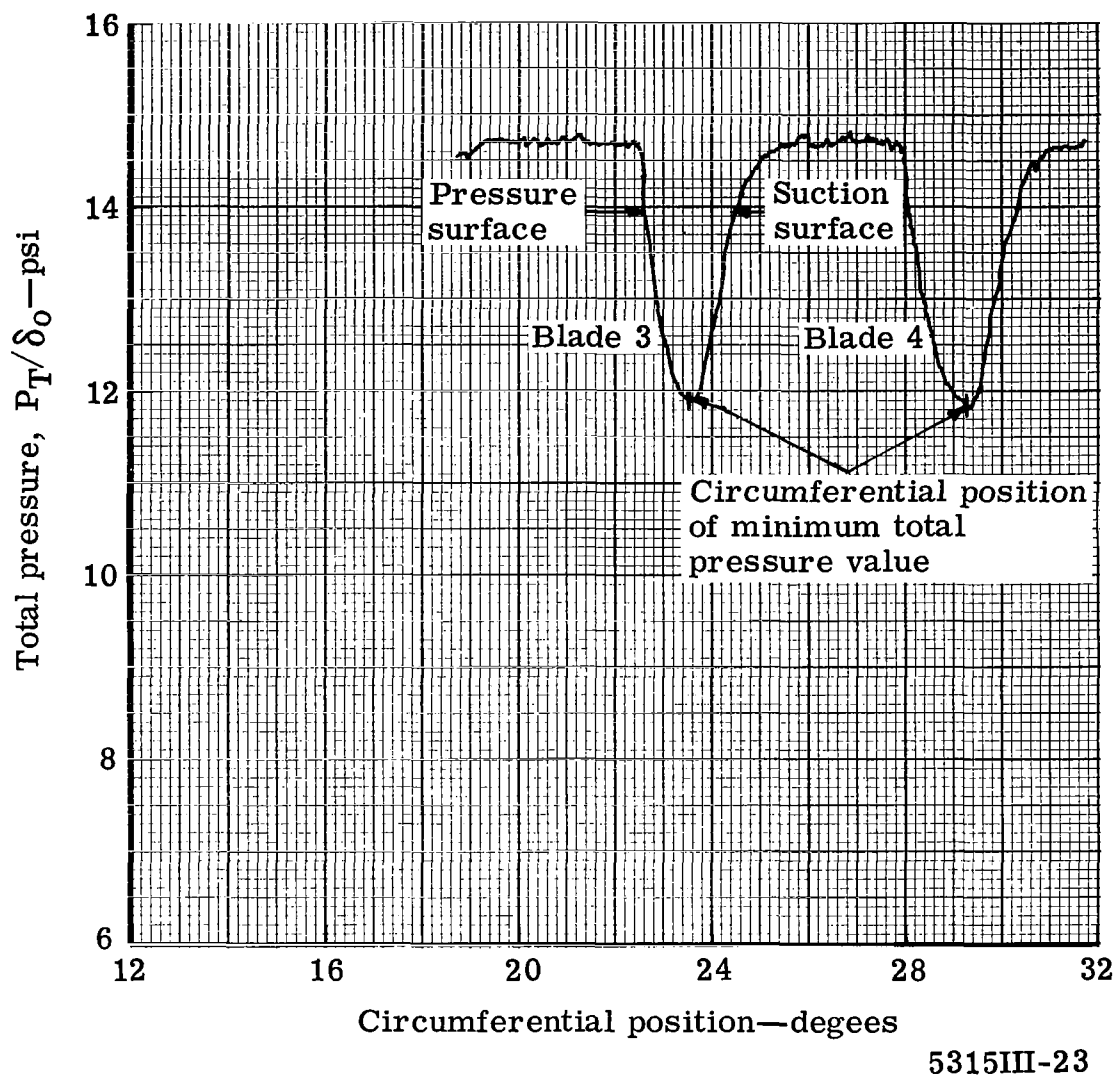
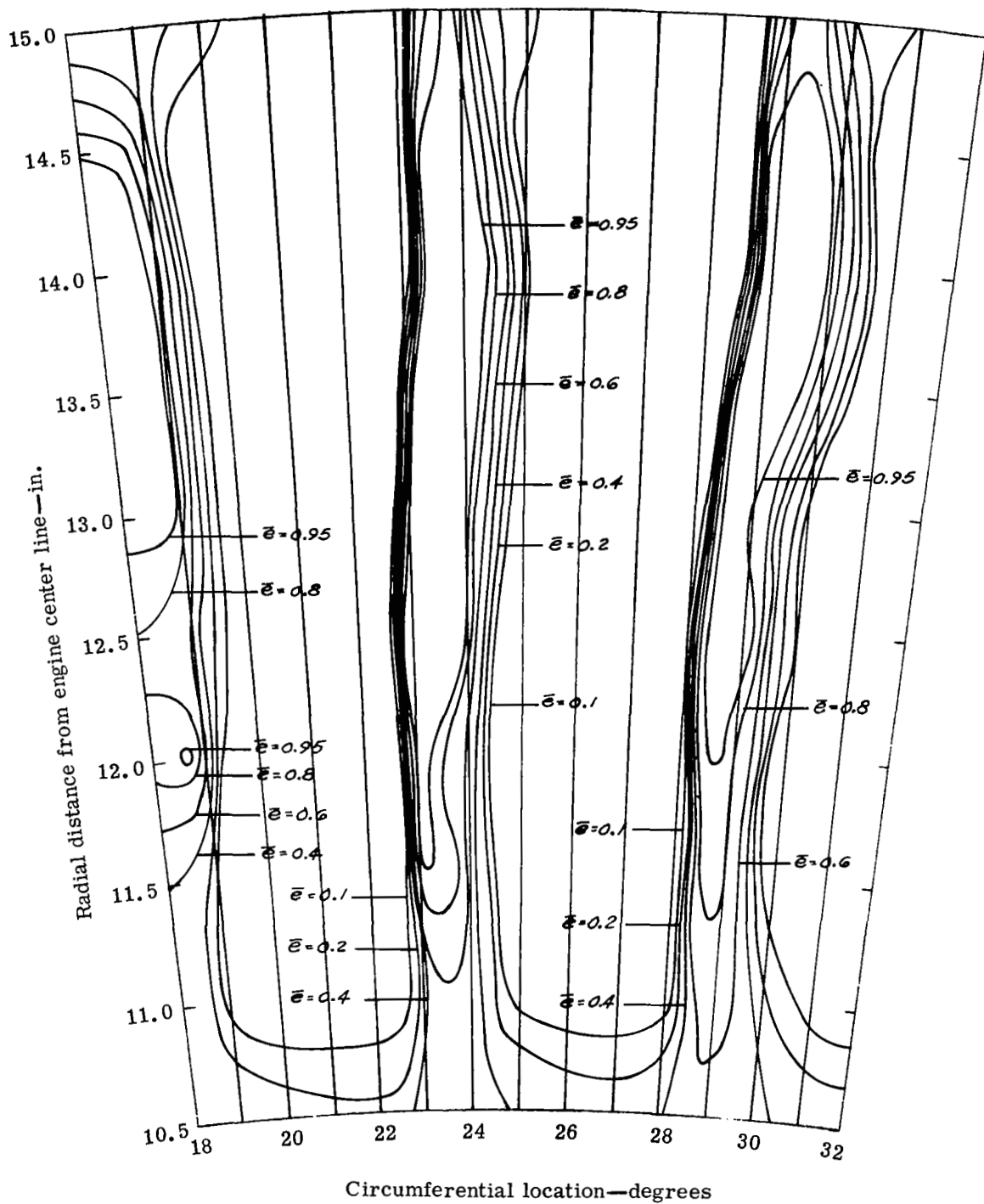
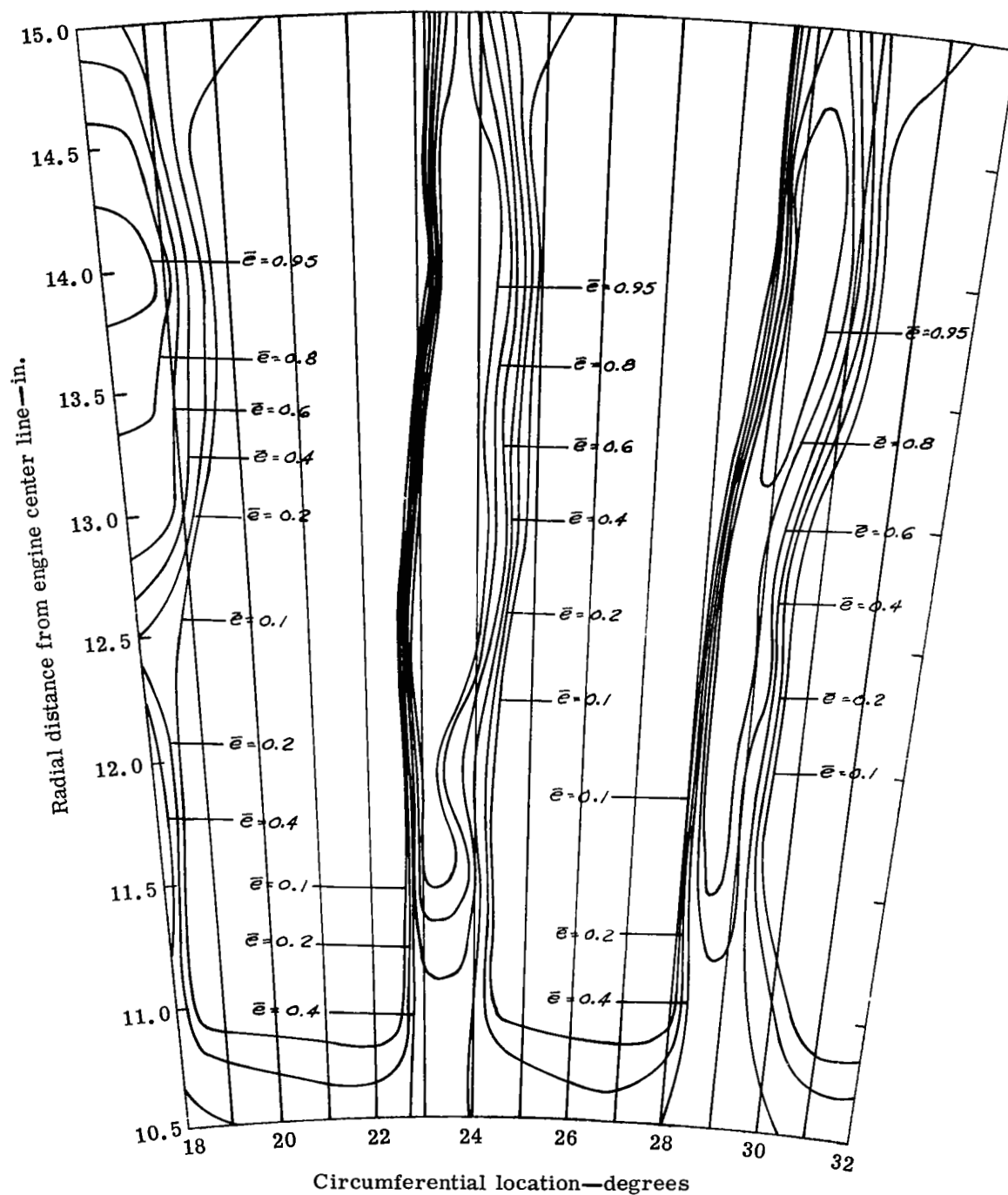


Figure 47. Plain blade exit wake survey total pressure distribution for radial position $R = 12.97$ in.



5315V-54

Figure 48. Contours of kinetic energy loss coefficient across one tangential jet No. 1 blade passage at Station 3 (0.020-in. slot, $\dot{m}_j/\dot{m}_p = 1.00\%$).



5315V-55

Figure 49. Contours of kinetic energy loss coefficient across one tangential jet No. 1 blade passage at Station 3 (0.020-in. slot, $\dot{m}_j/\dot{m}_p = 2.60\%$).

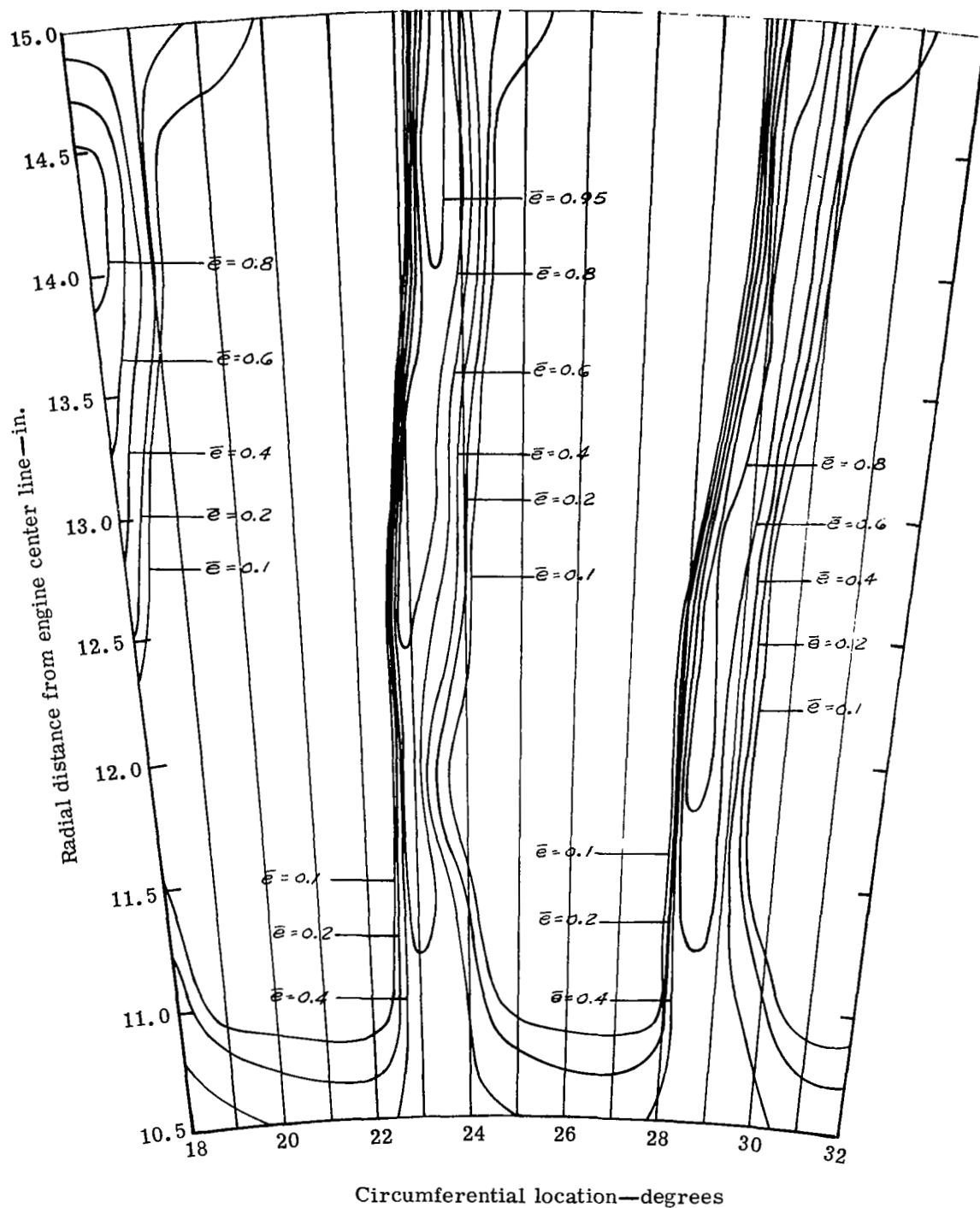


Figure 50. Contours of kinetic energy loss coefficient across one tangential jet blade passage at Station 3 (0.02-in. slot, $\dot{m}_j/\dot{m}_p = 4.00\%$).

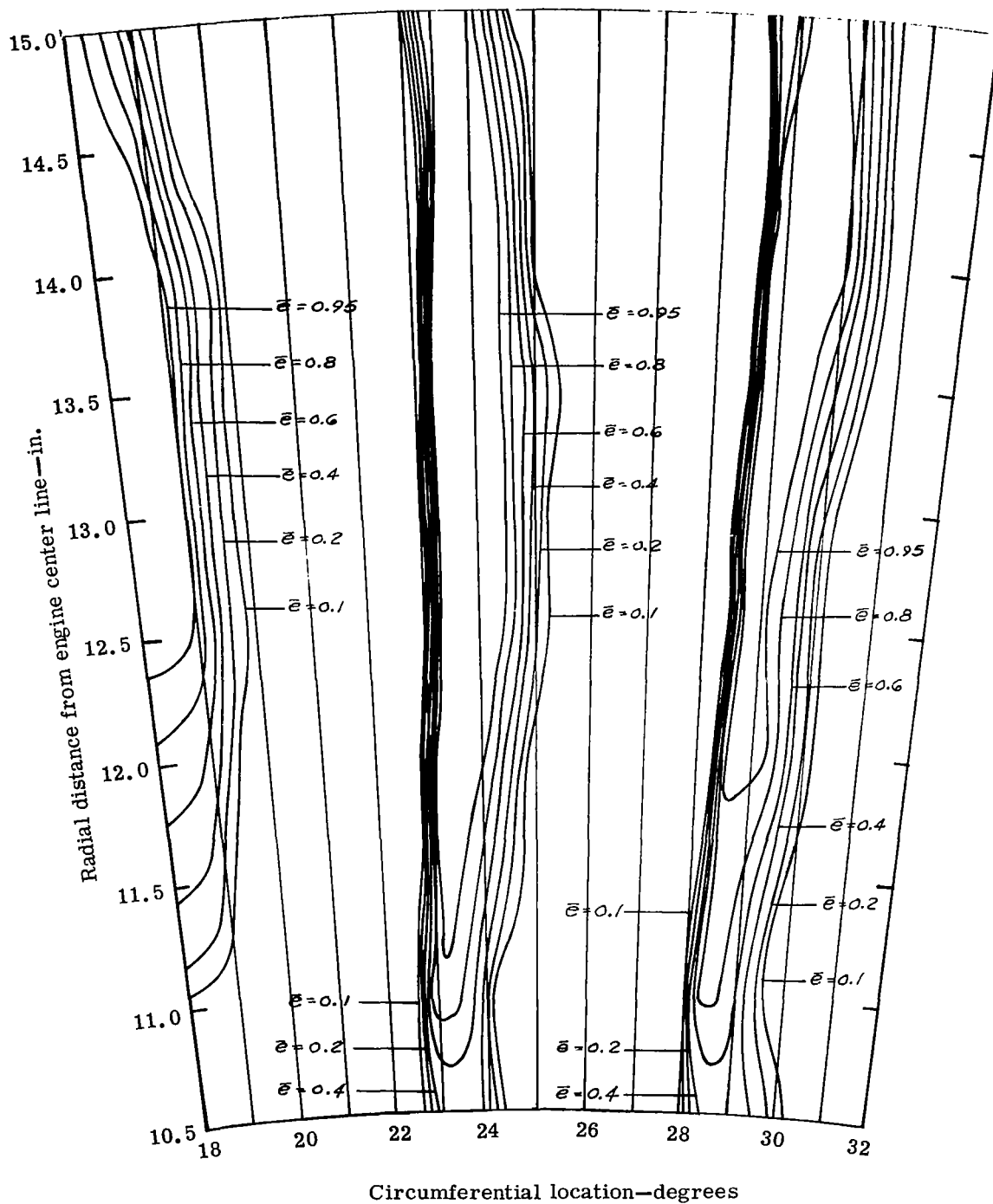


Figure 51. Contours of kinetic energy loss coefficient across one tangential jet No. 1 blade passage at Station 3 (0.030-in. slot, $\dot{m}_j/\dot{m}_p = 2.50\%$).

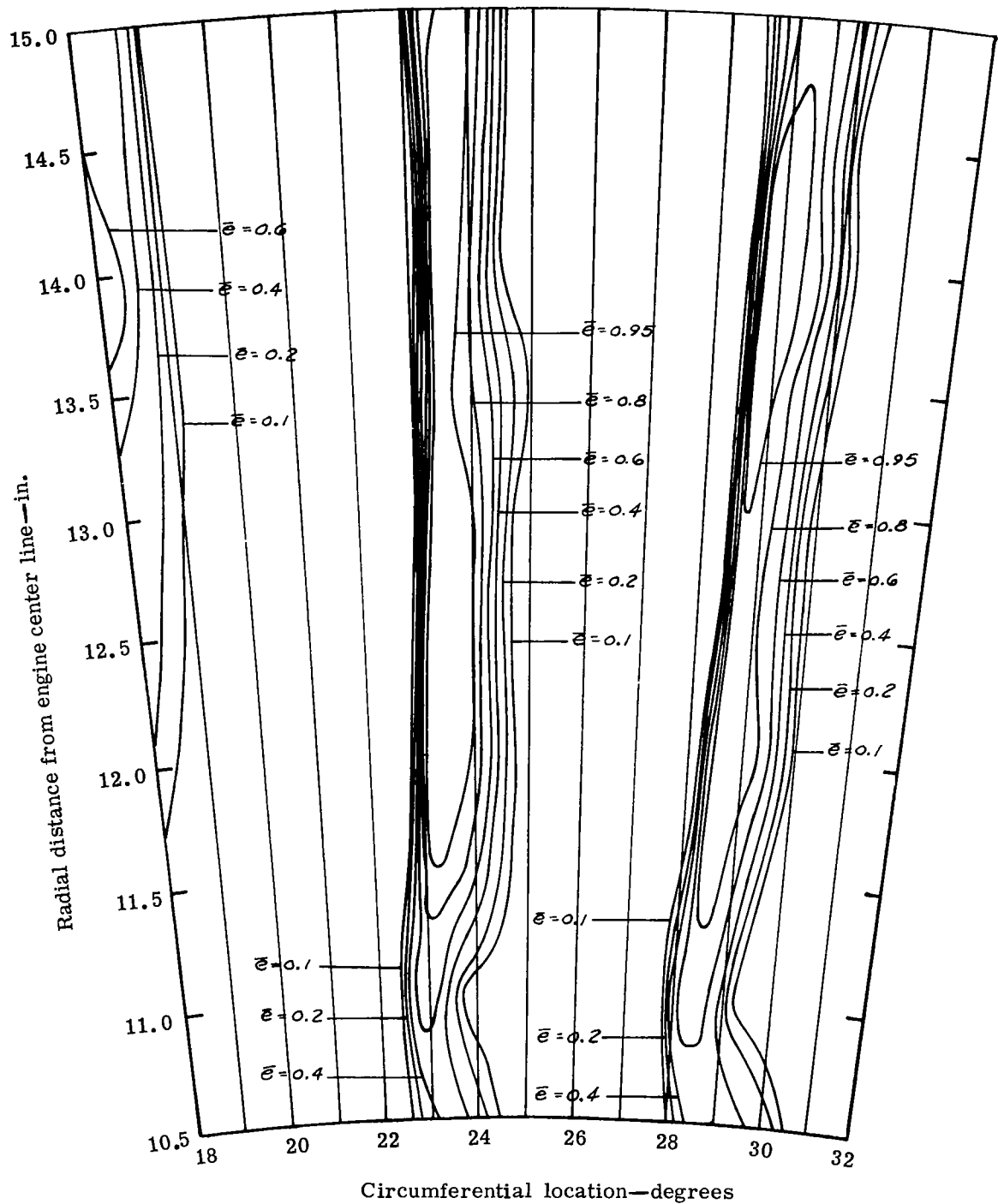
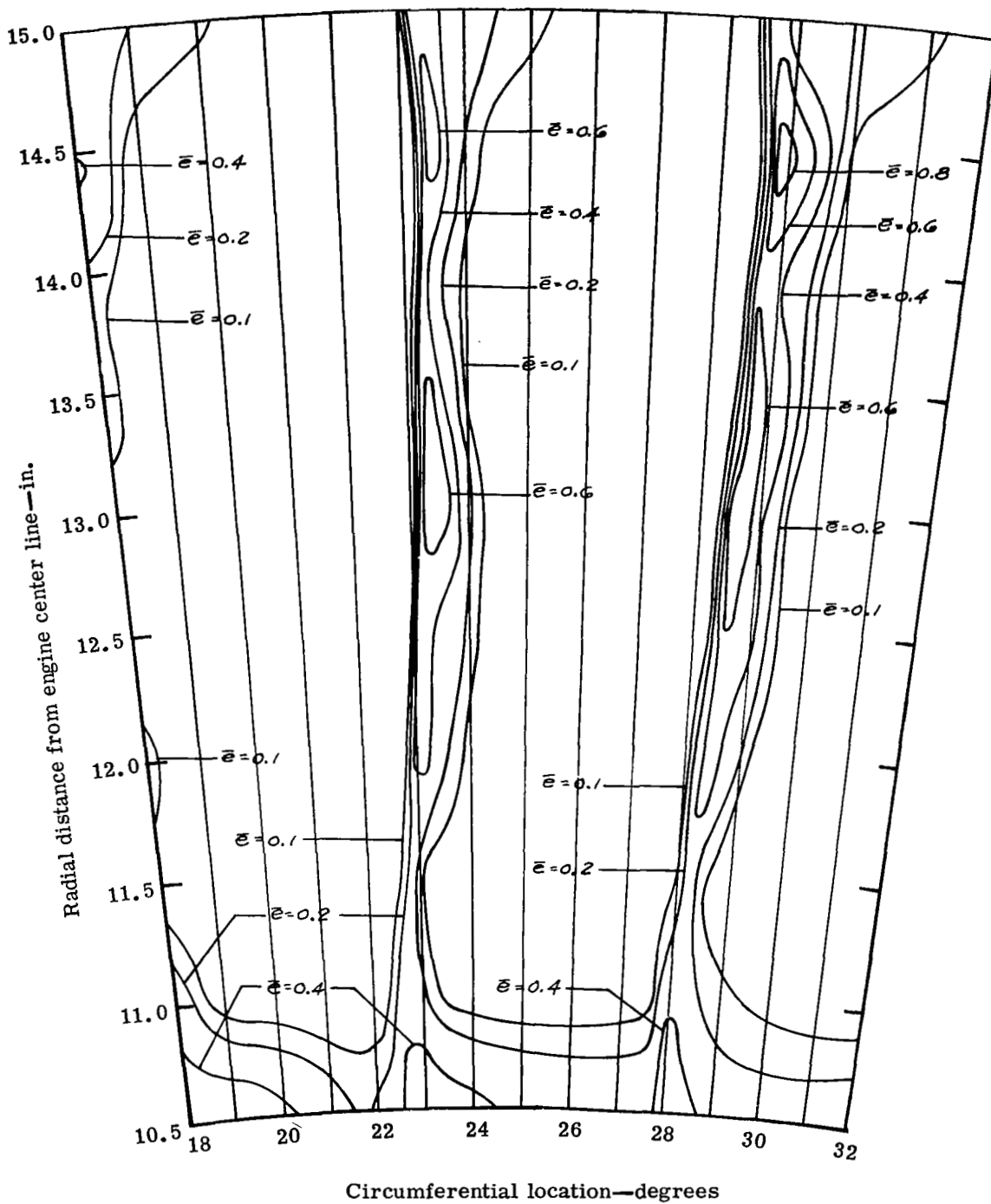
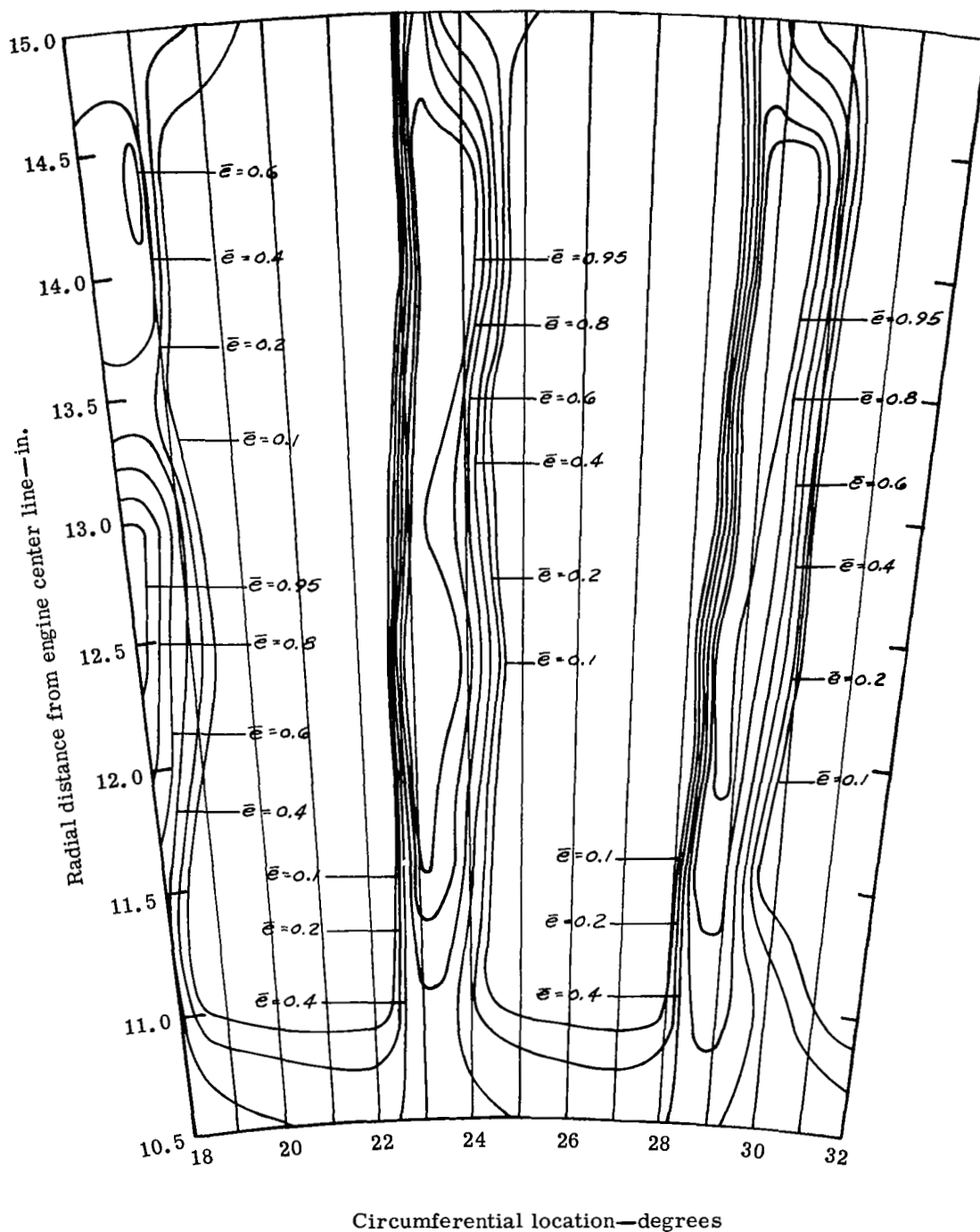


Figure 52. Contours of kinetic energy loss coefficient across one tangential jet No. 1 blade passage at Station 3 (0.030-in. slot, $\dot{m}_j/\dot{m}_p = 4.10\%$).



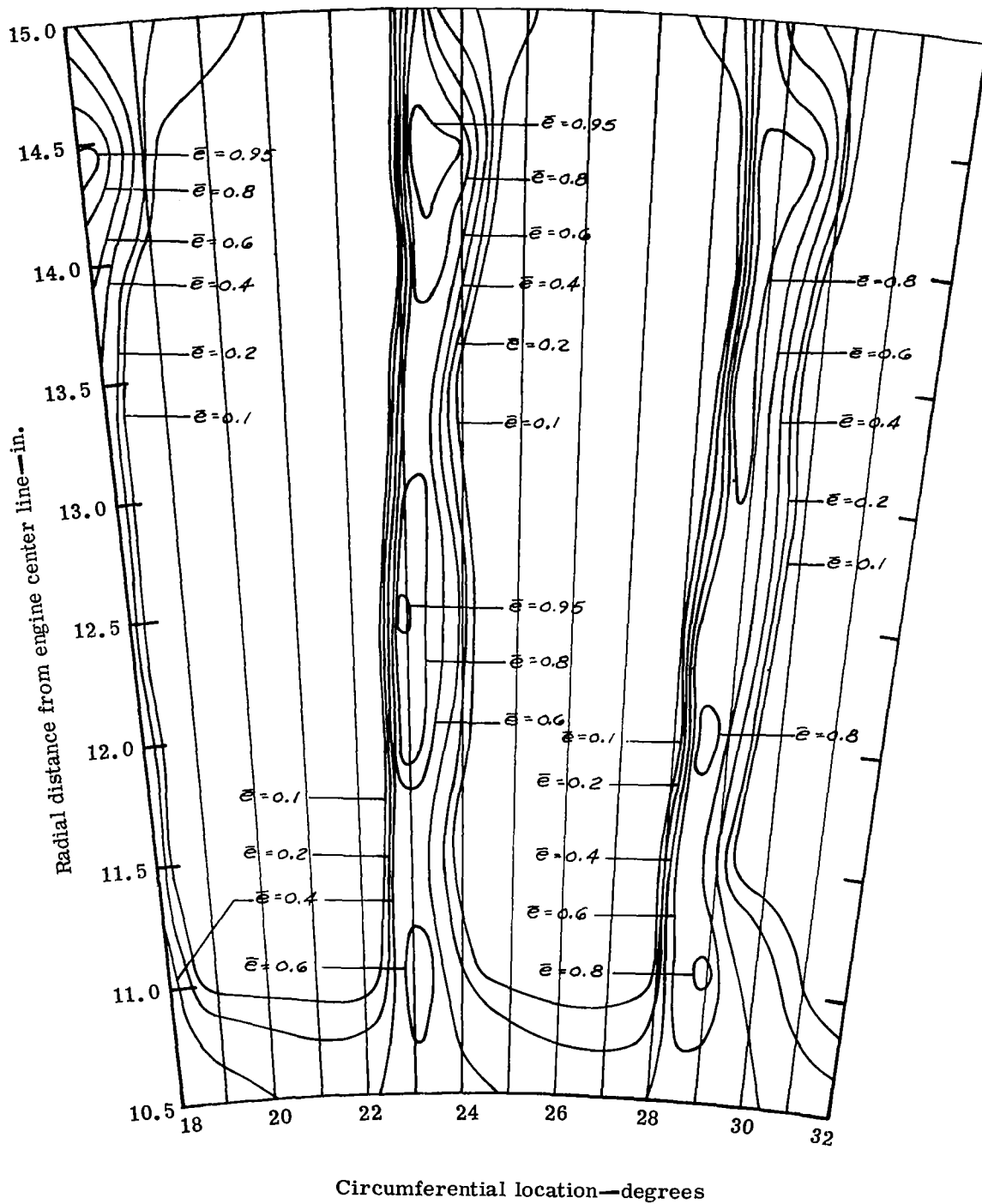
5315V-59

Figure 53. Contours of kinetic energy loss coefficient across one tangential jet No. 1 blade passage at Station 3 (0.030-in. slot, $\dot{m}_j/\dot{m}_p = 6.30\%$).



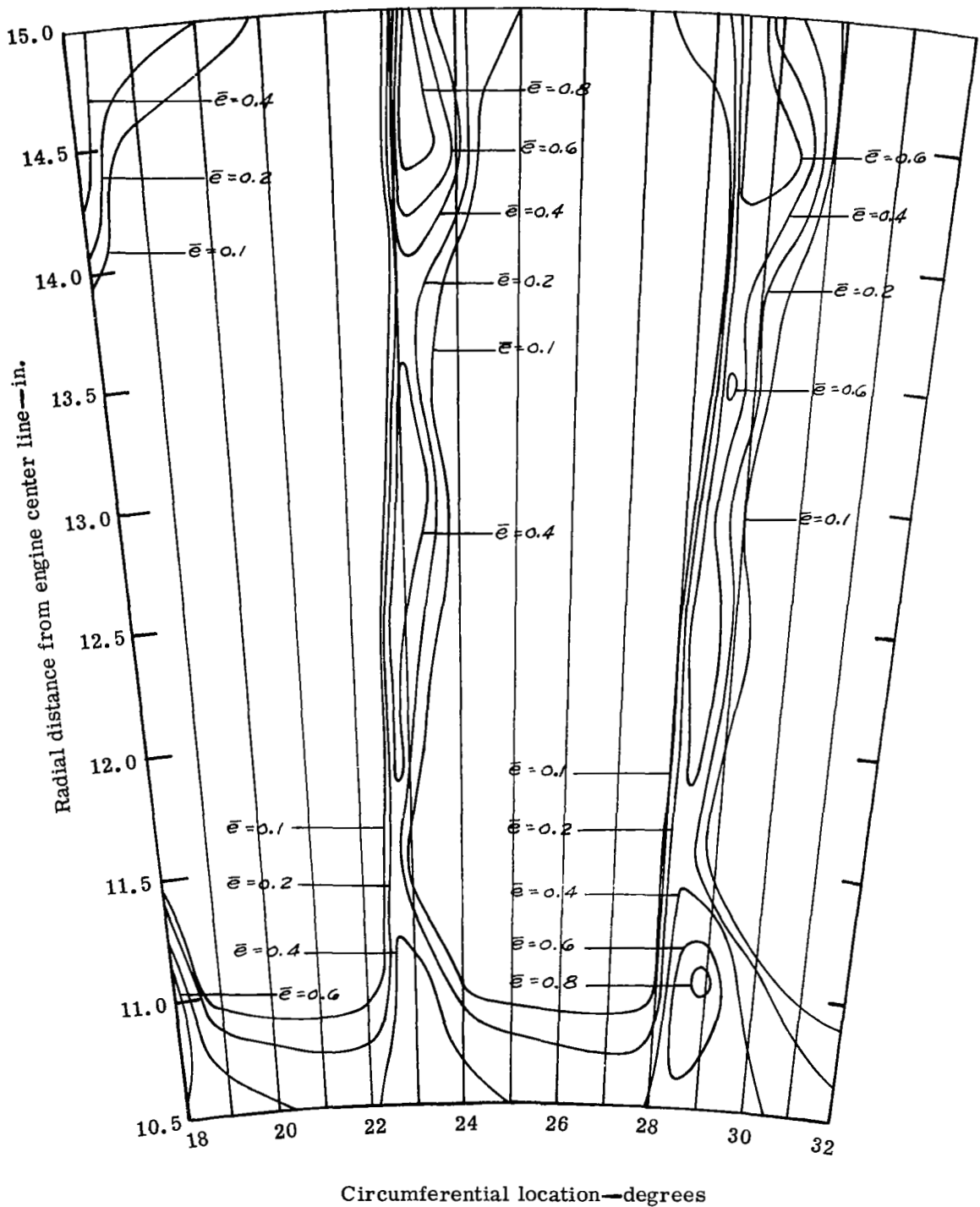
5315V-60

Figure 54. Contours of kinetic energy loss coefficient across one tangential jet No. 1 blade passage at Station 3 (0.040-in. slot, $\dot{m}_j/\dot{m}_p = 3.98\%$).



5315V-61

Figure 55. Contours of kinetic energy loss coefficient across one tangential jet No. 1 blade passage at Station 3 (0.040-in. slot, $\dot{m}_j/\dot{m}_p = 5.62\%$).



5315V-62

Figure 56. Contours of kinetic energy loss coefficient across one tangential jet No. 1 blade passage at Station 3 (0.040-in. slot, $\dot{m}_j/\dot{m}_p = 7.44\%$).

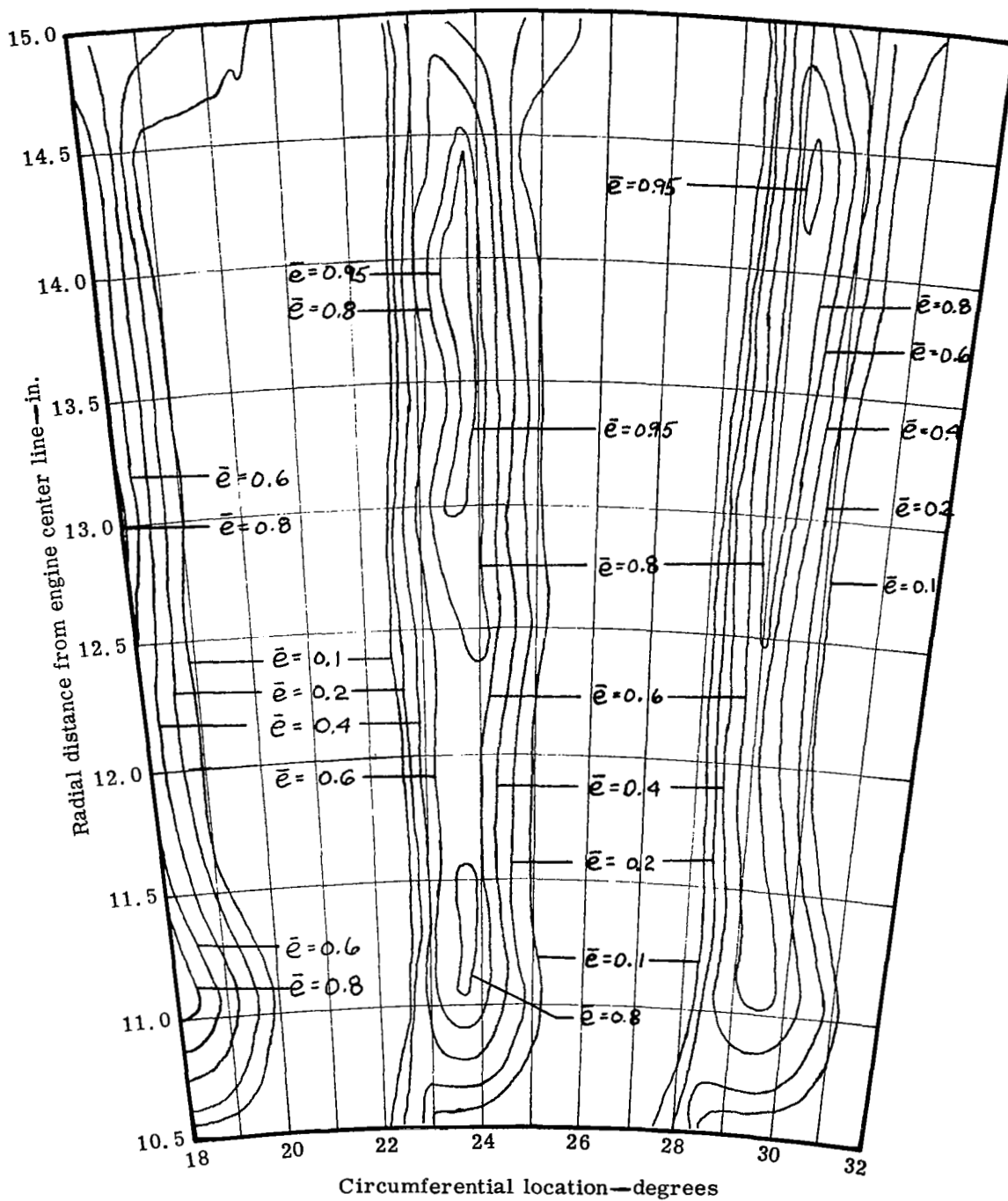
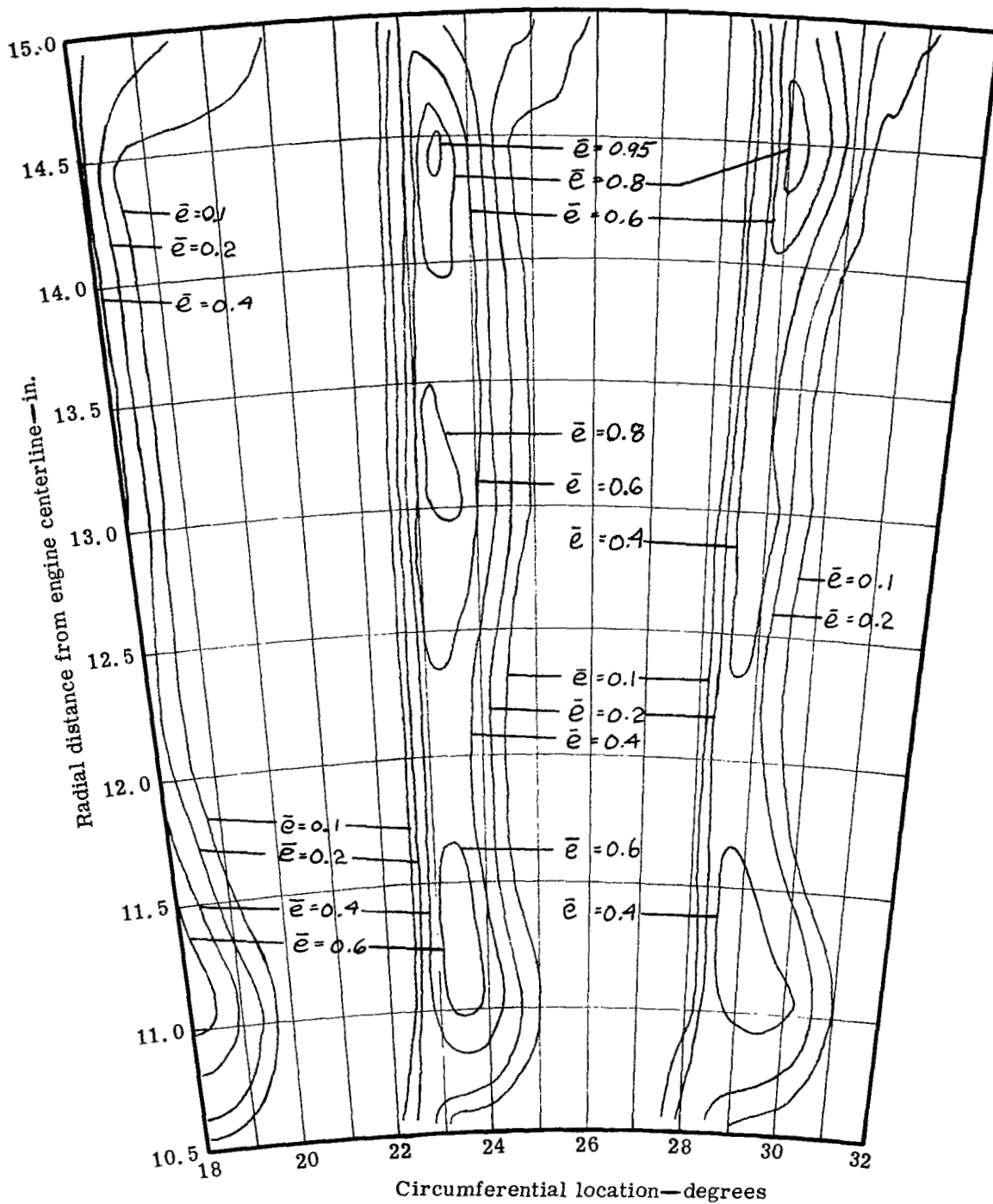
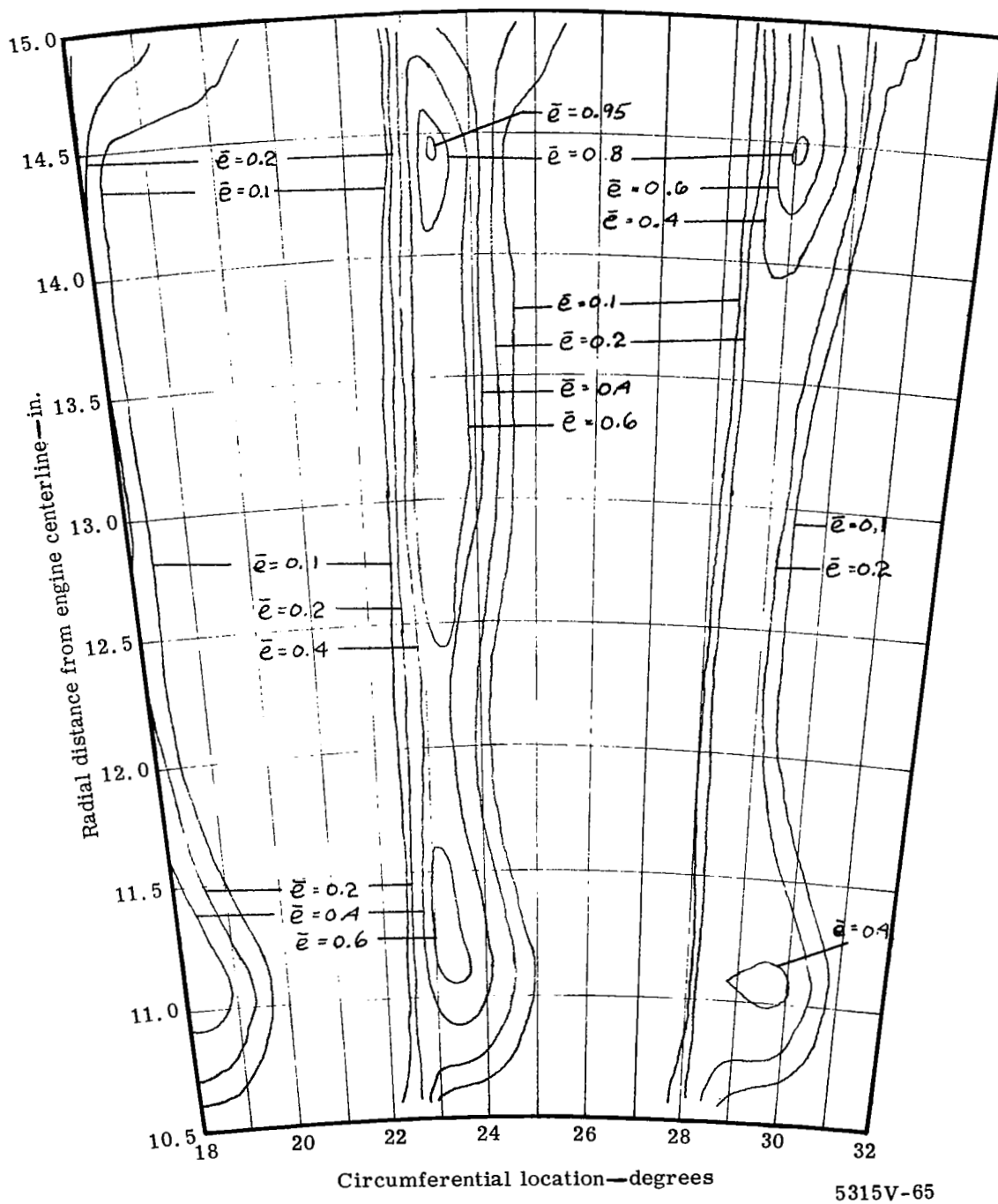


Figure 57. Contours of kinetic energy loss coefficient across one tangential jet No. 2 blade passage at Station 3 (0.020-in. slot and $\dot{m}_j/\dot{m}_p = 1.96\%$).



5315V-64

Figure 58. Contours of kinetic energy loss coefficient across one tangential jet No. 2 blade passage at Station 3 (0.020-in. slot and $\dot{m}_j/\dot{m}_p = 3.02\%$).



5315V-65

Figure 59. Contours of kinetic energy loss coefficient across one tangential jet No. 2 blade passage at Station 3 (0.020-in. slot and $\dot{m}_j/\dot{m}_p = 3.54\%$).

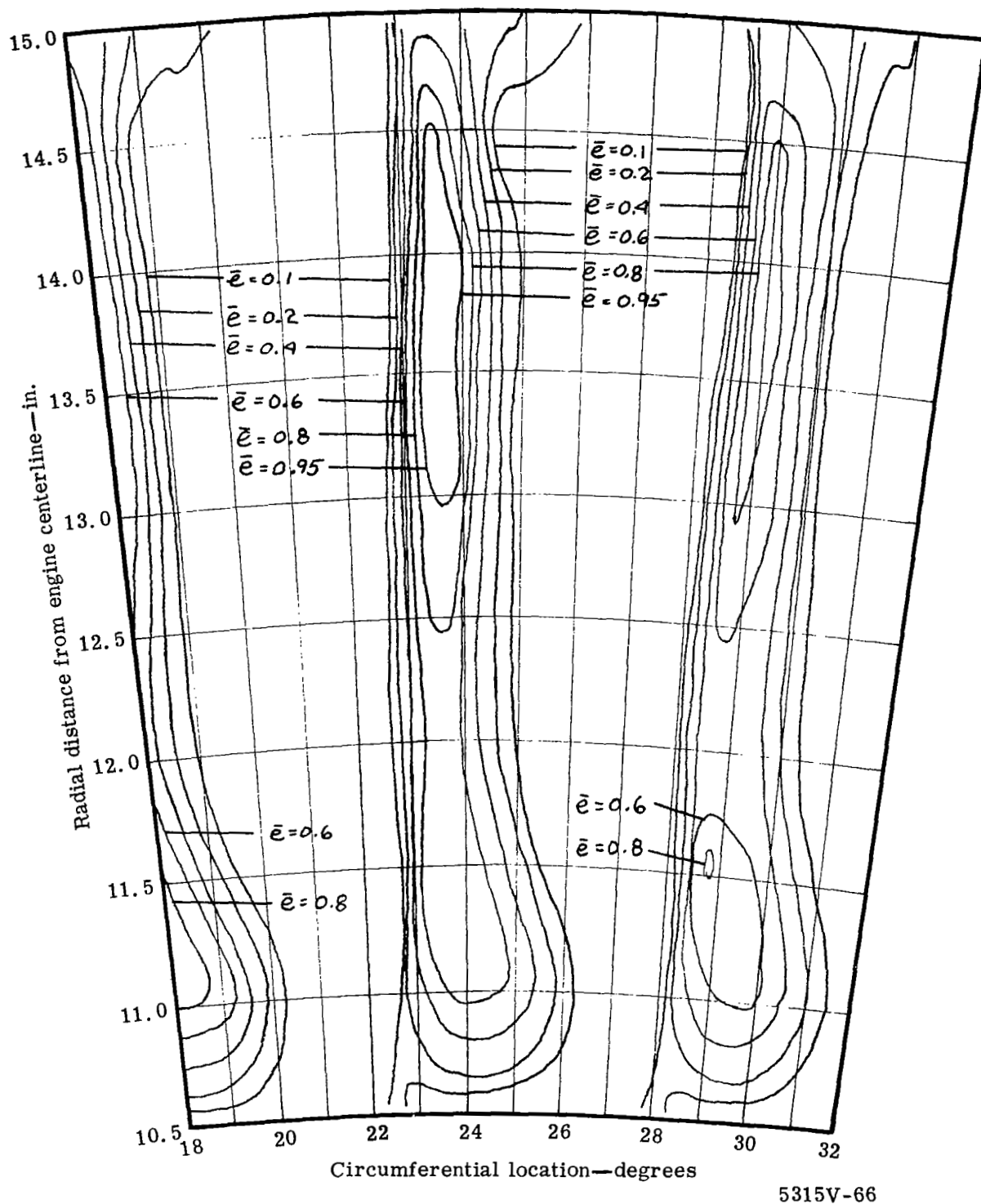
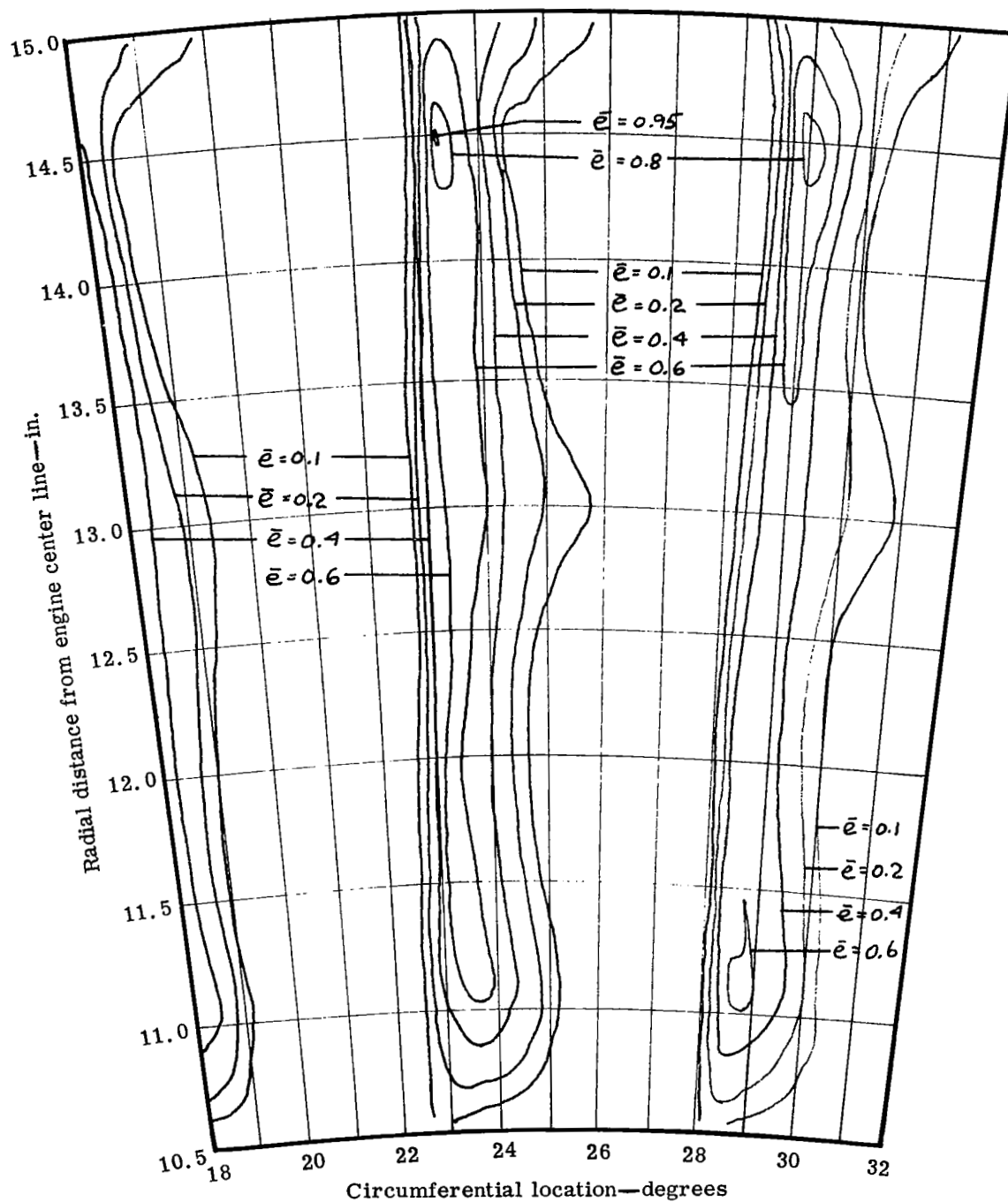


Figure 60. Contours of kinetic energy loss coefficient across one tangential jet No. 2 blade passage at Station 3 (0.030-in. slot and $\dot{m}_j/\dot{m}_p = 2.0\%$).



5315V-67

Figure 61. Contours of kinetic energy loss coefficient across one tangential jet No. 2 blade passage at Station 3 (0.030-in. slot and $\dot{m}_j/\dot{m}_p = 2.99\%$).

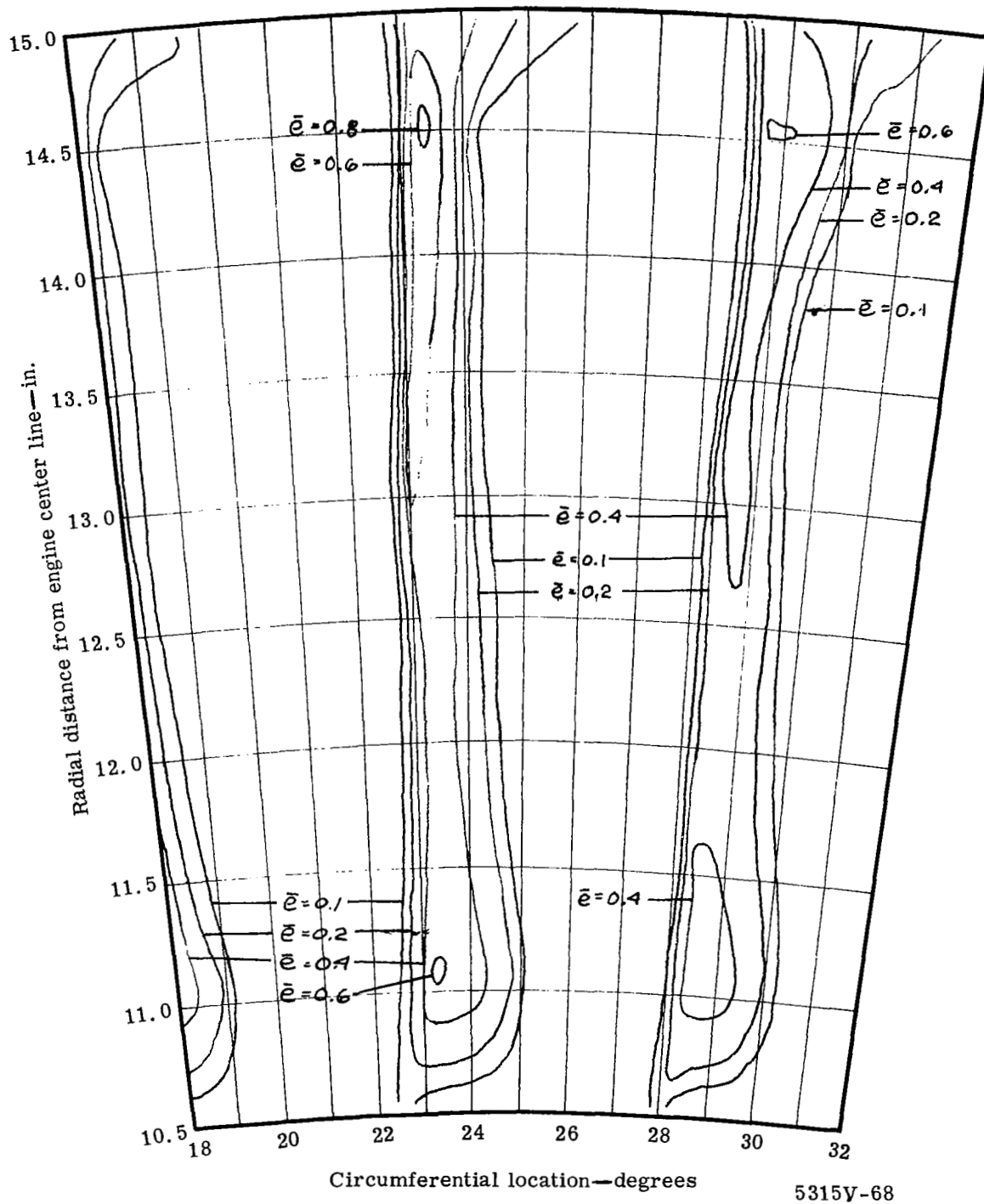


Figure 62. Contours of kinetic energy loss coefficient across one tangential jet No. 2 blade passage at Station 3 (0.030-in. slot and $\dot{m}_j/\dot{m}_p = 4.02\%$).

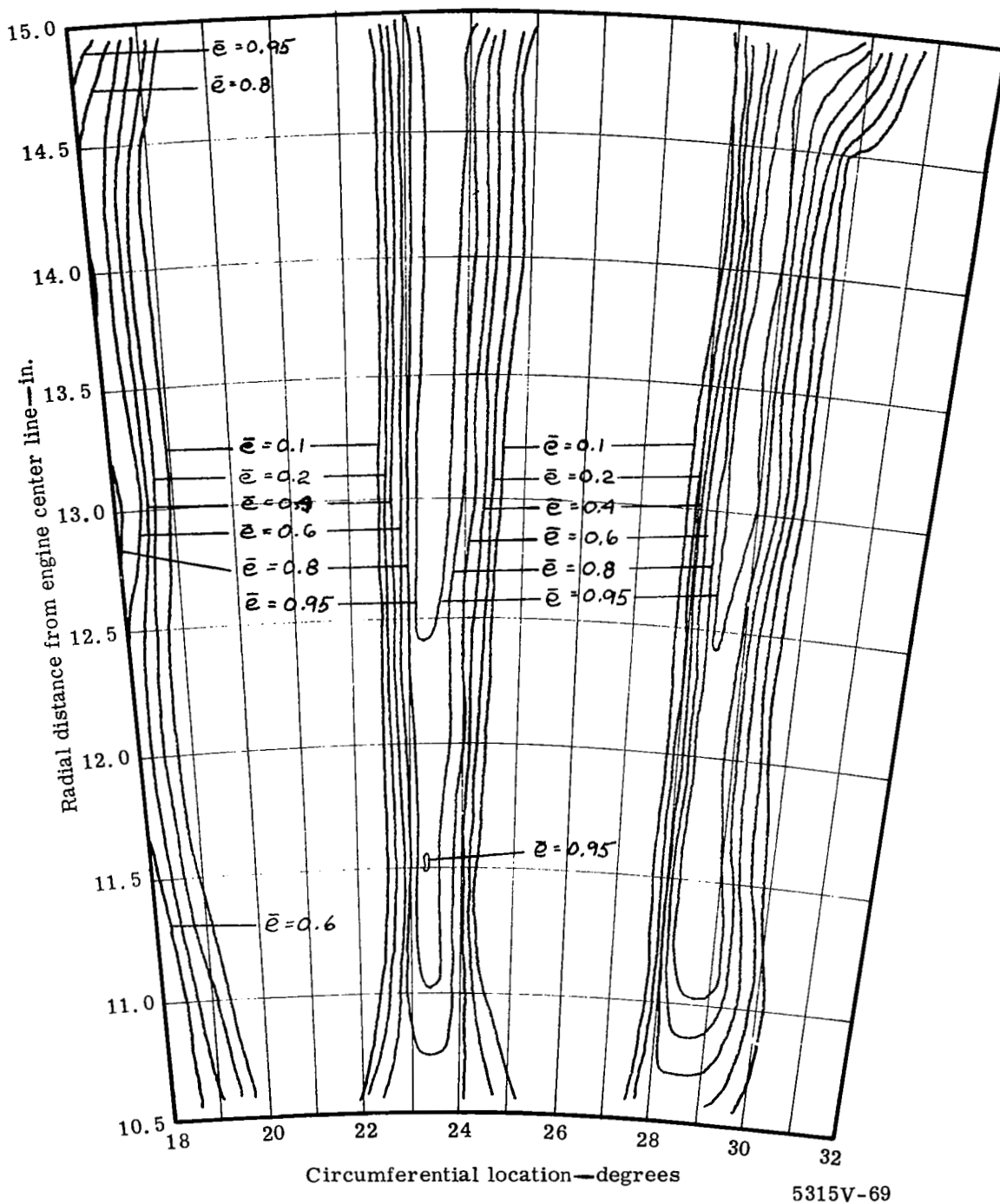


Figure 63. Contours of kinetic energy loss coefficient across one tangential jet No. 2 blade passage at Station 3 (0.040-in. slot and $\dot{m}_j/\dot{m}_p = 2.0\%$).

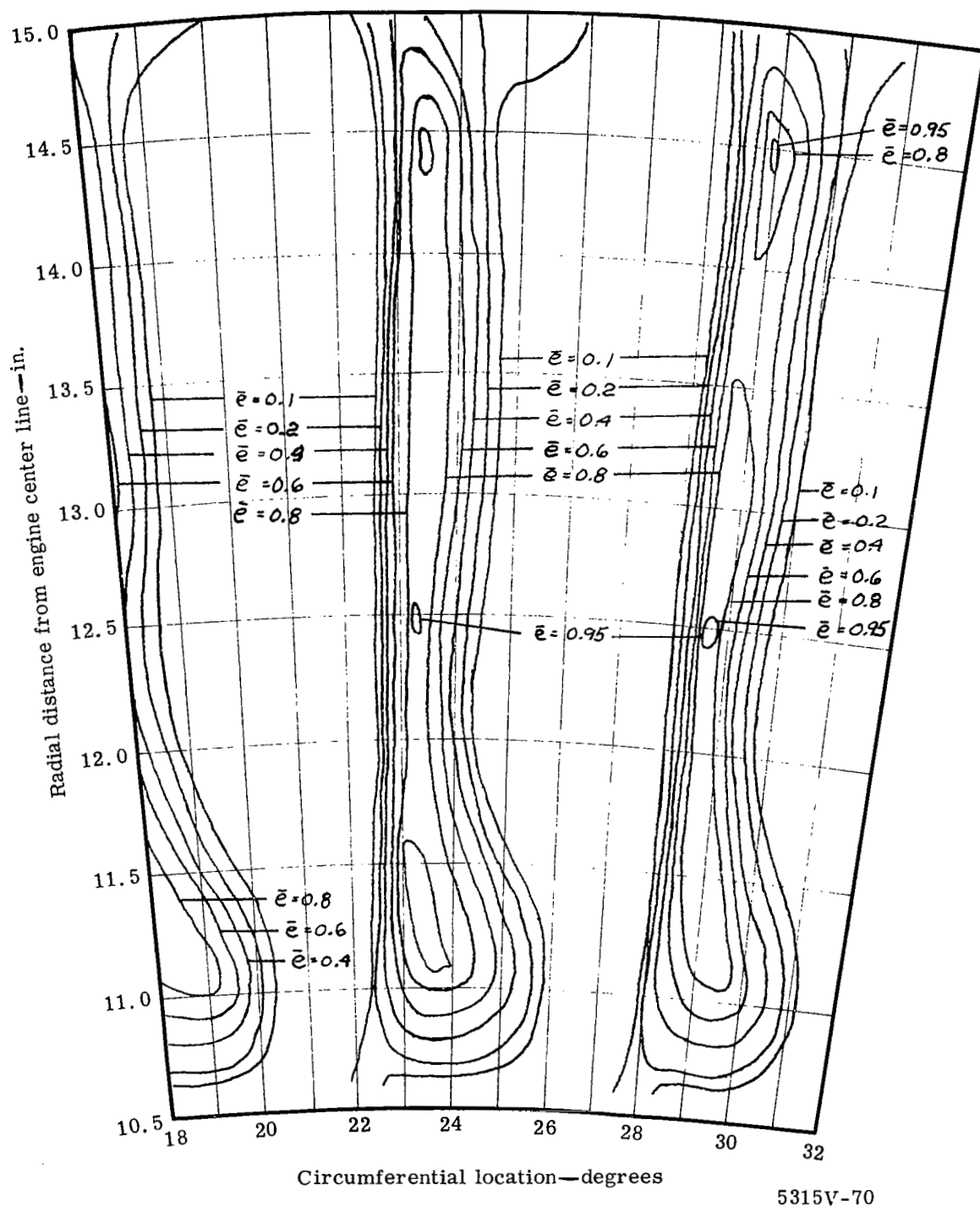


Figure 64. Contours of kinetic energy loss coefficient across one tangential jet No. 2 blade passage at Station 3 (0.040-in. and $\dot{m}_j/\dot{m}_p = 3.00\%$).

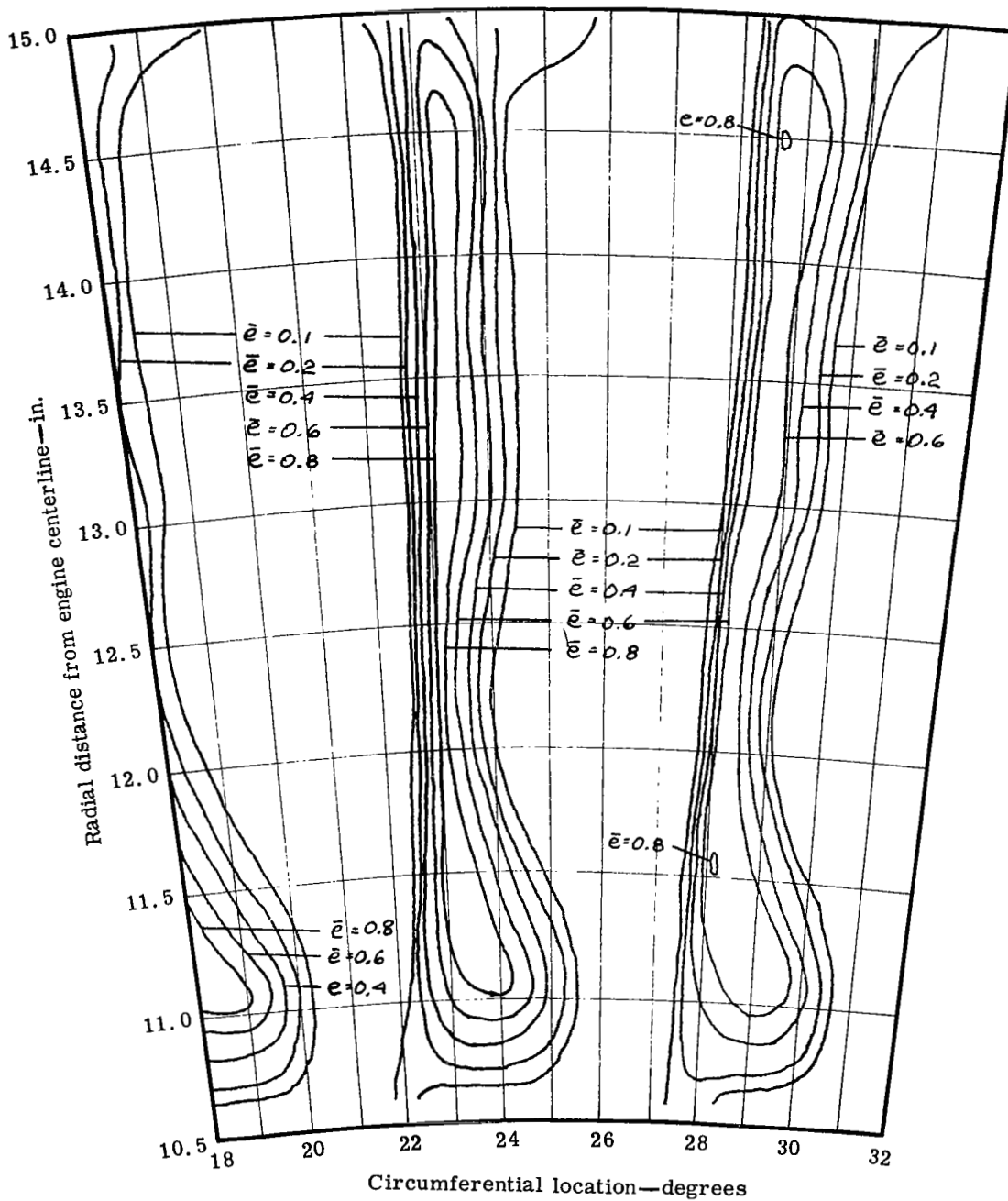
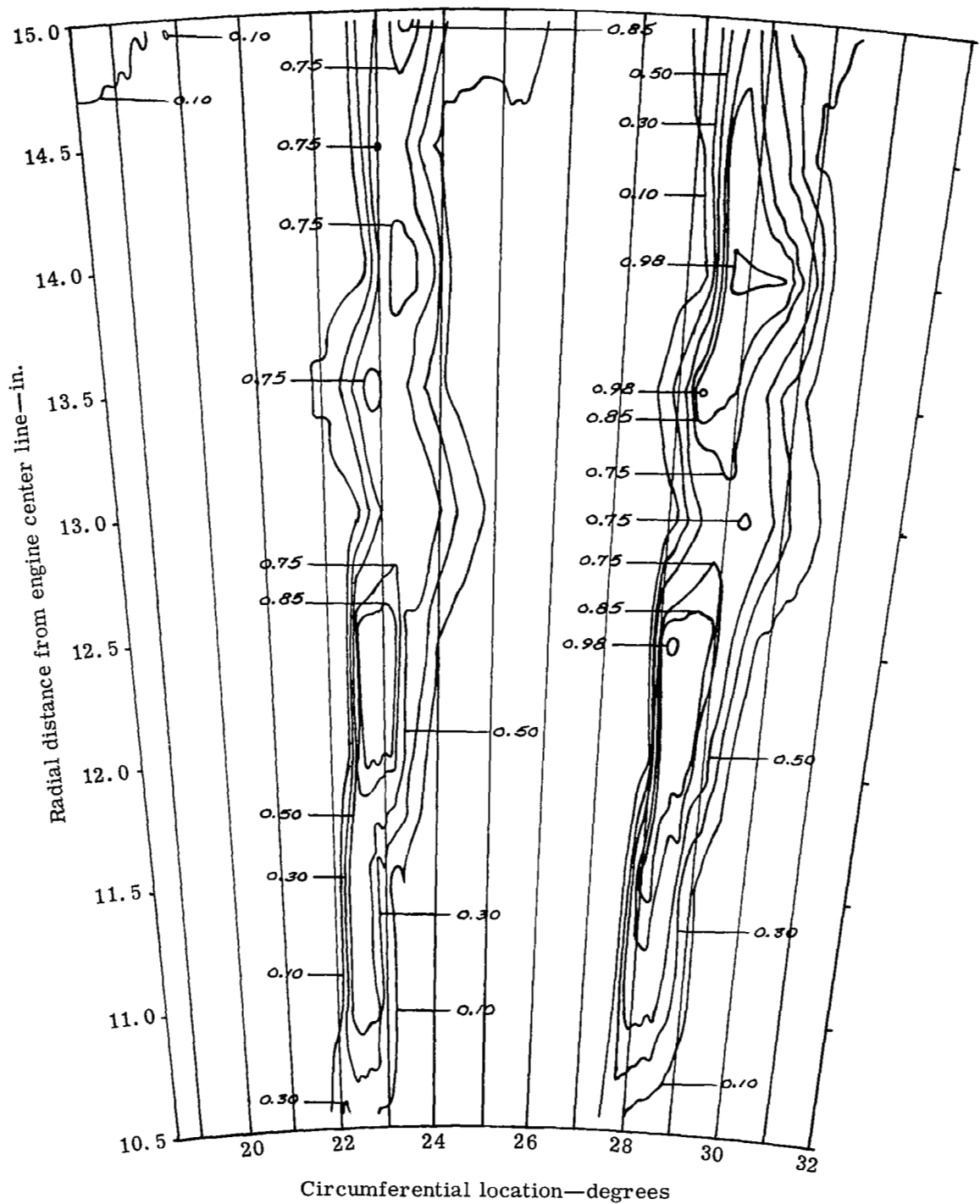
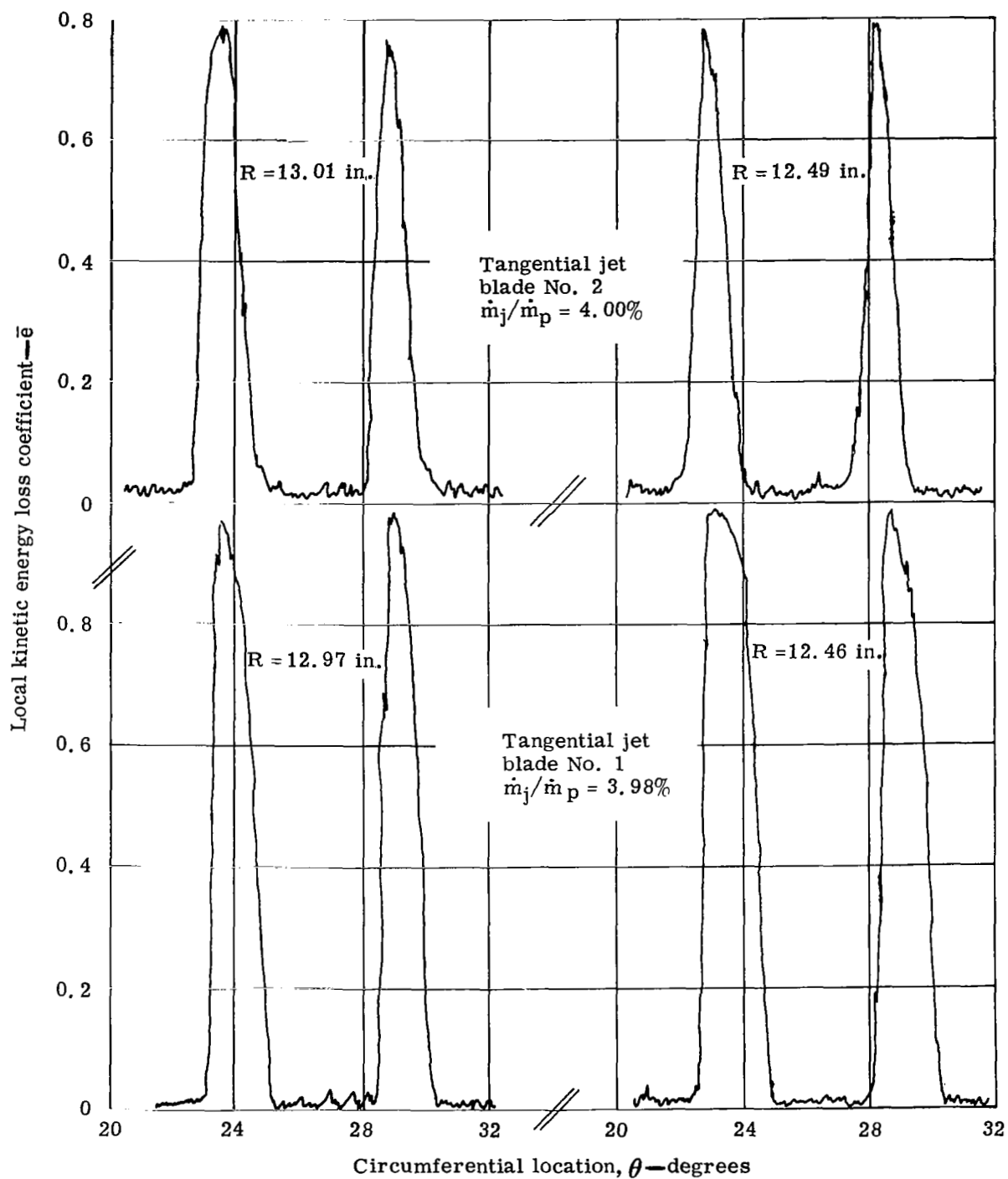


Figure 65. Contours of kinetic energy loss coefficient across one tangential jet No. 2 blade passage at Station 3 (0.040-in. and $\dot{m}_j/\dot{m}_p = 4.00\%$).



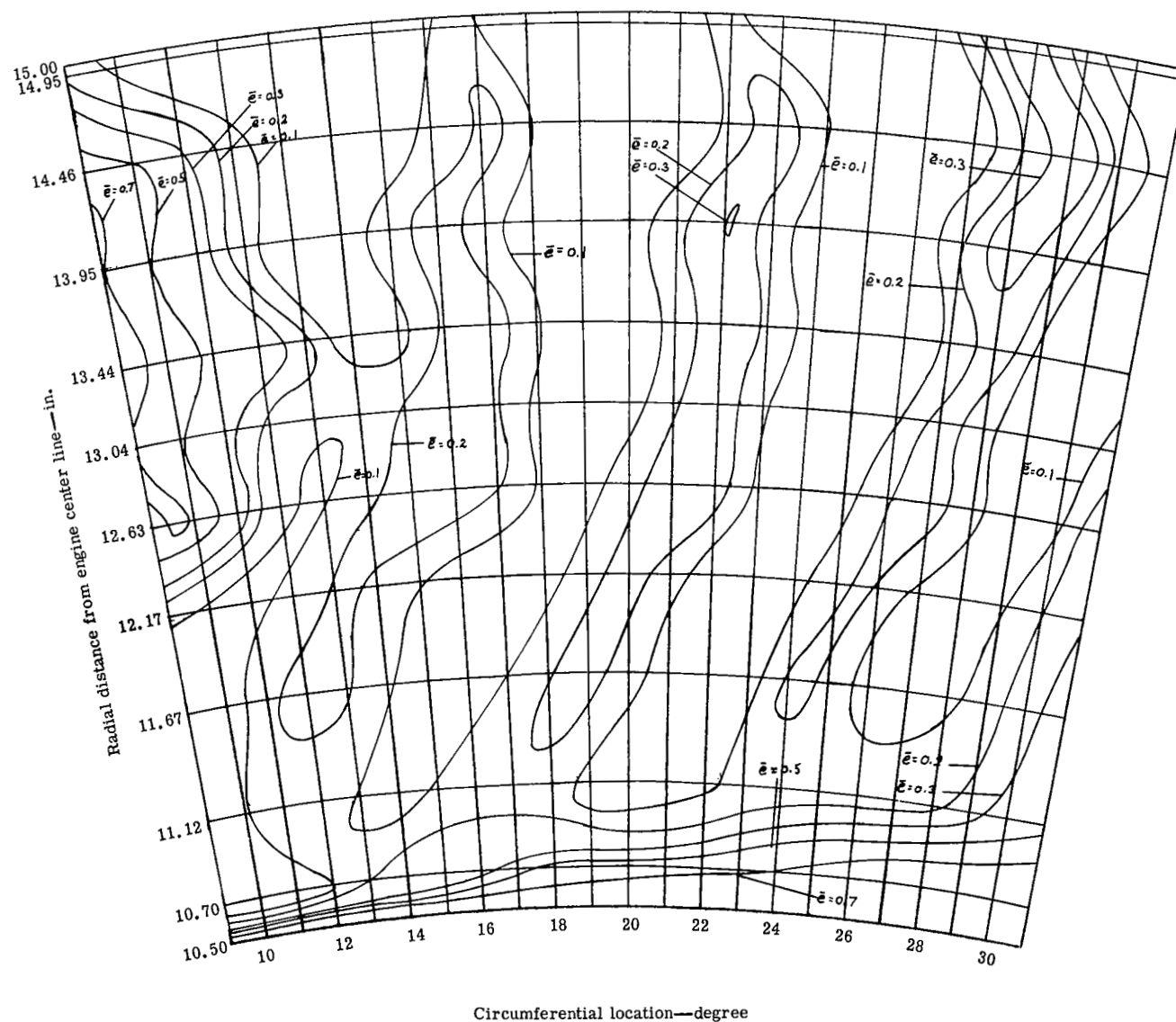
5315V-171

Figure 66. Contours of kinetic energy loss coefficient across one blade passage— plain blade exit wake survey.



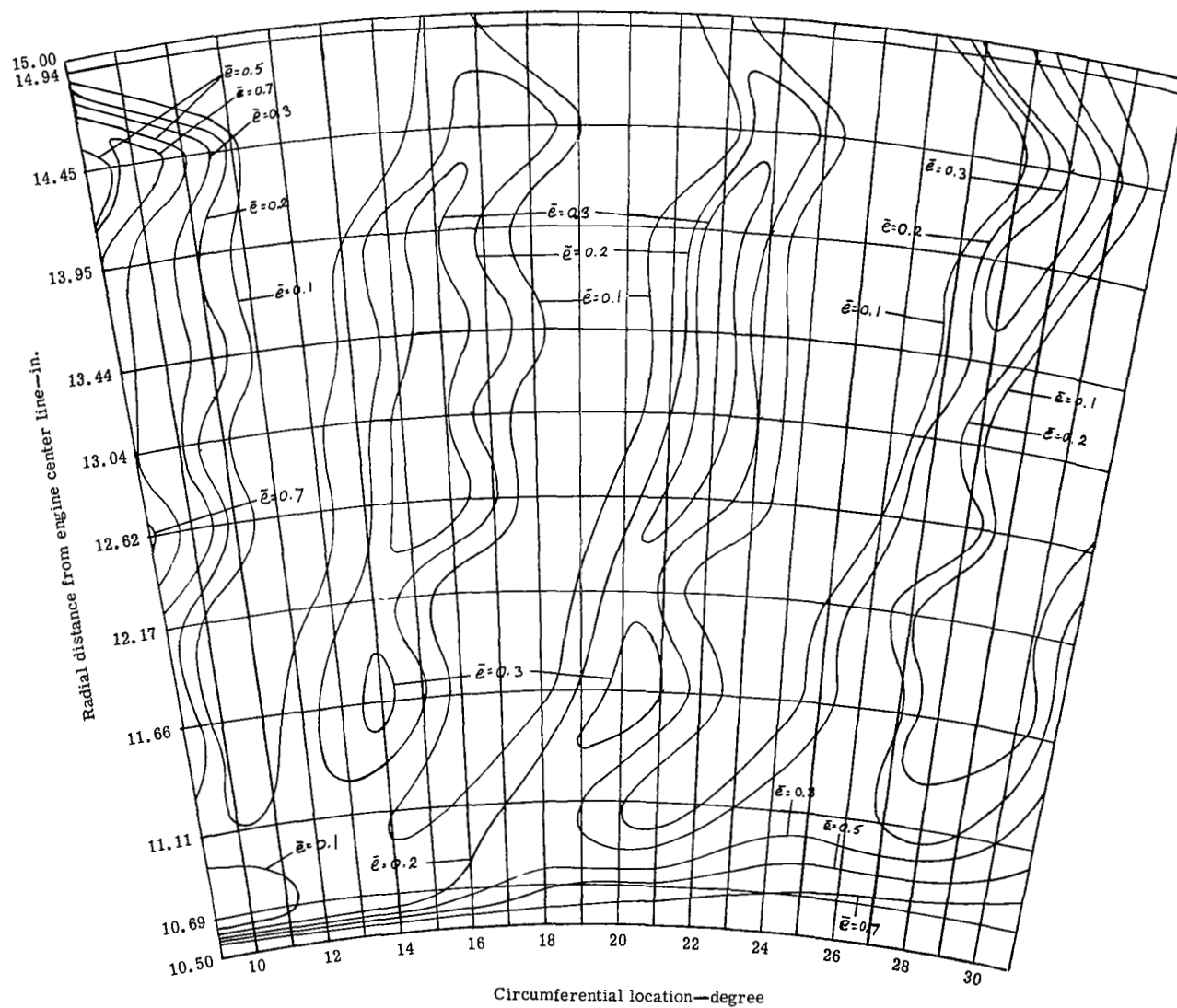
5315V-72

Figure 67. Circumferential variation of trailing edge midspan region wake \bar{e} distributions for the 0.040-in. slot No. 1 and No. 2 jet blades.



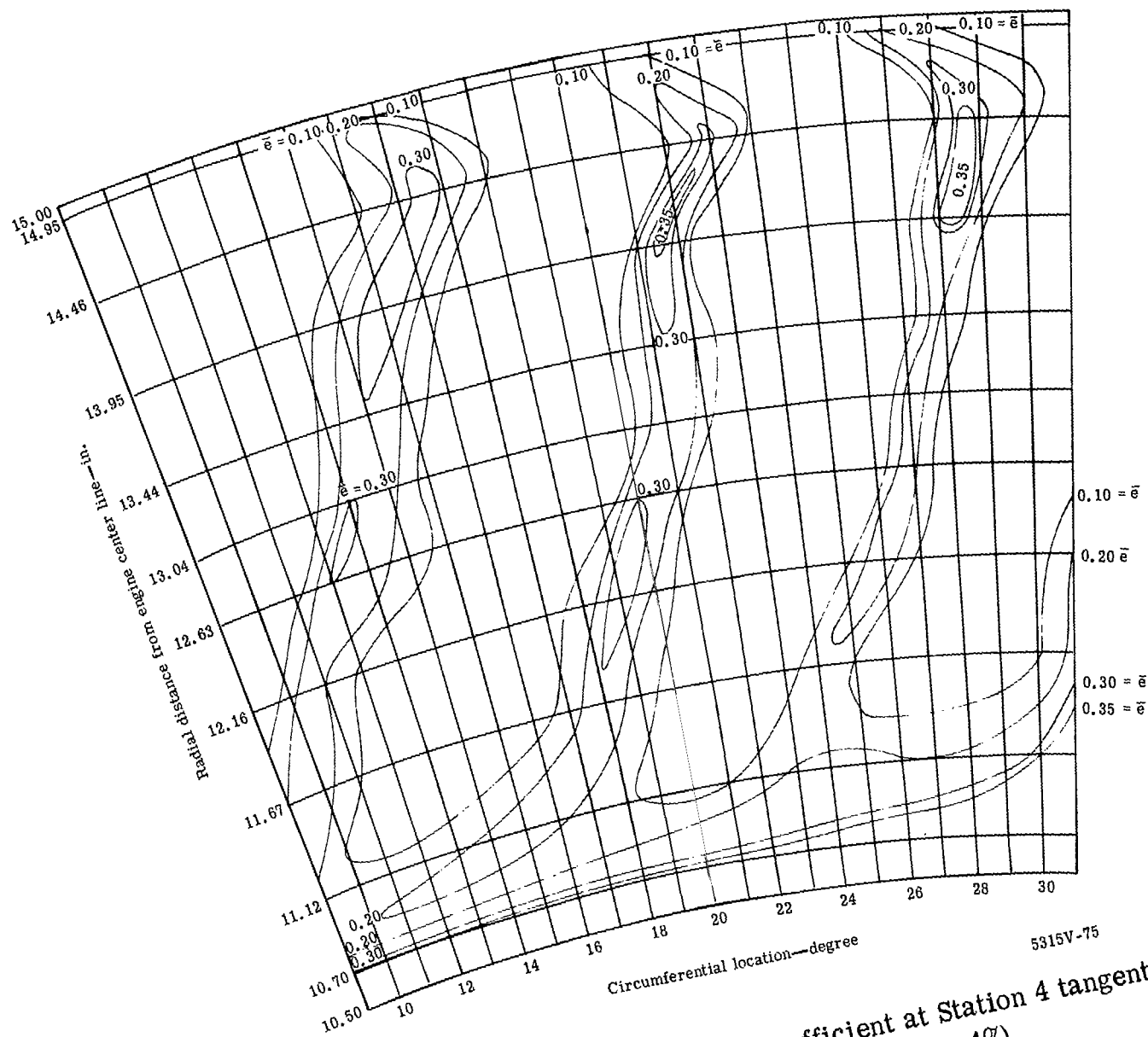
5315V-73

Figure 68. Contours of kinetic energy loss coefficient at Station 4 for tangential jet blade No. 1 (0.020-in. slot, $\dot{m}_j/\dot{m}_p = 1.0\%$).



5315V-74

Figure 69. Contours of kinetic energy loss coefficient at Station 4 for tangential jet blade No. 1 (0.020-in. slot, $\dot{m}_j/\dot{m}_p = 2.6\%$).



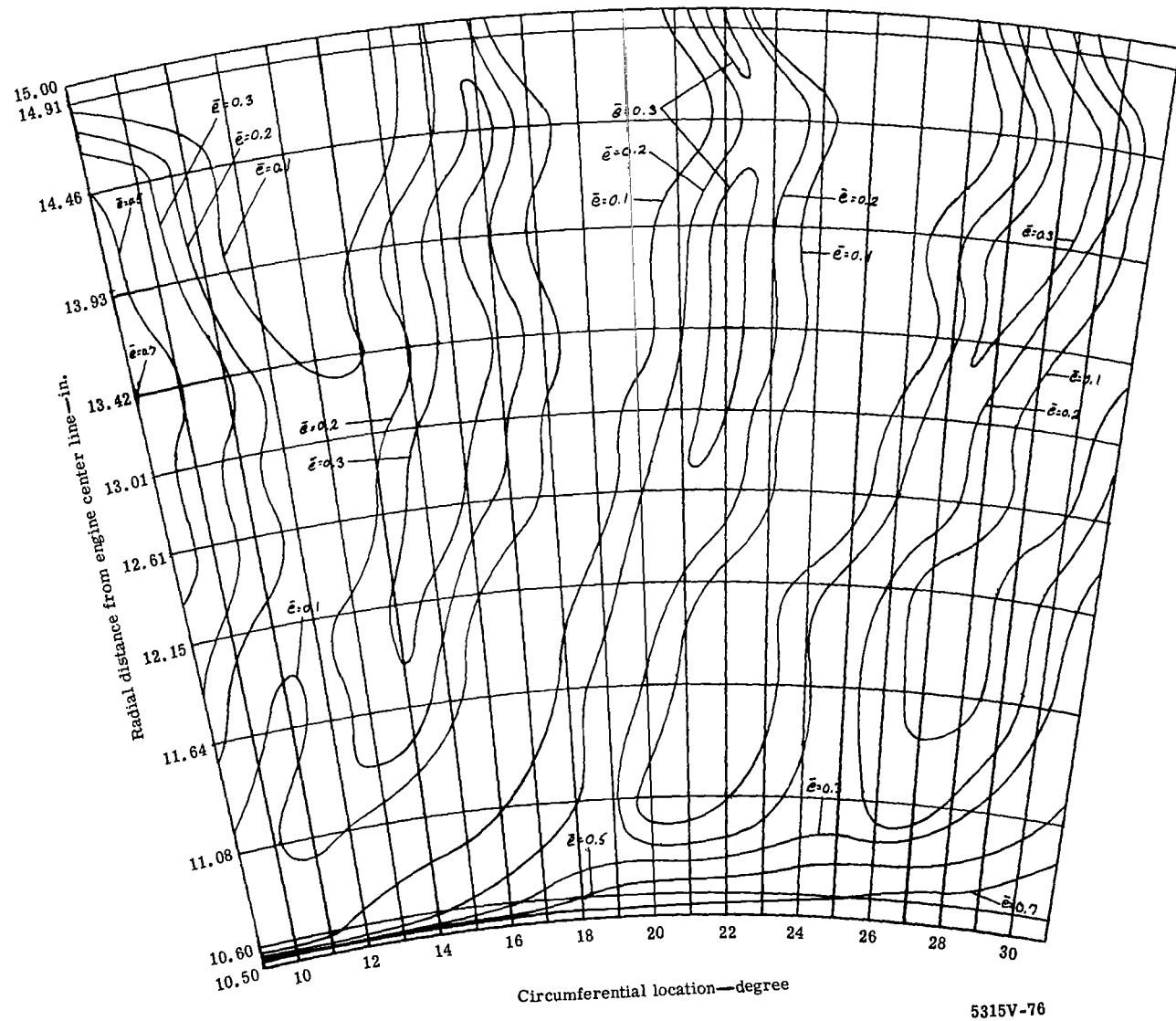


Figure 71. Contours of kinetic energy loss coefficient at Station 4 for tangential jet blade No. 1 (0.030-in. slot, $\dot{m}_j/\dot{m}_p = 2.5\%$).

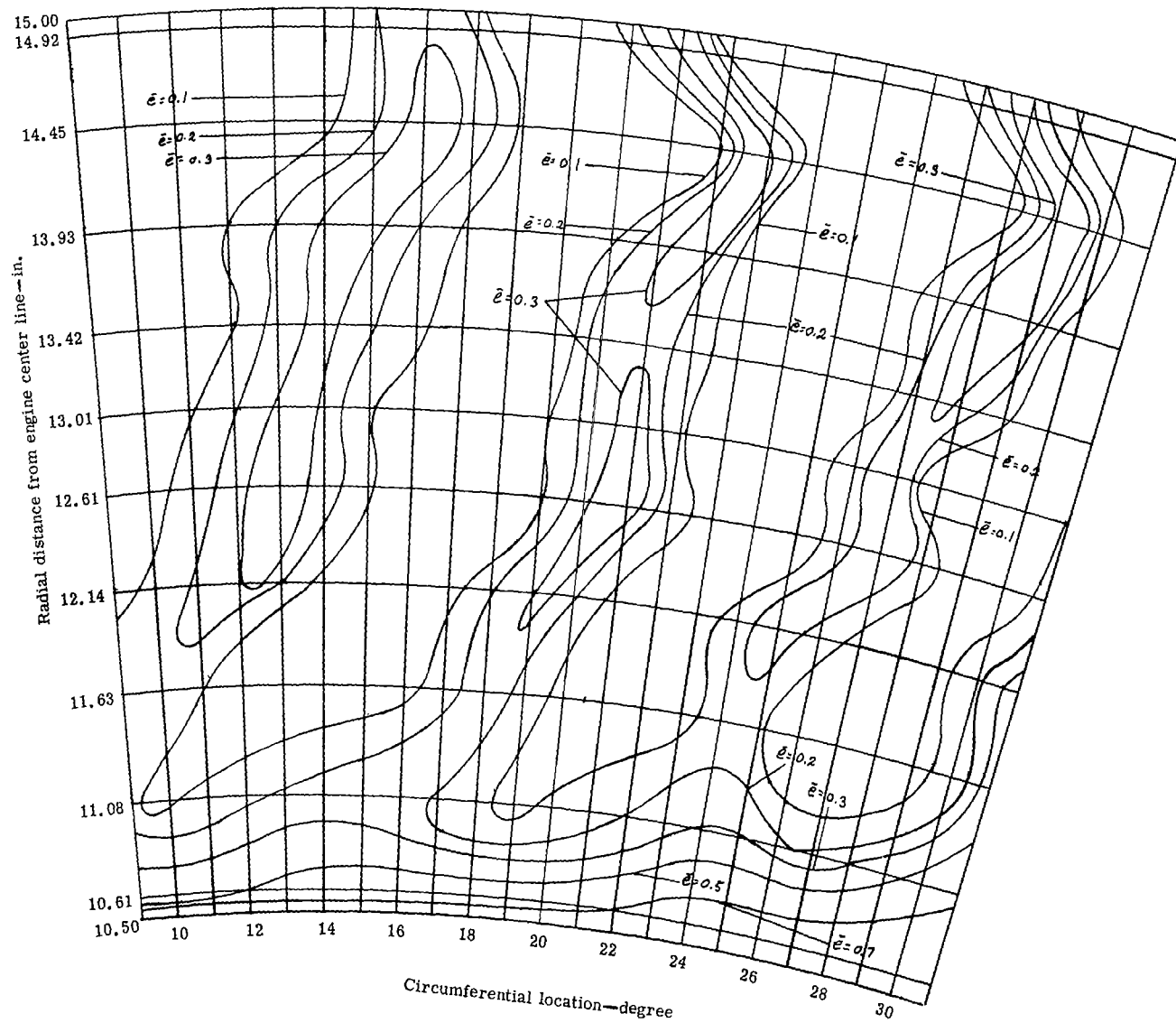


Figure 72. Contours of kinetic energy loss coefficient at Station 4 for tangential jet blade No. 1 (0.030-in. slot, $\dot{m}_j/\dot{m}_p = 4.2\%$).

5315V-77

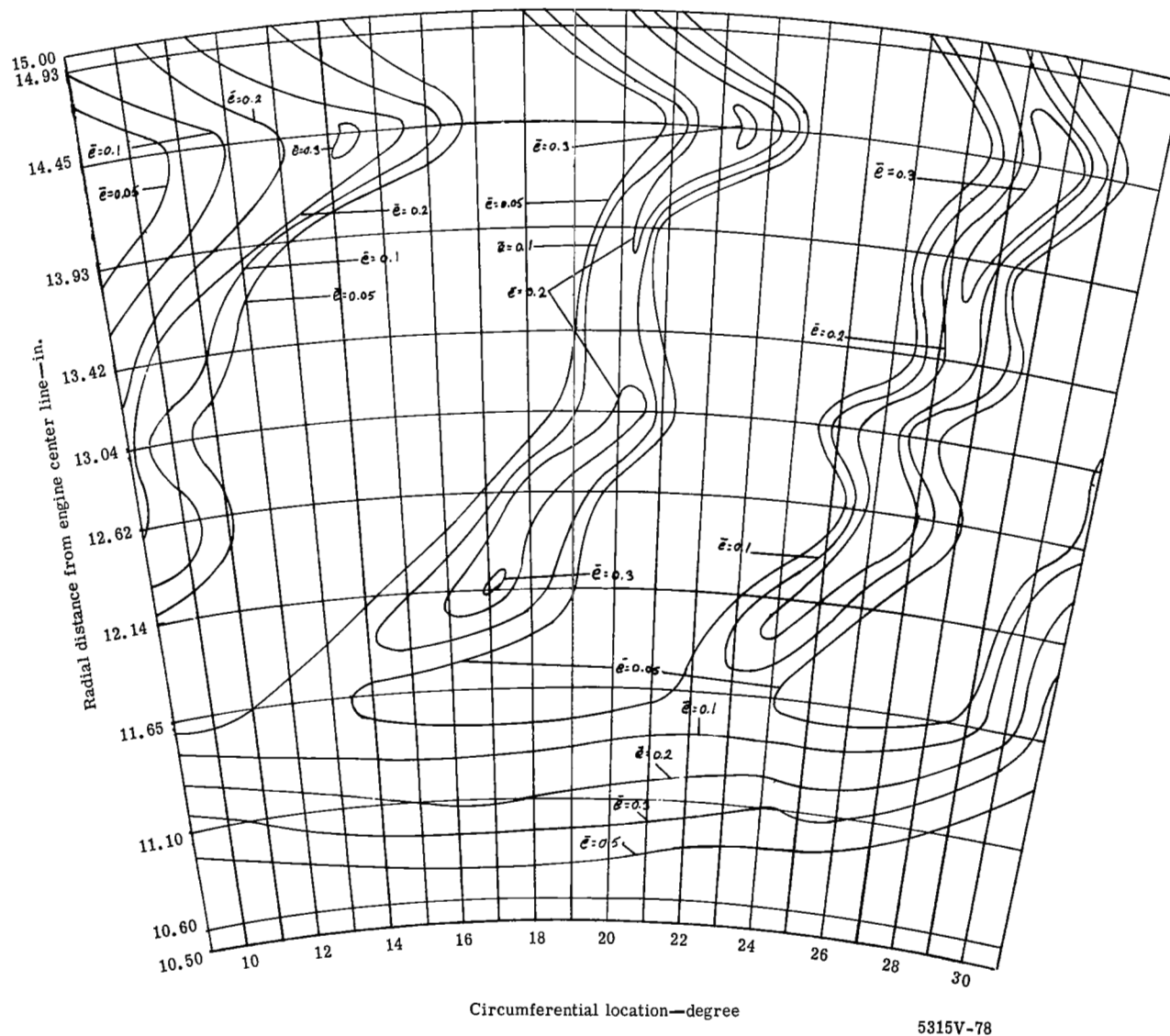


Figure 73. Contours of kinetic energy loss coefficient at Station 4 for tangential jet blade No. 1 (0.030-in. slot, $\dot{m}_j/\dot{m}_p = 6.4\%$).

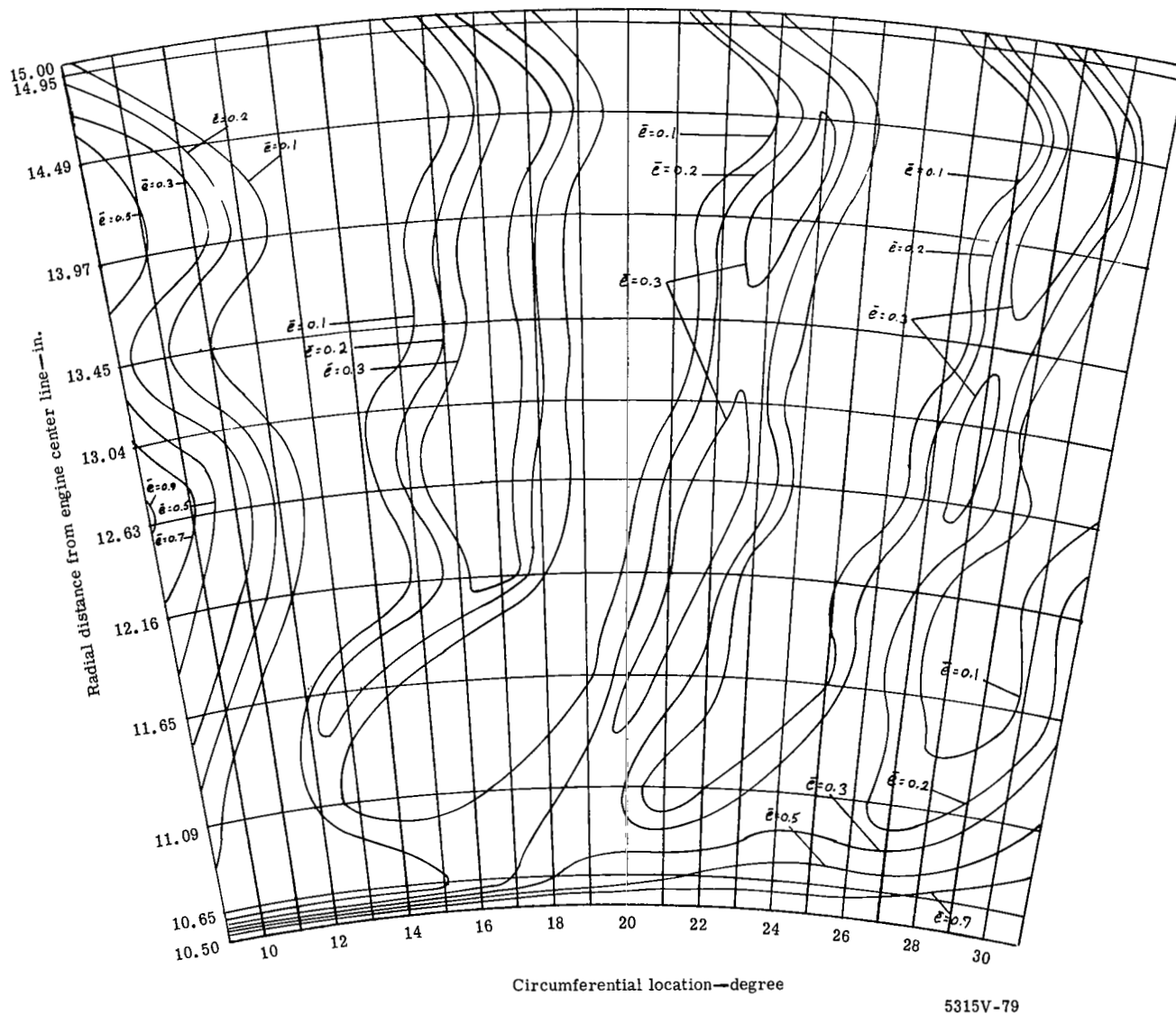


Figure 74. Contours of kinetic energy loss coefficient at Station 4 for tangential jet blade No. 1 (0.040-in. slot, $\dot{m}_j/\dot{m}_p = 3.94\%$).

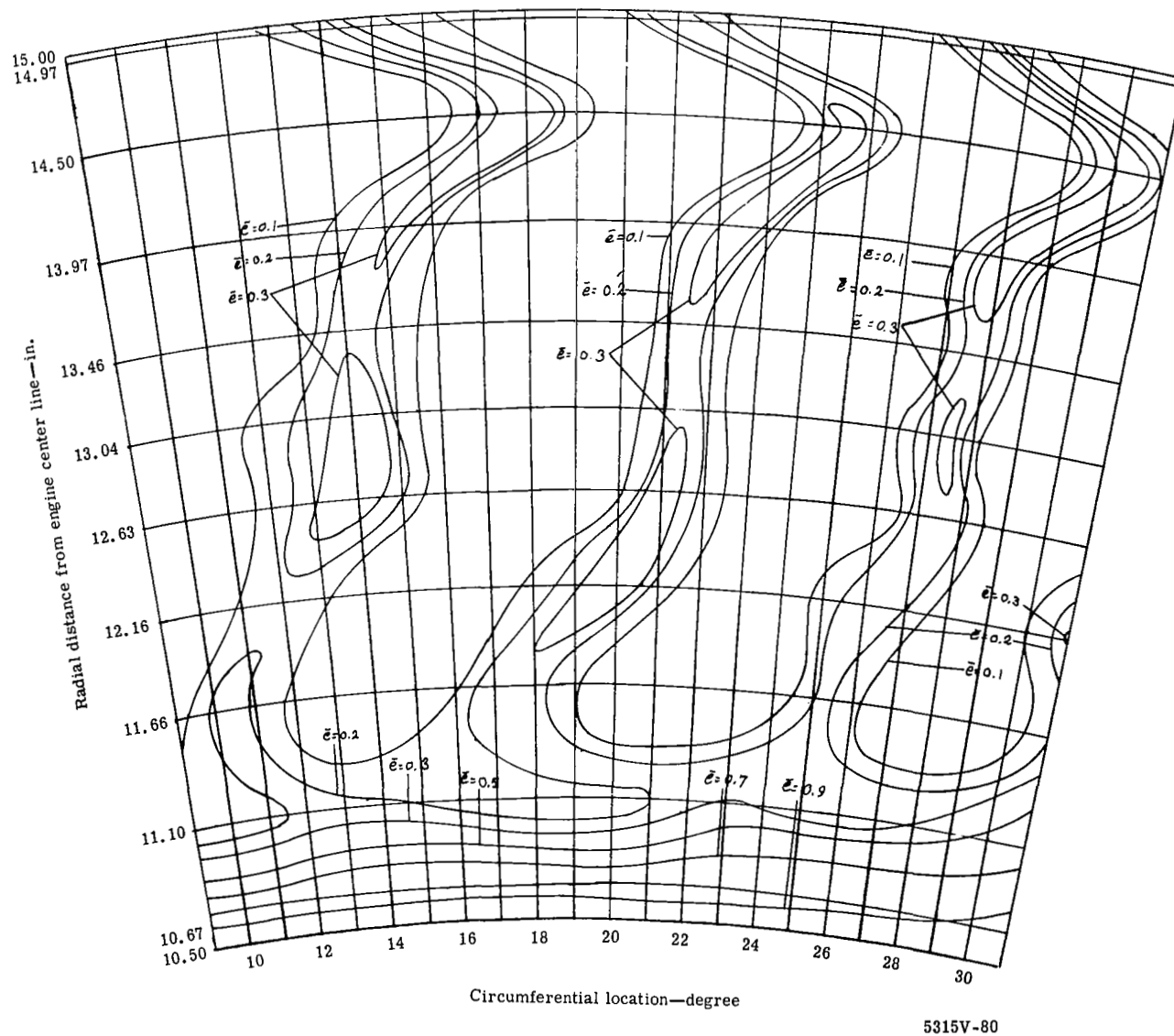
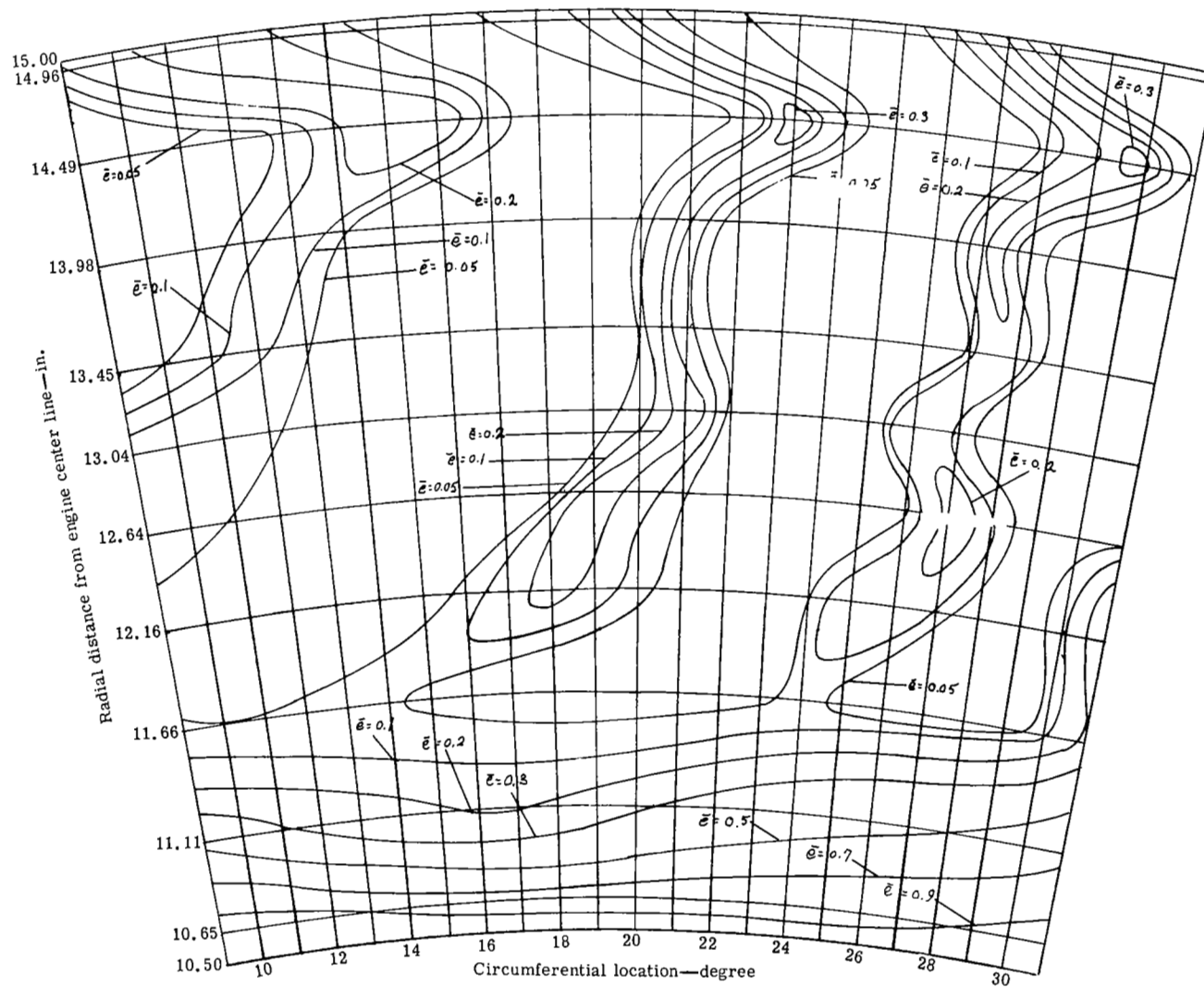


Figure 75. Contours of kinetic energy loss coefficient at Station 4 for tangential jet blade No. 1 (0.040-in. slot, $\dot{m}_j/\dot{m}_p = 5.64\%$).



5315V-81

Figure 76. Contours of kinetic energy loss coefficient at Station 4 for tangential jet blade No. 1 (0.040-in. slot, $\dot{m}_j/\dot{m}_p = 7.48\%$).

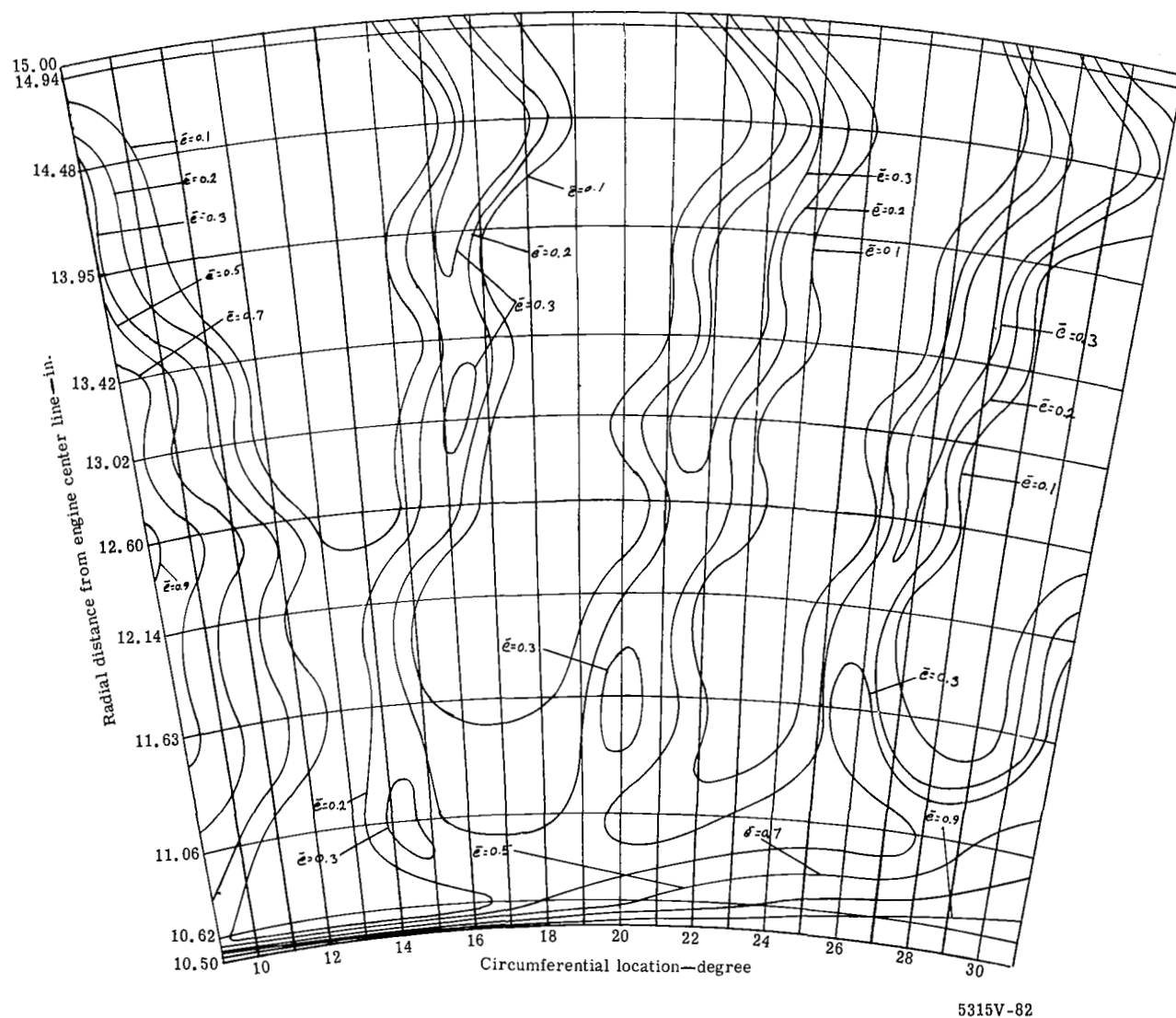
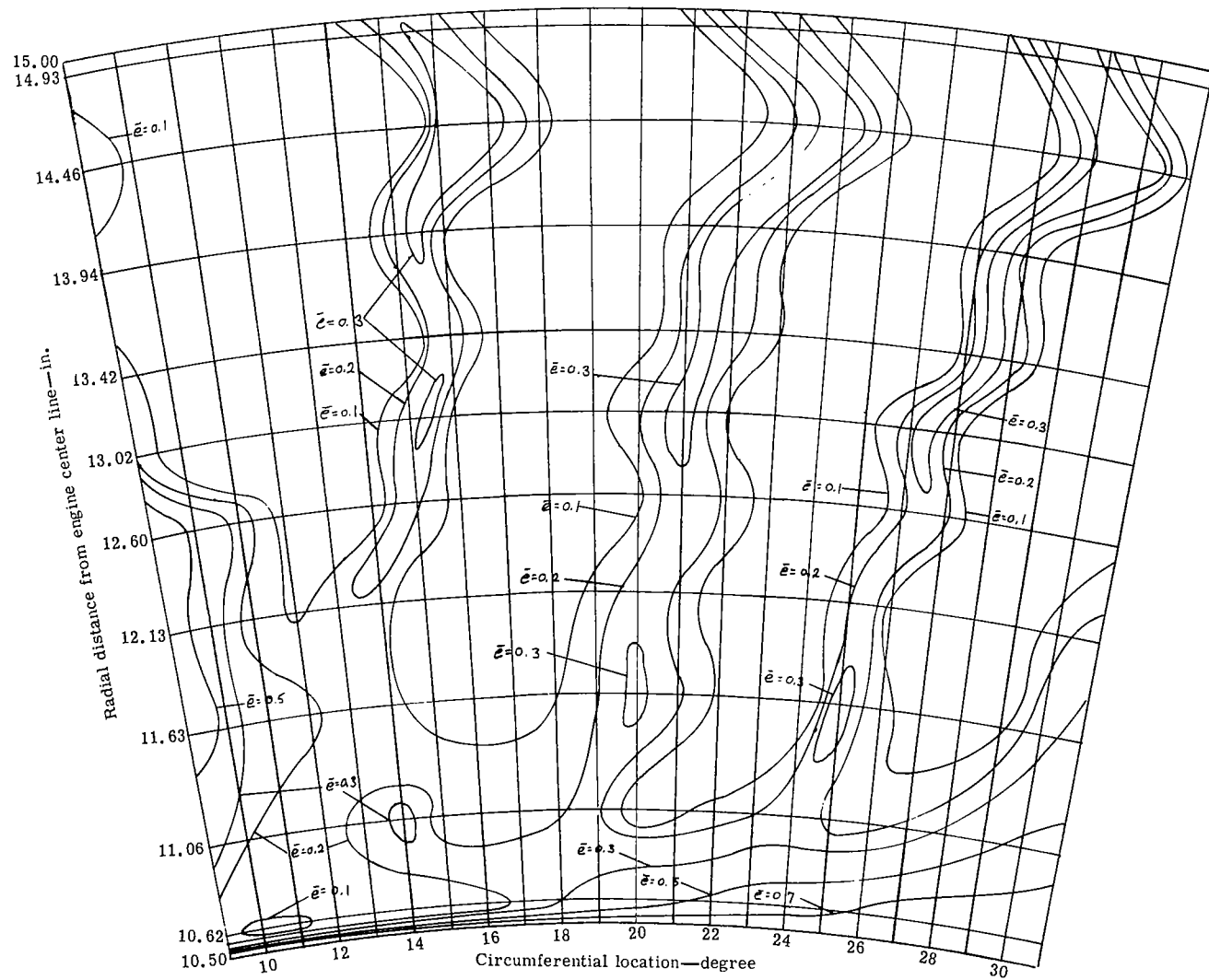


Figure 77. Contours of kinetic energy loss coefficient at Station 4 for tangential jet blade No. 2 (0.020-in. slot, $\dot{m}_j/\dot{m}_p = 1.97\%$).



5315V-83

Figure 78. Contours of kinetic energy loss coefficient at Station 4 for tangential jet blade No. 2 (0.020-in. slot, $\dot{m}_j/\dot{m}_p = 3.00\%$).

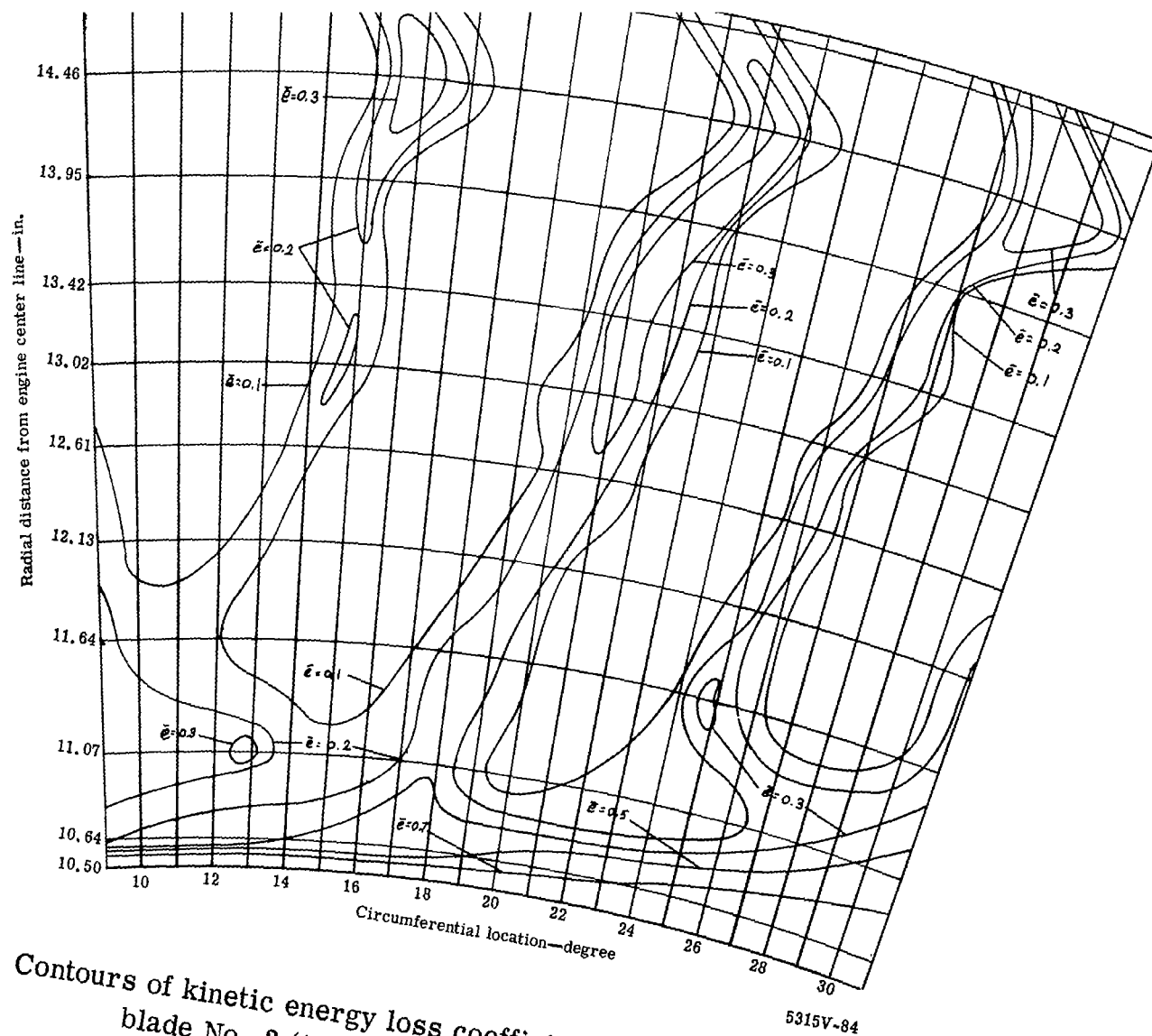


Figure 79. Contours of kinetic energy loss coefficient at Station 4 for tangential jet blade No. 2 (0.020-in. slot, $\dot{m}_j/\dot{m}_p = 3.50\%$).

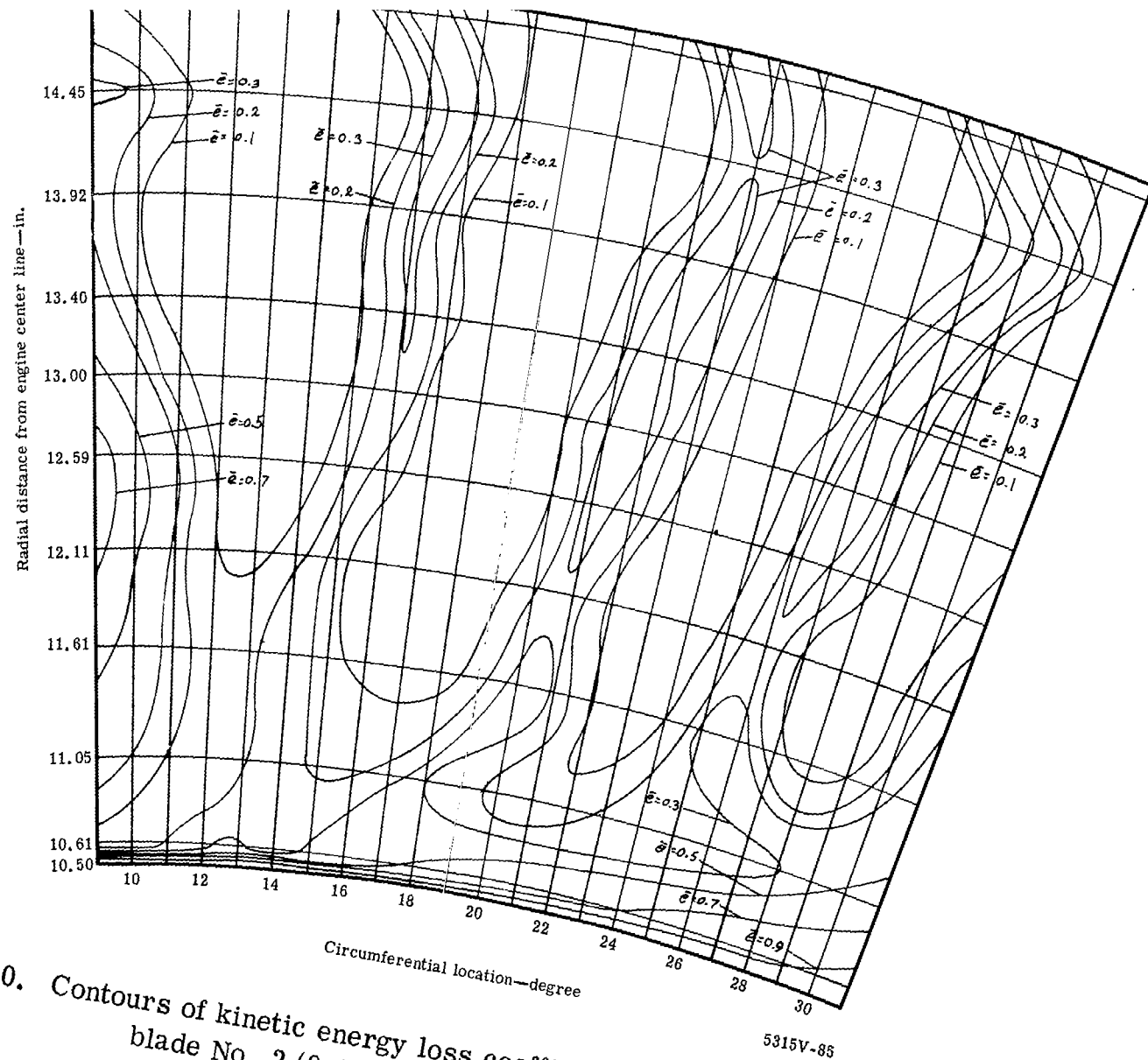


Figure 80. Contours of kinetic energy loss coefficient at Station 4 for tangential jet blade No. 2 (0.030-in. slot, $\dot{m}_j/\dot{m}_p = 2.01\%$).

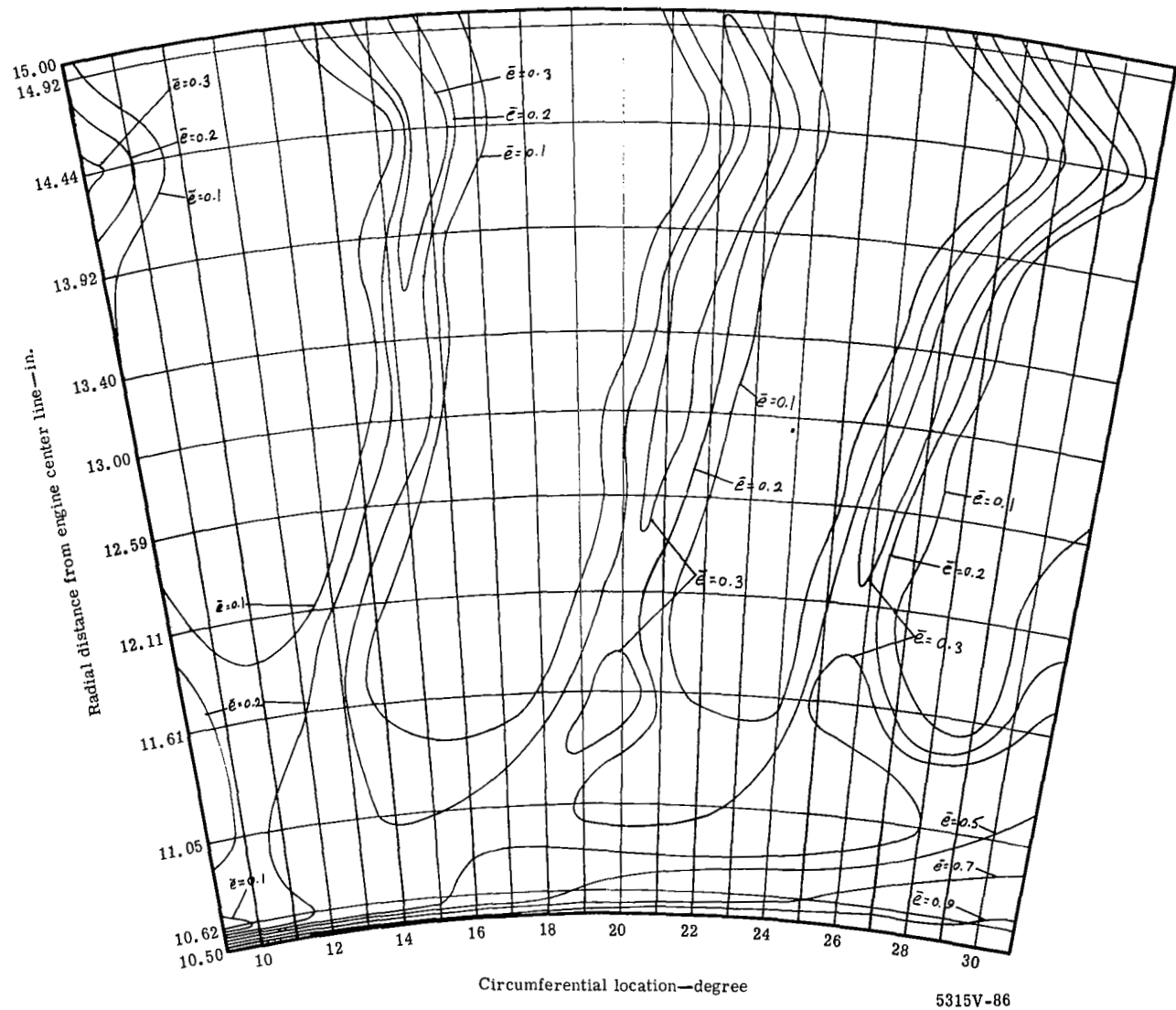


Figure 81. Contours of kinetic energy loss coefficient at Station 4 for tangential jet blade No. 2 (0.030-in. slot, $\dot{m}_j/\dot{m}_p = 3.08\%$).

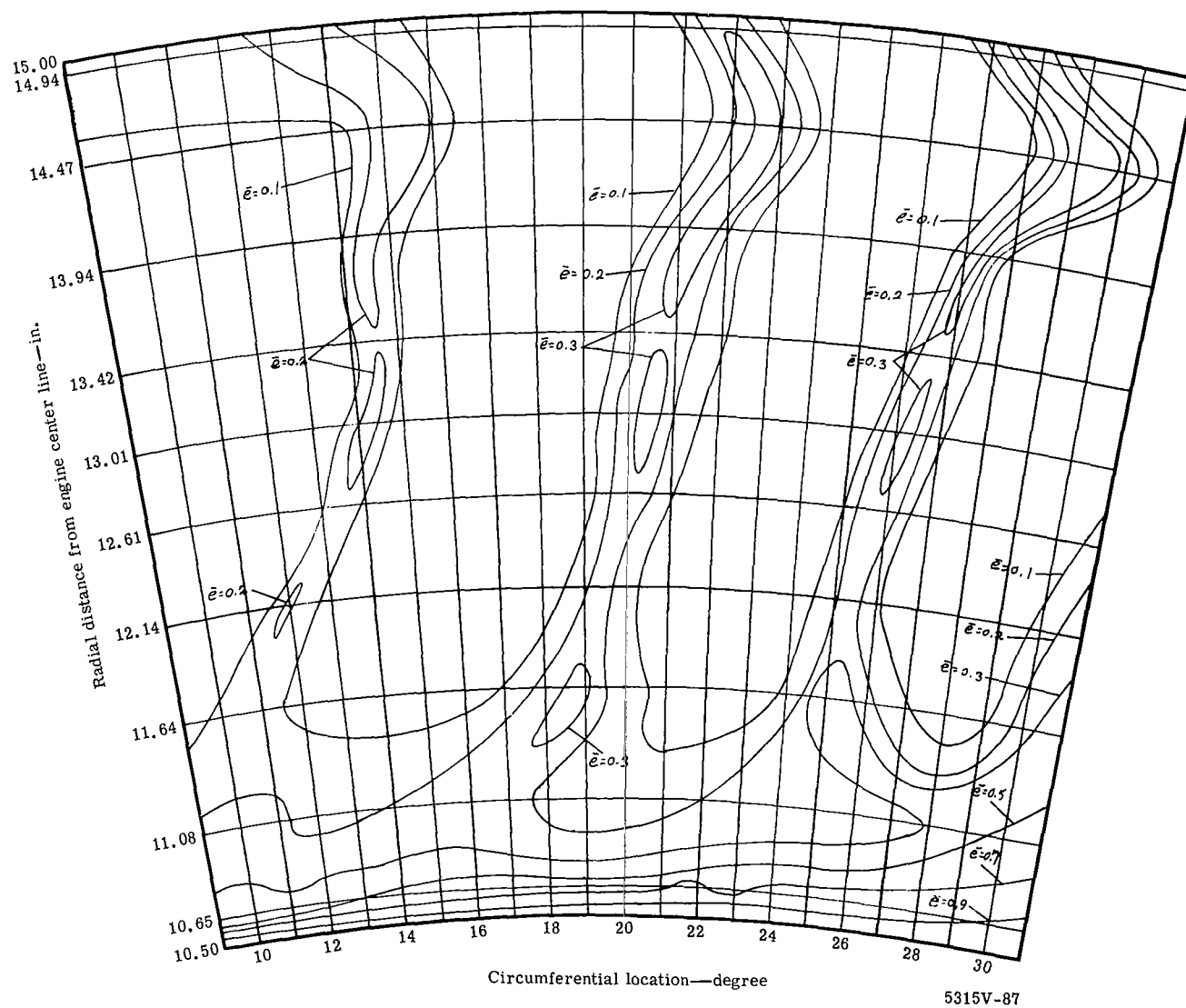


Figure 82. Contours of kinetic energy loss coefficient at Station 4 for tangential jet blade No. 2 (0.030-in. slot, $\dot{m}_j/\dot{m}_p = 4.04\%$).

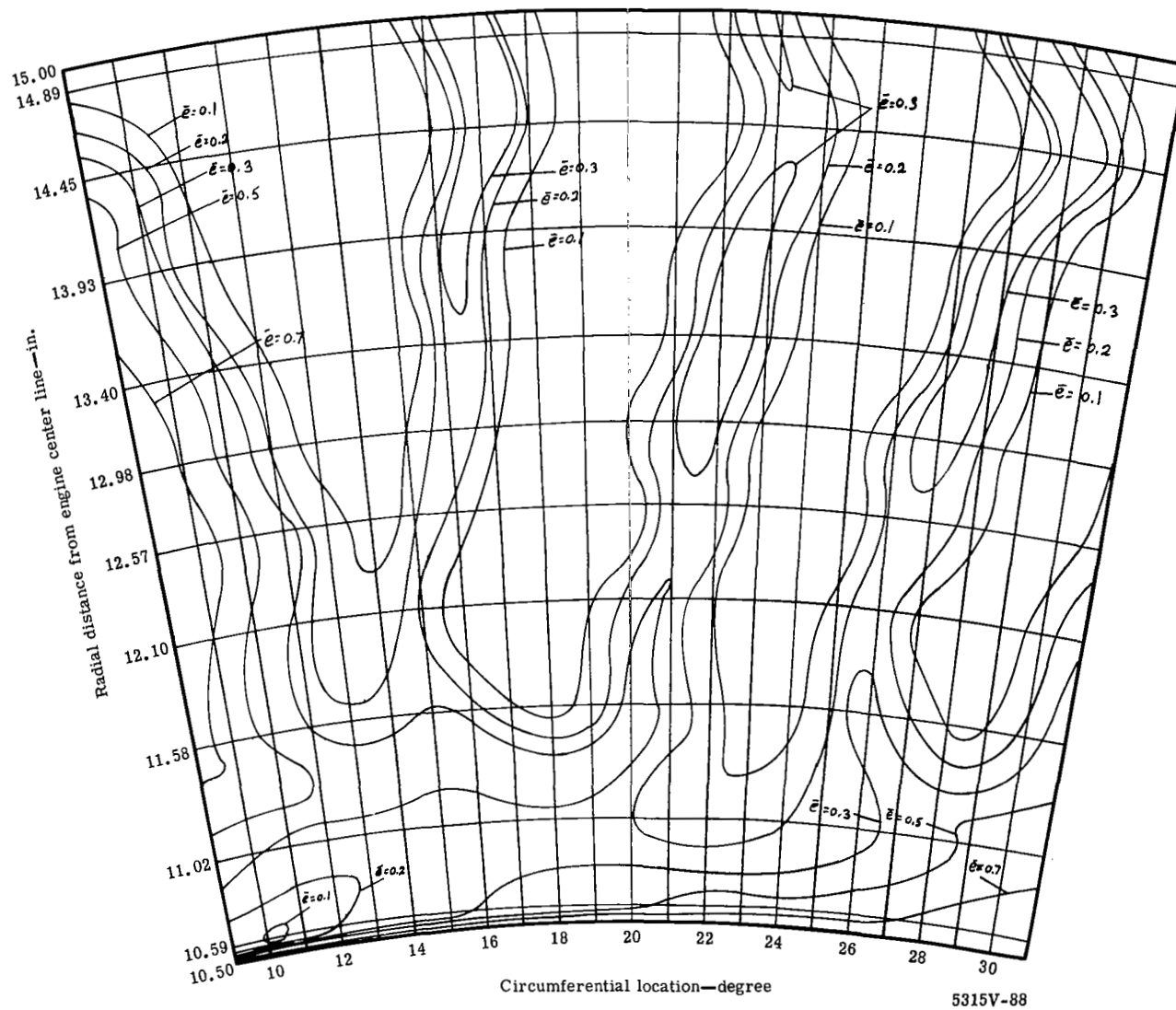


Figure 83. Contours of kinetic energy loss coefficient at Station 4 for tangential jet blade No. 2 (0.040-in. slot, $\dot{m}_j/\dot{m}_p = 2.03\%$).

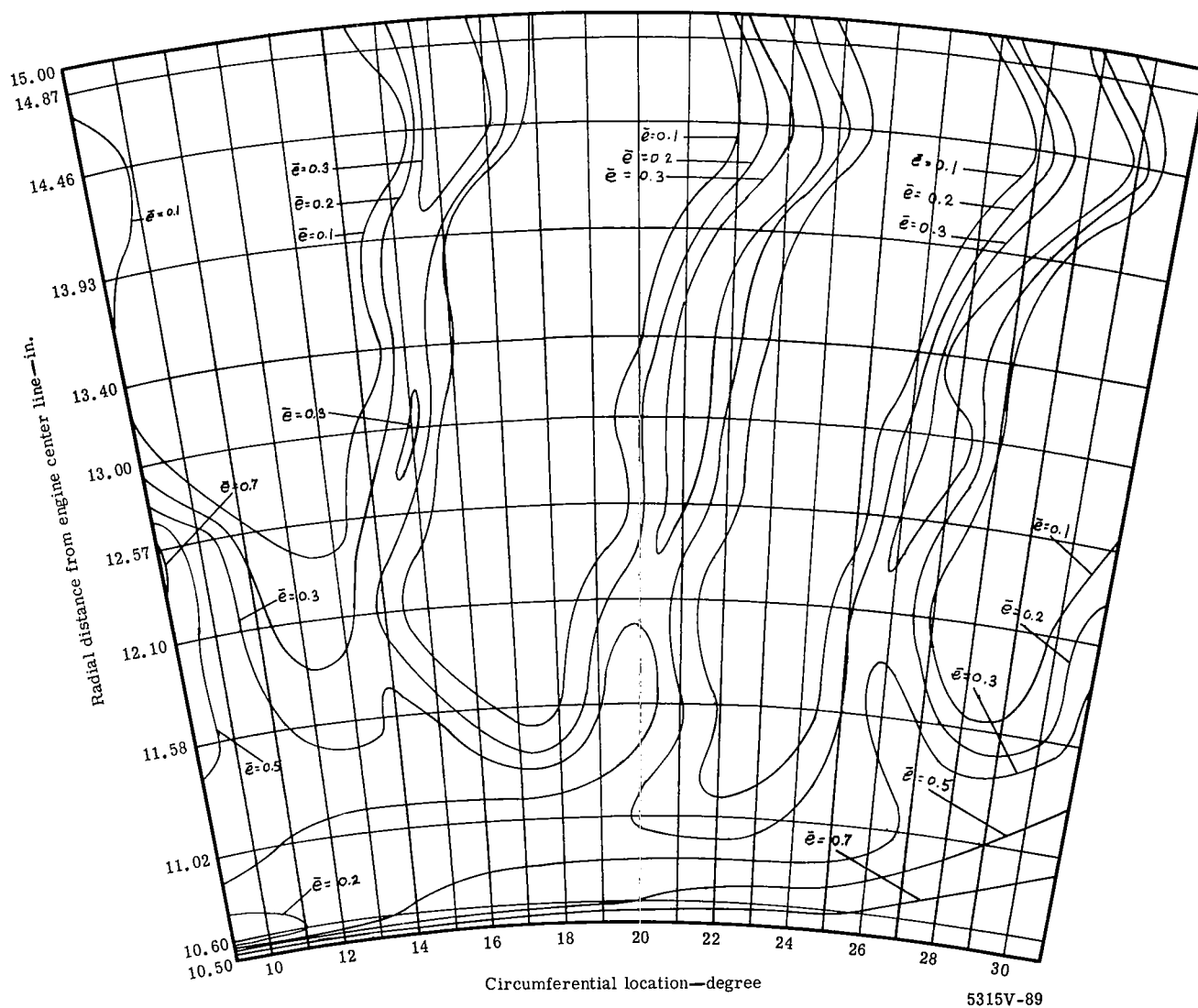


Figure 84. Contours of kinetic energy loss coefficient at Station 4 for tangential jet blade No. 2 (0.040-in. slot, $\dot{m}_j/\dot{m}_p = 3.00\%$).

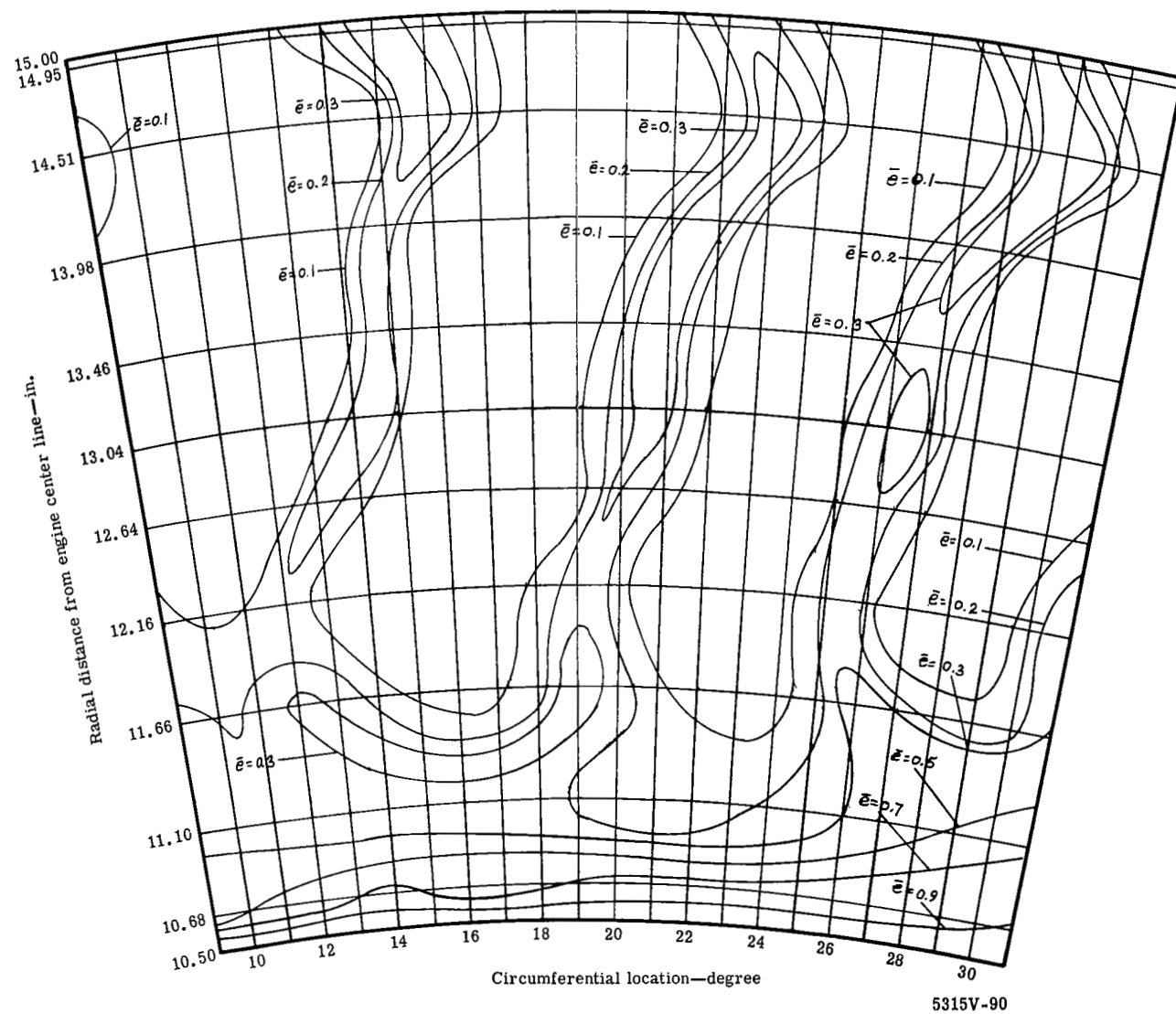
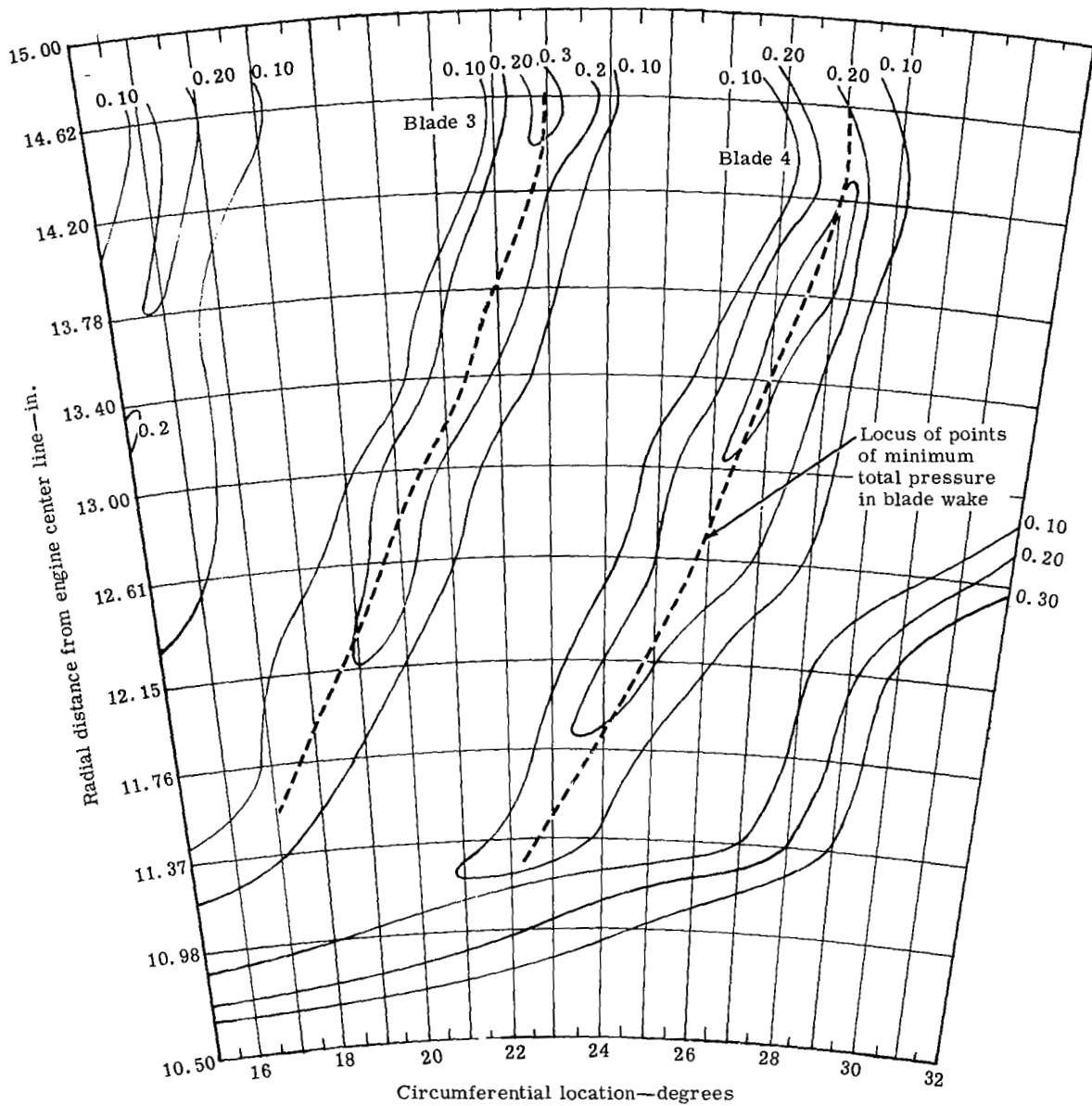


Figure 85. Contours of kinetic energy loss coefficient at Station 4 for tangential jet blade No. 2 (0.040-in. slot, $\dot{m}_j/\dot{m}_p = 3.85\%$).



5315V-178

Figure 86. Contours of kinetic energy loss coefficient—plain blade downstream wake survey.

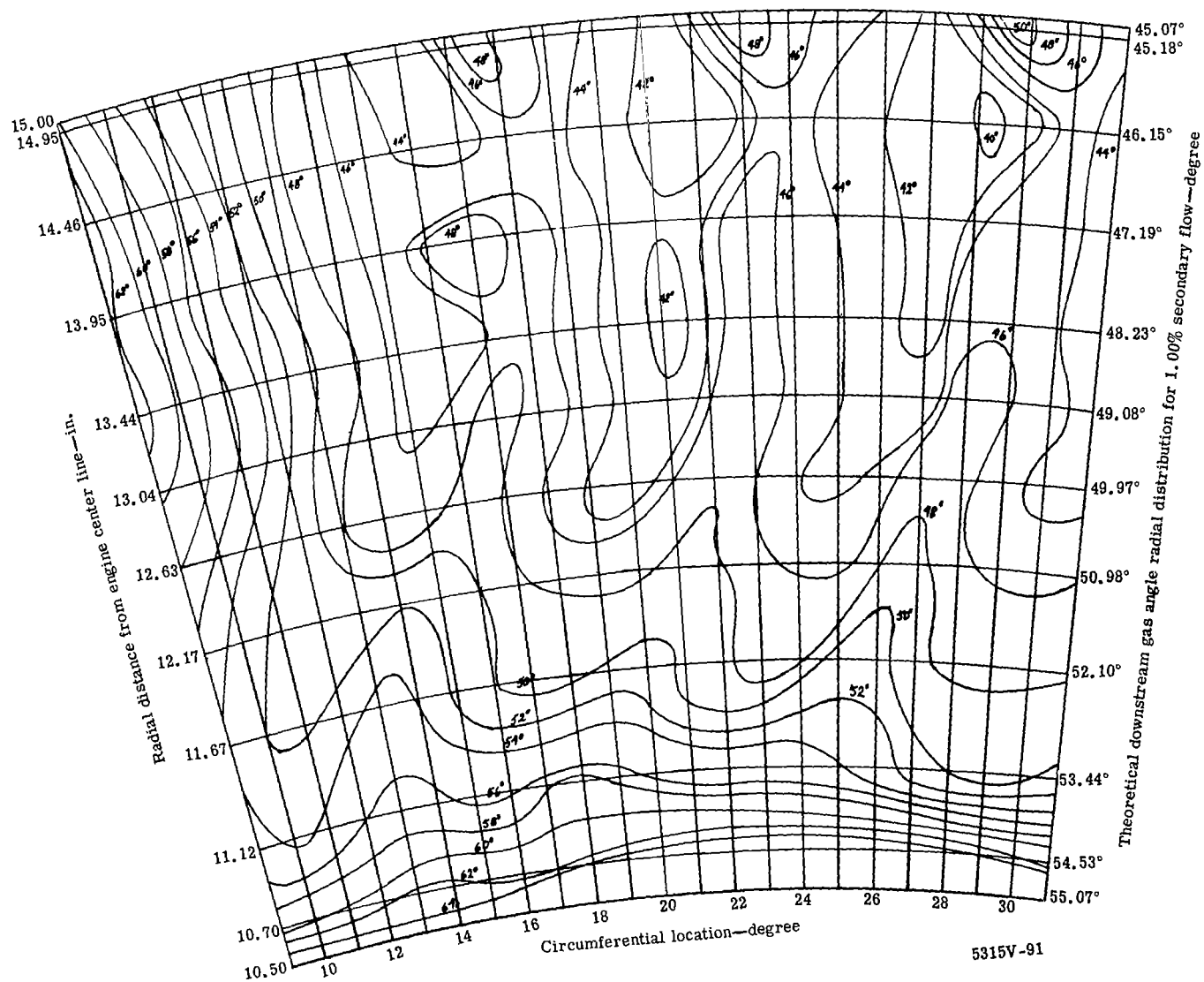


Figure 87. Contours of downstream gas angle measured from axial for the tangential jet blade No. 1 (0.020-in. slot, $\dot{m}_j/\dot{m}_p = 1.0\%$).

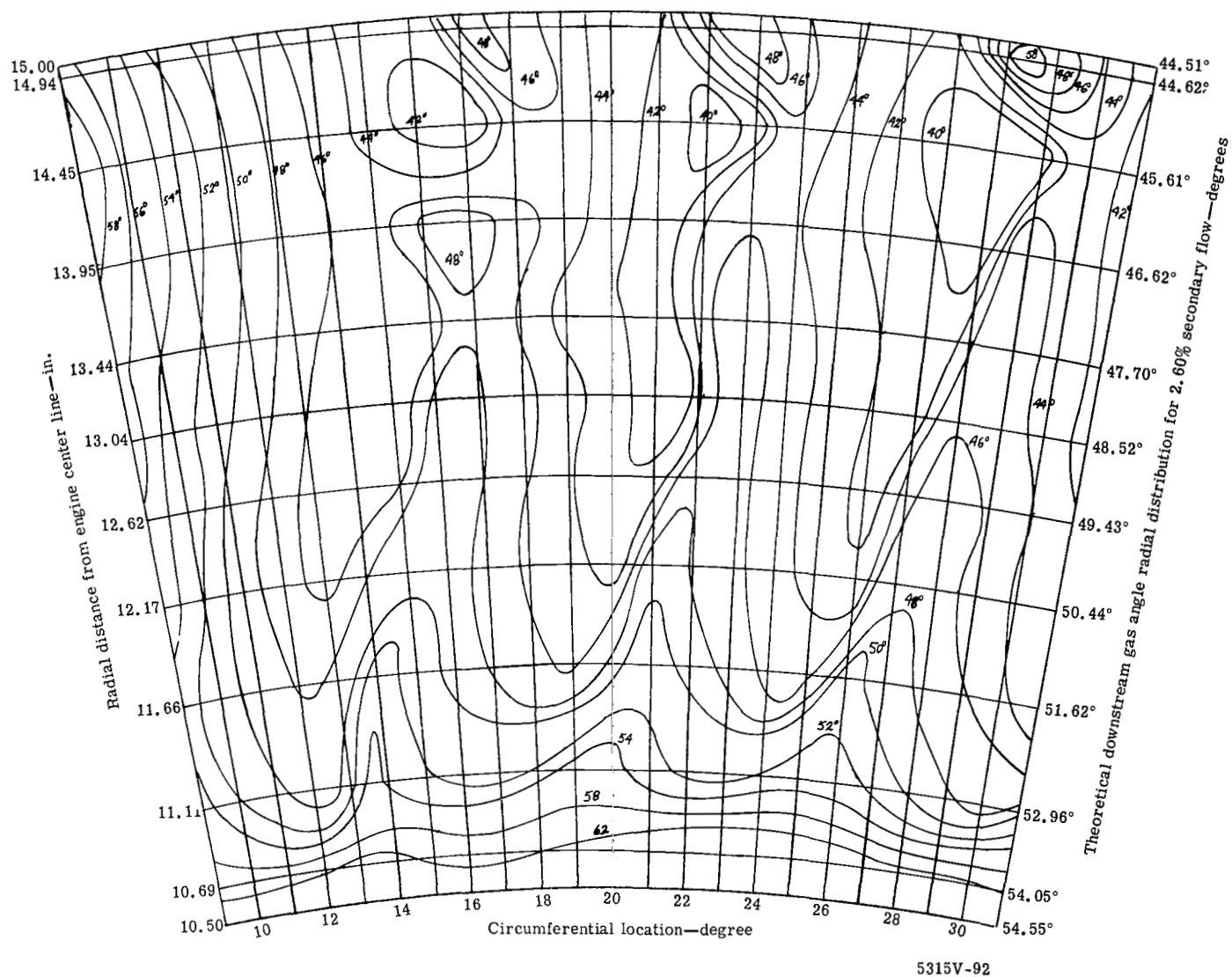
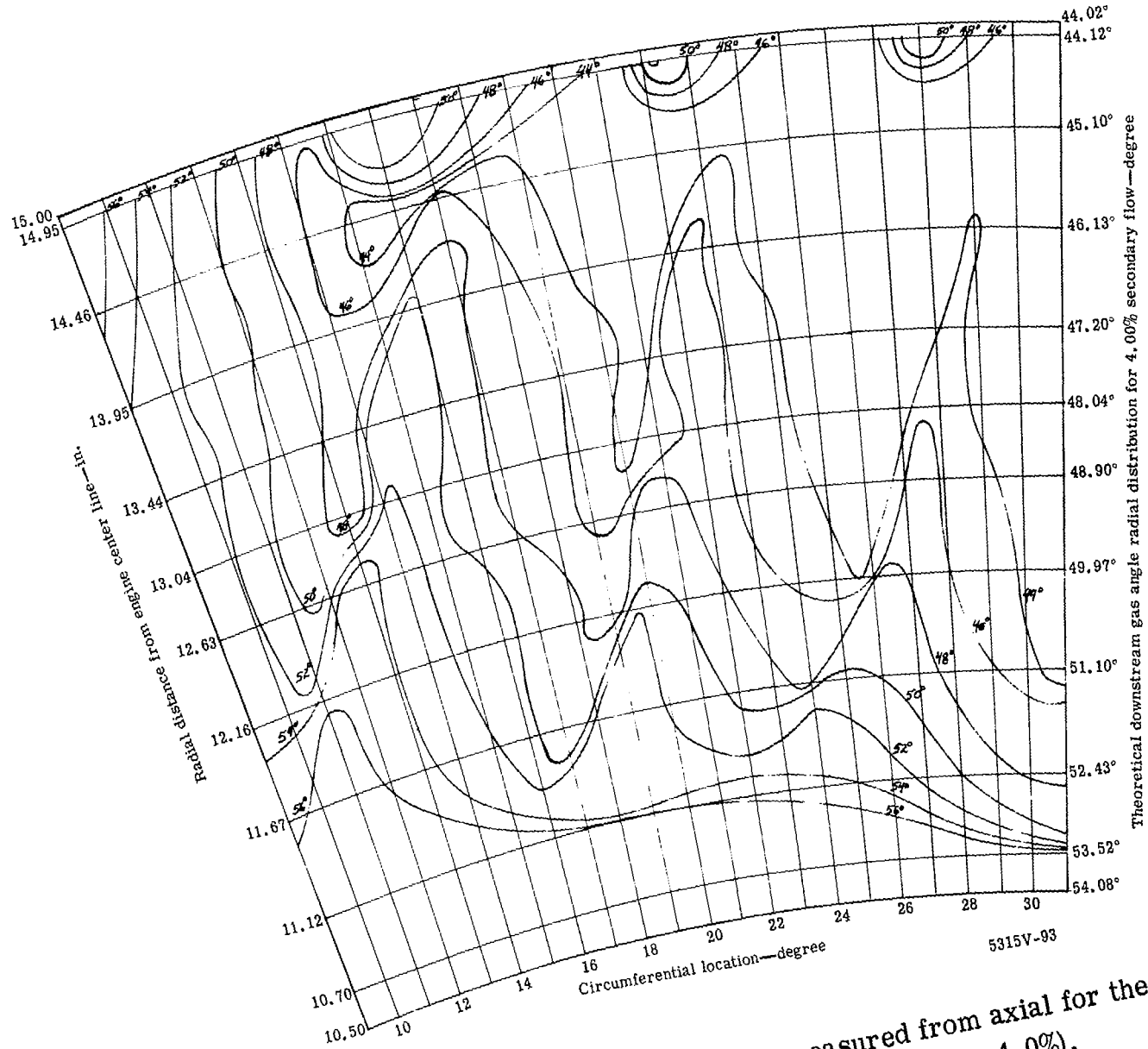


Figure 88. Contours of downstream gas angle measured from axial for the tangential jet blade No. 1 (0.020-in. slot, $\dot{m}_j/\dot{m}_p = 2.67\%$).



Theoretical downstream gas angle radial distribution for 4.00% secondary flow—degree
 (0.020-in. slot, $\dot{m}_j/\dot{m}_p = 4.0\%$).

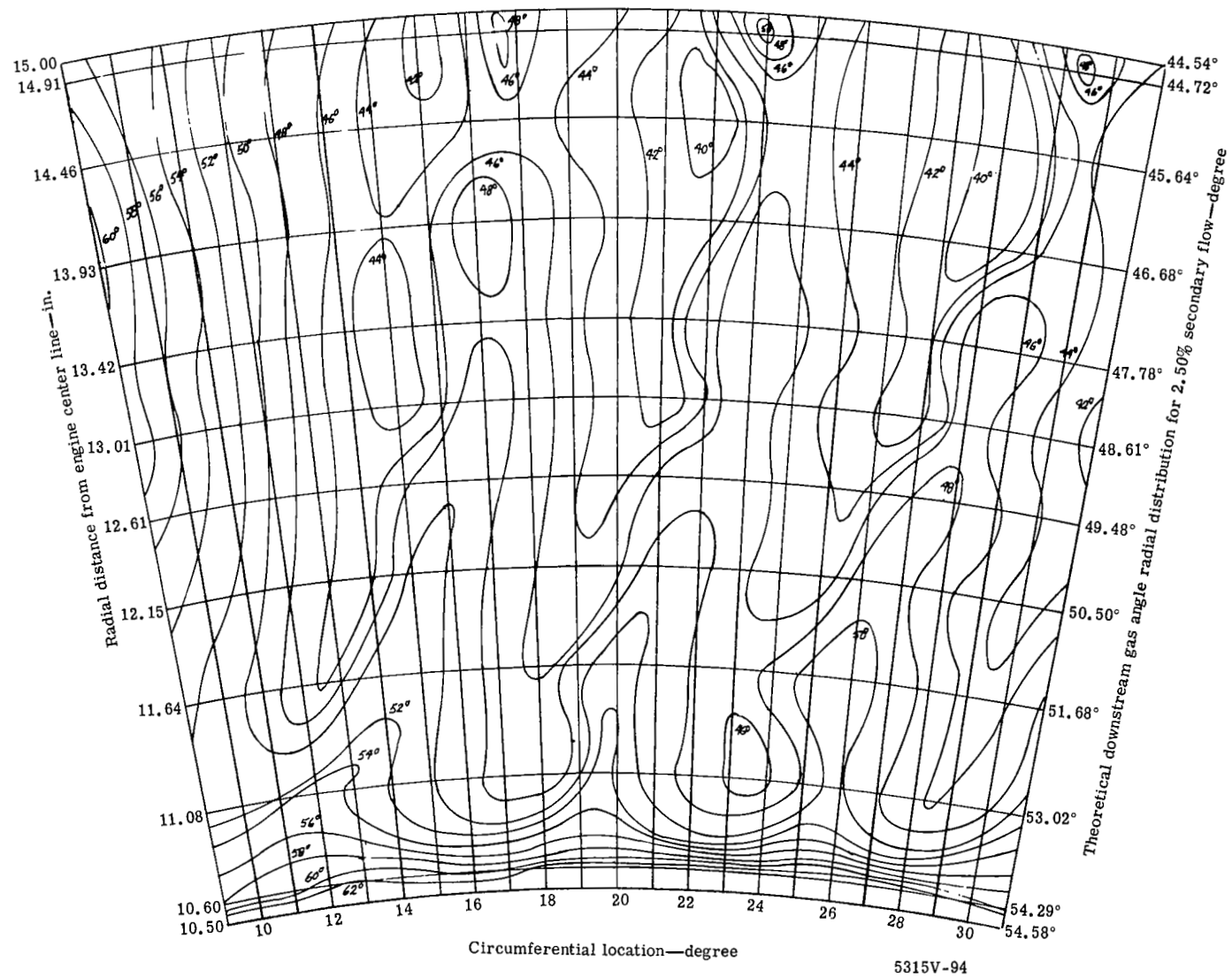


Figure 90. Contours of downstream gas angle measured from axial for the tangential jet blade No. 1 (0.030-in. slot, $\dot{m}_j/\dot{m}_p = 2.5\%$).

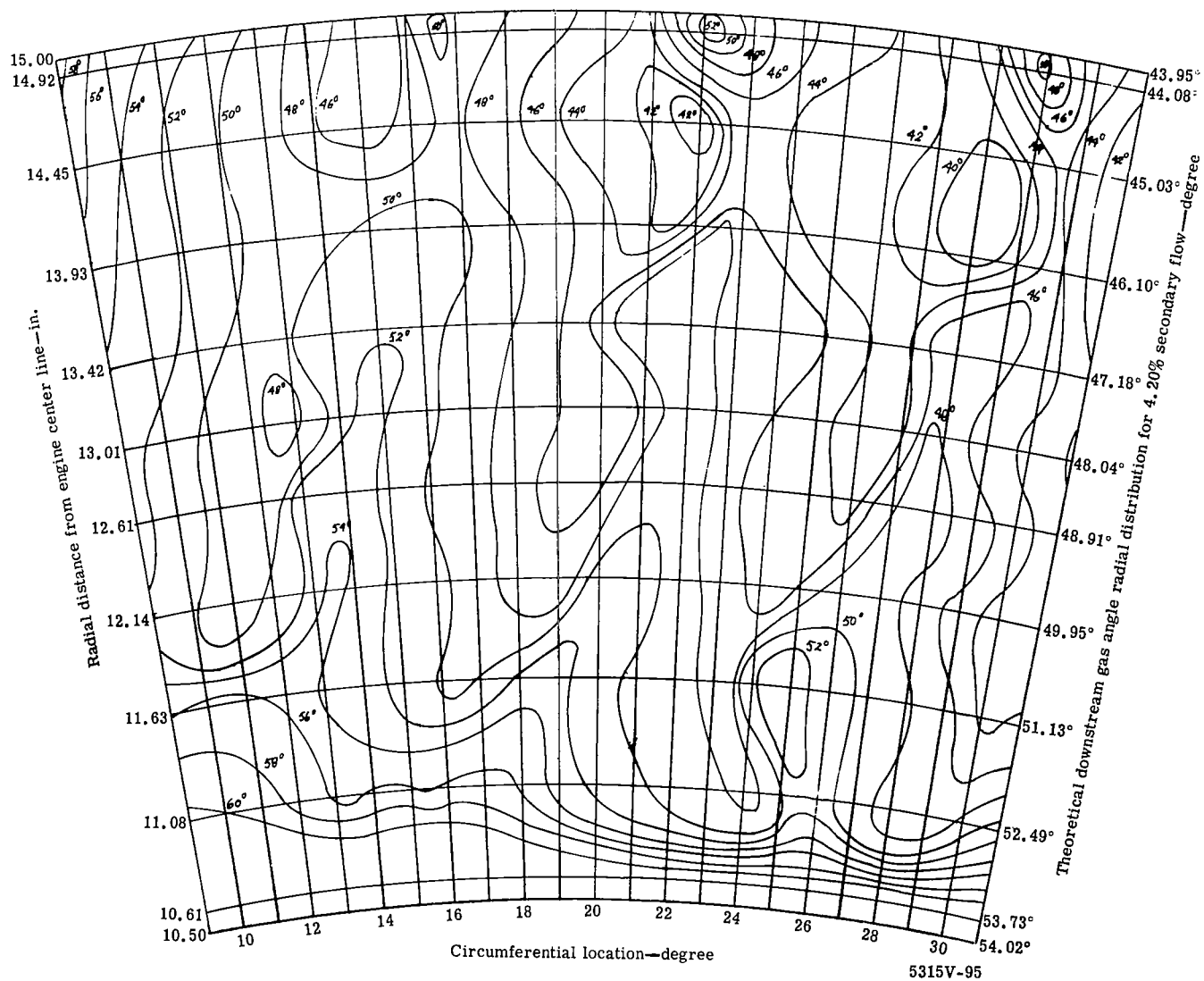
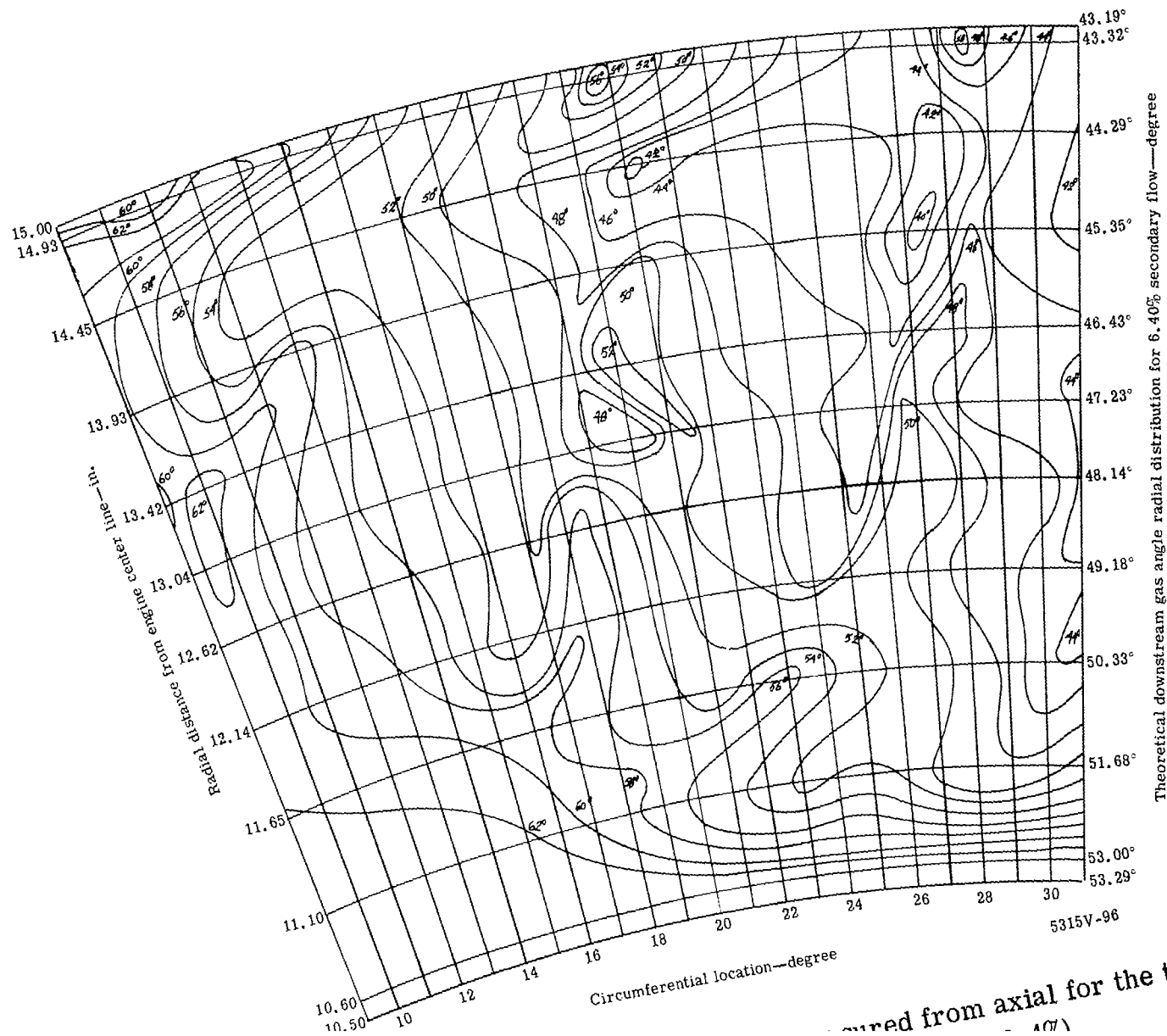


Figure 91. Contours of downstream gas angle measured from axial for the tangential jet blade No. 1 (0.030-in. slot, $\dot{m}_j/\dot{m}_p = 4.2\%$).



measured from axial for the tangential

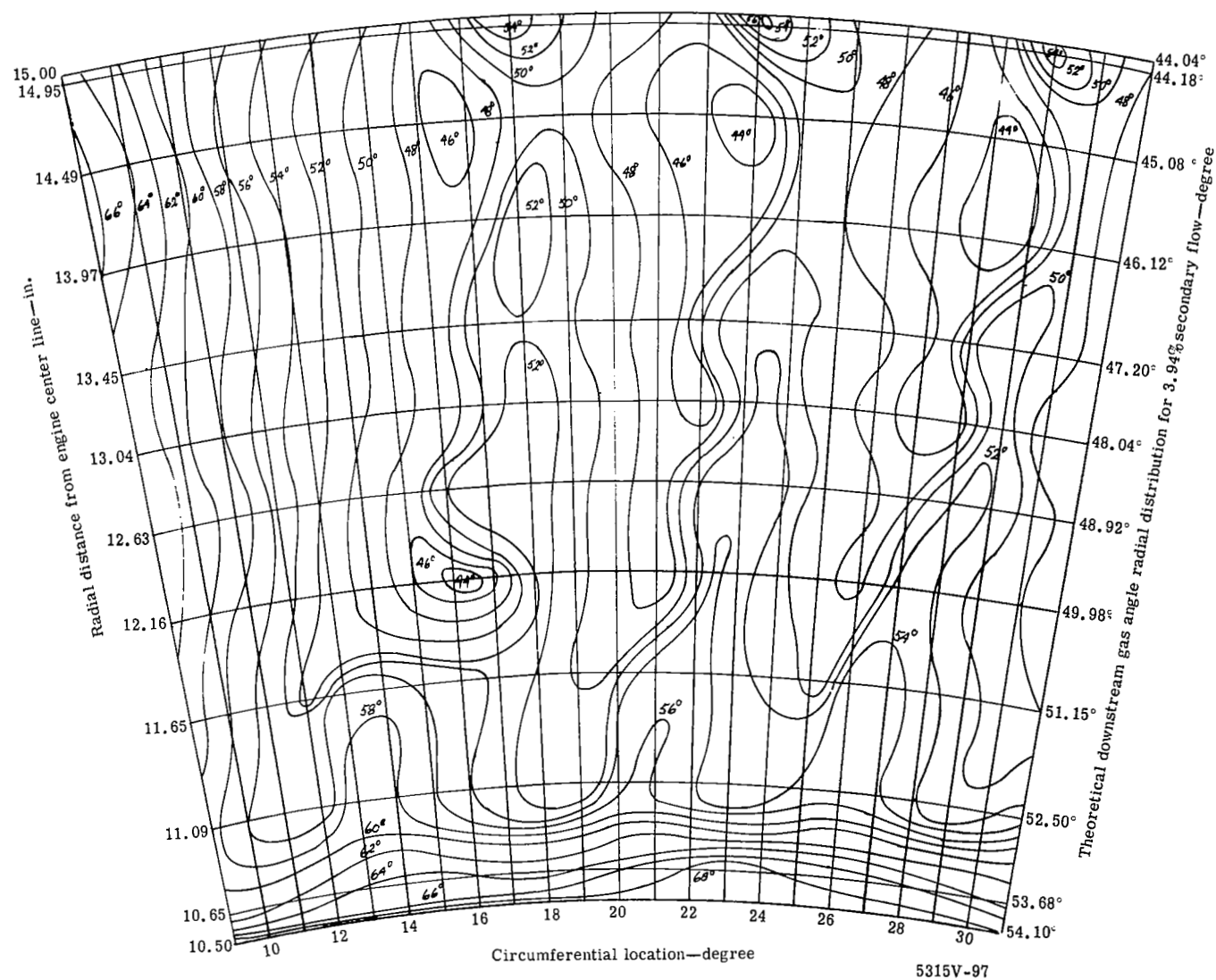


Figure 93. Contours of downstream gas angle measured from axial for the tangential jet blade No. 1 (0.040-in. slot, $\dot{m}_j/\dot{m}_p = 3.94\%$).

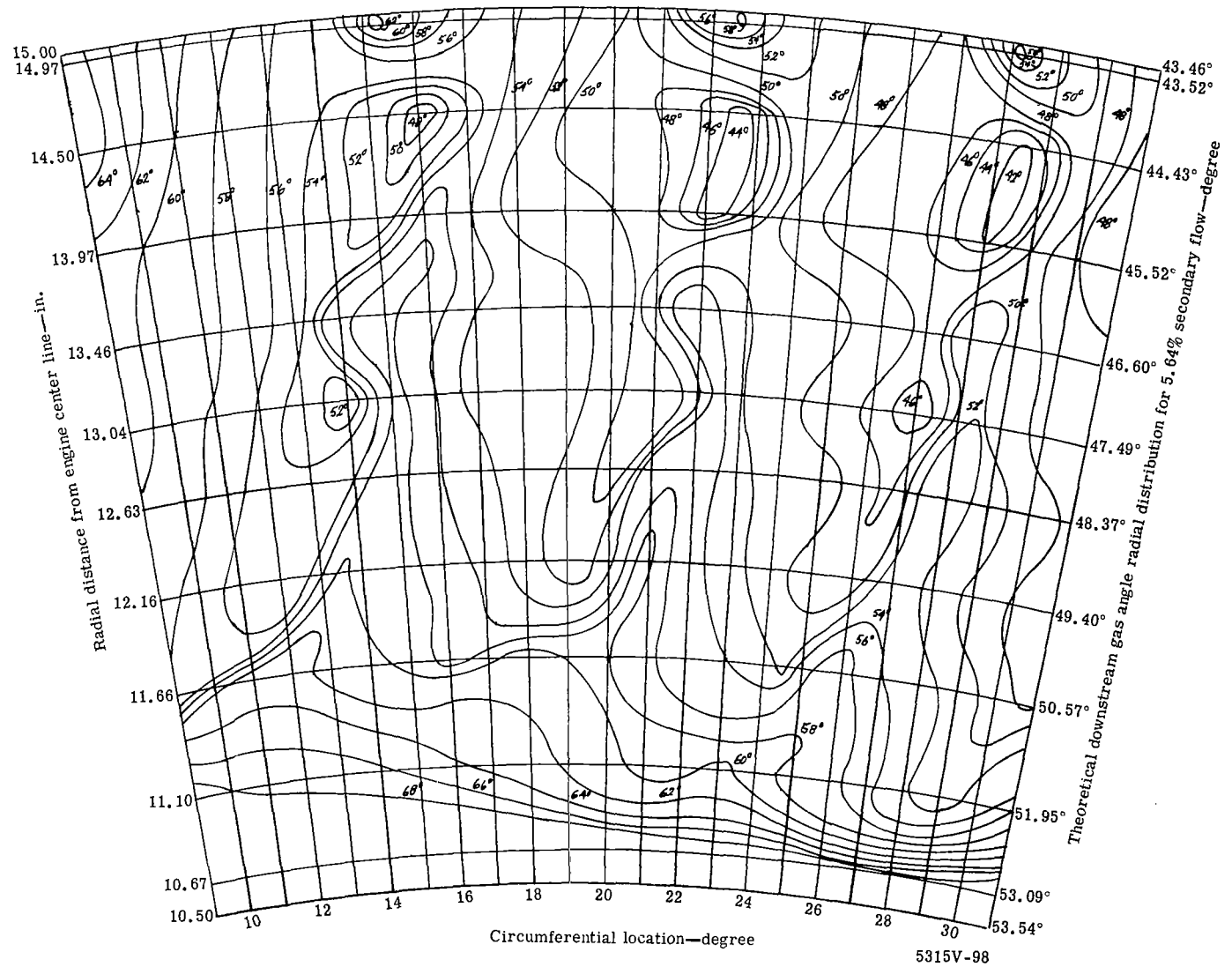


Figure 94. Contours of downstream gas angle measured from axial for the tangential jet blade No. 1 (0.040-in. slot, $\dot{m}_j/\dot{m}_p = 5.64\%$).

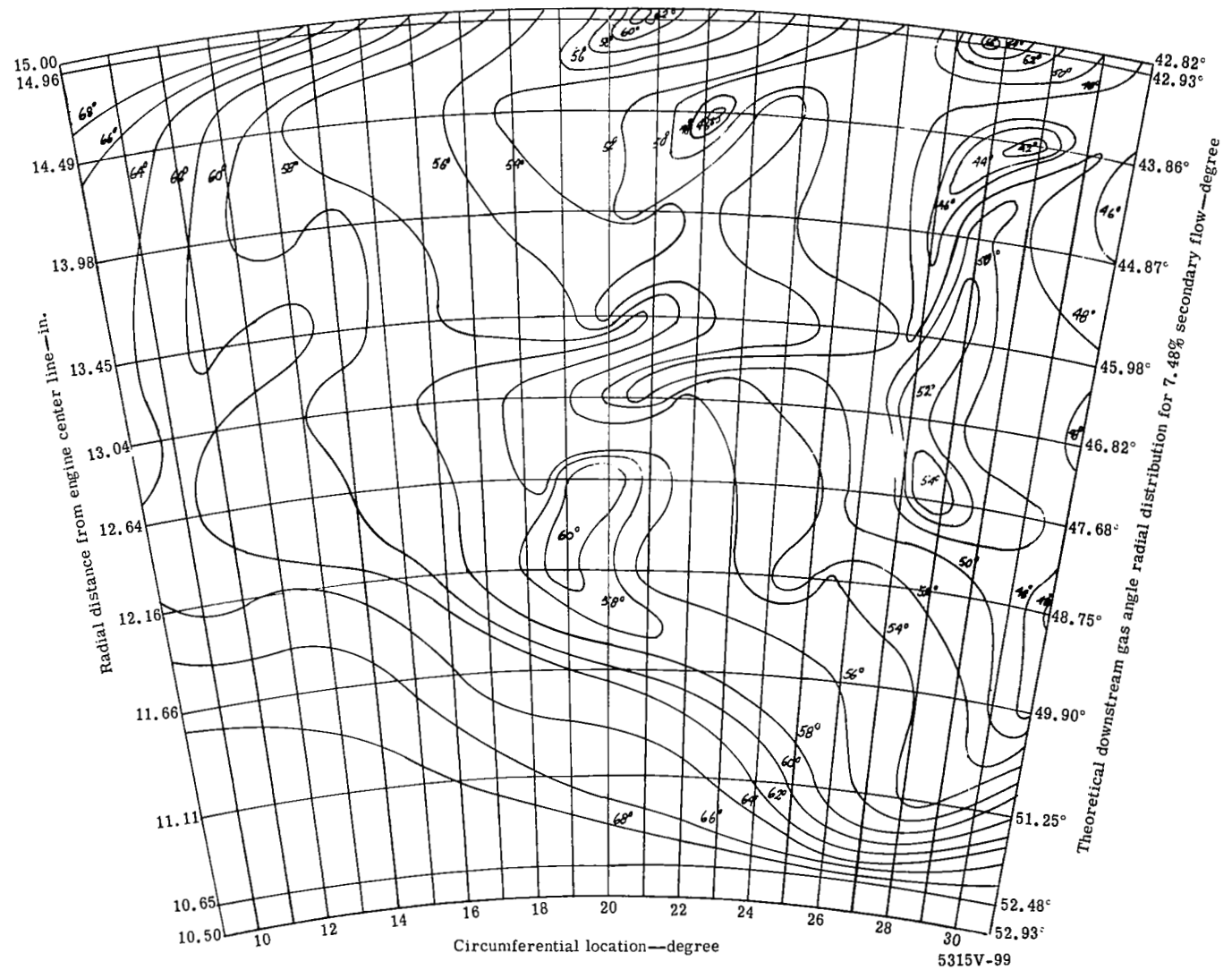
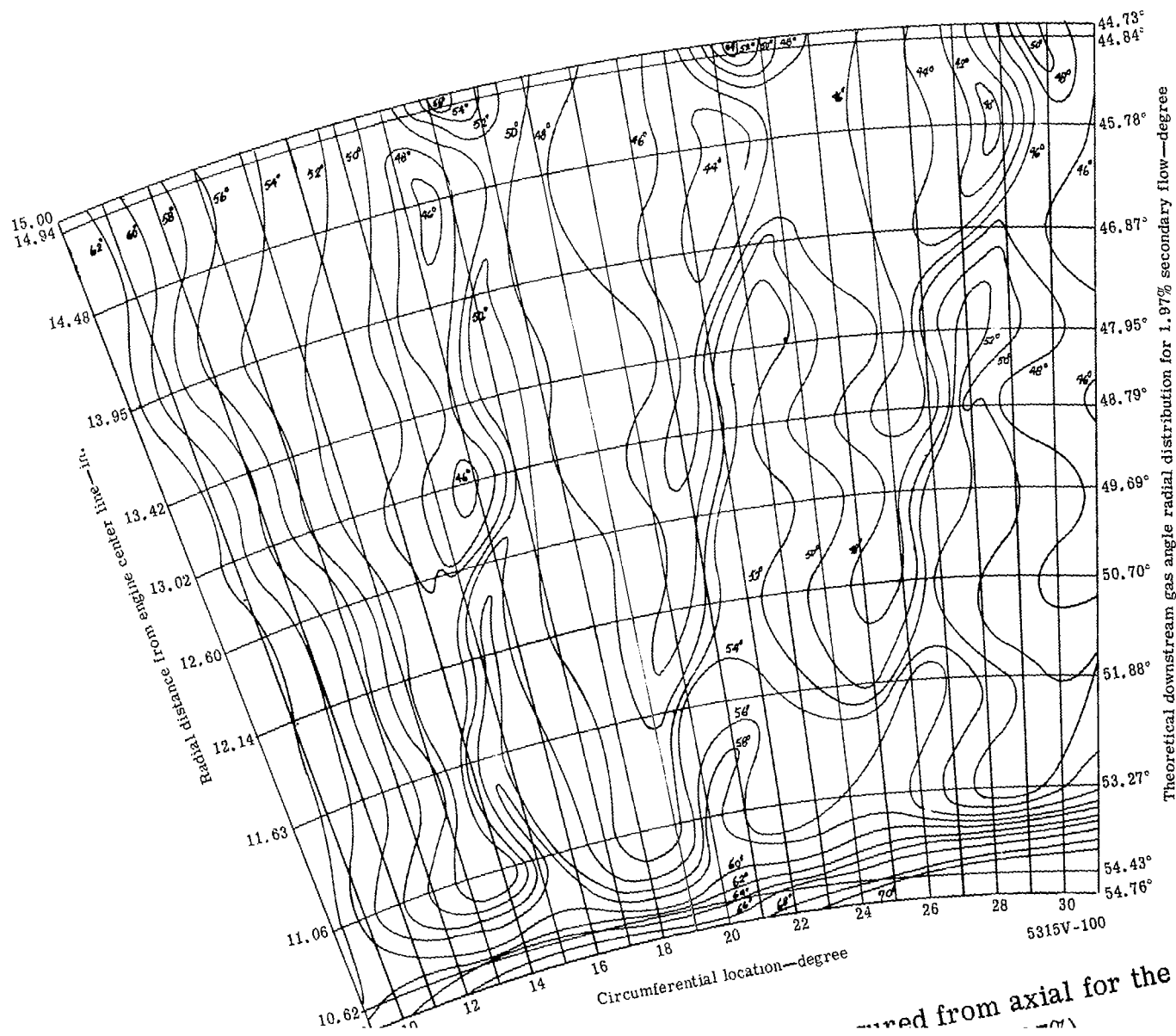
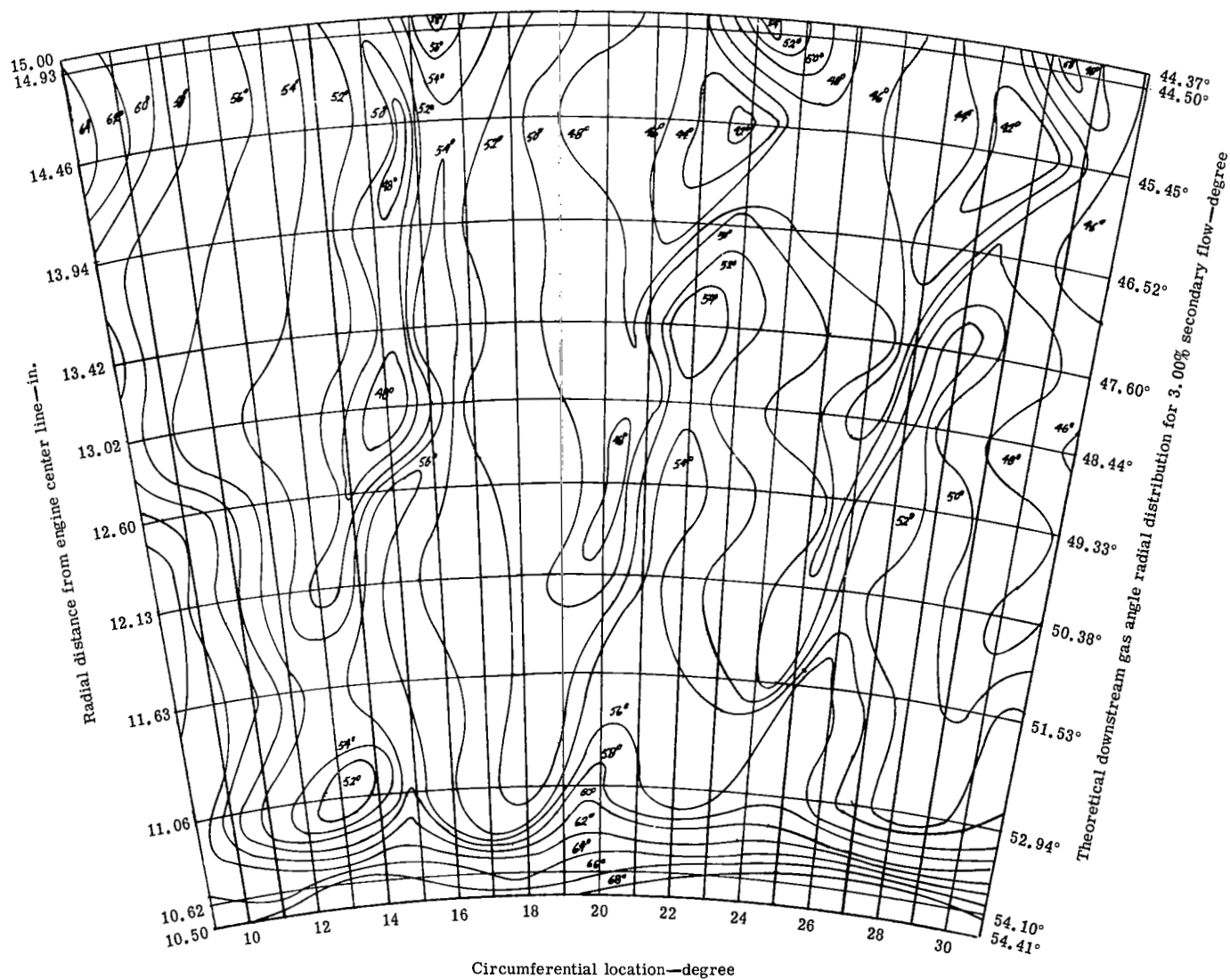


Figure 95. Contours of downstream gas angle measured from axial for the tangential jet blade No. 1 (0.040-in. slot, $\dot{m}_j/\dot{m}_p = 7.48\%$).

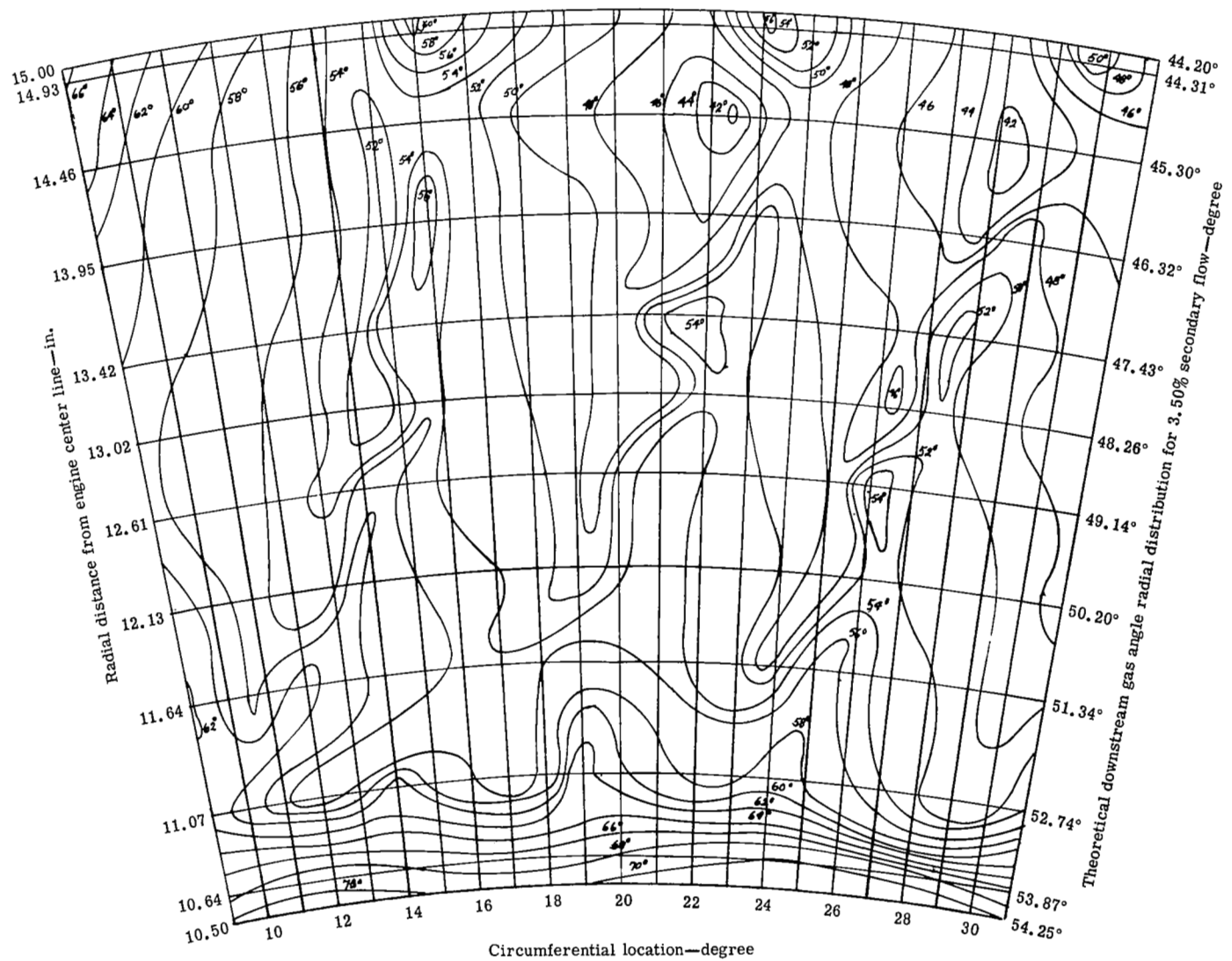


5315V-100
e
-ured from axial for the tangential
- 70A



5315V-101

Figure 97. Contours of downstream gas angle measured from axial for the tangential jet blade No. 2 (0.020-in. slot, $\dot{m}_j/\dot{m}_p = 3.00\%$).



5315V-102

Figure 98. Contours of downstream gas angle measured from axial for the tangential jet blade No. 2 (0.020-in. slot, $\dot{m}_j/\dot{m}_p = 3.50\%$).

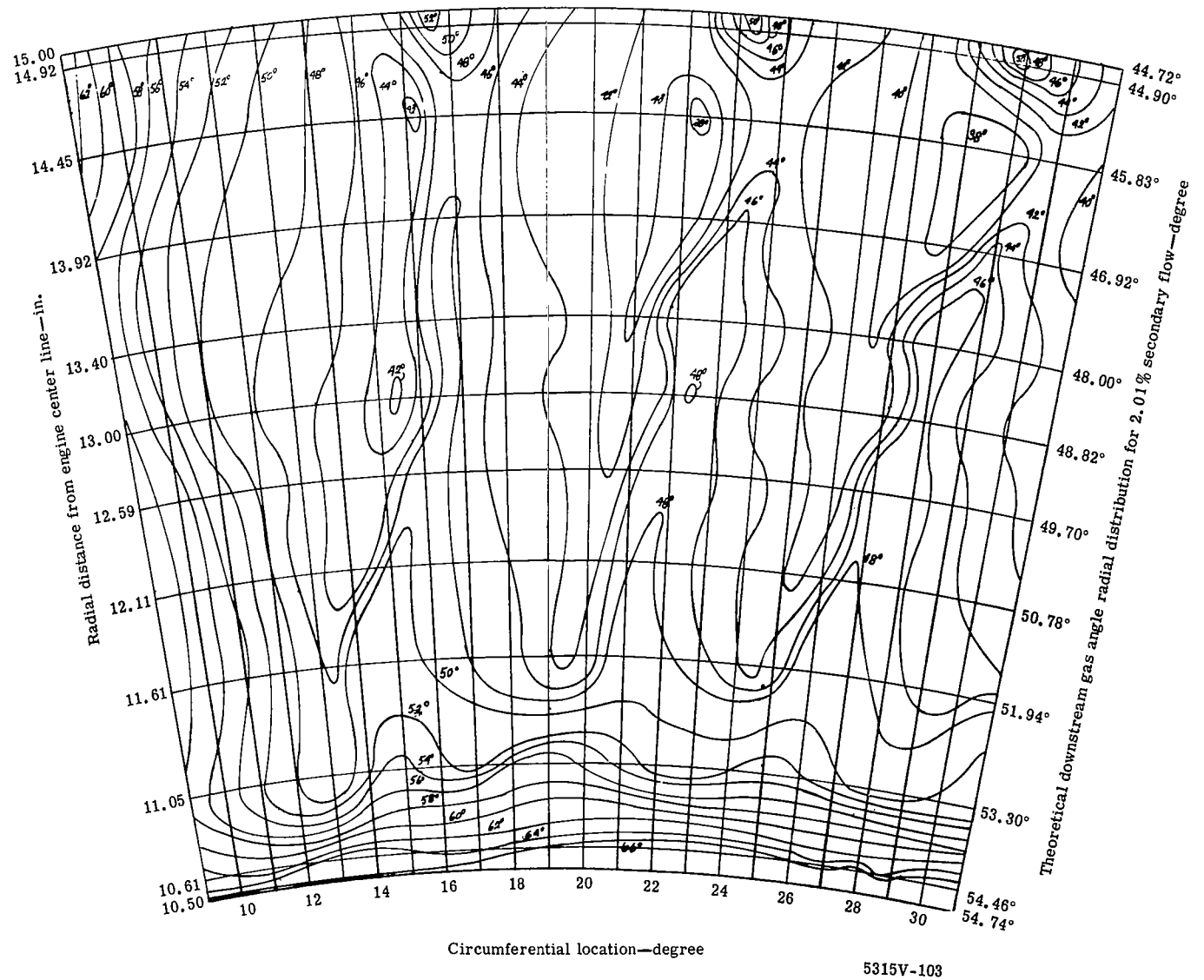
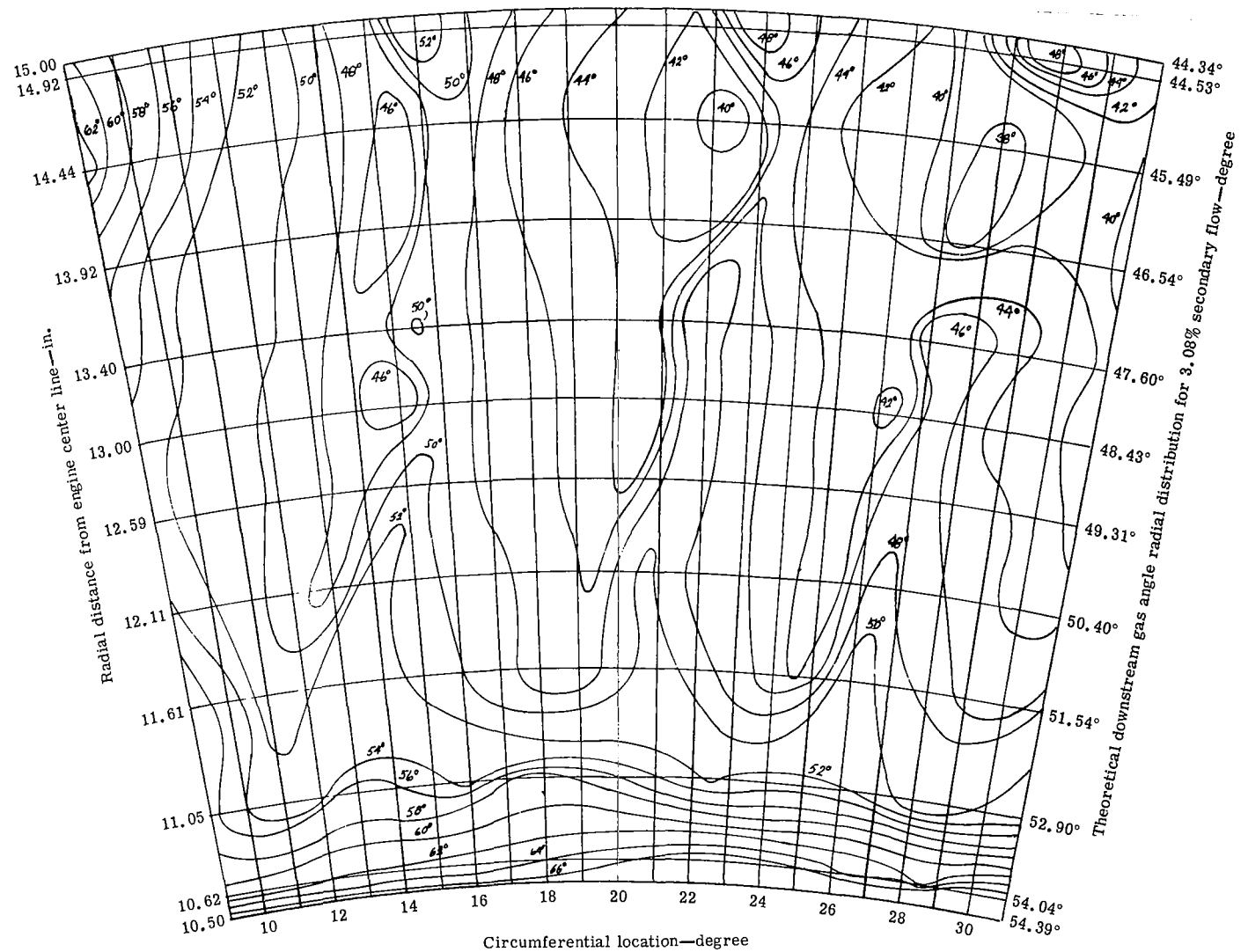


Figure 99. Contours of downstream gas angle measured from axial for the tangential jet blade No. 2 (0.030-in. slot, $\dot{m}_j/\dot{m}_p = 2.0\%$).



5315V-104

Figure 100. Contours of downstream gas angle measured from axial for the tangential jet blade No. 2 (0.030-in. slot, $\dot{m}_j/\dot{m}_p = 3.08\%$).

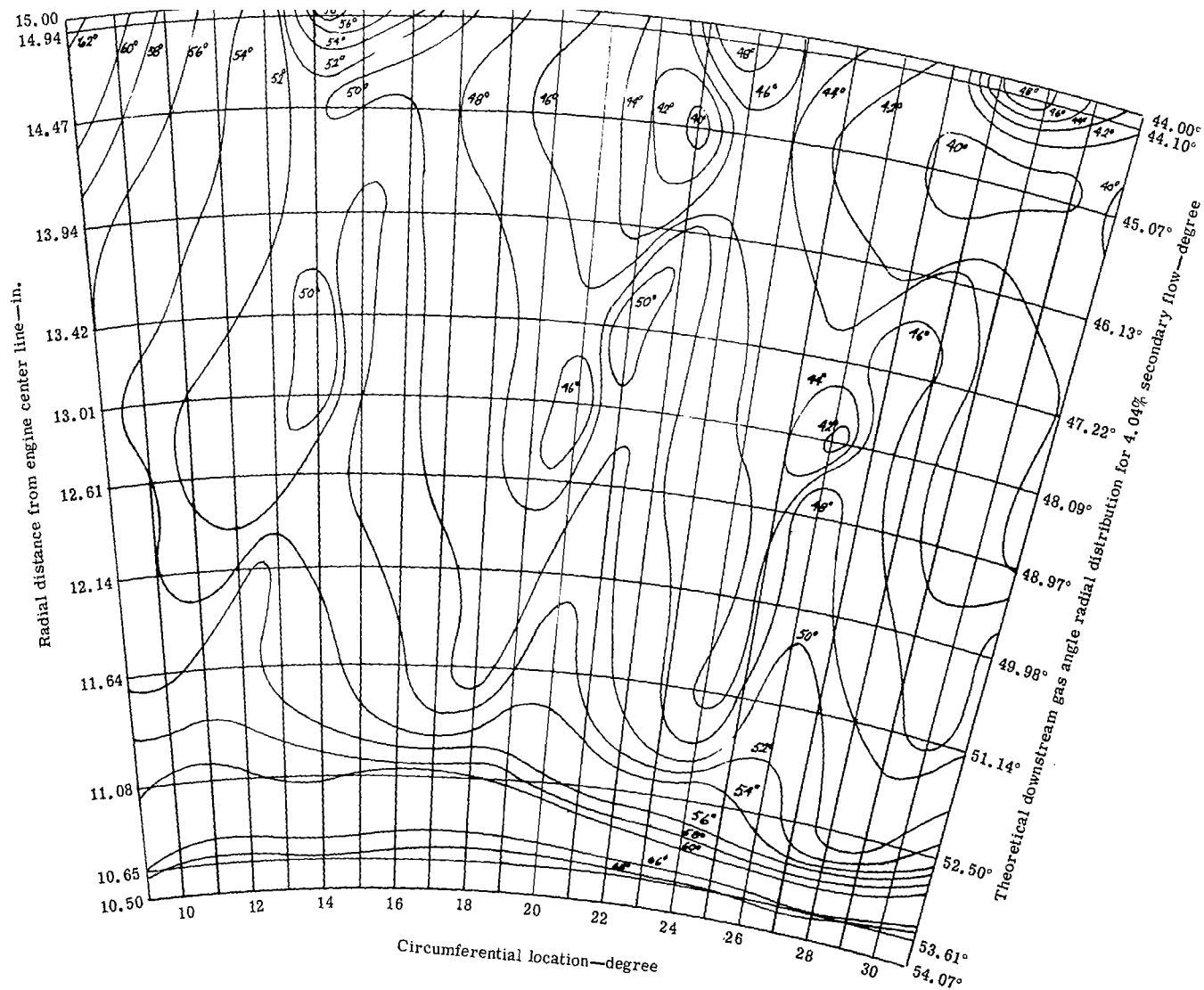


Figure 101. Contours of downstream gas angle measured from axial for the tangential jet blade No. 2 (0.030-in. slot, $\dot{m}_j/\dot{m}_p = 4.04\%$).

5315V-105

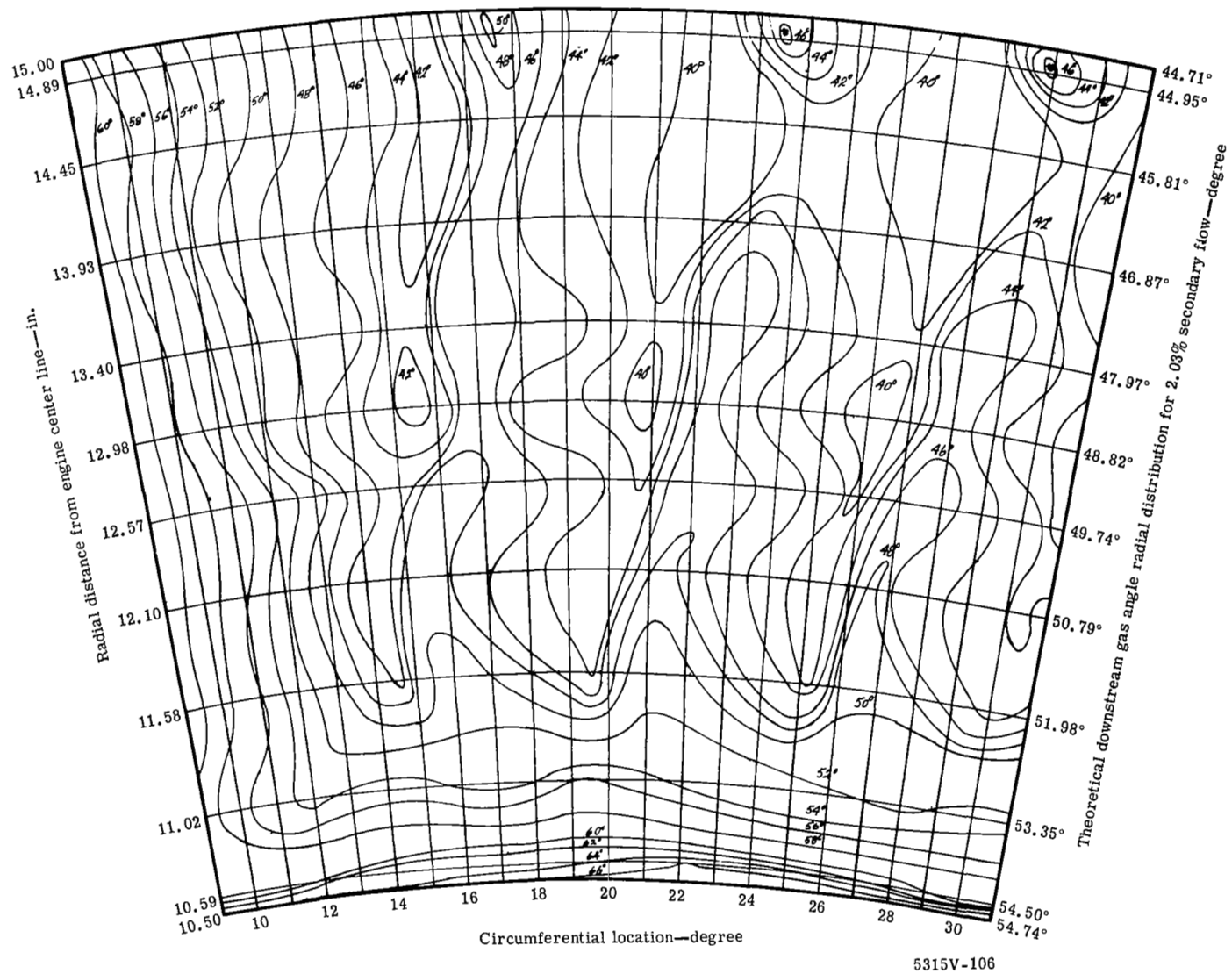


Figure 102. Contours of downstream gas angle measured from axial for the tangential jet blade No. 2 (0.040-in. slot, $\dot{m}_j/\dot{m}_p = 2.03\%$).

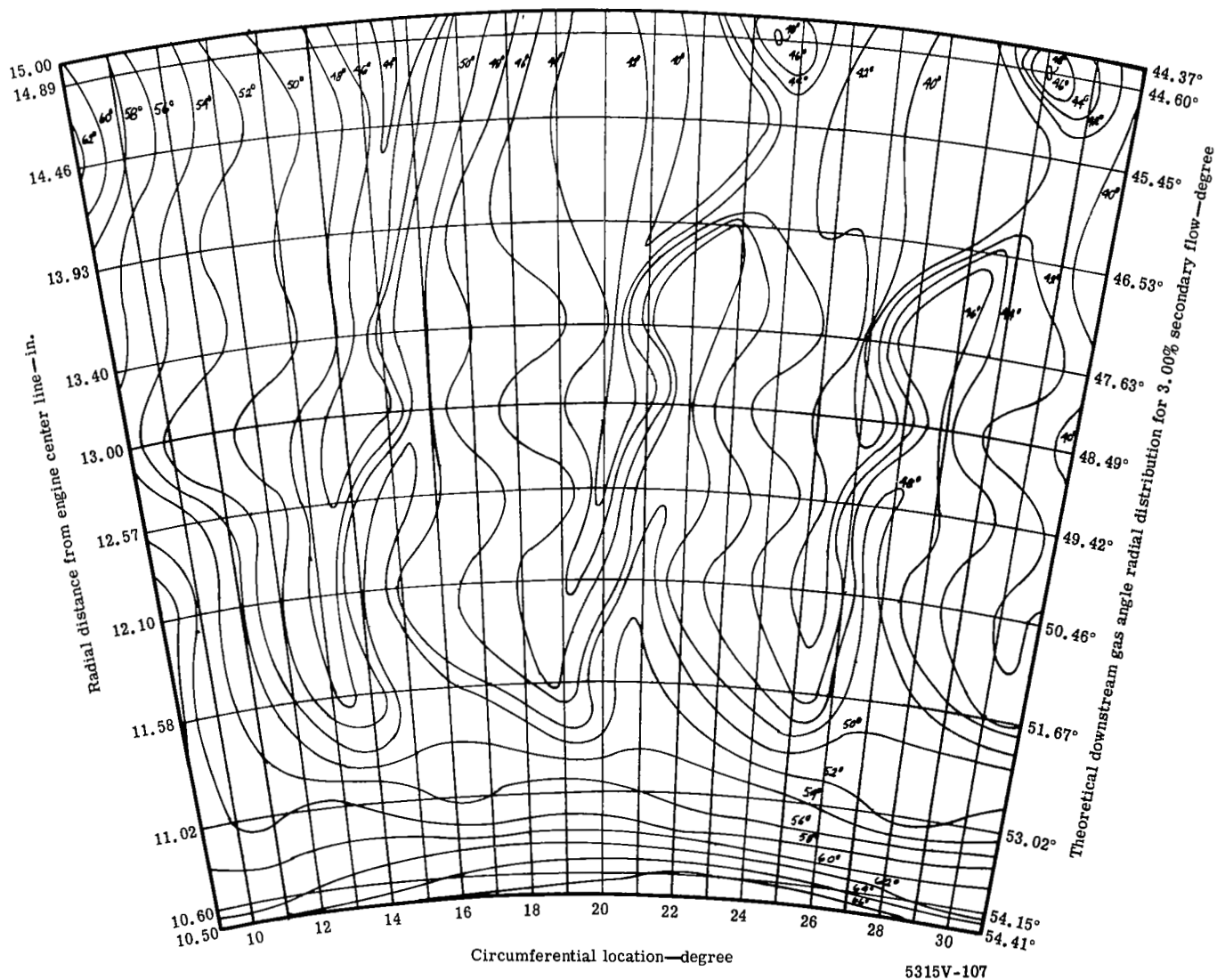


Figure 103. Contours of downstream gas angle measured from axial for the tangential jet blade No. 2 (0.040-in. slot, $\dot{m}_j/\dot{m}_p = 3.00\%$).

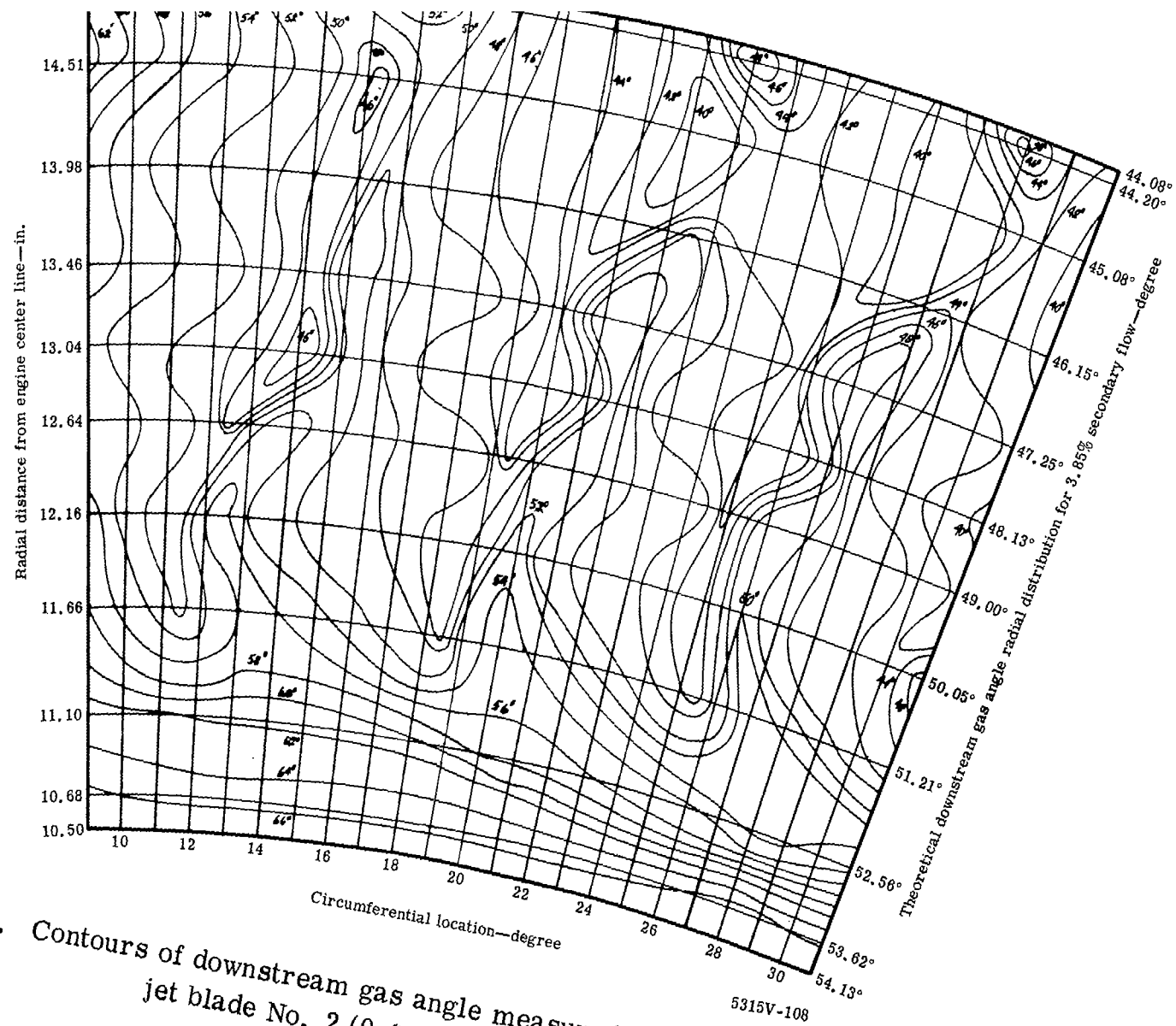
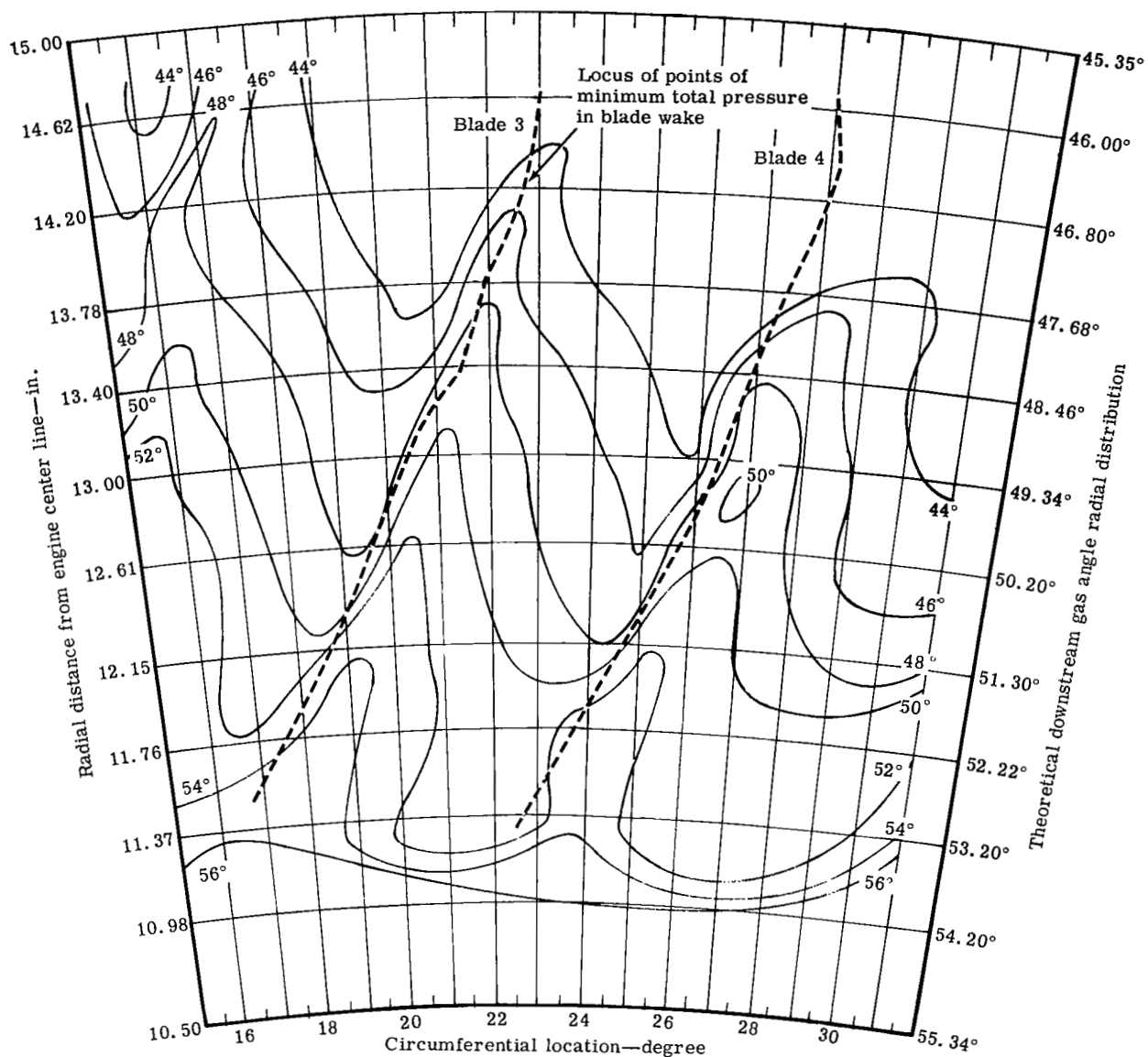


Figure 104. Contours of downstream gas angle measured from axial for the tangential jet blade No. 2 (0.040-in. slot, $\dot{m}_j/\dot{m}_p = 3.85\%$).



5315V-172

Figure 105. Contours of downstream gas angle—measured from axial—
plain blade downstream wake survey.

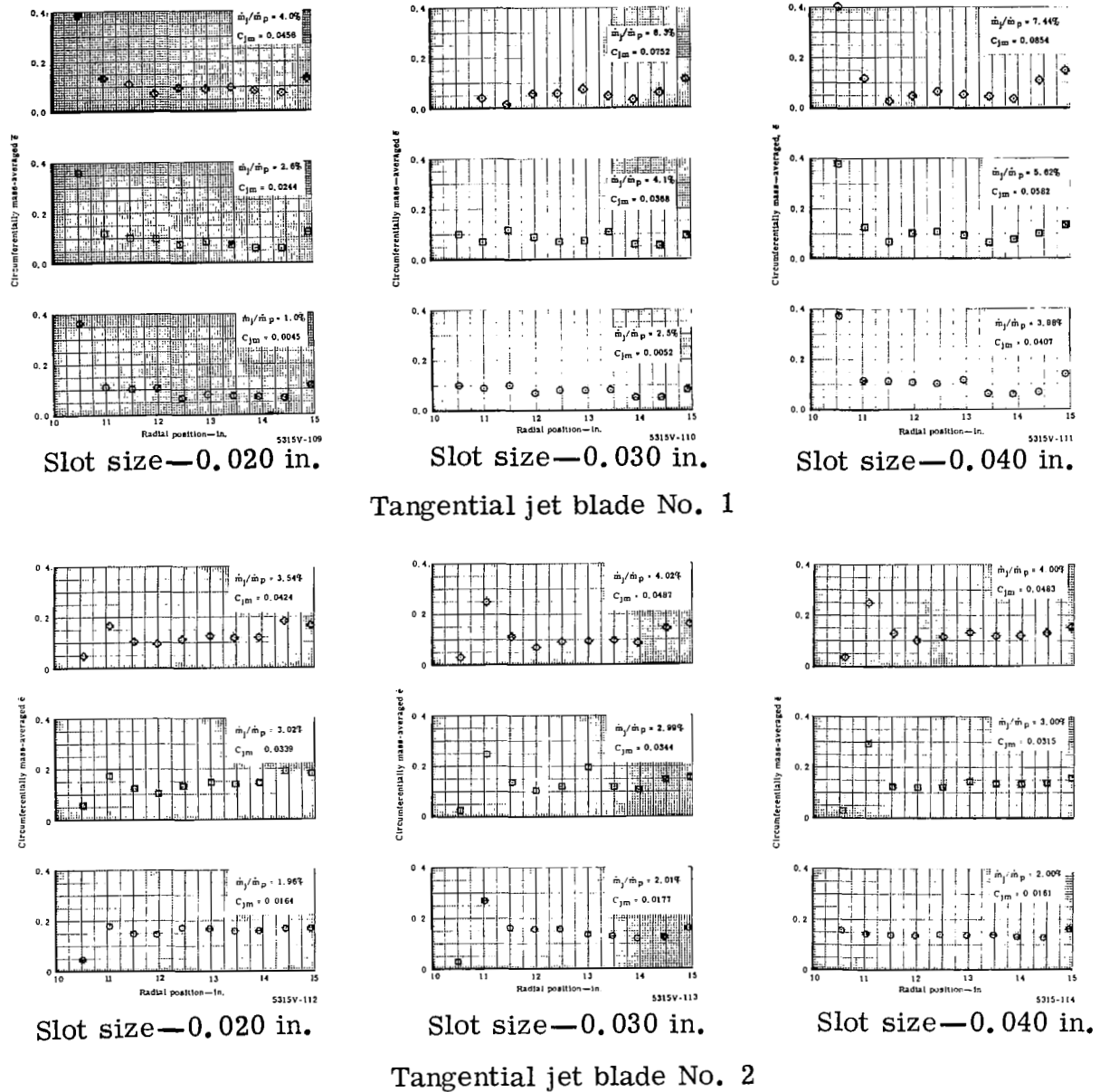


Figure 106. Radial variation of circumferentially mass-averaged kinetic energy loss coefficient at trailing edge (Station 3) for all tangential jet configurations.

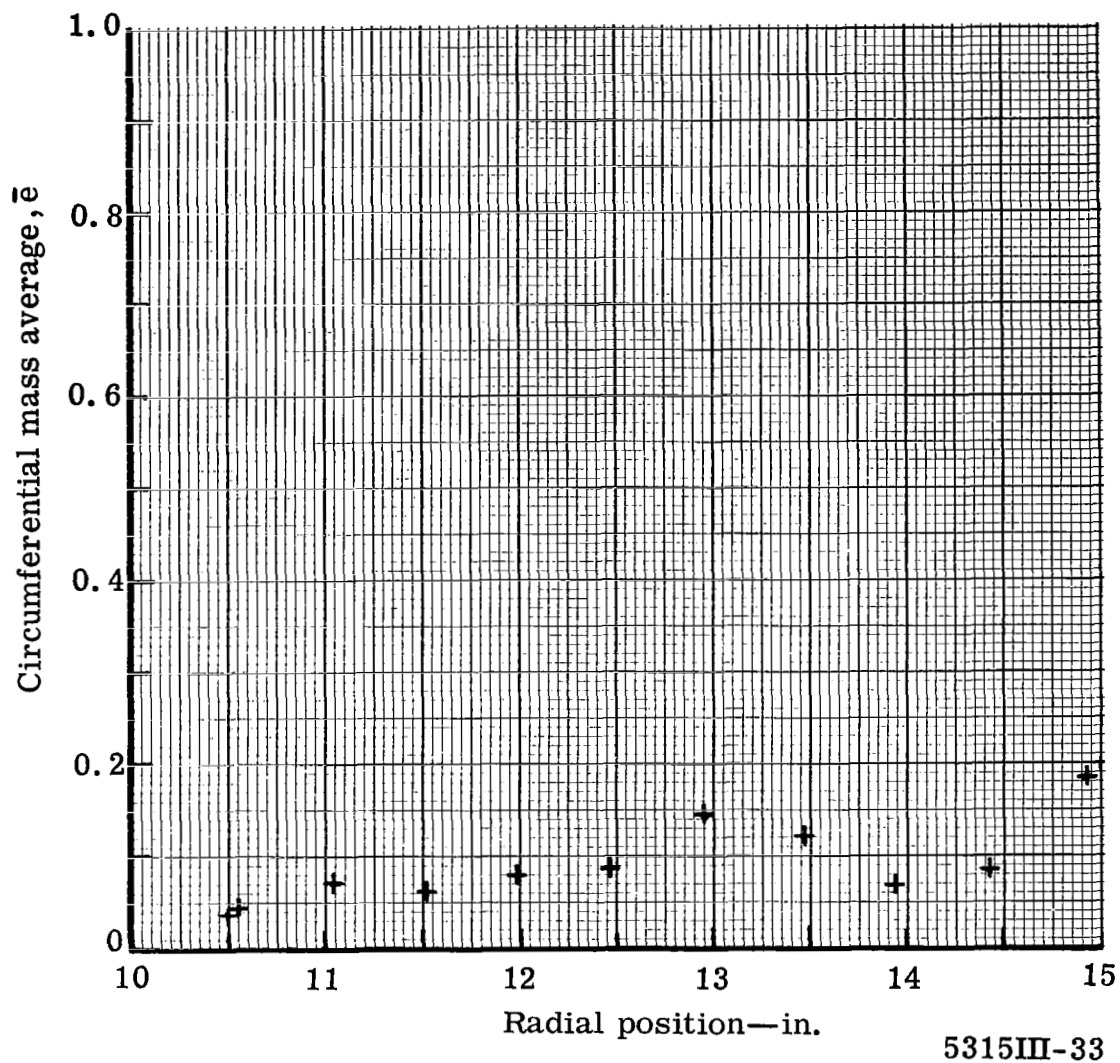
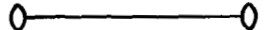



Figure 107. Plain blade exit wake survey—kinetic energy loss coefficient at Station 3.

Tangential jet blade		\overline{hb} in.	$\dot{m}_j/\dot{m}_p - \%$	Radial location-in.
	No. 1	0.040	3.98	12.97
	No. 2	0.040	4.00	13.01
				

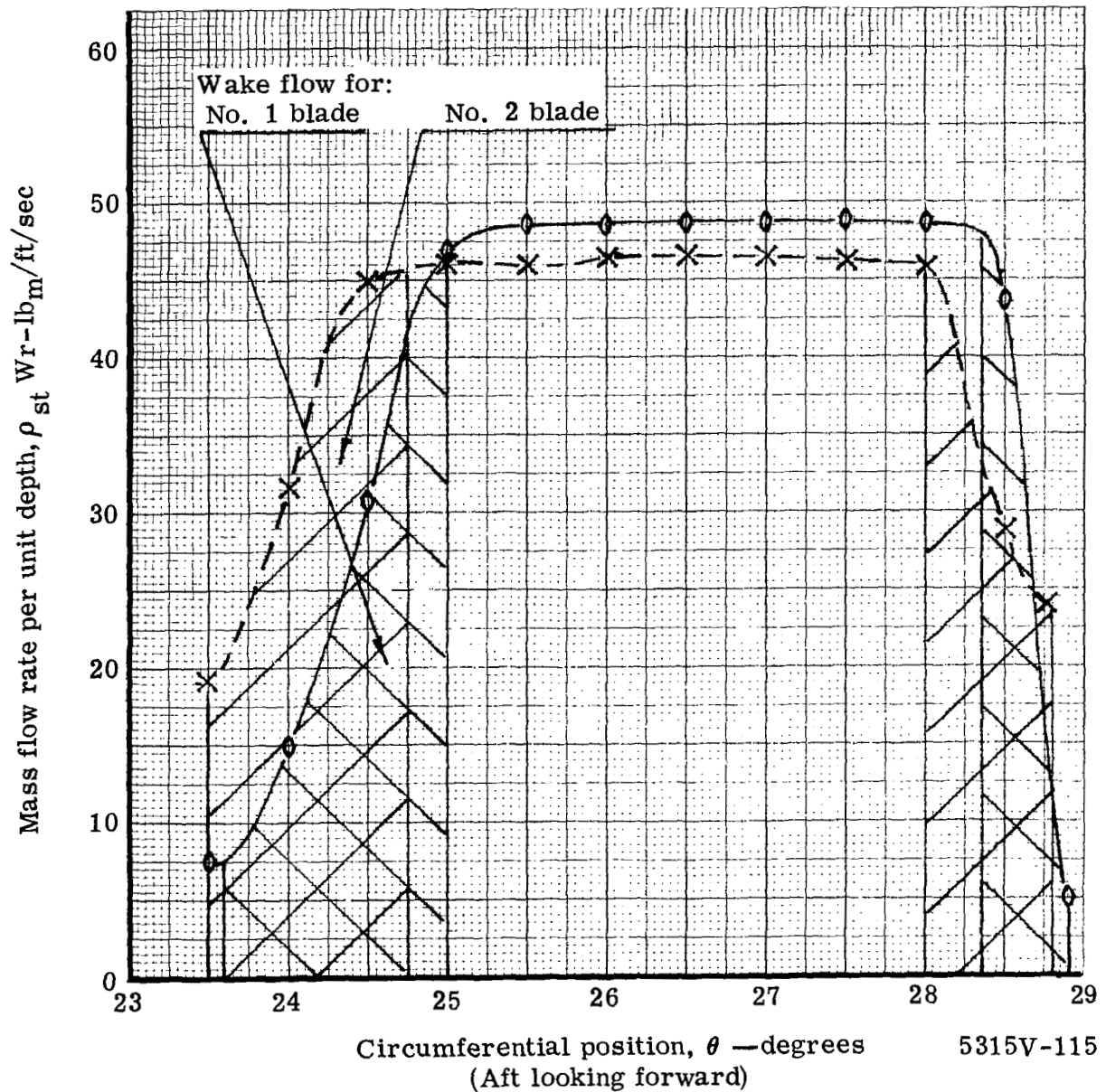


Figure 108. Circumferential variation of mass flow rate per unit depth near the cascade center passage mean section for two tangential jet blade configurations.

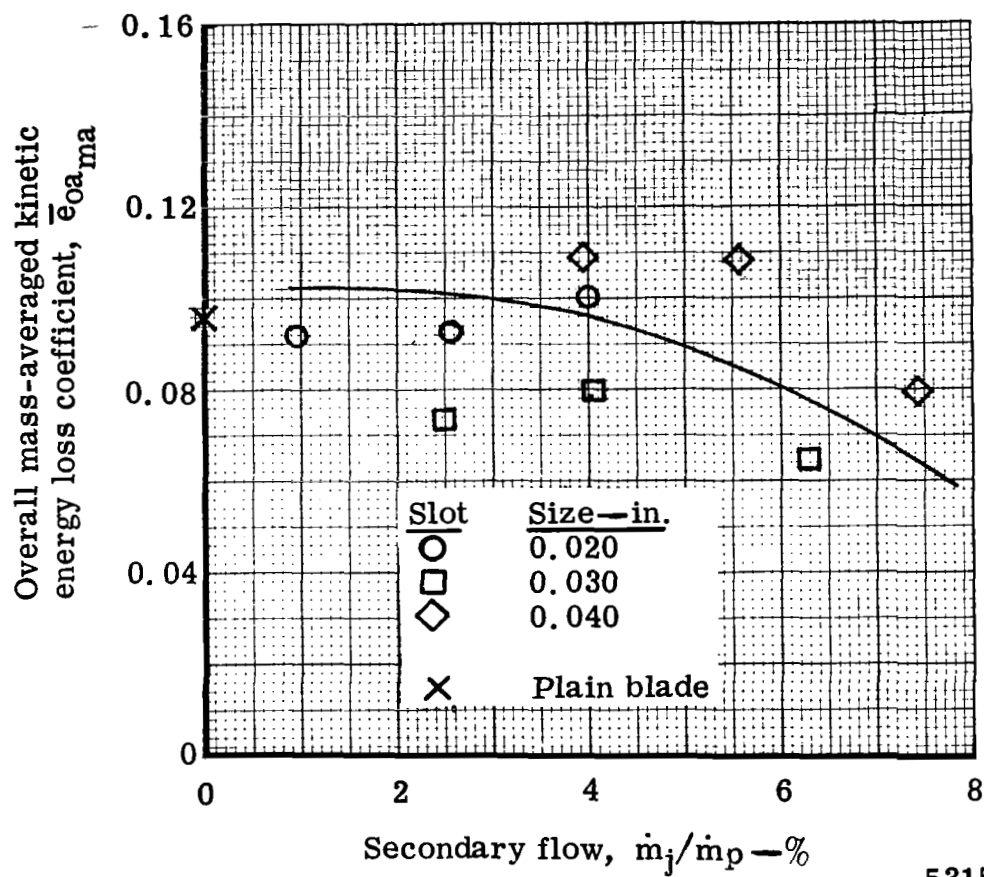


Figure 109. Variation of overall mass-averaged kinetic energy loss coefficient with percent of secondary flow at tangential jet blade No. 1 trailing edge.

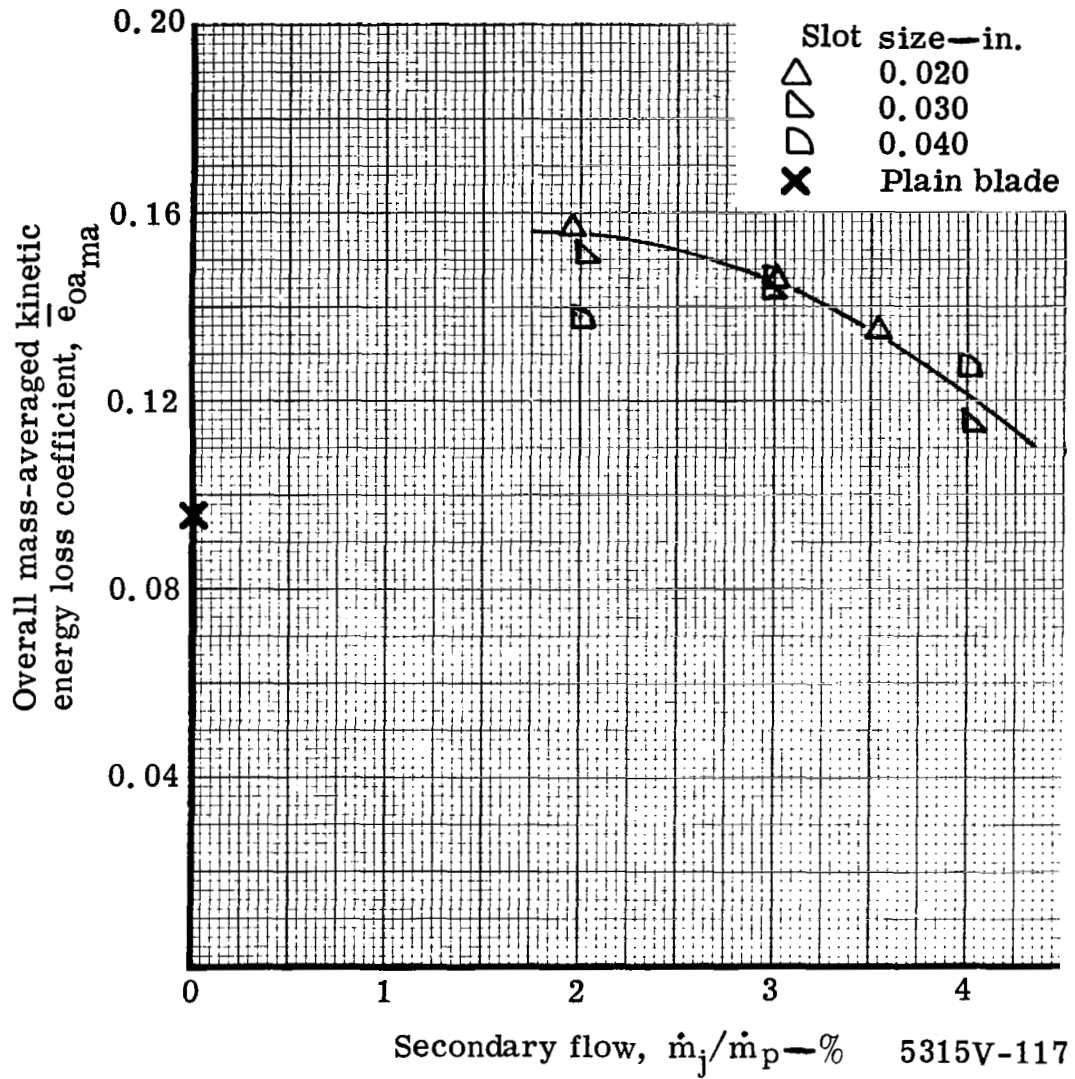
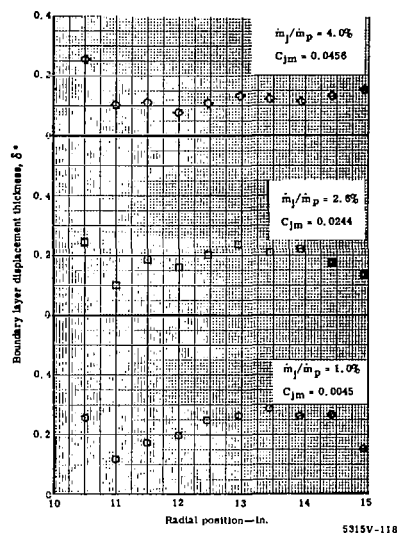
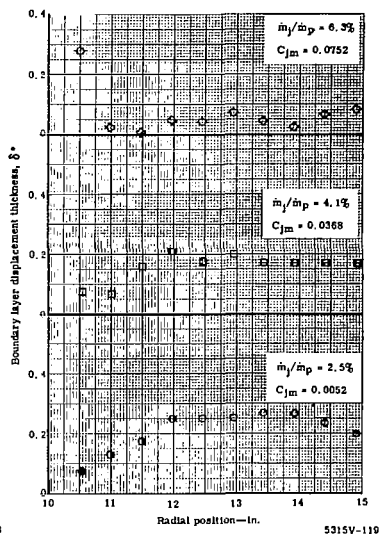


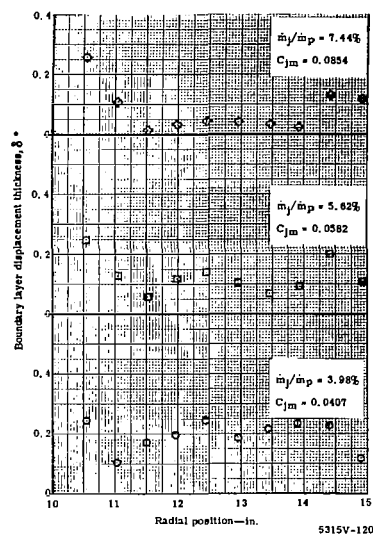
Figure 110. Variation of overall mass-averaged kinetic energy loss coefficient with percent secondary flow at tangential jet blade No. 2 trailing edge.



0.020-in. slot

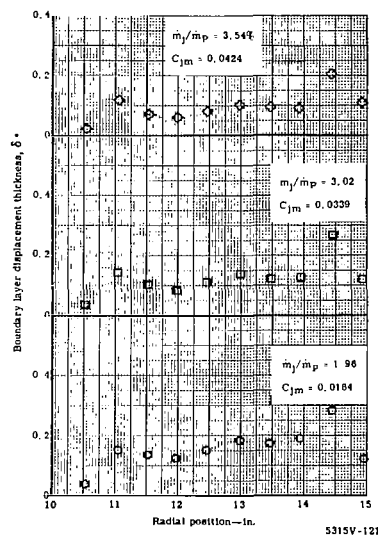


0.030-in. slot

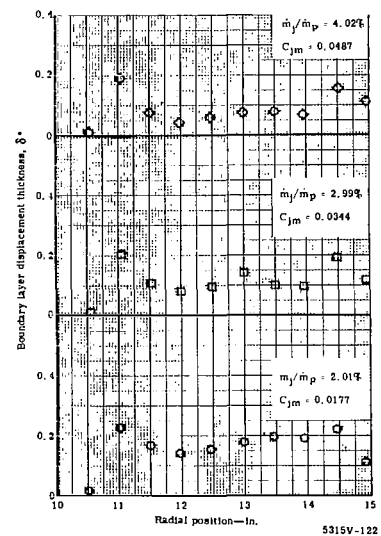


0.040-in. slot

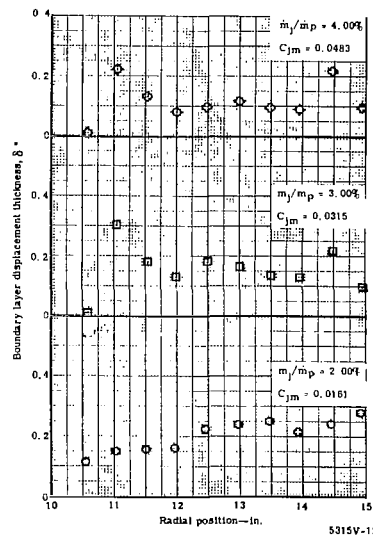
Tangential jet blade No. 1



0.020-in. slot



0.030-in. slot



0.040-in. slot

Tangential jet blade No. 2

Figure 111. Radial variation of boundary layer displacement thickness at trailing edge (Station 3) for all tangential jet configurations.

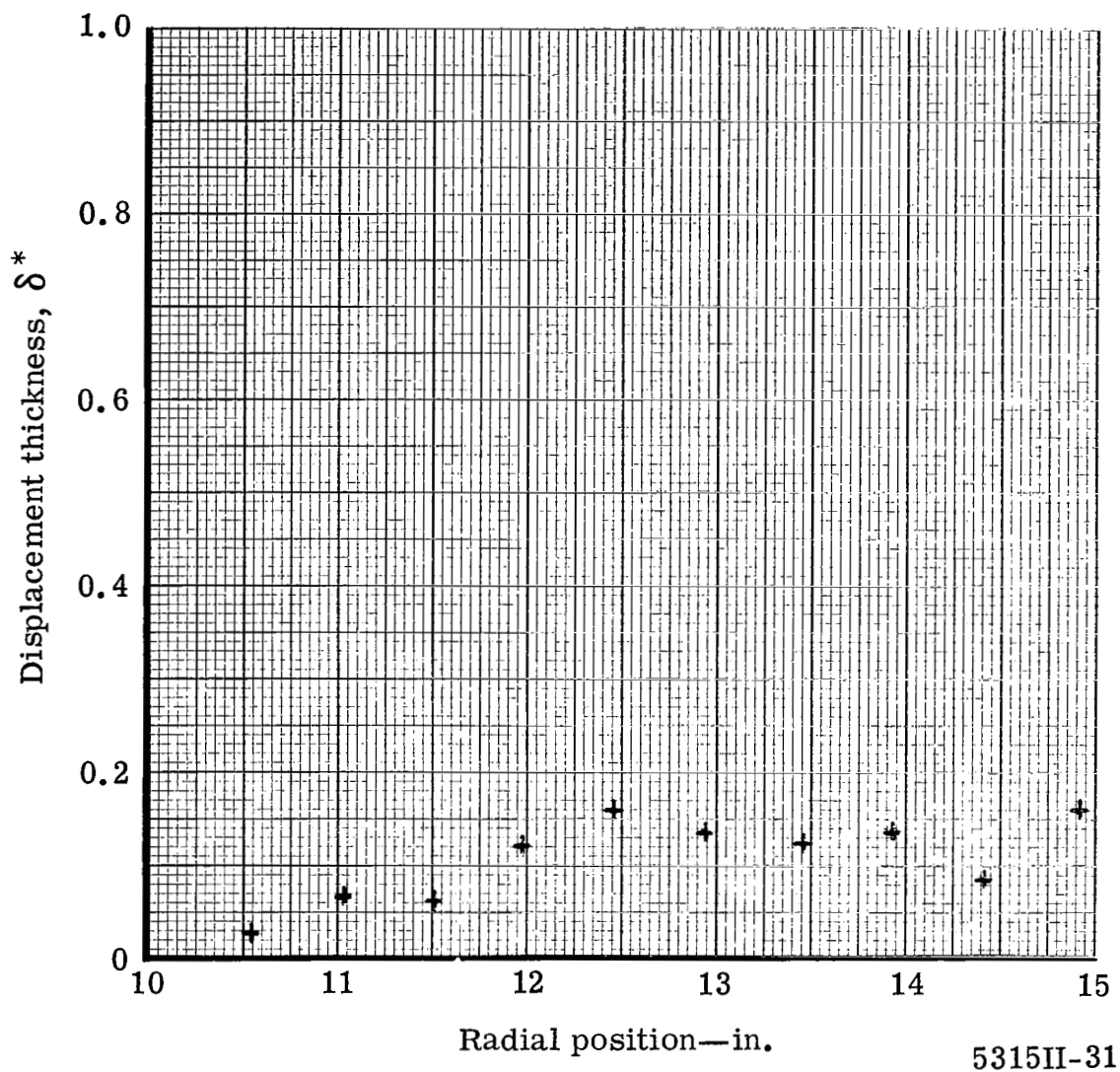
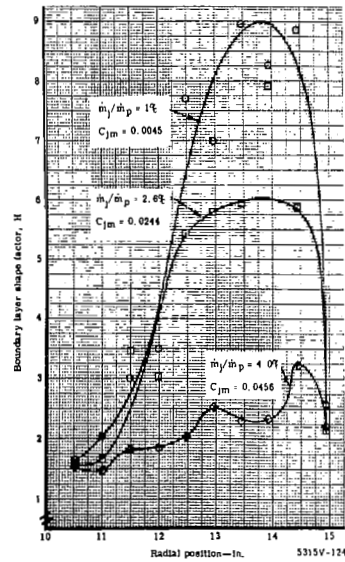
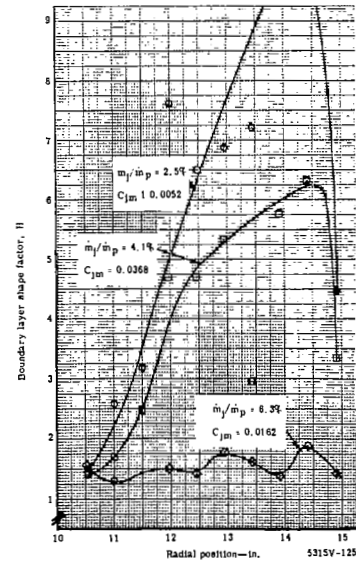
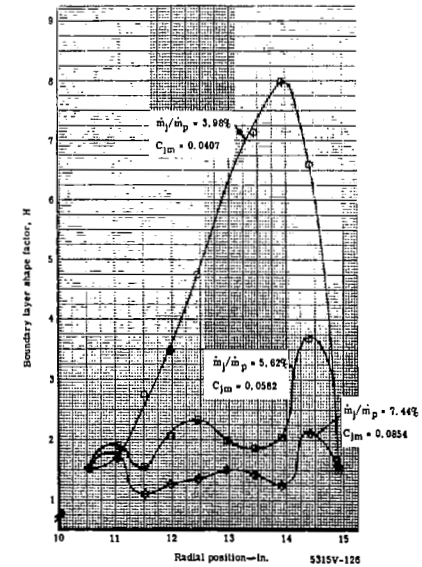


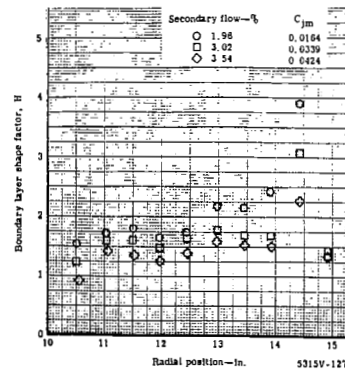
Figure 112. Plain blade exit wake survey—displacement thickness distribution at Station 3.



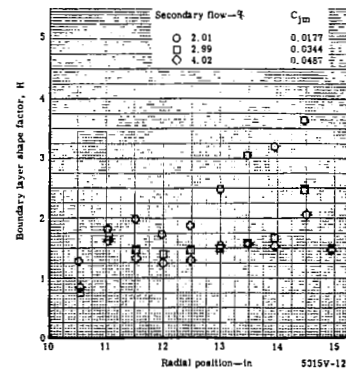
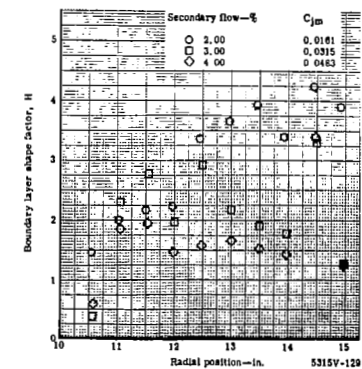
Slot size = 0.02 in.

Slot size = 0.03 in.
Tangential jet blade No. 1

Slot size = 0.04 in.

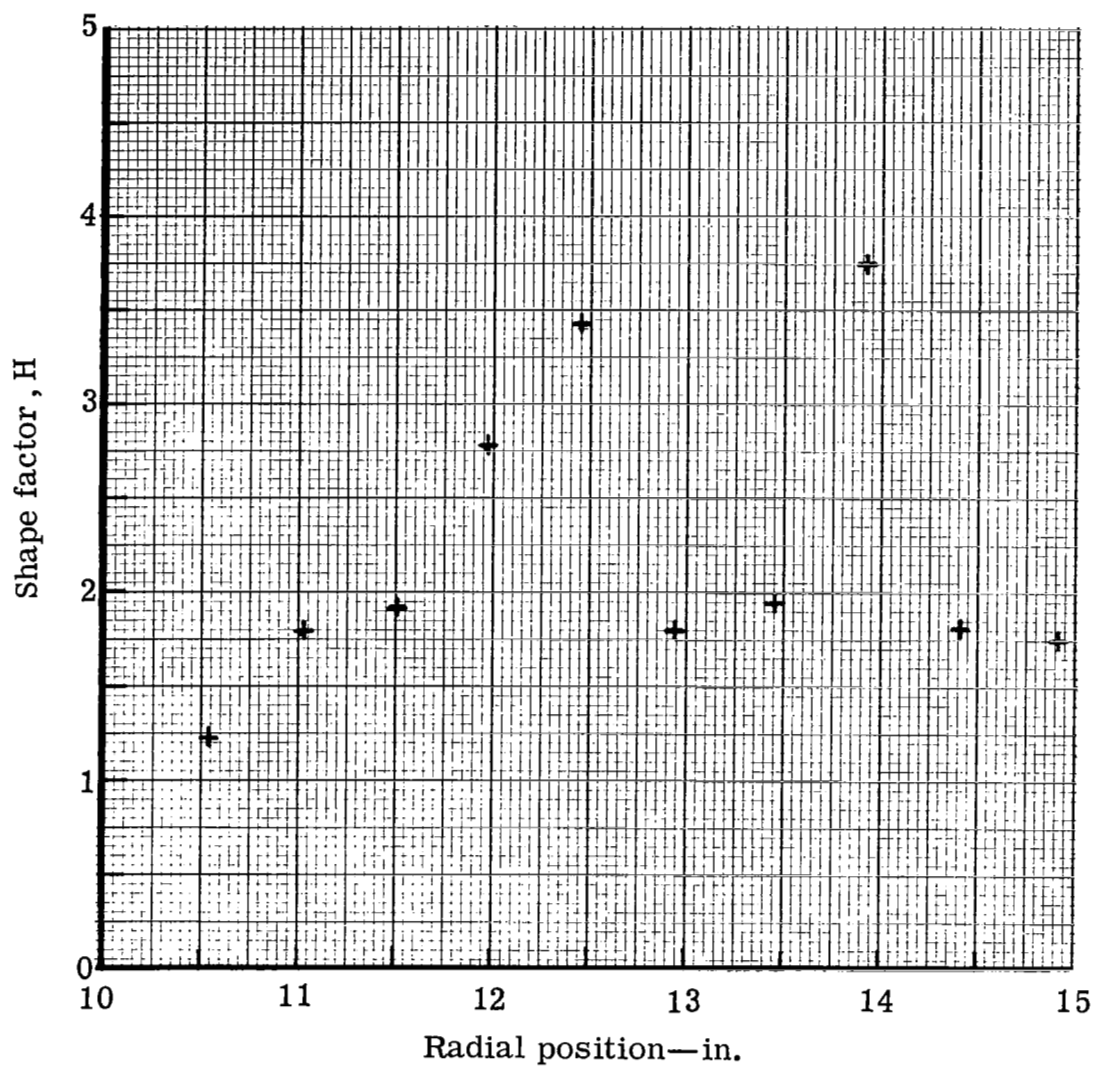


Slot size = 0.02 in.

Slot size = 0.03 in.
Tangential jet blade No. 2

Slot size = 0.04 in.

Figure 113. Radial variation of boundary layer shape factor of trailing edge (Station 3) for tangential jet configurations.



5315III-38

Figure 114. Plain blade exit wake survey—shape factor distribution at Station 3.

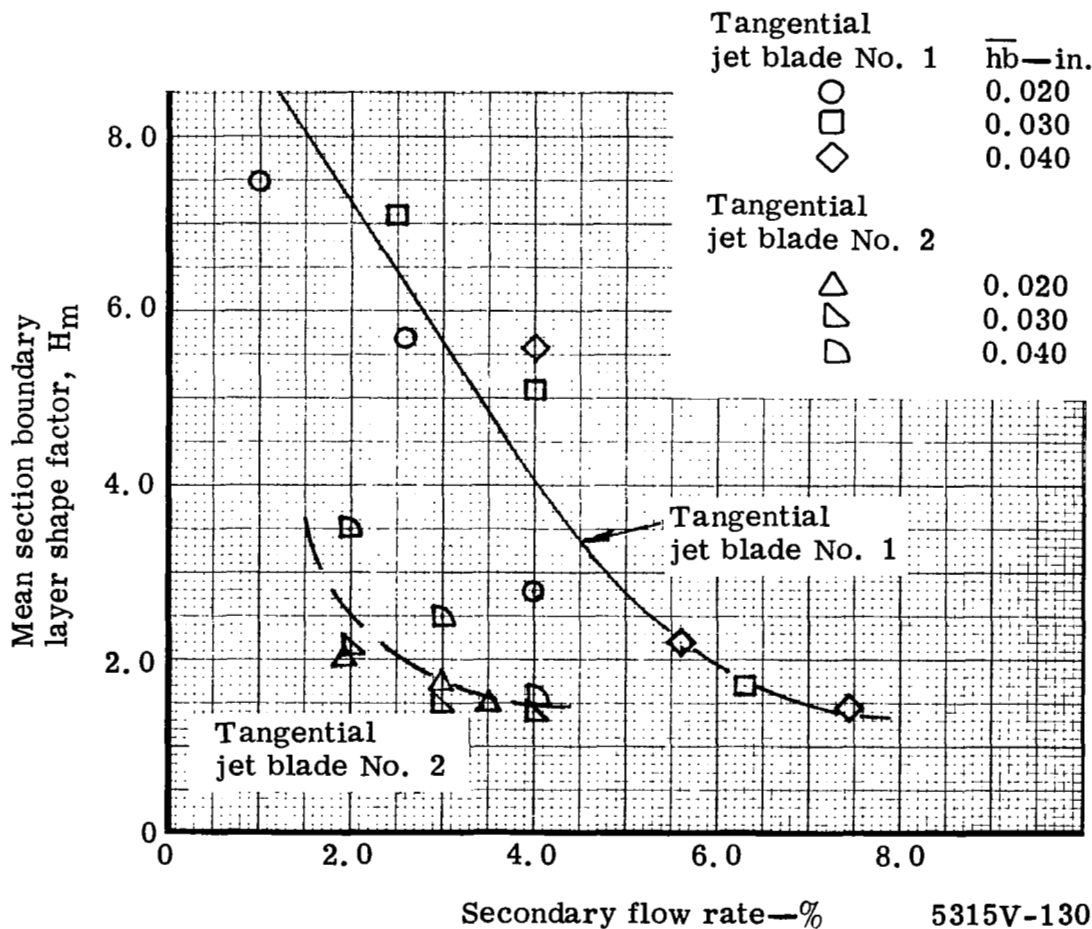
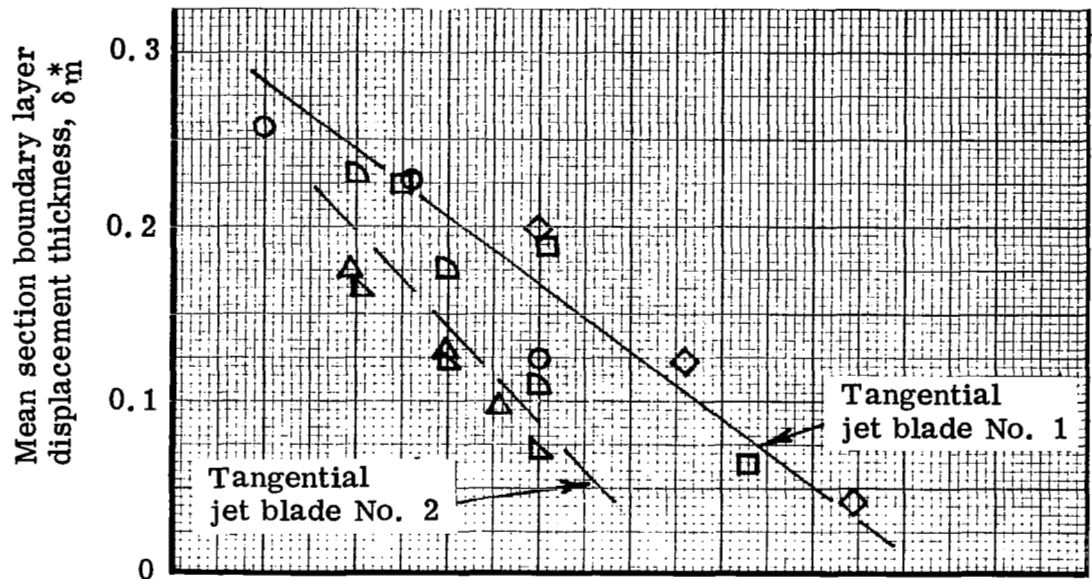
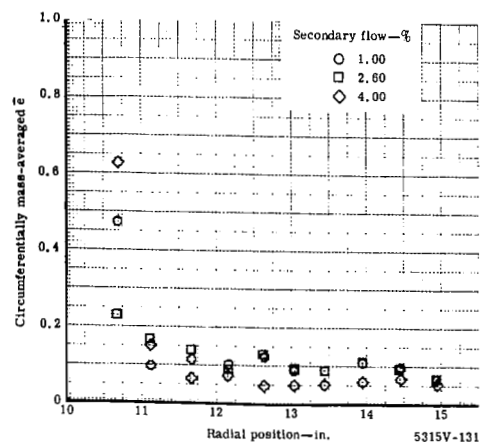
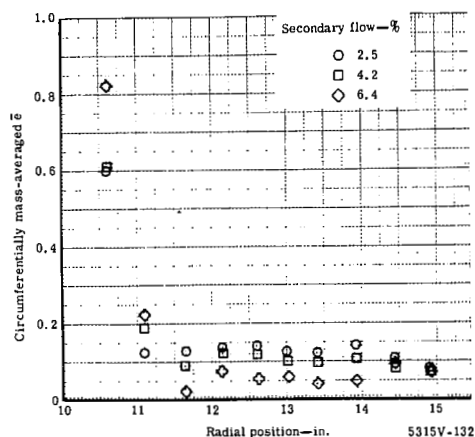


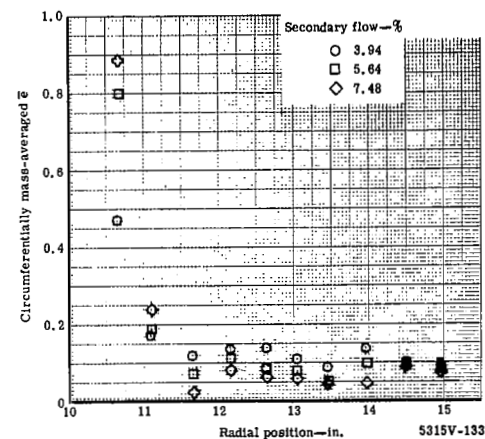
Figure 115. Effect of secondary flow on trailing edge mean section δ^* and H for tangential blades No. 1 and 2.



Slot size—0.020 in.

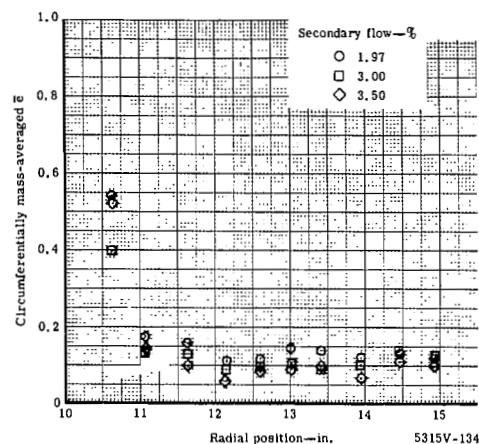


Slot size—0.030 in.

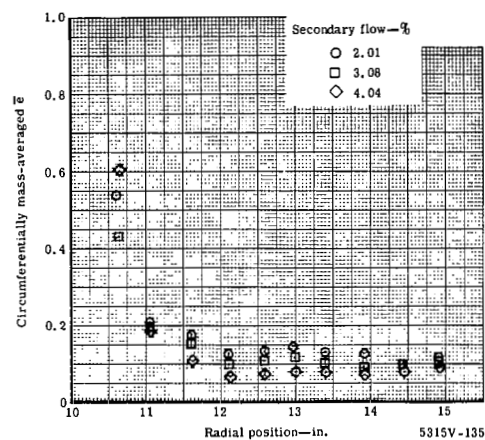


Slot size—0.040 in.

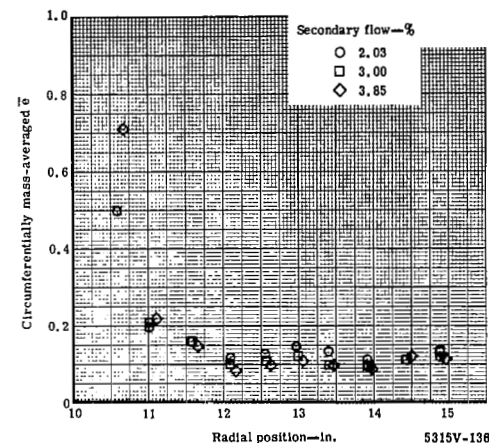
Tangential jet blade No. 1



Slot size—0.020 in.



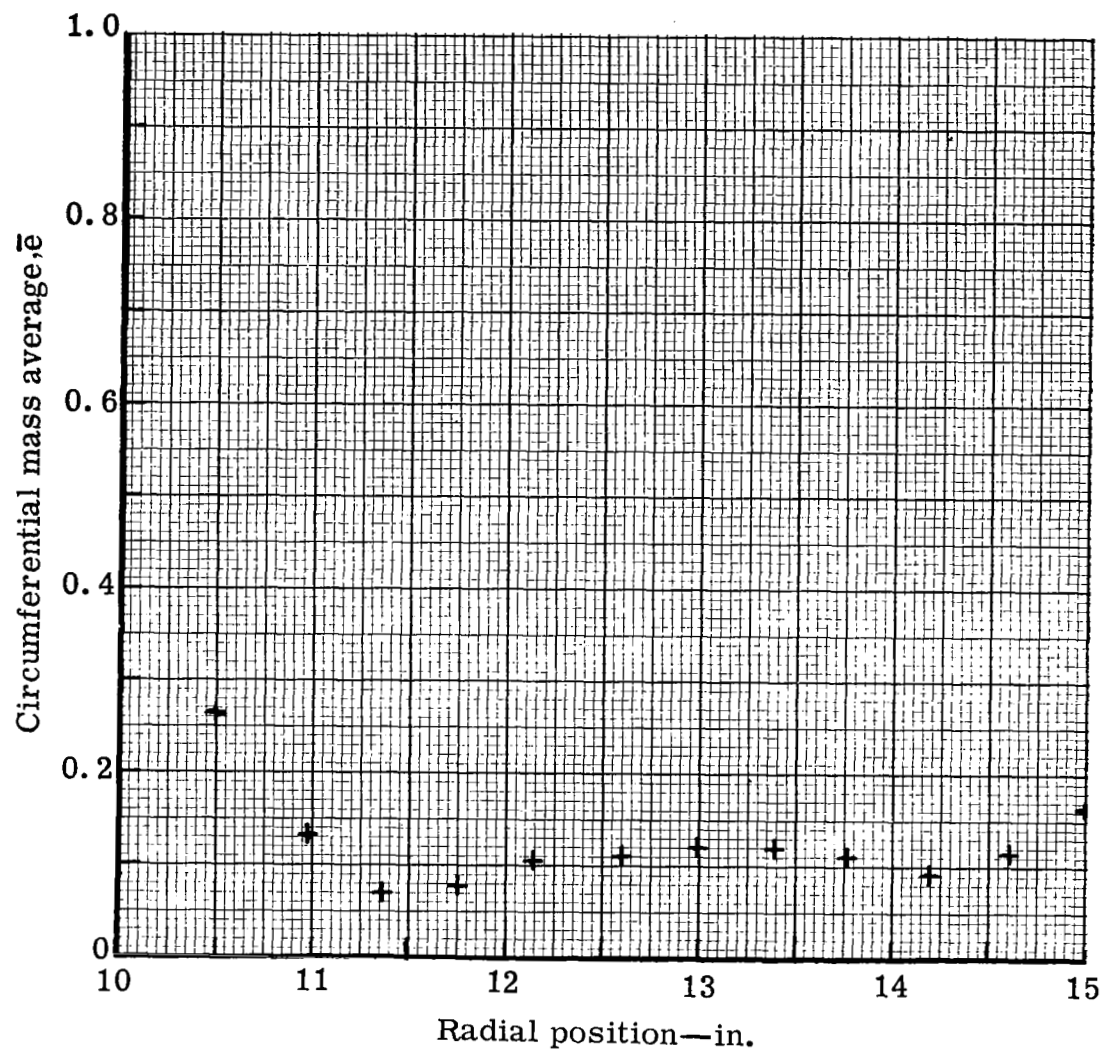
Slot size—0.030 in.



Slot size—0.040 in.

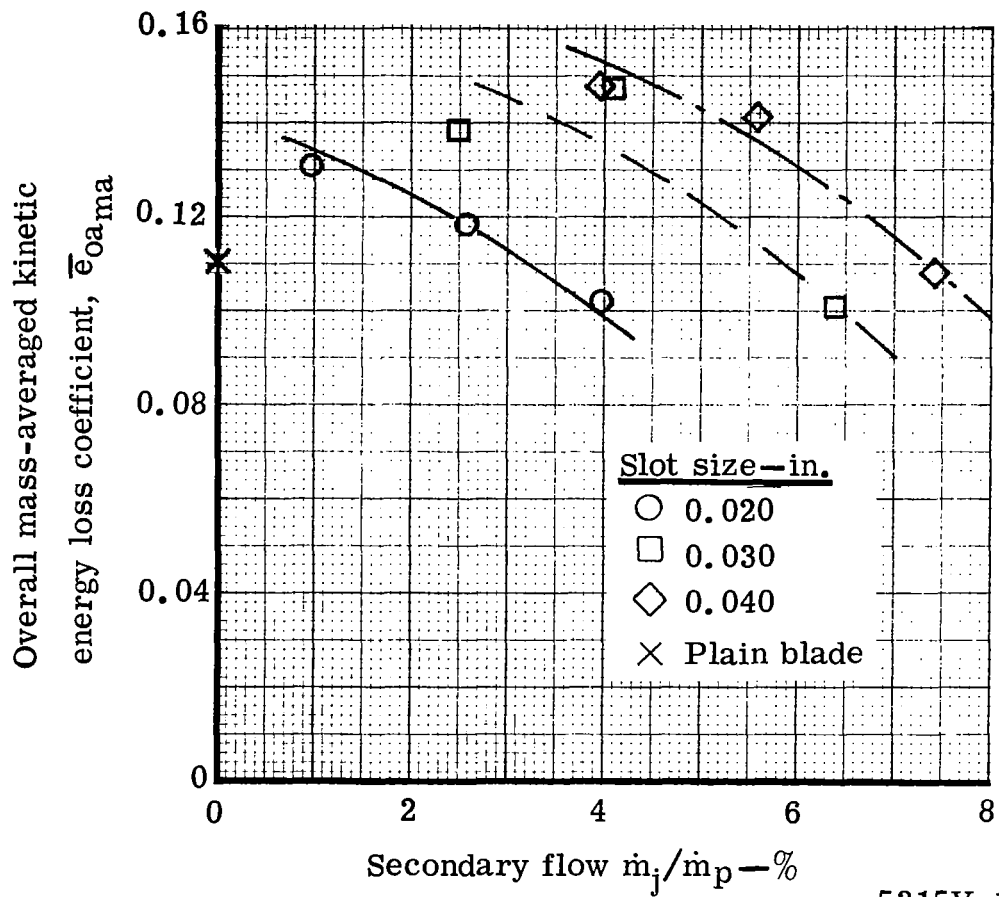
Tangential jet blade No. 2

Figure 116. Radial variation of circumferentially mass-averaged kinetic energy loss coefficient at Station 4 for all tangential jet configurations.



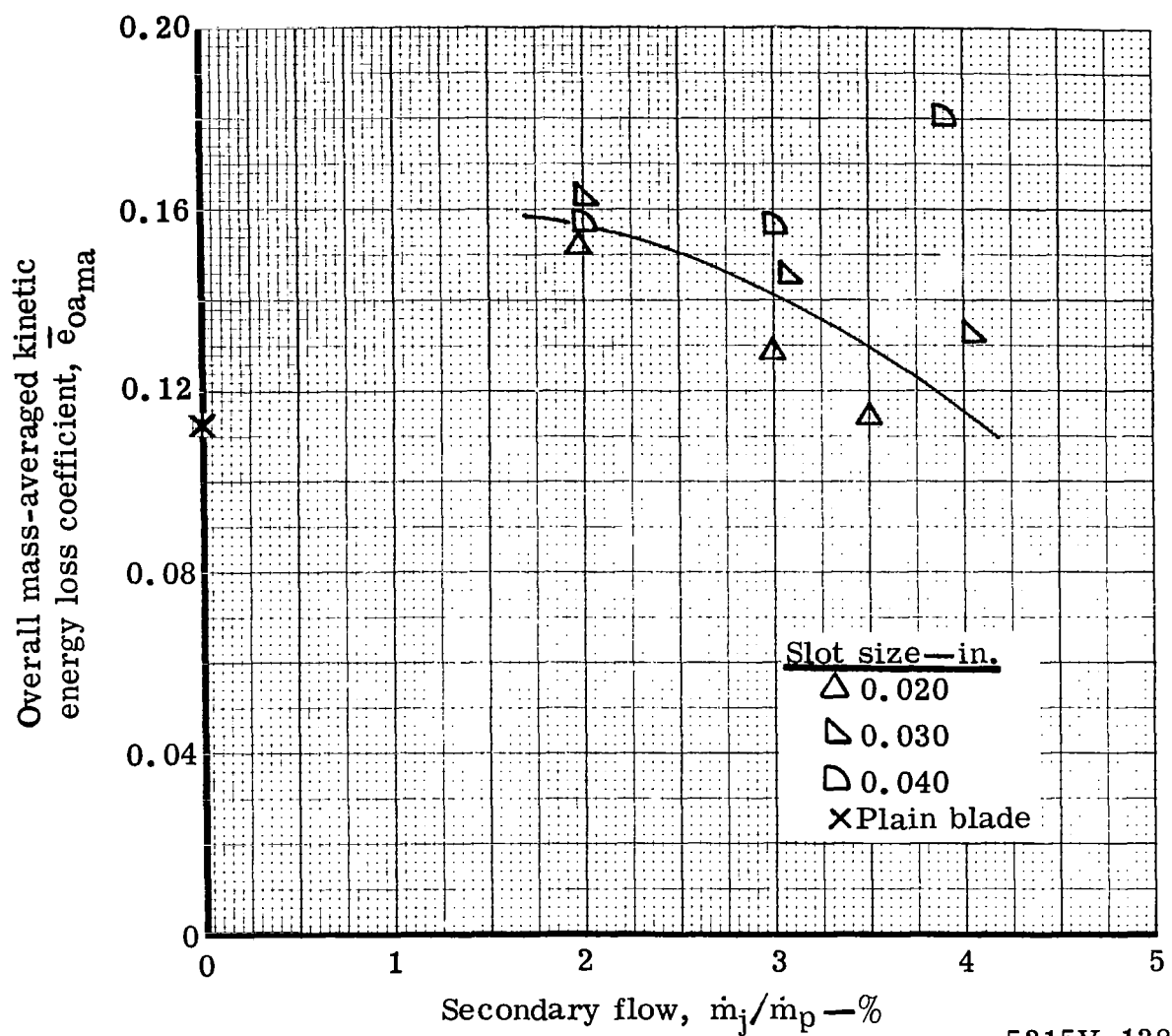
5315III-40

Figure 117. Plain blade downstream wake survey—kinetic energy loss coefficient distribution at Station 4.



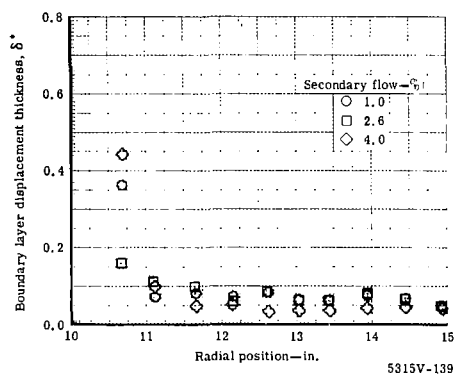
5315V-137

Figure 118. Variation of overall mass-averaged kinetic energy loss coefficient with percent secondary flow at tangential jet blade No. 1, Station 4.

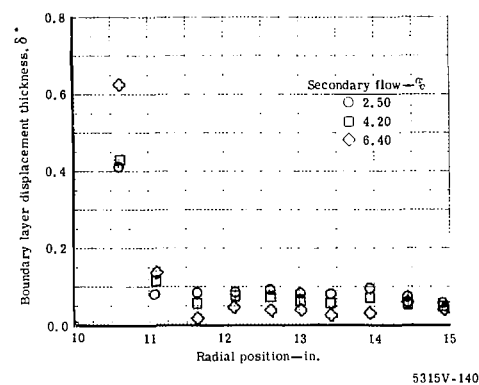


5315V-138

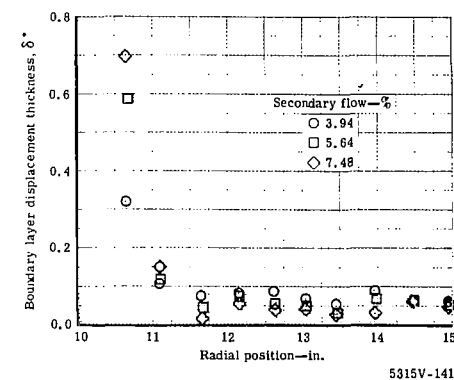
Figure 119. Variation of overall mass averaged kinetic energy loss coefficient with percent secondary flow at tangential jet blade No. 2, Station 4.



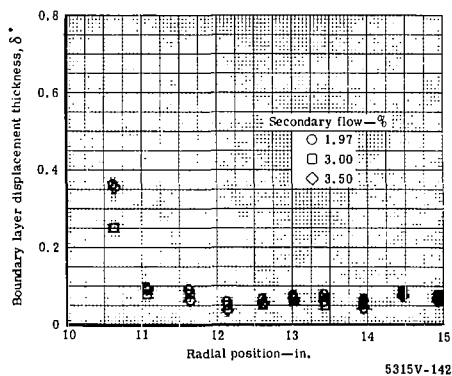
Slot size = 0.020 in.



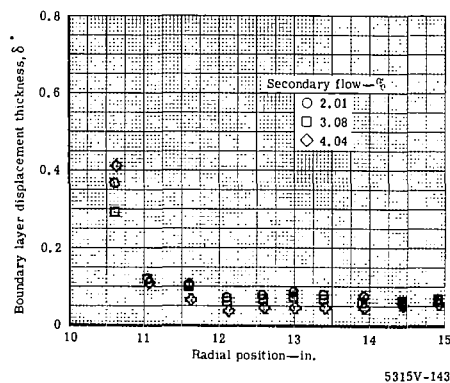
Slot size = 0.030 in.
Tangential jet blade No. 1



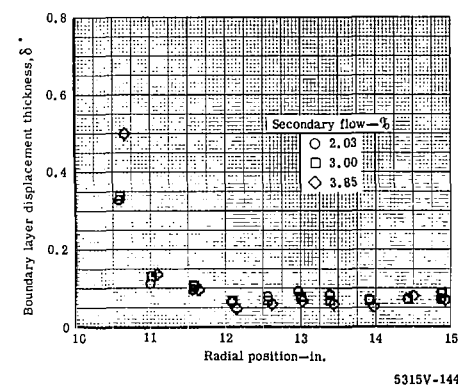
Slot size = 0.040 in.



Slot size = 0.020 in.

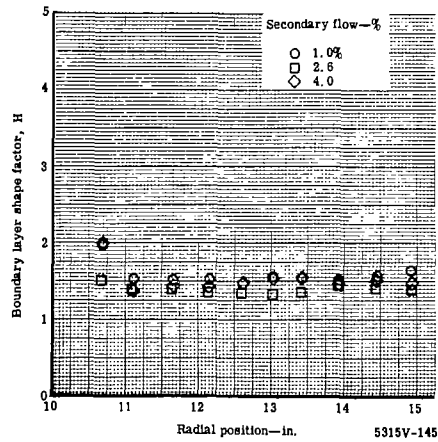


Slot size = 0.030 in.
Tangential jet blade No. 2

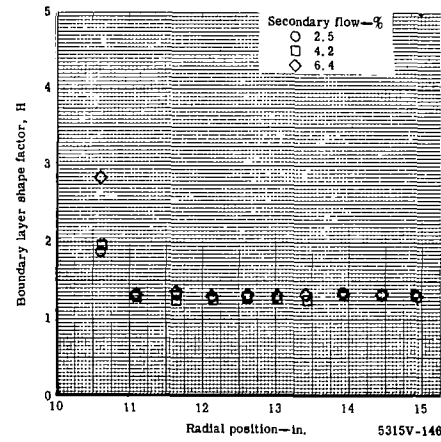


Slot size = 0.040 in.

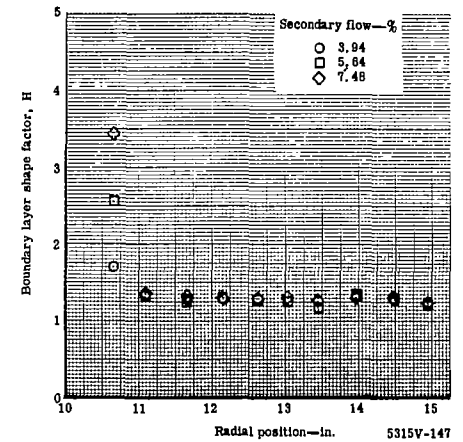
Figure 120. Radial variation of boundary layer displacement thickness at Station 4 for all tangential jet configurations.



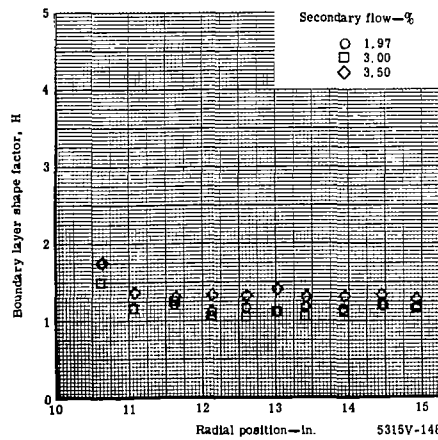
Slot size = 0.020 in.



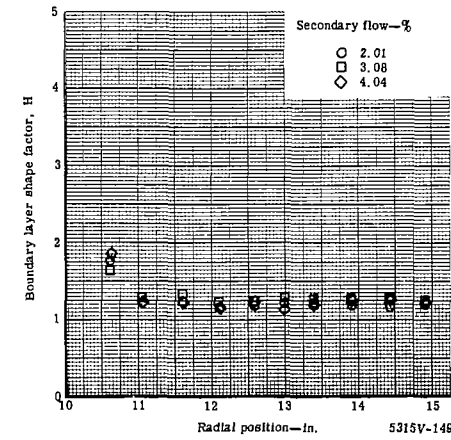
Slot size = 0.030 in.
Tangential jet blade No. 1



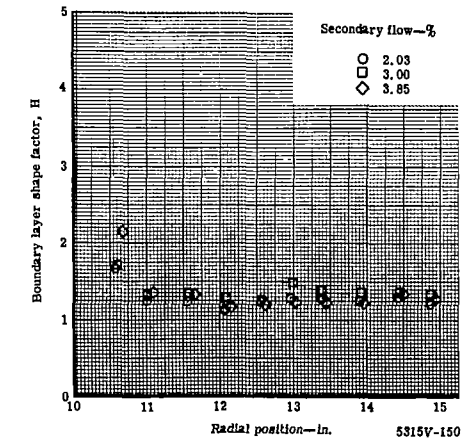
Slot size = 0.040 in.



Slot size = 0.020 in.



Slot size = 0.030 in.



Slot size = 0.040 in.

Tangential jet blade No. 2

Figure 121. Radial variation of boundary layer shape factor at Station 4 for tangential jet configurations.

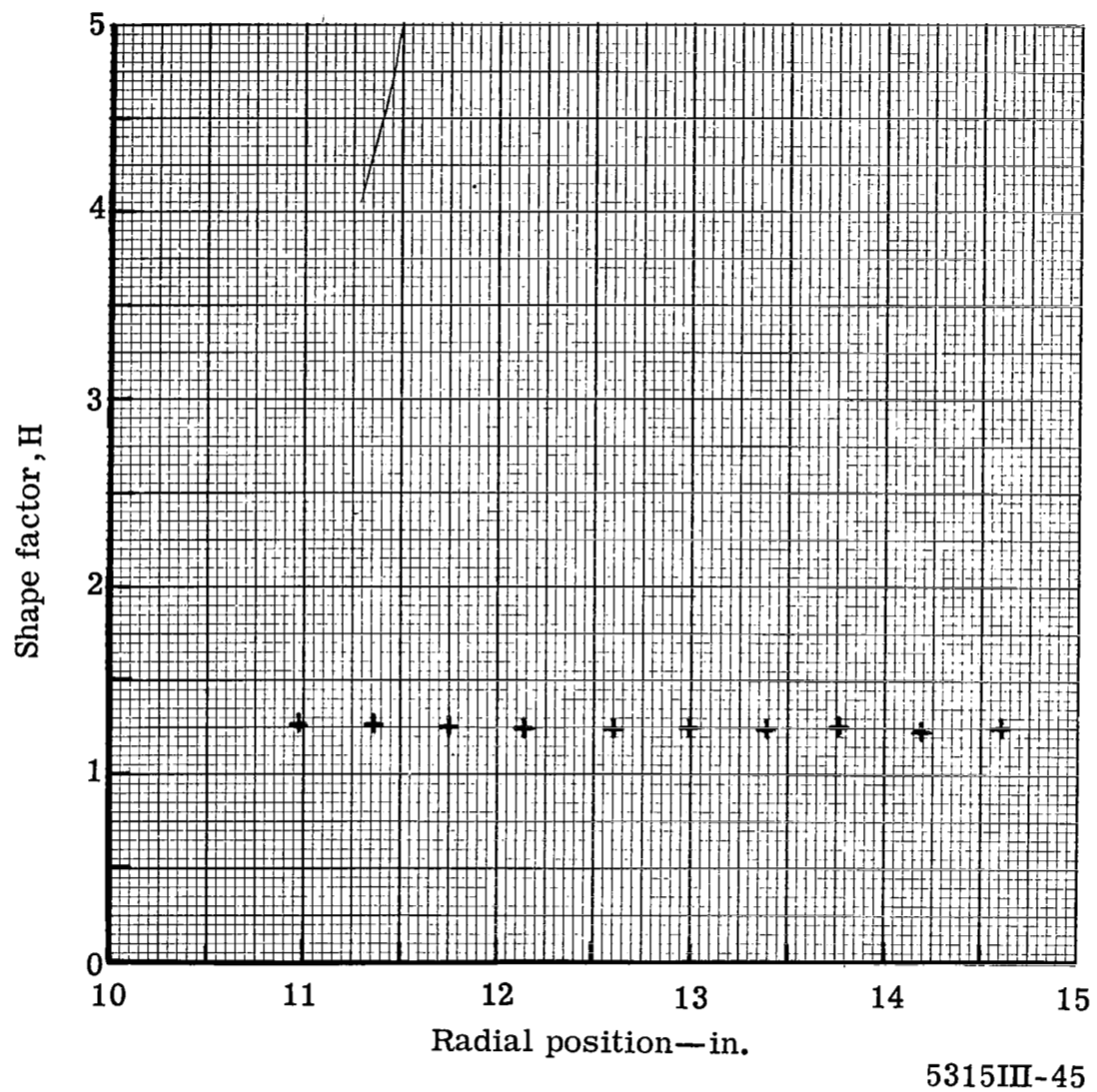


Figure 122. Plain blade downstream wake survey-shape factor distribution at Station 4.